UCLA
UCLA Electronic Theses and Dissertations

Title

Mitochondrial Protein Dynamics in Cardiac Remodeling

Permalink

https://escholarship.org/uc/item/3sj7b8gc

Author

Lau, Edward

Publication Date

2014

Peer reviewed|Thesis/dissertation

UNIVERSITY OF CALIFORNIA

Los Angeles

Mitochondrial Protein Dynamics in Cardiac Remodeling

A dissertation submitted in partial satisfaction of the requirements for the degree

Doctor of Philosophy

in Molecular, Cellular, & Integrative Physiology

by

Edward Lau

2014

ABTRACT OF THE DISSERTATION

Mitochondrial Protein Turnover in Cardiac Remodeling

by

Edward Lau

Doctor of Philosophy in Molecular, Cellular & Integrative Physiology

University of California, Los Angeles, 2014

Professor Peipei Ping, Chair

The cardiac mitochondrial proteome contains ~1,500 distinct proteins that carry out necessary metabolic and energetic processes in the heart. To sustain cardiac function, the mitochondrial proteome must be maintained in constant renewal, or turnover, especially under stress conditions. Disruptions of protein turnover can lead to protein damage and proteotoxicity, a hallmark of many heart disease etiologies. Current quantitative proteomics experiments largely focus on the measurement of the steady-state abundance, or changes therein, of proteins that are present in a system, and give little insights into the underlying regulations of protein synthesis, degradation, and homeostasis. Protein turnover rates provide this missing temporal dimension of information, and can inform on the potential mechanism through which protein abundance may permute during the development of disease (e.g., via increased synthesis or decreased degradation). Currently, such investigations are hampered by the fact that the technology to measure protein turnover in animals on a large scale has not been well developed. This dissertation outlines a new method to measure protein turnover half-life in the cardiac mitochondrion. Basic features of the regulation of protein turnover in the mitochondrion are discussed, and how protein dynamics permutes in early-stage heart failure after hypertrophic stimuli is described. In total, we measured the turnover rates of 2,986 proteins in the mouse heart under basal conditions, isoproterenol stimulus, and post-stimulus recovery, including 1,078 proteins

from isolated mitochondria. The data revealed widespread, bidirectional changes in protein turnover in 35 functional categories, and further identified a number of novel candidate disease proteins with significantly up-regulated turnover rates in disease, including HK1, ALDH1B1, and PHB, which have been obscured from previous investigations due to their inconspicuous changes in steady-state abundance. Combinatorial analysis of protein expression and protein turnover data indicates that the remodeling heart is characterized by decreased turnover but increased expression of a cohort of mitochondrial proteins including FXN, LETM1, and CYC1, suggesting a potential class of candidate disease proteins whose impaired degradation is associated with remodeling. I further discuss the implications of the data to the cardiac remodeling process at large and how such investigations may be translated to human studies in the future. Taken together, the results suggest that comparisons of protein turnover rates can be a powerful new tool to understand the temporal dynamics of disease progression in the heart.

The dissertation of Edward Lau is approved

by

James N. Weiss

Enrico Stefani

Robert J. Beynon

Aldons J. Lusis

Peipei Ping, Committee Chair

University of California, Los Angeles

2014

TABLE OF CONTENTS

I. Turnover of mitochondrial proteins in the heart

II. Mitochondrial protein dynamics during cardiac remodeling

III. Mechanisms of proteolysis in cardiac mitochondria

IV. Translational potential and future perspectives

LIST OF FIGURES

LIST OF TABLES

RECURRING NOTATIONS AND ABBREVIATIONS

2DE	Two-dimensional electrophoresis
A_0	Fractional abundance of the 0th isotopomer
ATP	Adenosine triphosphate
DIGE	Differential gel electrophoresis
GC	Gas chromatography
^2H_2O	Deuterium oxide ("heavy water")
IEF	Isoelectric focusing
i.p.	Intraperitoneal
k	Protein turnover rate constant
k_p	Precursor turnover rate constant
LC	Liquid chromatography
LVAD	Left-ventricular assist device
MIDA	Mass isotopomer distribution analysis
MS	Mass spectrometry
MS/MS	Tandem mass spectrometry
PAGE	Polyacrylamide gel electrophoresis
Ppm	Parts per million
p_{ss}	Precursor steady-state enrichment level
PTM	Post-translational modifications
RIA	Relative isotope abundance
ROS	Reactive oxygen species
SDS	Sodium dodecyl sulfate
SILAC	Stable isotope labeling by amino acid in cell culture
UPS	Ubiquitin-proteasome system

PREFACE

This dissertation details the progress I made between 2011 and 2014 in collaboration with my colleagues in the Ping laboratory at UCLA to examine the turnover and proteolysis of mitochondrial proteins in normal and diseased hearts. The majority of the work has been published in peer-reviewed journals: Chapter I contains in part an updated version of the work in our publications (Chan et al., 2014; Kim et al., 2012; Lam et al., 2014). Chapter II contains in part an updated version of our publication (Lam et al., 2014). Chapter III contains in part an updated version of our publication (Lau et al., 2012). Chapter IV contains in part an updated version of our publications (Lam et al., 2014; Wang et al., 2014). The reader is encouraged to refer to these publications for a concise summary of the studies. As the medium of this dissertation presents an opportunity for additional material not permissible by the strict word limits of journals, additional analyses have been included for the purpose of discussion and for providing a more coherent narrative of the rationales behind the studies. For the sake of organization, methods are summarized at the end of each chapter, and insofar as reasonable discussions on the technical aspects of experiments are separated from those on the biological implications of the results.

The co-authors of the publications contributed to study design, data collection, and data analysis to various extents. For the work in our publication (Kim et al., 2012), Tae-Young Kim, Ding Wang and Allen Kim in particular contributed to study design, animal models, data generation and data analysis. For the work in our publication (Lam et al., 2014), Maggie Lam in particular contributed to study design, data collection, data analysis, and software production. David Liem in particular contributed to animal models. Allen Kim and Xiangbo Liang in particular participated in the mathematical model and software production. For the work published in Reference (Lau et al., 2012), Ding Wang in particular contributed to data collection and analysis. For the work published in our publication (Wang et al., 2014), David Liem in particular

contributed to clinical study design. Jason Tabaraki in particular contributed to sample collection. Maggie Lam and Dominic Ng in particular participated in data collection and analysis. In all of the aforementioned published studies and in unpublished studies included in this dissertation, I played major roles in any or all of study design, planning, data collection, data interpretation, data presentation, manuscript preparation, and revision. I declare that this dissertation in its entirety represents my original work except where due acknowledgment is made, and that it has not been previously included in a thesis at any institution. As biomedical research is an increasingly collaborative endeavor, on the occasions where it has become infeasible to clearly separate contributions from close collaborative efforts in the aforementioned published projects, particular elements in the published works may be construed as necessary backgrounds and introduction to the subject instead of experimental results of this dissertation work.

BIOGRAPHICAL SKETCH

Education and employment:

B.A.   Molecular & Cell Biology, University of California, Berkeley, CA, 2006
M.Phil.   Chemistry, University of Hong Kong, Hong Kong, 2010

2006-7   Lab Helper, Dept. of Chemical Physiology, The Scripps Research Institute, CA
2007-8   Research Assistant, Dept. of Chemistry, Univ. of Hong Kong, Hong Kong
2008-10   Graduate Student Researcher, Dept. of Chemistry, Univ. of Hong Kong, Hong Kong
2010-4   Graduate Student Researcher, Dept. of Physiology, UCLA
2012,3,4   Teaching Assistant, Dept. of Microbiology, Immunology & Mol. Genetics, UCLA

Peer reviewed publications: (***** equal contributions as first author; **corresponding authorship)

Most relevant to this dissertation:
1. Lam MP*, Wang D*, **Lau E***, Liem DA*, Kim AK, Ng CM, Liang X, Bleakley BJ, Liu C, Tabaraki JD, Cadeiras M, Wang Y, Deng MC, Ping P. Protein kinetic signatures of the re-modeling heart following isoproterenol stimulation. Journal of Clinical Investigation, 2014;124:1734-44.

2. Wang D, Liem DA, **Lau E,** Ng CM, Bleakley BJ, Cadeiras M, Deng MC, Lam MP, Ping P. Characterization of human plasma proteome dynamics using deuterium oxide. Proteomics Clinical Applications, 2014;8:610-9.

3. Chan XC, Black CM, Lin AJ, Ping P, **Lau E****. Mitochondrial protein turnover: methods to measure turnover rates on a large scale. Journal of Molecular and Cellular Cardiology, 2014, In press: doi:10.1016/j.yjmcc.2014.10.012.

4. Kim TY*, Wang D*, Kim AK*, **Lau E***, Lin AJ, Liem DA, Zhang J, Zong NC, Lam MP, Ping P. Metabolic labeling reveals proteome dynamics of mouse mitochondria, Molecular & Cellular Proteomics, 2013;11:1586-94.

5. **Lau E***, Wang D*, Zhang J, Yu H, Lam MPY, Liang X, Zong NC, Kim TY, Ping P. Substrate- and isoform-specific proteome stability in normal and stressed cardiac mitochondria, Circulation Research, 2012;110:1174-8.

Other selected peer-reviewed publications (out of 21 total):
6. Zong N, Ping P, **Lau E**, Choi HJ, Ng DCM, Meyer D, Fang C, Li H, Wang D, Zelaya IM, Yates JR, Lam MP. Lysine Ubiquitination and Acetylation of Human Cardiac 20S Pro-teasomes. Proteomics Clinical Applications, 2014;8:590-4.

7. Lotz C, Lin AJ, Black CM, Zhang J, **Lau E**, Deng N, Wang Y, Zong NC, Choi JJ, Xu T, Liam DA, Korge P, Weiss JN, Hermjakob H, Yates JR, Apweiler R, Ping P. The characterization, deign and function of the mitochondrial proteome: from organs to organisms, Journal of Proteome Research, 2014;13:433-46.

8. Lam MPY, **Lau E**, Liem DA, Ping P, Cyclophilin D and acetylation: a new link in cardiac signaling, Circulation Research, 2013;113:1268-9.

9. Lam MPY*, **Lau E***, Scruggs SB, Wang D, Kim TY, Liem AD, et al., Site-specific quantitative analysis of cardiac mitochondrial protein phosphorylation, <u>Journal of Proteomics</u>, 2013;81:15-23.

10. Martin LJ, **Lau E**, Singh H, Vergnes L, Tarling EJ, Mehrabian M, Mungrue I, Xiao S, Shih D, Castellani L, Ping P, Reue K, Stefani E, Drake TA, Bostrom K, Lusis AJ. ABCC6 localizes to the mitochondria-associated membrane, <u>Circulation Research</u>, 2012;111:516-20.

11. Lam MP, Scruggs SB, Kim TY, Zong NC, **Lau E**, Wang D, Kim TY, Liem DA, Zhang J, Ryan CM, Faull KF, Ping P. An MRM-based workflow for quantifying cardiac mitochondrial protein phosphorylation in murine and human tissue, <u>Journal of Proteomics</u>, 2012;75:4602-9.

12. **Lau E**, Lam MP, Siu SO, Chu IK, Combinatorial use of offline SCX and online RP-RP chromatography for iTRAQ-based quantitative proteomics applications, <u>Molecular Biosystems</u>, 2011;7:1399-408.

13. Lam MP, **Lau E**, Siu SO, Ng DCM, Lo C, Chu IK, Online combination of reverse-phase/reverse-phase and porous graphitic carbon liquid chromatography for multicomponent separation of proteomics and glycoproteomics samples, <u>Electrophoresis</u>, 2011;32:2930-40.

14. Liu H, **Lau E**, Lam MPY, Chu H, Li S, Huang G, et al., OsNOA1/RIF1 ifunctional homolog of AtNOA1/RIF1: implication for a highly conserved plant cGTPase essential for chloroplast function, <u>New Phytologist</u>, 2010;187:83-105.

15. Lam MPY, Siu SO, **Lau E**, Mao Z, Sun HZ, Chiu PCN, et al., Online coupling of reverse-phase and hydrophilic interaction liquid chromatography for protein and glycoprotein characterization, <u>Analytical and Bioanalytical Chemistry</u>, 2010; 398:791-804.

Lectures and presentations:

• 2014/09/23 "Proteome Biology of the Heart", UCLA MCIP CVRL New Student Orientation

• 2013/11/17 "Protein half-life in normal and diseased heart", AHA Scientific Sessions 2013, Dallas, TX

• 2008/07/30 "Understanding the molecular mechanisms of skeletal dysplasia through quantitative proteomics of mutant collagen X protein-expressing chondrocytes", 25th Annual Trent Conference on Mass Spectrometry, 2008, Toronto, ON, Canada.

Awards and honors:

• Winner, International Poster Competition, 33rd International Society for Heart Research North American Section Annual Meeting, 2012, Banff, AB, Canada

• American Heart Association Pre-doctoral fellowship 12PRE11610024, "Protein degradation pathways in cardiac mitochondria", Edward Lau (PI), 07/01/2012 – 06/30/2014

• Poster Award for "Substrate- and isoform- specific proteome stability in cardiac mitochondria, Lau et al.", NHLBI Proteomics Center Third PI/Advisory Panel Meeting, 2012.

• Co-inventor, UC Case 2013-137/ Tech ID: 23601 "Platform for Large-Scale Determination of Biomolecular Turnover Rate" (http://techtransfer.universityofcalifornia.edu/NCD/23601.html)

I. Turnover of mitochondrial proteins in the heart

This chapter describes the development a ^2H_2O labeling strategy with which protein dynamics within cardiac mitochondria may be discerned. We developed a novel mass spectrometry and data analysis method to measure the half-life in vivo of proteins in mouse models. The data revealed over 500 mitochondrial proteins were measured from the mouse heart, mouse liver, and mouse kidney. The median half-life of mitochondrial proteins in the heart was 15.4 [3.5 – 33.0] days, and in the liver 4.7 [1.2 – 7.3] days, the kidney 4.8 [1.5 – 7.5] days. Mitochondrial proteins display diverse individual turnover rates both within and across multiple tissues, whereas proteins belonging to complexes tend to have closer half-life. We further consider some of the properties of in-vivo protein half-life and their implications on the regulation of the mitochondrial proteome. These method developments serve as a foundation for comparisons between normal and diseased hearts in the subsequent chapters. The material presented in this chapter was published and can be found in our publications (Chan et al., 2014; Kim et al., 2012; Lam et al., 2014).

Methods to measure in vivo mitochondrial protein turnover

Mitochondria are the site of numerous essential cellular processes, ranging from energy metabolism to calcium handling, redox balance, and cell death (Balaban, 1990; Zhang et al., 2012). In the mammalian heart, cardiac mitochondria can make up to ~35% of cardiac volume (Schaper et al., 1985), and produces 95% of the ATP that sustains the enormous energetic needs of cardiac functions (Neely and Morgan, 1974). Recent discoveries in cardiac research

1

have converged upon the importance of mitochondrial physiology in the development of multiple human heart diseases, spurring hope that a new generation of therapies can be discovered that target molecules within these organelles.

To support mitochondrial structure and functions, cardiac mitochondria contain a distinct repertoire of proteins that localize specifically to the organelle. These mitochondrial proteins may originate from both the nuclear genome or the mitochondrial genome, and may reside in mitochondria obligatorily or transiently – translocating into the mitochondria after particular stimuli. Mitochondrial proteins can be found localized to four sub-organellar compartments: the outer membrane, which has been estimated to contain approximately 10% of all mitochondrial proteins, the intermembrane space (~10%), the inner membrane (~20%), and the matrix (~60%), as reviewed in (Zhang et al., 2012). As proteins are biomolecules that carry out the bulk of biological functions, the global protein pool (proteome) represents a critical intermediate phenotype between gene expression and functional outcome. They also offer a robust reflection of the cell state (with the half-life of a protein pool on the order of days) relative to its mRNA counterpart (with half-life on the order of hours) (Vogel and Marcotte, 2012). As such, tremendous interests have been shown toward characterizing the anatomy and physiology of cardiac mitochondrial proteins to interrogate their alterations in disease mechanisms.

With advances in mass spectrometry and bioinformatics techniques in the last decade, the entire set of proteins from a system (the proteome) may now be interrogated to identify protein molecular signatures in disease and to the regulation of protein expression, localization, modification, and interaction at a global level. Such large-scale studies of proteins have been widely applied to identify the complement of mitochondrial proteins in multiple organisms and tissues, including in mouse, human, and Drosophila, as reviewed in (Zhang et al., 2012) and their involvement in disease mechanisms. In the Ping laboratory in particular, there has been a longstanding interest in defining the role of the cardiac mitochondrial proteome in cardiac and

injury. To identify bona fide mitochondrial proteins, our laboratory has developed rigorous protocols to isolate mitochondrial fractions from tissue lysates via differential centrifugation, followed by purification with a stepwise Percoll density gradient, then followed by shotgun proteomics using high-resolution mass spectrometry and stringent bioinformatics filters. Recent surveys in the laboratory of cardiac mitochondrial proteome, which we define as the complement of proteins reproducibly identifiable by proteomics techniques from mitochondrial purifications, revealed approximately 1,300 distinct proteins that span over five orders of magnitude in concentration (Lotz et al., 2013), representing one of the most comprehensive atlas of mitochondrial proteins to-date.
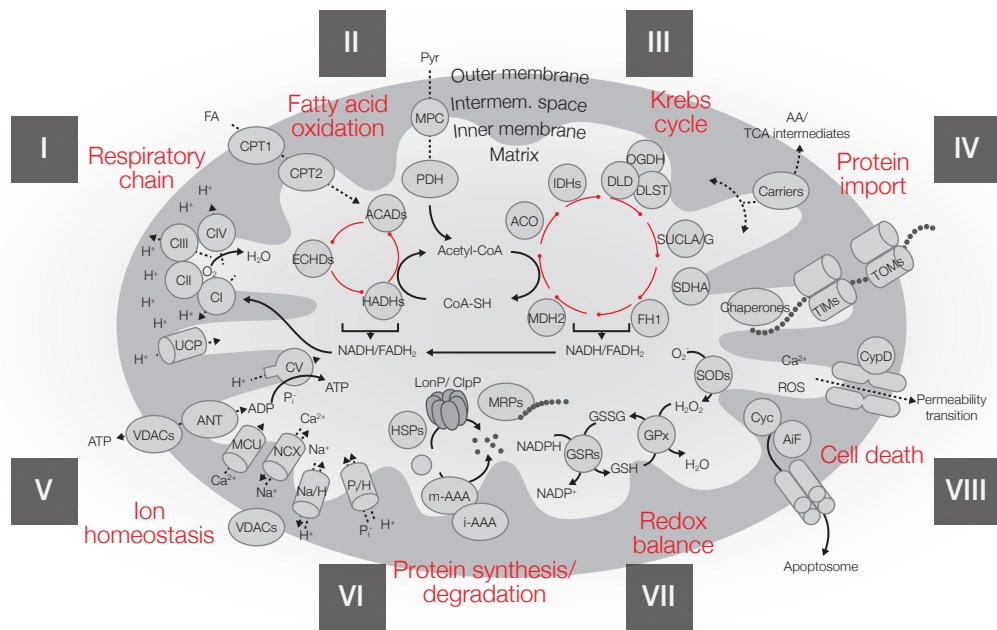
FIGURE 1.1   Elements of the mitochondrial proteome

FIGURE 1.1 depicts components of the identified cardiac mitochondrial proteome. Collectively the identified mitochondrial proteins belonged to diverse functional categories, from which at least eight major overlapping sub-proteomes might be identified: the respiratory chain compo-

nents, TCA cycle and anaplerotic enzymes, fatty acid oxidation enzymes, protein import machineries, ion homeostasis and inner membrane channel proteins, proteolytic and chaperone systems, redox proteins, and apoptotic proteins (Zhang et al., 2012). Furthermore, to investigate how alterations of proteins in various functional categories are reflected in disease development, members in the Ping group delineated the complements of core vs. facultative mitochondrial proteins in the heart (Zhang et al., 2008a). More recently, we conducted quantitative mass spectrometry comparisons of the relative abundance of mitochondrial proteins amongst different organs and organisms. Mitochondria from different tissues have vastly distinct proteome composition to support specialized functions. The results suggest that cardiac mitochondria are especially rich in ATP synthesis proteins, whereas liver mitochondria contain higher abundance of proteins in amino acid metabolism (Lotz et al., 2013). To examine the agents of cardioprotective signaling in the mitochondrion, we further developed highly sensitive, targeted multiple-reaction monitoring (MRM) methods to quantify mitochondrial protein post-translational modifications in site-specific manners (Lam et al., 2012, 2013).

Given the importance of mitochondrial protein functions, damage to mitochondrial proteins such as by reactive oxygen species (ROS) is expected to disrupt critical cellular processes and accordingly has been associated with numerous disease phenotypes. To preserve metabolic and energetic functions, the proteome that composes functional mitochondria must be constantly maintained in homeostasis. This is normally achieved in part by the degradation of existing proteins into free amino acids, and the subsequent synthesis of new proteins to replenish the protein pool. Alterations of this protein dynamic equilibrium often lead to changes in static protein abundance, though as we shall see this is not always the case, and changes in protein synthesis may be balanced by changes in degradation and lead to no overt changes in steady-state level. Until recently, most investigations of the mitochondrial proteome have focused on the steady-state quantities of mitochondrial proteins in health or disease, but the measurement of the static abundance of a protein alone lacks temporality and gives little in-

4

sight into the underlying temporal processes such as its homeostasis renewal, or the window of impact of a new protein. This barrier leads to an incomplete description of the proteome, and may contribute to the inability to detect some important features of biological and pathological processes when the crucial disease correlation is masked from the method of investigation. Protein turnover is thought to provide this "missing dimension" of protein function and allows one to draw inference into the homeostasis and windows of impact of a particular protein (Pratt et al., 2002).

Protein turnover and homeostasis have also taken on particular significance in the study of mitochondrial biology due to the profound implications of mitochondrial quality control and mitochondrial dynamics in multiple human diseases. Cardiac mitochondria exhibit a remarkable degree of dynamism in that they continually adjust their functions, morphology, and molecular compositions according to the changing energetic demands of the heart. At the molecular level, this dynamism involves the simultaneous shifting of the dynamic equilibria of biomolecules towards new cellular states according to cellular needs. Meanwhile, increased ROS is a hallmark in the diseased heart that can exacerbate protein damage, misfolding, aggregation, malfunction, and creates severe protein quality control stress (Giordano, 2005). As the respiratory chain within the mitochondrion is a major source of ROS production in the heart (Balaban et al., 2005), the proximity of mitochondrial proteins to reactive oxygen species renders them highly susceptible to protein damage. Maintenance of mitochondrial quality and integrity involves coordinated turnover of compromised components to preserve cellular functions, and the accumulation of damaged proteins in mitochondria is thought to contribute to disease pathology (Hammerling and Gustafsson, 2014; Rosca and Hoppel, 2010). Disrupted protein homeostasis could further elevate cellular ROS and protein degradation stress, such as by producing further ROS through signaling and respiratory uncoupling (Divald et al., 2010; Gomes et al., 2006; Papa et al., 2007), leading to a vicious cycle of protein damage and dysfunctions, suggesting protein degradation insufficiency could act directly as a molecular trigger

5

of pathogenesis and presents an interesting aspect through which to measure the effect of gene and environment factors. Hence, understanding how mitochondrial proteins are maintained in homeostasis is an essential step towards a more complete understanding in the role of the proteome in cardiac disease mechanisms.
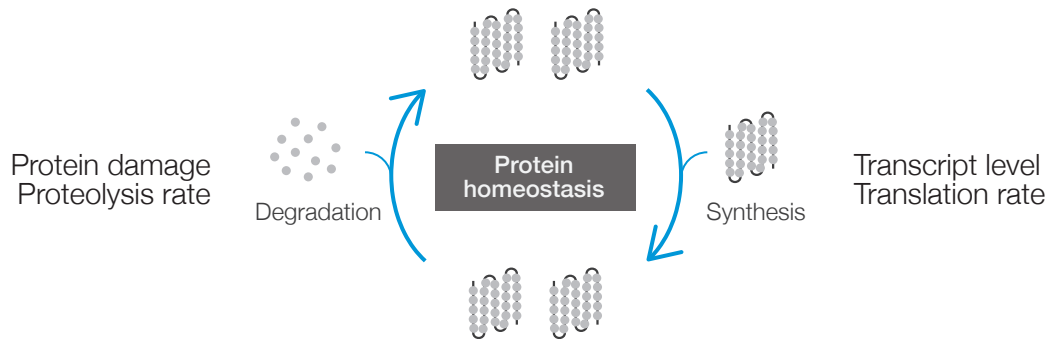
FIGURE 1.2   Protein turnover cycle

FIGURE 1.2 is a graphical representation of the protein turnover cycle. Proteins are not static entities, but instead exist in a dynamic equilibrium of continual synthesis and degradation, which orchestrate the steady-state abundance of the protein species. The dynamic equilibrium of a protein can be controlled by either the rate of protein synthesis or protein degradation, or both. Protein synthesis and degradation are regulated by different cellular processes, e.g., how much of a protein is being synthesized is regulated in part by the abundance of the cognate transcripts and other post-transcriptional regulations, whereas how much of a protein is degraded is influenced by the existence of protein damage and the activity of protein degradation machineries.

In the normal heart, protein translation and import constantly supplement the mitochondrial proteome, while mitochondrial fusion and fission may redistribute proteins, and proteolysis, returns protein-bound amino acid into the free pool. Mitochondrial proteins may be degraded via multiple means. Autophagy can engulf and degrade entire organelles, whereas the turnover

rates of individual proteins can be individually regulated by intra-mitochondrial proteases, proteasomes, by export via mitochondrial-derived vesicles, or by escaping autophagy via fusing with the ER (Saita et al., 2013). Under normal circumstances, the totality of continual synthesis and degradation of proteins make up the protein turnover cycle and maintain protein abundance in homeostasis (Claydon and Beynon, 2012; Hinkson and Elias, 2011).
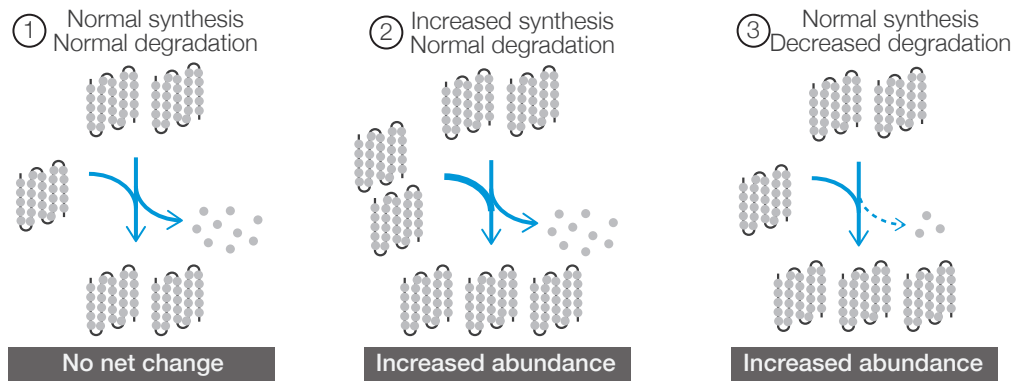
FIGURE 1.3   Degeneracy of the protein turnover cycle

FIGURE 1.3 illustrates protein abundance as an emergent property of the permutation of synthesis and degradation. Because either the rate of protein synthesis or degradation must deviate from normal values in order for the protein pool size to adjust to a new level, any permutation of proteome states leaves behind a kinetic signature, in the form of the fraction of newly synthesized proteins in the protein pool (Claydon and Beynon, 2012; Doherty and Beynon, 2006). This kinetic signature can be measured through the incorporation of isotopes into protein over time, and can be exploited to identify unexpected disease proteins and their pathological implications independently of abundance measurements. On the other hand, a particular profile of static abundance may be the outcome of multiple combinations of synthesis and degradation scenario. As the final protein level is degenerate with regard to the quantitative permutation of synthesis rate or degradation rate, measurement of steady-state abundance alone can conflate disparate scenarios – a protein of increased abundance could

7

owe it to increased synthesis or decreased degradation, whereas a protein with shortened half-life may show no abundance change. These kinetic scenarios represent different biological realities, e.g., a protein under irreversible ROS damage will require increased turnover in order to stay above the threshold of functionality. For example, a drastic increase or decrease in protein half-life in early hypertrophy is highly indicative of a switch in functional manifestation, and thus reveals a probable causal relationship to pathological remodeling. On the other hand, prolonged half-life amid elevated ROS in the decompensated heart is symptomatic of protein damage or impaired proteolysis – because the previously existing protein pool accumulates. Yet alternatively, cellular signaling may accelerate synthesis and degradation to shorten protein half-life without altering protein abundance, which has been hypothesized to facilitate the generation of spatial gradients (Varshavsky, 2011). These and other pathologic scenarios present only in the time dimension, and are obscured from steady-state protein abundance measurements. Taken together, protein dynamics is significant because it provides an important view into the remodeling heart that cannot be otherwise obtained.

To understand how normal mitochondrial proteins are maintained in homeostasis to preserve cardiac metabolic and energetic functions and how the process fails in the diseased heart, at minimum one must know how, which and how fast mitochondrial proteins are being replaced, i.e., their turnover rates. The synthesis rate of a protein is conventionally explored via microarray studies, which implicitly utilize the abundance of mRNA transcripts as surrogates (albeit very poor ones) for protein abundance. On the other hand, the degradation and turnover of proteins are relatively underexplored due to technical difficulty in its measurement, but their importance is paramount, as impairments can drive pathologic remodeling in the heart (Chen et al., 2005; Wang and Robbins, 2006) , and abnormal protein accumulation within cardiac cells is a general observation in many etiologies of human heart failure (Day, 2013; Nojiri et al., 2006).

The measurement of protein turnover dynamics has long captured the attention of biomedical research. Early experiments were pioneered by Rudolf Schoenheimer and David Rittenberg at Columbia University in New York (Kennedy, 2001; Kresge et al., 2005; Shemin and Bentley, 2001; Simoni et al., 2002), who became interested to study cellular metabolism at a time when the physical sciences were beginning to be applied to biology (Kohler Jr., 1977). In 1939 Schoenheimer used isotope labeling to establish that proteins in the body, and thus life itself, are in a dynamic state of interactions with the environment even in the absence of obvious growth (Schoenheimer et al., 1939). These tenets ran contrary to popular beliefs of the day, which posited that organic molecules acquired through diet were solely combusted for fuel, but they soon gained wide acceptance and are now held as self-evident. Studies from the 1950's onward coincided with biochemists' interest in measuring the flux and dynamics of biochemical pathways, and led to the elucidation of the bulk protein synthesis rate in the human body (Rittenberg and San Pietro, 1953) and of the rate constant of turnover (k) of specific cellular compartments, and a few easily isolatable proteins (Glass and Doyle, 1972).

In cardiac biology, Murray Rabinowitz at the University of Chicago was one of the early investigators to realize the important metabolic links between mitochondrial dynamics and cardiac hypertrophy (Getz, 2013; Rabinowitz and Zak, 1975). Rabinowitz was in particular interested in the synthesis and turnover of mitochondrial proteins, and in 1973 he was the first to compare protein turnover in heart failure when he made the discovery that following aortic banding, rat heart cytochrome c abundance increased on the first day then subsequently decreased, whereas its degradation decreased consistently throughout (as measured by pulse-chase of a radioactive heme precursor tracer, δ-amino-laevulinate) (Albin et al., 1973; Rabinowitz, 1973). He concluded that the decreased destruction of cytochrome c was responsible for its early increase in hypertrophy, and that a dissociation in the myofibrillar and mitochondrial growth responses ultimately led to energetic decline. In subsequent years, his group also compared the turnover rates of myofibrillar proteins, and from the data made critical inference on the

assembly sequences of the myofibril subunits (Zak et al., 1977). Meanwhile, a number of contemporary studies began to establish the turnover of mitochondrial sub-compartments (outer membrane vs. inner membrane) or few individual mitochondrial proteins such as cytochrome c (Brunner and Neupert, 1968; Glass and Doyle, 1972; Lipsky and Pedersen, 1981). Two observations from these early studies were of interest. First, they showcased the idea that protein turnover is a regulated cellular parameter that responds to disease stimuli. Second, it was realized that individual mitochondrial compartments and proteins exhibit different turnover rates. These studies however largely lacked the technical prowess to discern individual protein turnover on a large scale, and the ponderous experimental design and large variability of the results both hindered the studies of disease models until modern proteomics techniques became available.

In the intervening years, the focus of research has remained fixated on the turnover of structural proteins that are easy to isolate, in particular the highly abundant myofibril proteins (Martin, 1981; Simpson et al., 1996), with a general consensual concept arising from these studies to suggest that differential regulations of synthesis and degradation often accompany stress, hypertrophy, or remodeling in myocytes both in vitro and in vivo. In another study, the gap junction protein connexin 43 was found to have very short half-life in perfused hearts (Beardslee et al., 1998), which may have implications on rapid dynamic remodeling of gap junctions in the heart. Increased synthesis of collagen III and degradation of collagen I are found to be markers of hypertrophy and fibrosis in hypertrophic cardiomyopathy patients (Lombardi et al., 2003).

More recent studies on mitochondrial turnover shifted focus to whole-organelle level turnover and dynamics, which describes the regulatory behaviors at the organizational level of the entire mitochondria. A number of studies of mitochondrial protein turnover in models of caloric restrictions and aging simply assume mitochondria as turning over as a unit (Miller et al., 2012;

Miwa et al., 2008), from which conclusions were drawn without considerations of the individual turnover rates of proteins.

Since abundance measurements conflate disparate kinetic scenarios, investigations restricted to steady-state measurements have limited power to discern particular time-dimensional features of disease progression. This limitation has perhaps led to failures in identifying causal events during hypertrophic responses, and the obscuration of potential drug target proteins for which abundance is not the correlating parameter in its disease association. Assessing global protein turnover kinetics in the remodeling heart therefore provides new opportunities to understand cardiac remodeling and identify molecular changes that presage functional debilitations. The aforementioned knowledge gap obstructs our understanding of heart diseases, and arises in part because the dynamic process of cardiac remodeling is inadequately captured by our static conceptualization of the cardiac proteome: current techniques produce fragmented snapshots of protein expression in the myocardium that are difficult to interpret in the context of other key cellular processes.

Several terms are used interchangeably in the following chapters to describe various aspects of the synthesis and degradation of proteins. The protein turnover rate constant (k) is the preferred parameter to describe how fast the protein pool is replaced and is irreplaceable in certain technical description. On many occasions the logarithm of this parameter is presented ($\log_{10} k$), because k typically spans several orders of magnitude in a proteome. Some find half-life more intuitive to visualize, but its use in graphs is minimized because the reciprocal transformation from k to half-life has the tendency of distorting sample distributions. In general, I use the term protein temporal dynamics where it concerns the biological state of the cell, protein kinetics where it reflects the behavior of isotope incorporation and speed of protein pool replacement, and protein turnover where it denotes the combined synthesis and degradation of protein pools.

A number of techniques exist for measuring protein turnover or stability in cultured cells in vitro, including simple immunobiological approaches to measure the decrease in protein abundance following synthesis inhibition by cyclohexamide, or the use of the decay of protein fluorescence signals from fluorescent protein timers (Khmelinskii et al., 2012; Yen et al., 2008), or stable isotope labeling by amino acids in cell culture (SILAC) (Andersen et al., 2005; Pratt et al., 2002; Schwanhausser et al., 2011). However, the proteome dynamics of exponentially dividing cells in vitro does not recapitulate the full range of physiological regulations that occur in multicellular organisms. More importantly, proteins in cultured cells may turn over both via degradation or dilution into daughter cells, which confounds the inference of physiological turnover rates. Cyclohexamide experiments in vitro typically report protein half-life of hours as the minimum turnover rates of proteins are set by the doubling time of cells, as opposed to the half-life in the range of days to weeks measured from mammalian systems in vivo.

To measure the physiological protein turnover rates in mammals, i.e., the rate at which existing proteins are replaced in vivo, it follows that a method is needed to differentiate a newly synthesized protein from pre-existing proteins after the protein sample is drawn from the living organisms. This is typically accomplished using isotope analogs of protein precursors that are ingested by the animal through food or water supply. Since 1935, a number of isotope-labeling methods have been developed to label cellular proteins and trace their bulk turnover. Deuterium was among the earliest of isotope labels to be used as an analog for biomolecules, when Schoenheimer explored protein metabolism using molecules tagged with the stable isotopes ^{2}H and ^{15}N. However, the laborious analytical methods to discern ^{2}H content of amino acids from protein hydrolysate using combustion and interferometry, or ^{15}N with the Kjeldahl method, led to the gradual displacement of stable isotopes by the advent of radioisotopes in the 1940s. The specific activity of radioisotope analogs such as ^{3}H or ^{14}C- labeled amino acids were easy to detect from various samples directly using scintillation counters. Since late 1990s, however,

there has been a marked return to the use of stable isotopes driven by advances in biological mass spectrometry techniques with which stable isotopes can be separated by mass. Labeling with stable isotopes followed by mass spectrometry thus enables one to differentiate between pre-existing and newly-synthesized proteins via the relative isotope abundance of the target proteins, and thus to trace the continual turnover of the proteome in living systems (Beynon and Pratt, 2005). The advantages of using stable isotope and mass spectrometry methods over radioisotope scintillation counters include the ability to detect and differentiate multiple labeled proteins at once, and detecting a peptide with multiple numbers of label, which allows easy turnover determination through precursor-product relationship.

A challenge of deducing turnover in higher organism is that the isotopes need to be effectively delivered into the organisms via injection or oral intake. Under most scenarios the protein precursor cannot be enriched fully due to dilution with existing precursors, compartmentalization, and potential toxicity. Converting the amount of label present to the fraction of new proteins was a challenging problem where true precursor enrichment is difficult to ascertain, since it creates an uncertainty in how the labeled molecule appears in terms of relative isotope abundance (analogous to specific activity in radioisotope labeling), which creates an uncertainty in deducing the fraction of newly-synthesized products.

A general solution to deduce protein synthesis from isotope labels is to assume a combinatorial probability model, which dictates that a biological polymer of more than one monomer will exhibit statistical distribution of labels following polynomial expansion of the proportion of labeled and unlabeled precursors. This was exploited in 1986 by Kalderon and colleagues to measure glycogen synthesis from ^{13}C-labeled glucose (Kalderon et al., 1986), and by Marc Hellerstein and colleagues in 1991, who put forth an application of the technique to mass spectrometry data, named Mass Isotopomer Distribution Analysis (MIDA) as reviewed in (Hellerstein and Neese, 1999). Mass isotopomers are isomers containing different isotopes that

become resolved by a mass analyzer. Thus as a protein is synthesized by a population of monomers (protein precursor) containing a fixed proportion of heavy isotopes, the resulting statistical distribution of protein isotopomers containing zero, one, two, or more heavier isotopes will follow a mathematically deducible polynomial distributions determined by three MIDA parameters: n, the number of monomer units in the protein, p, the proportion of labels in the precursor, and f, the fraction of newly made polymers (whose amounts of labels are diluted by the presence of unlabeled polymers in the pool). The feasibility of this method for calculating protein turnover was first demonstrated on serum albumin in $[^2H_3]$-leucine labeled rats (Papageorgopoulos et al., 1999).

Variations of the combinatorial probability model have since been widely used to analyze MS data in protein turnover experiments. For instance, Robert Beynon at the University of Liverpool devised a method to identify the precursor relative isotope abundance in single amino acid labels (e.g., $[^2H_8]$-valine) that uses the combinatorial probability model to compare the isotopomer distributions of peptide clusters containing two instances of the labeled amino acid, in order to deduce the true precursor enrichment, which is then used to calculate the fraction of newly synthesized peptides for all peptides containing at least one instance of the labeled amino acid. In combination with high-throughput proteomics techniques, this led to the first large-scale measurements of individual protein half-life in vivo in higher organisms (Doherty et al., 2005).
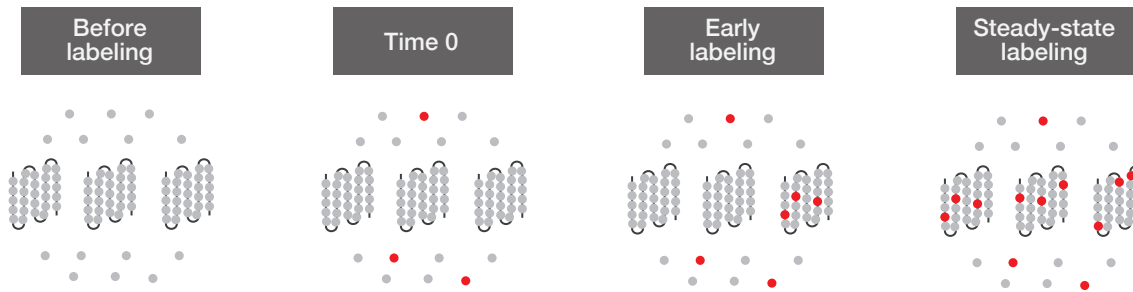
FIGURE 1.4   Principle of stable isotope labeling

FIGURE 1.4 illustrates the principle of isotope labeling to deduce protein turnover, whether by stable isotopes or radioisotopes. In metabolic labeling experiments, the protein precursors are subjected to an artificial enrichment of the stable isotope through the intake or injection. The isotope tags serve as homologs to protein precursors that allow the isotope label to be incorporated into newly synthesized proteins, which can then be differentiated by physical methods that differentiate isotopes. The protein synthesis process could therefore be detected by mass spectrometry and described as the gradual incorporation of isotopes into the protein population. With additional cycles of protein synthesis and degradation, the cellular proteins increase in the labeled fraction until the overall isotope enrichment reaches equilibrium with the relative isotope abundance of precursors in the organism. Since a protein is a polymer of protein precursors, the amount of label incorporated into a newly made protein follows a combinatorial probability model. The accumulation rate of isotopes into cellular proteins over time is then used to estimate the turnover of the protein pool in a systematic manner from the perspective of the substrate pool.

Since 2005, multiple studies have demonstrated the use of stable isotope labeling and mass spectrometry to study protein turnover (Busch et al., 2006; Claydon et al., 2012; Kasumov et al., 2011; Price et al., 2010, 2012a; De Riva et al., 2010), making use of several types of stable isotope tags that were introduced into cellular proteins, either in the form of essential amino

acids in diet or the precursors of non-essential amino acids. Currently, three major types of isotope labels are available for large-scale studies:

(i) Stable isotope-labeling of essential amino acids: A popular method is the introduction of amino acids labeled with heavy isotopes (^{13}C, ^2H, or ^{15}N), such as $[^2H_3]$-leucine, into the animal, either through injection or through an enriched synthetic diet. A major advantage of labeled amino acids is the simplicity in data analysis workflow. Since these heavy amino acids have fixed number of labeled atom centers, no intermediates in the amount of labeling per newly synthesized protein exist. Secondly, precursors with +6 or +8 Da (e.g., $[^{13}C_6]$-arginine $[^2H_8]$-valine) are available, which are sufficiently different in mass from the light variant such that isotope clusters do not overlap. A drawback is the requirement for a synthetic diet supplemented with the labeled amino acid, which may unbalance metabolism or spur protein synthesis. Analytical complications may also arise through the loss of α-carbon deuteron through enzymatic transamination, which can result in the experimental mass shift of labeled peptides being less than expected (Beynon and Pratt, 2005). Labeled amino acids were first exploited by Beynon and colleagues to deduce the first proteome-wide protein turnover study in higher organisms (Doherty et al., 2005), and have been employed in a number of studies in diverse animals including mouse (Claydon et al., 2012; Hsieh et al., 2012), chicken (Doherty et al., 2005), zebrafish (Westman-Brinkmalm et al., 2011), and carp (Doherty et al., 2012). Using $[^2H_3]$-leucine, the Rabinovitch group recently determined the in vivo turnover rates of ~400 mouse liver and heart mitochondrial proteins (Hsieh et al., 2012).

(ii) Metabolic ^{15}N or ^{13}C labeling via diet: Alternatively, proteins can be enriched via metabolic precursors. Enrichment of ^{15}N atoms in an animal has been achieved for SILAC mice (SILAM), a method for creating >95% ^{15}N-labeled mice to be used as internal standards for protein quantitation, where the isotopically pure foodstuff for animals labels all mouse amino acids metabolically. Similar to dynamic SILAC experiments, a non-saturated labeling curve can be used to

measure protein turnover in live animals. This method is compatible with proteome-wide turnover inquiry (Price et al., 2010; Zhang et al., 2011), and has recently been demonstrated for the measurement of turnover rates of over 1,700 proteins in the brain, liver, and blood of mice fed with the ^{15}N-enriched Spirulina algae for up to 32 days (Price et al., 2010). Besides ^{15}N, metabolic ^{13}C labeling has also been demonstrated by enriching mouse diets with ^{13}C-labeled glucose, which is metabolized into amino acid precursors (Vogt et al., 2005).

One potential drawback of metabolic ^{15}N or ^{13}C labeling is the complex isotope patterns generated as compared to SILAC approaches. As the mice gradually acquire excess heavy atoms, the labeled peptide peaks will shift gradually both in relative abundance of heavy isotopes (due to protein turnover) and in the amount of horizontal mass shifts exhibited by the heavy labeled peptides (due to increasing numbers of heavy atoms in newly synthesized proteins), creating a complex pattern of isotopic shifts (Guan et al., 2011; Lyon et al., 2014) which demands more complicated data processing to deconvolute the spectra into component peptide ions with different numbers of incorporated heavy atoms.

(iii) Metabolic labeling with heavy water: ^{2}H$_2$O is gaining in popularity as a protein label for animal studies (Lam et al., 2014; Price et al., 2012a; Rosca et al., 2008). One primary advantage of ^{2}H$_2$O is that can be straightforwardly introduced into the animal by free drinking in the drinking water supply, which avoids potential physiological impacts of dietary modifications or amino acid infusion. The ingested ^{2}H$_2$O molecules quickly equilibrate with body water, and thus precursor isotope enrichment can be measured accurately from any biofluid. Deuterium atoms from body water is conferred to the carbon-hydrogen bonds of free non-essential amino acids during their enzymatic biosynthesis (Busch et al., 2006), which has been measured to complete within 30 minutes (Kasumov et al., 2011). Unlike in deuterium exchange experiments, the enzymatically labeled C-H bonds are chemically stable and do not back-exchange during sample processing. Essential amino acids are labeled by transaminases. ^{2}H$_2$O labeling does

not create separate peptide clusters (which essentially doubles the complexity of the prote-omics sample), and thus is very amenable to large-scale analysis. Recently ^2H_2O labeling has been demonstrated for proteome-wide turnover measurements in multiple organisms including the mouse, rat, and human (Kasumov et al., 2013; Price et al., 2012a, 2012b; Shekar et al., 2014). A potential drawback is that deuterated peptides elute slightly earlier in liquid chroma-tography, which may introduce errors in peak area quantification. Secondly, the number of ^2H accessible labeling sites may be uncertain in some systems with different biochemistry of amino acid utilization than mammals.
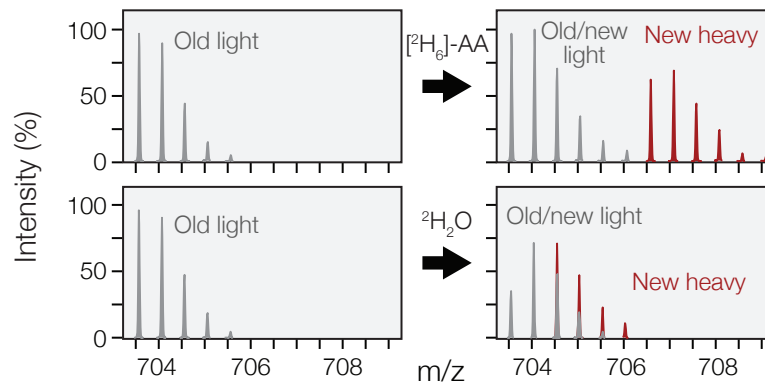
FIGURE 1.5   Appearance of heavy isotopes in mass spectra

FIGURE 1.5 shows the use of two kinds of isotope tracers for measuring protein turnover in animals. The optimal isotope label for an experiment depends greatly on the available analyti-cal instrumentation and computational workflows. Economy, physiological impacts, and ease of data analysis are all valid concerns that may influence decision as has been reviewed else-where (Claydon and Beynon, 2012). In the above stable labeling experiments, the incorporated labels may be detected by mass spectrometry. Most modern proteomics platforms have been successfully employed for protein turnover studies including Orbitrap (Shekar et al., 2014), Q-ToF (Price et al., 2012a), MALDI-ToF (Doherty et al., 2005), and LTQ-FT (Hsieh et al., 2012; Price et al., 2010) instruments. On the top graph is shown the changes in peptide isotope

patterns following enrichment with a stable isotope labeled amino acid (e.g., $[^2H_6]$-leucine). The spectrum on the left shows the old (pre-existing) proteins, which only contain light isotopes. The introduction of heavy isotopes and the production of new proteins create a new isotope envelope that contains a fixed amount of heavy isotopes. Some new proteins also contain light isotopes due to incomplete relative isotope abundance (RIA). On the bottom is shown the changes in peptide isotope patterns following enrichment with ^2H_2O. Instead of forming a new isotope envelope, new proteins shift the isotopic distribution of the pre-existing envelope.

In the following studies, we have chosen to develop analytical methods for ^2H_2O labeling, which acts as a heavy-labeled precursor to cellular amino acids. ^2H_2O quickly confers ^2H atoms from cellular water to the carbon-hydrogen bonds of free nonessential amino acids during their enzymatic biosynthesis (Busch et al., 2006) within 30 minutes (Kasumov et al., 2011). Unlike labile N-H or O-H bonds, these C-H bonds are stable and the incorporated ^2H atoms in non-essential amino acids do not back-exchange during sample processing. Additionally, H in the α-carbon of essential amino acids is reversibly accessible to ^2H by transamination. The ^2H-labeled amino acids are integrated into newly synthesized protein via amino acyl-tRNAs, and with each cycle of turnover, into proteins until their ^2H content reaches steady-state equilibrium with surrounding ^2H_2O. The rate of protein turnover is determined by tracking the time evolution of mass isotopomer distributions.
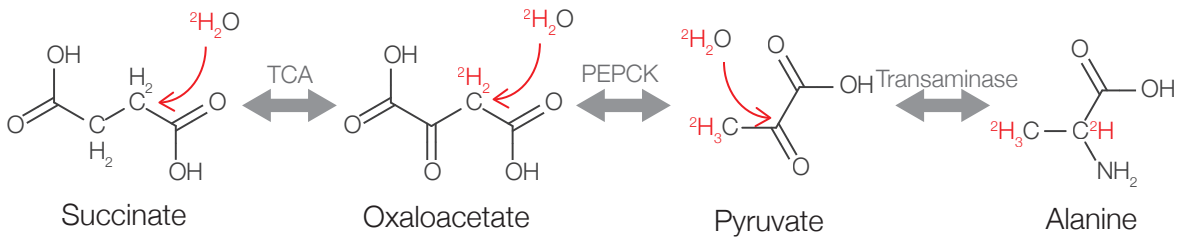
FIGURE 1.6   Mechanism of amino acid labeling by ^2H_2O

FIGURE 1.6 shows one mechanism whereby orally ingested ^2H_2O can confer ^2H atoms onto protein precursors. As ^2H_2O permeates body water, the ^2H atoms (red) are quickly transferred from the surrounding onto the carbon-hydrogen bonds of nonessential amino acids during their biosynthesis (Busch et al., 2006), which are in turn integrated into newly synthesized proteins. Alanine, for example, is labeled via its synthesis from the tricarboxylic acid (TCA) cycle intermediates succinate and oxaloacetate, and contains a characteristic four ^2H-accessible labeling sites per amino acid.

Several properties of ^2H_2O make it in our opinion an attractive choice as a tracer for protein turnover measurements in vivo. Compared to ^{15}N-labeled essential amino acids, ^2H_2O has the technical advantage that precursor enrichment can be measured by GC-MS, either in place of or in conjunction with MIDA analysis. Since water is assumed to equilibrate with all body and cellular compartments, ^2H_2O content can be measured in accessible tissues or fluids such as plasma or saliva to reflect the enrichment level in the tissue of interest, which also avoids compartmentalization effects where the dietary precursor does not equilibrate with the precursor pool in the target tissue. As an isotope analog of water, ^2H_2O is generally considered bioorthogonal at low concentration, and does not have physiological impacts that may result from dietary modifications. Lastly, labeling with low percentages of ^2H_2O also doesn't create a new isotope clusters, which introduces minimal additional complexity to the mass spectra.
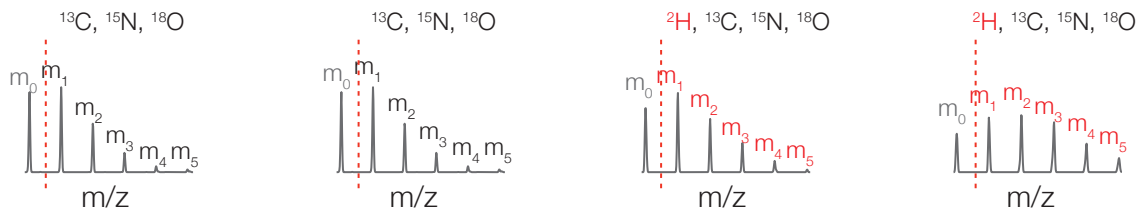
FIGURE 1.7   Peptide isotopomer shift

FIGURE 1.7 illustrates the expected shifts in protein/peptide mass spectra during a metabolic ^2H_2O labeling experiment. As the protein precursors are subjected to an artificial enrichment of stable isotopes, the protein synthesis process is detected by mass spectrometry as the gradual incorporation of isotopes into the protein population. With additional cycles of protein synthesis and degradation, the cellular proteins increase in the labeled fraction until the overall isotope enrichment reaches equilibrium with respect to the relative isotope abundance of precursors in the organism. The stable isotopes being used can be introduced to proteins through the essential amino acids in diet (e.g., ^{15}N-labeled amino acids (Price et al., 2010)) or the precursors of nonessential amino acids, such as in ^2H labeling through ^2H_2O.

Thus, ^2H_2O has the potential for measuring protein turnover on a very large scale. Currently, the major hindrances to the adoption of ^2H_2O to trace cellular protein turnover are data analytical constraints. One challenge arises because the mass shift induced by low percentages of ^2H_2O overlaps with the natural isotope envelope. Secondly, the number of labeling site on peptides which dictates the resulting statistical distribution of isotopomers after enrichment is not completely known. A number of prior works have shown the feasibility of using ^2H_2O labeling to measure protein half-life, as reviewed previously, but in general, analytical methods for large scale ^2H_2O labeling data remain under-developed.

To illustrate the analytical challenges of interpreting ^2H_2O labeling data, we consider here the general workflow of kinetic curve-fitting. For the sake of simple calculation, protein turnover is often assumed to be a first-order kinetic process, which comprises of protein synthesis as a

zero-order process, i.e., independent of protein concentration, and protein degradation as a first-order process, i.e., proportional to protein concentration to the first power. In a labeling experiment, ^{2}H accumulation in protein causes the addition of mass to the parental peptide ion peaks, thus shifting the relative abundance of the natural isotope distribution of peptide due to ^{13}C, ^{15}N, ^{18}O, ad ^{35}S atoms. As the heavy labels are integrated into the newly synthesized proteins, with eventual turnover of the protein pool the amount of label will reach steady-state equilibrium with the surrounding free amino acids. The mass isotopomer distribution changes at multiple time points of measurements can be effectively resolved by high-resolution mass spectrometry. Hence by experimentally deducing the isotope abundance of a given peptide in its approach to the steady state, and by assuming its rise-to-plateau follows first-order kinetics, the rate constant of protein turnover may be deduced. The challenge, then, is that the steady-state enrichment level of each peptide differs by the number of ^{2}H label sites, which is determined by the peptide amino acid sequence, and thus must be measured or modeled individually. Moreover, proteins with relatively slow turnover takes a long time to reach plateau enrichment, which would either significantly lengthen the labeling time or significantly reduce the portion of the proteome that can be covered.

An effective ^{2}H$_2$O data analysis strategy must therefore deduce the relative isotope abundance of peptide ions at different time points and calculating the turnover rates based on a kinetic model that corresponds to the protein turnover process. In practice, after the fraction of newly synthesized proteins are experimentally measured at one or more time points, the data must be extracted and arranged into a time series, then fitted to a kinetic model. Multiple models have been proposed. In most cases, simple rise-to-pleateau kinetics is assumed, and the isotope distribution before labeling and at steady-state can be calculated to determine the remaining unknown, i.e., the protein turnover rate (Claydon and Beynon, 2012). In a variation to this method, Kasumov and colleagues have used the quasi-linear region of the first-order kinetic curve to calculate k for long-half-life proteins (Li et al., 2012). More complex multi-

compartment modeling has also been formulated that are thought to more closely resemble true turnover kinetics (Guan et al., 2012).

Several current limitations accompany the existing ^2H_2O studies that constrain their overall proteome coverage and thus utility in uncovering biological insights. Although the isotope labeled spectra can be manually analyzed to yield turnover rates, high-throughput studies demand the aid of computational software automation. Many existing tools can integrate the peak areas of native or isotope-labeled peptide ions for protein quantification process. Since these software applications must add together the relative peak areas of each isotope, they may be co-opted for protein turnover studies when a custom kinetic model is supplied to handle the integration data. Hence there is a general need for automated software solutions to deconvolute complex isotope relationship.

In order to enable the analysis stable isotope labeling data on a truly proteome scale, my colleagues and I developed a computation-assisted method based on multivariate optimization where all relevant parameters describing the kinetic curve can be found using multi-parameter fitting.

The method can be divided into two functional modules. (i) The first module automates the quantification of peptide ion mass isotopomer distribution of mass spectra. To quantify the fractional abundance of each isotopomer within the isotope envelope, the software creates the extracted ion chromatogram for each identified peptide ion. To determine whether a peak is a genuine peptide signal or noise, the software using a mass isolation window (set to $\pm$ 100 ppm), retention time information from protein identification file, as well as peak-width ($\geq$ 0.1 minute at half-height) and intensity (median of all signals multiplied by a user-definable factor) filters. Note that the utilized mass window filter is considerably wider than the delta mass identification because in order to capture all the signal intensity of the ion it has to cover the whole

peak along the m/z axis, and not only the apex of the peak to deduce median mass. Once the true isotopomer peak is selected from the chromatogram, integrating for the area under the peak gives the abundance of the isotopomer ion. The abundances of mass isotopomers thus determined are normalized by the total abundances in the particular peptide. The end result is that the acquired mass spectrum sets are automatically deconvoluted into the isotopomer distributions for every identified peptide, which constitutes the quantity that will determine the fractional stable isotope enrichment.

(ii) The second module takes the data series and determine the rate constants of protein turnover. We implemented a computationally efficient solution to aggregate all isotopomer distributions and perform multivariate fitting to model the isotopomer distribution to first-order kinetics by fitting all three parameters of the kinetic equation: initial abundance ($A_i(0)$), steady-state abundance ($A_i(\infty)$), and the rate constant of synthetic replacement (k). The final computation of protein turnover aggregates the isotope incorporation data from multiple mass isotopomers of each peptide, and from all eligible peptides from each protein, and does a second fitting to solve for least squares. Uncertainty in the rate constant is determined by propagating the variance of the dataset in respect to the predicted model to the rate constant using a first-order series expansion. This simplified method takes advantage of the ability to acquire multiple sampling time point and the power of computerized multivariate fitting, and has the advantage that it does not require overt use of the MIDA parameters (p, n, f) and can deduce the parameter of interest (k) in a single step. The ability to forego asymptotic enrichment, at least in principle, also facilitates the analysis of long-lifetime proteins without prolonged labeling, which also gives greater agility to detect temporal changes in turnover rate in disease.

$$A_0(t) = I_0(t) / \sum I_i(t)$$

$A_0(0) = 0.52$

$A_0(12) = 0.32$

$A_0(90) = 0.18$
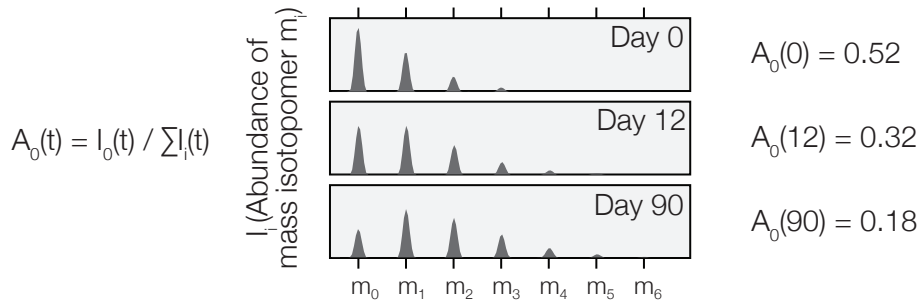
FIGURE 1.8   Peptide isotopomer patterns following labeling

FIGURE 1.8 illustrates the concept of parameterizing the fractional abundance of mass isoto-pomers in a peptide isotopomer cluster as a means to calculate protein turnover. At any given time point during the enrichment process, t, the normalized peak area for the first mass isoto-pomer (I_0), $A_0(t)$, can be determined by dividing the peak area of the first mass isotopomer (m_0), $I_0(t)$, over the summation of peak areas from all mass isotopomers (m_0, m_1, m_2, m_3...) in the same spectrum ($I_0(t)$, $I_1(t)$, $I_2(t)$, $I_3(t)$...). $A_0(t)$ reflects the mass isotopomer shift and decreases in value over time in a manner that follows the turnover of the peptide. This is illustrated in the figure at day 0, day 12, and day 90 of a labeling experiment for an example tryptic peptide LVESLPQEIK, $[M + 2H]^{2+}$ = 578.33 m/z, from the mitochondrial 39S ribosomal protein L12 (MRPL12). Prior to the start of ^2H_2O labeling (day 0), the first mass isotopomer (m_0) represented the most intense peak ($A_0(0)$ = 0.52) in the envelope. At 12 days of labeling, the peak intensity of m_0 became comparable to that of m_1, and one new feature corresponding to m_4 was ob-served ($A_0(12)$ = 0.32). After 90 days of labeling, m_0 became the third most intense mass isoto-pomer and the high-mass isotopomer peak m_5 became observable ($A_0(90)$ = 0.18).
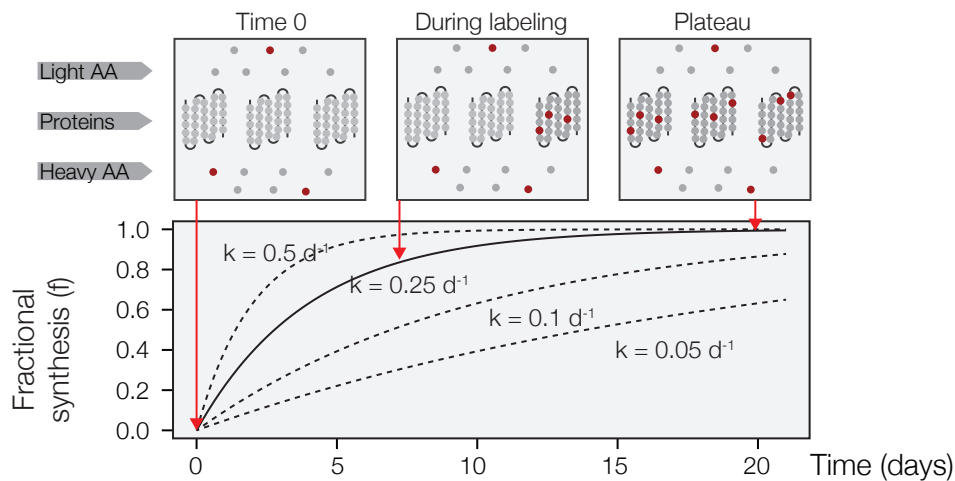
FIGURE 1.9   Fitting of data to kinetic curve

Figure 1.9 illustrates the general concept of kinetic curve fitting. Because we assume protein turnover to follow simple first-order kinetics, the introduction of ^{2}H results in an anticipated evolution of $A_0(t)$ in an enrichment experiment that can be modeled using a first-order exponential decay equation, where the rate constant of the equation, k, is the rate at which proteins are newly synthesized to replace the existing protein pool in the cell. If we assume equilibrium in the protein pool, k also equates the rate at which proteins are degraded and thus the protein turnover rate. Computer optimization algorithms can therefore be employed that iterate different values of k in order to minimize the residual between the equation and empirical data points, and determine the most probable value of k, as shown in the four different curves on the graph that correspond to k = 0.5, 0.25, 0.1, and 0.05 d^{-1} respectively.

$$A_0(t) = A_0(0) + [A_0(\infty) - A_0(0)] \cdot (1 - e^{-kt})$$

$$f(t) = 1 - e^{-kt}$$

Fractional abundance of m_0 [$A_0(t)$]

$A_0(0)$

$A_0(0) = 0.52$
$A_0(\infty) = 0.18$
$k = 0.066$
$R^2 = 0.99$

$A_0(\infty)$

Time (days)

Fractional synthesis [$f(t)$]

$k = 0.065$ d^{-1}
$t_{1/2} = 10.6$ d
$R^2 = 0.98$

Time (days)
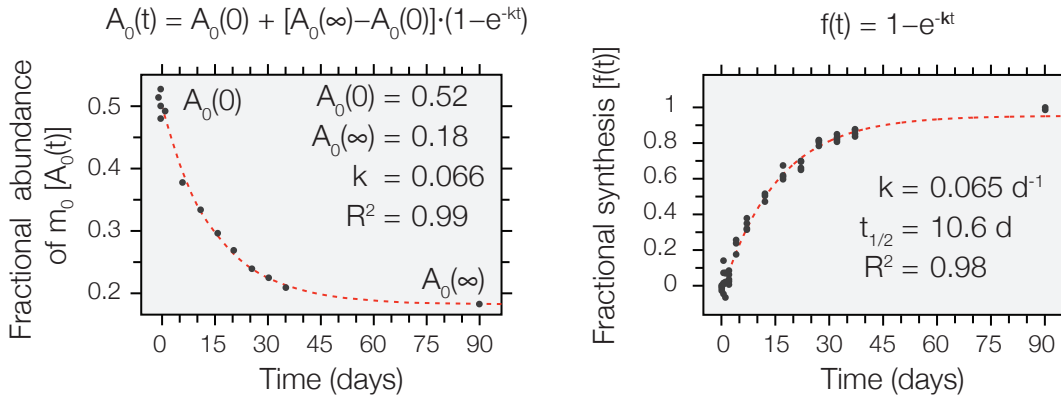
FIGURE 1.10   Deduction of turnover rate from peptide isotopomers

FIGURE 1.10 visualizes the experimental deduction of the turnover rate constant via three-parameter fitting for the example tryptic peptide above. On the left, the fractional abundance values of the first isotopomer ($A_0(t)$ at each experimental time points as they were measured by the mass spectrometer were plotted (points). We then performed a three-parameter non-linear fitting on the time-series data via the Nelder-Mead simplex method (Nelder and Mead, 1965). The fractional abundance at the initiation of labeling (t = 0), $A_0(0)$; at full plateau enrichment, $A_0(\infty)$; and the protein turnover rate constant, k; are defined from the time-series data of each mass isotopomer by the best-fitted first-order kinetics equation (red dashed line). Note that this time-series and the derived values occur at the peptide level and originates from only a single peptide from the protein. We next rescaled this equation into a simple first-order kinetics equation on the right by transforming the time-series data of fractional abundance of m_0 into the fractional synthesis of the protein, f(t), which represents the proportion of total proteins that are newly synthesized through turnover since labeling begins. This rearrangement essentially describes how far the measured data point is between $A_0(0)$ and $A_0(\infty)$ alone the exponential decay equation.

The rearranged equation is agnostic to the values of $A_0(0)$ and $A_0(t)$, which are dependent upon the peptide sequence since the fraction of unlabeled peptides depends upon the atom compo-

sition and deuterium-accessible labeling sites of the peptide. This allows the rescaled peptide-level fractional synthesis data from multiple peptides corresponding to the same proteins to be combined, and a second, protein-level, optimization process to deduce the best-fitted value of k to all data points. This improves statistics and error estimation. Note that in addition to $A_0(t)$, in principle other isotopomers ($A_1(t)$ and $A_2(t)$ (the time evolution of the fractional abundance of the m2 isotopomer) also follows the exponential rise/decay curve and in principle can also be used for turnover rate calculation ($A_1(t)$ are not always suitable because its time evolution may be isosbestic for some peptides. These are automatically filtered because they don't fit to curve). However, in reality and in our experimental setup, m_2 time-series with which the kinetic curve can be confidently quantified and modeled are rare presumably because of the lower relative abundance of m_2. Thus m_2 based quantification will not be considered in details in the results to follow.

A major advantage of the three-parameter fitting method is that the calculation of turnover rate constant no longer depends overtly on the precursor-product relationship, and the MIDA parameters p (precursor level) and n (isotope numbers on the peptides). Thus can be used in a large variety of systems including in organisms where the amino acid metabolism and thus deuterium accessible sites are not known (e.g., drosophila, or cultured cells). It also lends itself to simple implementation of computer optimization programs.

Several filtering heuristics are in place to ensure data quality and limit error propagation. For example, peptide time-series are excluded from the calculation of the protein fractional synthesis data if it shows a curve-fitting R^2 value of less than an arbitrary 0.7 at the peptide level, as well as peptide series containing data from less than 5 out of 13 time points. The chosen R^2 value of 0.7 was adjudged empirically to balance high accuracy and precision in the measurement of the kinetic data. As A_0 and A_∞ are theoretically bound between 0 and 1, only experimental values between -0.1 and 1.1, were included in fractional synthesis calculation. For m_0

at some early time points, experimentally measured $A_0(t)$ could be larger than the computationally determined $A_0(0)$ due to measurement error and/or fitting error, which may lead to an erroneous negative fractional synthesis value. We found that filtering the data by their peptide-level R^2 value at this point was effective in excluding the majority of unquantifiable isotopomers and greatly improved the accuracy of turnover rate calculation without significantly impacting the number of analyzed proteins. In future work, a weighting algorithm may also be considered that allows peptides with good fitting (higher R^2 values) or high intensity (thus presumably more accurate isotope fractional abundant measurements) to contribute more to the overall evidence for turnover rate calculation.

To reiterate, we have applied here two distinct criteria for peptide selections. The first concerns with the protein identification, where Scaffold was used to validate and filter peptides based on their confidence levels. The second addresses the precision of curve fitting by using a R^2 threshold filter. Mass isotopomers that met these two criteria were accepted for protein turnover rate calculations.

Distributions of turnover rates in heart and liver mitochondria

To validate the analytical approach described above and measure how fast proteins turn over in cardiac mitochondria in vivo, we labeled male Hsd:ICR (CD-1) mice (9 – 12 weeks old) with ^2H_2O over a period of 90 days. Outbred Hsd:ICR (CD-1) mice were chosen for their vigor and robustness to surgical procedures, as well as their direct comparability to many Hsd:ICR murine cardiac proteomics and physiology data collected in the Ping laboratory in the past decade.
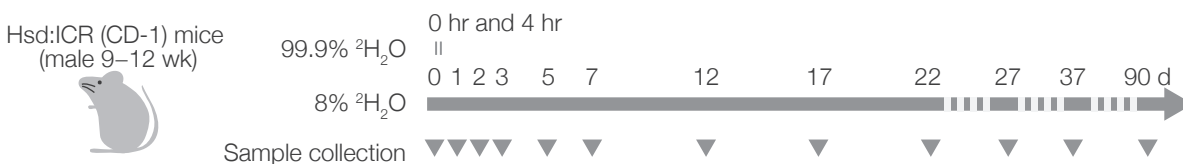
FIGURE 1.11 ^2H_2O labeling scheme to study protein turnover

FIGURE 1.11 presents an overview of the ^2H_2O labeling scheme in mice. Label enrichment was initiated on outbred Hsd:ICR (CD-1) mice (male, 9 – 12 weeks of age) through two successive 500-µL intraperitoneal injections of saline dissolved in 99.9% ^2H_2O spaced 4 hours apart (t = 0 hr and 4 hr). The animals were then given access to 8% ^2H_2O in their drinking water supply ad libitum. We euthanized three biological replicate groups of animals, each containing three mice at 13 time points: 0, 0.5, 1, 2, 4, 7, 12, 17, 22, 27, 32, 37, and 90 days after the first ^2H_2O injection (t = 0 hr). From each time point, we harvested heart, liver, and blood samples from the euthanized animals. All three biological replicate groups of animals from each time point were used to determine the extent of ^2H labeling in body water using gas chromatography-mass spectrometry (GC-MS). One of the three groups of mice at each time point was selected in random to be processed for the determination of protein turnover rates with high-resolution mass-spectrometry. During the labeling period, we maintained a record of the overall body weight of the animals, and observed no significant change due to ^2H_2O labeling (~40 g) (data not shown).
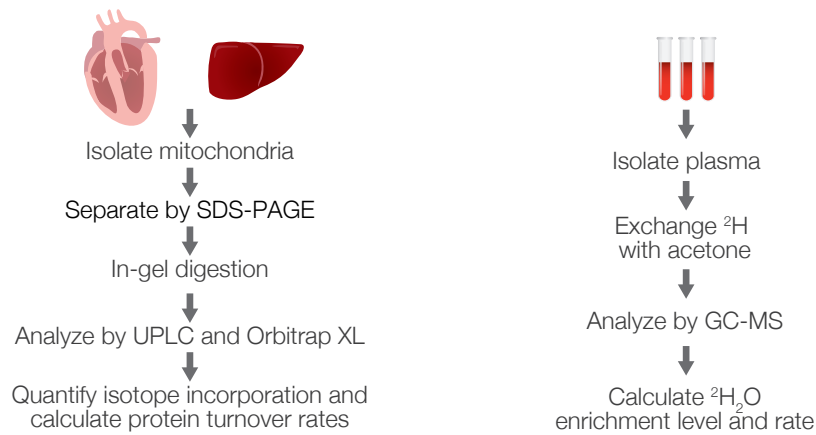
FIGURE 1.12 Sample processing scheme (heart and liver mitochondria)

FIGURE 1.12 illustrates the experimental workflow for processing the collected mouse samples. On the left, the steps for processing cardiac and hepatic samples for protein analysis is shown. At each of 13 time points, we removed the heart and the liver from the animals and extracted mitochondrial proteins. The proteins were separated by SDS-PAGE, digested, then analyzed by mass spectrometry to measure turnover rates. On the right is shown the workflow for measuring the ^2H_2O enrichment level in the plasma water pool of the animals. To quantify the level of precursor (^2H) incorporation during labeling, the serum of the animals was sampled at all experimental time points for GC-MS analysis following acetone exchange. In the experiments in this chapter, the ^2H_2O enrichment levels were not used for turnover rate calculation but only to determine that label enrichment was fast and steady as expected. Kidney mitochondrial preparations were procured in according manner (not depicted).

Because water molecules quickly equilibrate throughout the body and permeate all cellular compartments, the body water content from the serum serves as a close surrogate for the level of ^2H incorporation in all cell and organ types. Results from the GC-MS experiments confirm that the protocol achieved a fast enrichment of ^2H_2O in the body water. The GC-MS measurements quantify the molar ratio of $^2H/^1H$ in the serum water pool, which reached 3.5% within 12 hours following the priming injections. Throughout the labeling period, ad libitum feeding of 8%

^2H_2O maintained at a steady-state labeling level at ~4.3% in body water in Hsd:ICR mice. The speed and stability of ^2H incorporation provide the basis for calculating the fractional synthesis of proteins while assuming constant precursor enrichment. The lower actual body water enrichment than the enrichment provided in drinking water is likely attributable to other sources of water including metabolic water.

We next measured the isotope abundance of peptides in the samples by high-resolution mass spectrometry on an Orbitrap XL instrument, and calculated fractional protein synthesis at each time point based on the three-parameter fitting method. The intensities of mass isotopomers were quantified by an in-house computational software program as described above. The software integrates the areas under peak in the extracted ion chromatograms, then normalized by the intensity of all isotopomers in a particular peptide ion to determine its relative abundance. For every mass isotopomer with quantification data at five or more time points, the relative abundances from all time points were fitted to an exponential decay equation as described above. For a particular mass isotopomer, multiple normalized peak intensities may exist due to detection of the identical peptides in multiple gel bands, different charge states, or the oxidized forms. Identical isotopomers from multiple gel bands were combined, but otherwise were fitted independently. The fitting was extrapolated to yield the normalized abundance of the mass isotopomer at its initial, $A_0(0)$, and steady, $A_0(\infty)$, states.
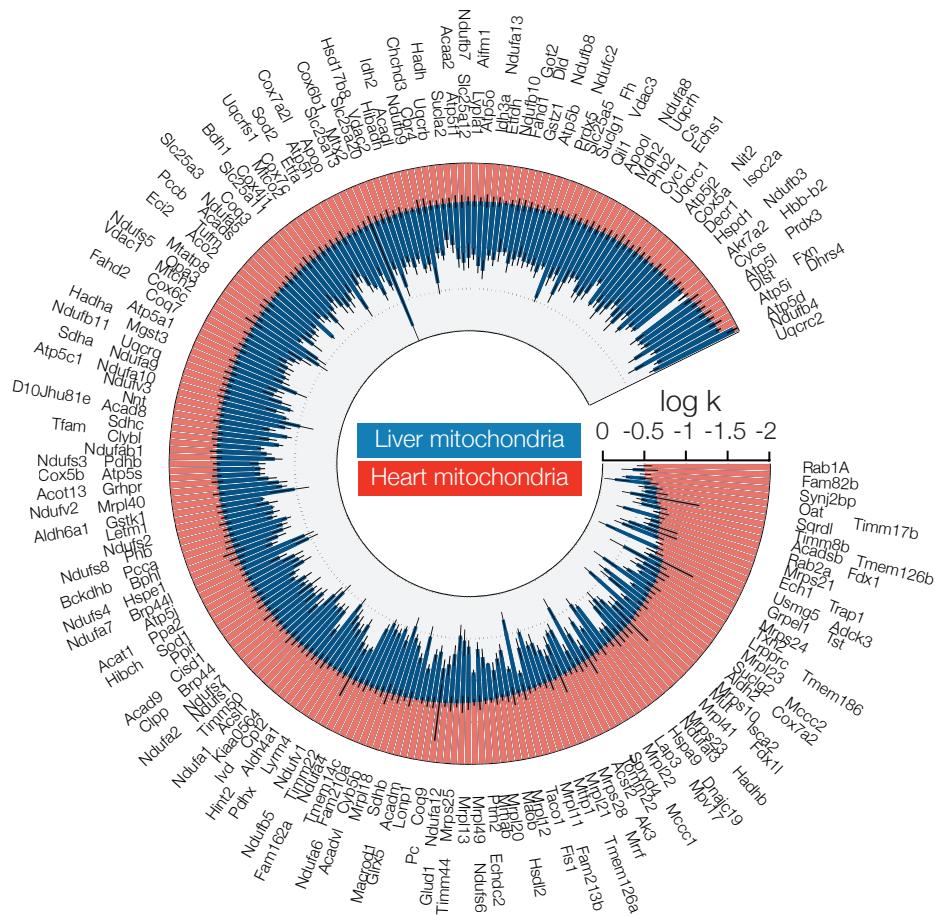
FIGURE 1.13   Turnover rates of cardiac and hepatic mitochondrial proteins

FIGURE 1.13 is a circularized bar chart that demonstrates the turnover rates of 242 mitochondrial proteins commonly quantified in the heart and in the liver. The circumferential axis lists each protein species whereas the radial axis denotes their respective protein turnover rate constant in cardiac mitochondria (red) and hepatic mitochondria (blue). A large difference in turnover rates was apparent between identical mitochondrial proteins in the two tissue types. The median turnover rate was more than three times higher in the liver than in the heart (0.150 d^{-1} and 0.045 d^{-1}, respectively). With the exception of only three proteins (MRPS24, RAB1A, and SYNJ2BP), all 242 commonly analyzed proteins shown here exhibited slower turnover (i.e. longer half-life) in cardiac mitochondria than in the hepatic mitochondria. This observation corroborates other recent studies on the in-vivo turnover rates of proteins amongst multiple mouse tissues (Claydon et al., 2012; Price et al., 2010) and illustrates that the large range of

turnover rates are determined at least in part by physiological regulation and cellular environments rather than protein sequence.
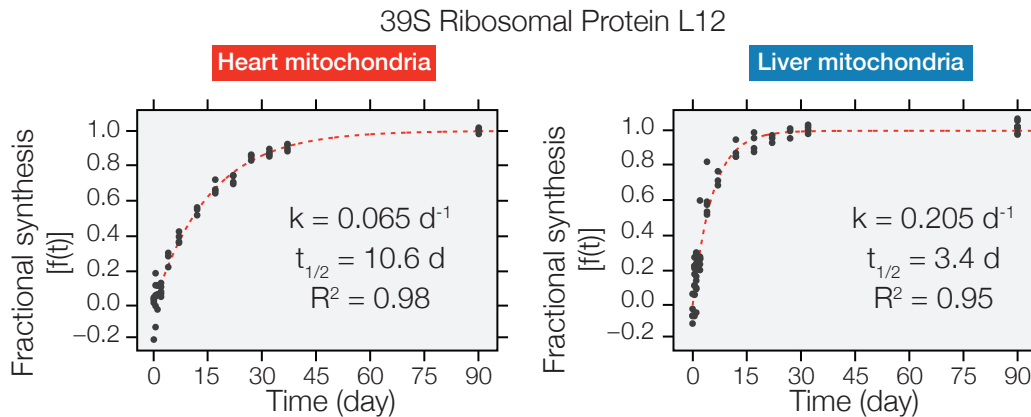
FIGURE 1.14   Tissue-specific differences in turnover rates

FIGURE 1.14 further demonstrates the significant differences in turnover rates that an identical mitochondrial protein in the heart and the liver may exhibit. The graph reflects the time-evolution of the fractional of the MRPL12 protein, which was encountered in previous figures. The fractional synthesis data from individual time-points were fitted to an exponential rise curve to yield the protein turnover rate, k. In the heart, MRPL12 turns over at the rate of 0.065 $\pm$ 0.004 d^{-1} (R^2 = 0.98) corresponding to a half-life of 10.7 days; whereas in the liver, the MRPL12 protein pool turns over almost three times faster, at 0.205 $\pm$ 0.028 d^{-1} (R^2 = 0.95), corresponding to a half-life of 3.4 days.

In total, this pilot study captured the turnover of 314 proteins in cardiac mitochondria and 386 in hepatic mitochondria, among which 458 are distinct. Mitochondrial proteins in all major functional categories including respiratory chain, tricarboxylic acid cycle, and fatty acid oxidation proteins are represented in the dataset. Detailed kinetic data and the fractional synthesis

curves of all quantified proteins are listed in Supplemental Table S1 and Supplemental Figures S1 and S2 of our publication (Kim et al., 2012) and are not reproduced herein.

Some considerations in evaluating the performance of the presented method and workflow are given here. Firstly, the sensitivity and dynamic range of concentration of the quantification method could be informally inferred by two means. We evaluated the range of protein concentration for which we could deduce confident turnover rates by comparing our results to the label-free quantification data from very exhaustive experimentation my colleagues and I previously conducted on cardiac and hepatic mitochondria (Lotz et al., 2013). The data suggest that protein turnover rates were determined for proteins spanning approximately five orders of magnitude in concentration, ranging from ATP5B at the highest abundance (NSAF: 3.9×10^{-2}) to RAB2A (NSAF: 5.6×10^{-7}). This limit is likely due to mass spectrometry method in detecting quantifiable peaks.

The minimal dynamic range of turnover rates in the system was estimated similarly by considering the distribution of values that were confidently quantified. In the dataset presented above, reliably quantified turnover rates spanned approximately three orders of magnitude, in line with a few recent ^2H_2O labeling studies in the literature. The observed turnover rates ranged from hours (ATP1A1, half-life: 19.3 hours) to months (UQCRC2; half-life: 61.8 days), but the majority of proteins fall within a more narrow range (interquartile range: 10.9 to 22.7 days). The range of sampling time points possibly places a limit to the dynamic range of turnover rates that can be measured. For instance, the earliest sampling time point must occur before the protein with the fastest turnover approaches its enrichment plateau where there is no information on turnover rate; likewise, a slow-turnover protein must accumulate sufficient label by the last sampling time points for its turnover to be measured. Some proteins that were shown to have extremely long half-life may have thus escaped detection. These proteins may be enumerated and classi-

fied by examining manually the raw data from amongst the proteins that were not fitted confidently to the kinetic curves.

The precision of measurements can be estimated by considering the errors of fitting at the protein level, based on the assumptions that: (i) individual peptides from an identical protein ought to have identical in-vivo turnover rates; and that (ii) each individual peptide isotope cluster represents an independent observation of the true turnover rate of the protein. We used the Monte Carlo method to estimate the fitting error, which, briefly, deduces the average and standard deviations of the measurements of A(t), then generate random values over 10,000 iterations according to the distribution and feed the values into the multivariate optimization algorithm to calculate the average and standard deviations of the values of k. Under our method and filtering criteria, the median of the relative standard error values of k at the protein level was 14.9% in the heart, and 21.1% in the liver. These values suggest that in general, our method deduced very similar turnover rates from independent peptides of the same proteins and thus were reasonably precise. In actuality, as in protein quantification experiments, some systematic bias in turnover rates exist from different peptide sequences: certain peptide sequences consistently and reproducibly reported lower turnover rates than other peptides matched to the same proteins. This may be due to unknown splicing isoforms and/or post-translational modifications. Since dk/dA is solvable in the kinetic equation, one could additionally estimate the standard errors of the calculated values of k directly through the non-linear curve fitting equation. In general, the Monte Carlo method appears to be more conservative and returns slightly larger standard errors. A comparison of the two methods was included in our publication (Kim et al., 2012) and is not reproduced here. Note that these analyses additionally assumes that in kinetic fitting each group of animals from each time point constitutes an individual biological replicate, since these individual animals contribute independently to the final fitted curve. In actuality, some time points will fall near the inflection point of the kinetic curve and contribute more to the error, i.e., dk/dA is a function of time. When the whole set of

labeling experiments were repeated over the course of a year, a root-mean-square error of ~25% was observed and is not discussed in details here.

The accuracy of quantification is more challenging to estimate in light of the paucity of existing gold standards of in vivo protein turnover against which one could judge the data. The use of standard curves has been demonstrated in early MIDA experiments and in more recent ^2H_2O investigations, where normal and deuterated peptides were synthesized and mixed in specific ratios, which is informative on the performance of the mass spectrometer in measuring protein isotope fractional abundance but not how well the determined turnover rates matches the true rates inside the cell. Alternatively, the measurement accuracy of mass isotopomer could be estimated using MIDA, by comparing the empirically measured unenriched mass isotopomer abundance at day 0 to theoretical values based on the natural occurrence of heavier isotopes.
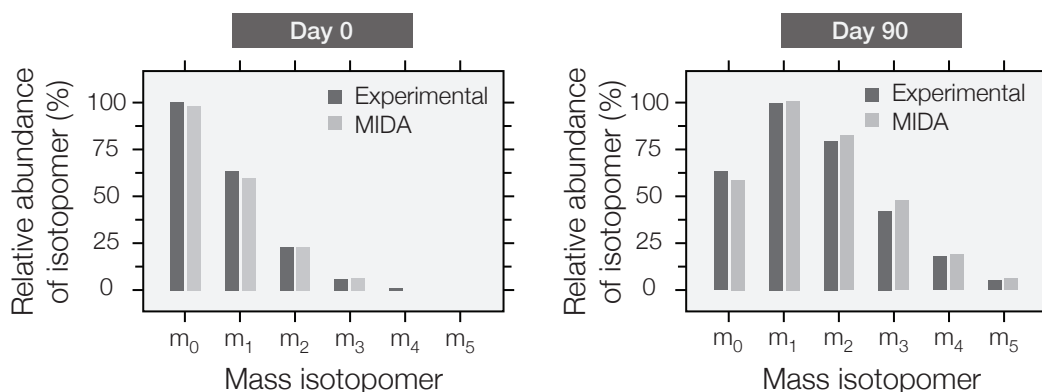
FIGURE 1.15   Eperimental and theoretical isotopomer abundances

FIGURE 1.15 compares the experimental values of mass isotopomer distributions to theoretical values acquired via MIDA before ^2H_2O enrichment (left) and after 90 days of ^2H_2O enrichment (right) for the MRPL12 peptide LVESLPQEIK. On the left, the MIDA theoretical distribution is based on the combinatorial probability of isotopes due to the natural occurrence of heavier isotopes (e.g., ^2H ^{13}C, ^{15}N, ^{18}O). It can be seen that the experimental distribution closely match-

es that of the theoretical values, indicating that in the experiments spectra with accurate relative isotope abundance were acquired. On the right, a slight discrepancy is seen between the experimental value of the peptide and the MIDA value, which may be due to incomplete plateau of the peptide at day 90, or an underestimation for the MIDA parameters p (precursor enrichment) and n (labeling sites). The present example notwithstanding, over the whole dataset such discrepancy is minor and uncommon, as will be seen in the next chapter where a new analytical method that makes overt uses of the MIDA parameter to derive the peptide enrichment plateau isotope abundance is shown to correctly predict labeling plateau.

Another method to indirectly gauge the accuracy of the dataset is to compare with common proteins in other labeling methods (^2H_2O or other labels). In addition, some values on the turnover of particular human plasma proteins, such as serum albumin and serotransferrin, have been validated over larger ranges of subjects and in different methods in single-protein investigations, to which we will attempt to compare our human data in Chapter IV.

Here we discuss the potential sources of errors in the derived turnover rate values. Unlike protein expression quantification, metabolic labeling experiments are not affected by incomplete sample recovery, but several other sources of error are possible, ranging from variations of the experimental sources to more systematic errors, which will be considered below.

Firstly, several experimental parameters contribute to measurement errors, which can include the accuracy of peak area measurement by the Orbitrap instrument, the effective separation of overlapping chromatographic peaks, isobaric peptides with overlapping isotope clusters, spectral accuracy, and absolute peak intensities. Prior to data acquisition, we anticipated these experimental errors and attempted to keep them under control by heuristically altering several experimental parameters and filtering criteria. Upon several trials and errors, it was decided that a resolution of 7,000 on the Orbitral XL instrument afforded the most favorable trade-off in

protein identification performance and acquiring accurate mass isotope fractional abundance, where the majority of unenriched mass isotope clusters fall within 5% of the theoretical value, as discussed above. It was also discovered that the use a stringency filter of $R^2 = 0.7$ or above at the peptide fitting level minimized the propagation of many poorly fitted peptide data to the protein level. These filtering parameters are by necessity empirical and arbitrary, but are internally consistent and do not make use of population averages to remove outliers.

Secondly, some systematic errors exist in the assumptions of the analytical model that cannot be easily removed. For example, the data analysis method assumes first-order kinetics of protein turnover in the curve-fitting model. Under scenarios where the molecular turnover kinetic is forced to conform to this assumption, a larger error will result. It is possible that the first-order kinetics model used in the study does not hold true to a homogenous degree for all experimental errors, and all proteins whose turnover deviates from first-order kinetics would be fitted with larger errors.

Thirdly, the protein turnover measurements are contingent upon accurate protein identification. In scenarios where peptide identification is incorrect, larger inter-peptide variations for a protein will result. To minimize this source of error, we adopted conservative protein identification criteria in protein database search parameters (see Materials and Methods) and further required a peptide isotopomer to be explicitly identified and independently quantified in about half of all time points in order to remove false positives. Peptide sequences that are common to more than one protein would for obvious reasons not yield reliable kinetics information for either, and thus we filtered out all redundant peptides from known protein isoforms and used a highly curated database to ensure only unique peptides were selected for individual proteins and to avoid ambiguity in protein kinetics information. However, some peptides shared by undocumented or undiscovered protein isoforms or splice isoforms are likely to remain and consequently constitute a potential source of error.

Fourthly, questions have been raised by reviewers on whether partially synthesized or hydro-lyzed proteins may interfere with the normalization of peptide values, in other words, whether a partial peptide fragment will contain more label than pre-existing proteins and skew the aver-age label incorporation of the overall population. In theory, one can imagine a scenario where protein synthesis success rate is very low in the heart, such that the N-terminal half of the protein is repeatedly synthesized and aborted independently of the intact protein pool, contrib-uting to higher isotope incorporation rates of some peptides. However, these defective ribo-some products should not come into contact with the general protein pool and adulterate the overall isotope ratio, since they are readily degraded by the proteasomes (Schubert et al., 2000). Thus far, we have not observed evidence to suggest this to skew turnover measure-ments, as the turnover rates of multiple peptides belonging to the same proteins are largely in agreement with one another, especially when fitting criteria are sufficiently stringent, suggest-ing most of the intra-protein variability comes from low-quality data that do not conform well to standard kinetic behaviors. Secondly, turnover measurements from LC-fractionated samples (see Chapter II) are indistinguishable from the gel-fractionated samples presented in this Chap-ter, which would remove partial peptide fragments <10 to 15 kDa in size.

Lastly, precursor recycling is a major intrinsic problem for most isotope tracer strategies, in-cluding ^2H_2O labeled amino acids. Briefly, if non-labeled amino acids that result from the pro-teolysis of a pre-existing unlabeled protein are returned into the protein precursor pool and become incorporated into a newly synthesized protein, the new protein will not contain the signature of isotope labels and will be indistinguishable from a pre-existing protein. This may effectively cause the measurable turnover rate to be an underestimation of the true turnover rate inside the cell. Admittedly, this may be particularly problematic for cross-systems compar-ison such as the one conducted in this chapter, as the liver and the heart may recycle proteo-lytic amino acids to different extents and gives a false impression of systematic differences in

protein turnover behaviors – this is known to be true at least where the urea cycle is concerned. There are relatively few studies in the literature that address this problem directly, most of which attempting to deduce the "true" turnover rates by using a protein precursor that is presumably non-reutilizable. These specialized labels include sodium bicarbonate, which labels arginine and is presumably non-reutilizable as synthesis into protein competes with breakdown from the urea cycle precursor (Miwa et al., 2008)), whereas other non-reusable precursors can be used for particular proteins, e.g., delta-aminolevulinic acid for heme-containing proteins. But in general, these strategies are not suitable for measuring the turnover of the mitochondrial proteome in the heart, which does not exhibit urea acid cycle activities.

Notwithstanding the above, several observations suggest that the experimental errors from protein precursor reutilization are limited in magnitude. First of all, as discussed earlier how fast amino acids become labeled can be measured using GC-MS and will inform on how dynamically the amino acid pool equilibrates with ^2H_2O. If the incorporation of labels into amino acids is fast, the proteolytic amino acids would be easily labeled or replaced by other metabolic intermediates. On the other hand, if label incorporation is slow, the proteolytic amino acids will have plenty of chance to be incorporated into nascent proteins without labels. Thus far, evidence exists for the quick equilibration of cellular amino acids with ingested ^2H_2O, which reaches plateau isotope incorporation within 30 minutes (Kasumov et al., 2011), a timeframe that is significantly shorter than the protein half-life being measured (in the order of days). This includes essential amino acid such as leucine, which gains labeling through enzymatic transamination reactions. This is in contrast with the introduction of pre-labeled amino acids via diet, which are not expected to back-exchange significantly with unlabeled amino acids. In the current workflow, both the transamination process and the empirical labeling sites of amino acids used in kinetic curve-fitting (e.g., leucine has 0.6 effective label-able hydrogen atom (Commerford et al., 1983)) help rectify the dilution of labels from reutilization. A background level of reutilization of proteolytic amino acids continually exists in the cell, but such dilution

can be empirically accounted for in the effective labeling sites, the result of which may be verified considering that the theoretical plateau values of isotope incorporation, deduced from the labeling site counts, match closely to experimentally acquired distributions.

One method to distinguish the effect of label reutilization of ^2H_2O strategies is to compare the turnover rates acquired from deuterium oxide heavy water ^2H_2O and oxygen-18 heavy water ($H_2^{18}O$). $H_2^{18}O$ labeling is similar to ^2H_2O in labeling and bioavailability, but instead labels the carboxyl oxygen atoms of a free amino acid (Rachdaoui et al., 2009). Although it labels fewer numbers of atoms than ^2H_2O and so may be less amenable to large-scale analysis due to the lower label incorporation, it has the advantage of incorporating labeled oxygen atoms into amino acids upon their cleavage from a peptide bond or a t-RNA (Borek et al., 1958). Thus $H_2^{18}O$ labeling is believed to be able to circumvent the potentially confounding recycling of amino acids, since any proteolytic amino acids will subsequently become labeled with ^{18}O when they are re-incorporated into peptide bonds. Steven Previs and colleagues have compared the protein turnover rates of albumin in mice using both ^2H_2O and $H_2^{18}O$ methods, and found that although $H_2^{18}O$ appeared to yield higher measured turnover, the difference between the two methods did not reach statistical significance (0.325 ± 0.046 d^{-1} for ^2H_2O labeling versus 0.301 ± 0.039 d^{-1} for $H^2_{18}O$ labeling, $P = 0.17$).

Hence from the above, there is no conclusive evidence to suggest that the measured protein half-life in our experiment would misrepresent in-vivo protein turnover behavior. Furthermore, it may be argued that the differences in protein turnover behaviors among proteins (z scores from the mean) are more important than the absolute values of turnover rates for the objective of inferring candidate protein targets from the statistical extremes. This consideration is common practice in protein expression experiments, where the relative abundance change (up- or down- regulation) is more often the direct experimental goal than the absolute abundance of the protein species (number of copies of protein molecules per cell).

Heterogeneity and regulations of protein turnover

Our data therefore suggest that protein half-life is a highly varied cellular parameter and corre-lates to some biological parameters including subcellular localization. Proteome quality control may be of particular regulatory significance in the mitochondria as their bi-genomic nature is thought to introduce additional phenotypic buffering in protein interaction stoichiometry (Rep and Grivell, 1996). The multifarious tissue-specific adaptations of mitochondria, in spite of the dearth of known master mitochondrial transcriptional regulators, also suggest hitherto un-known modulatory mechanisms of mitochondrial physiology. We therefore considered whether further biological insights may be discerned from the variations of turnover rates at the basal level. It is thought that the precise regulation of protein turnover rates is under severe selective pressure due to the cost of protein production and replacement. A substantial amount (up to ~25%) of dietary energy intake is used to replace degraded muscle protein during normal metabolic turnover (Hawkins, 1991; Millward et al., 1975; Young et al., 1975). Any sustainable deceleration of protein turnover would therefore result in a substantial increase in the efficiency of energy usage and opportunities to divert extra energy to processes critical for survival and reproduction. This selective pressure may have led to the observation that many housekeeping proteins such as serum albumin have high abundance but slow turnover. The high copy num-bers of these housekeeping proteins means that a large amount of energy is nevertheless used to maintain the bulk protein flux, and the required energy expenditure would become prohibi-tive if their turnover were also fast.

On the other hand, more recently it has been theorized that a high turnover rate may be select-ed for amongst proteins that need to quickly alter in abundance in response to some physio-logical stimuli (Varshavsky, 2011). High turnover is energetically expensive. A protein with a

short half-life and fast continual synthesis and degradation would be able to alter in abundance if either synthesis or degradation changes. At least in bacterial systems, it has been observed that stress response elements such as heat shock proteins have preferentially faster turnover (Maier et al., 2011).

As stated above, turnover rates of mitochondrial proteins varied greatly between the heart and the liver. To further explore the biology of mitochondrial protein turnover in different tissues, we compared data from Hsd:ICR mouse heart, liver, and kidney in an independent dataset using identical methods as above (raw data not shown).
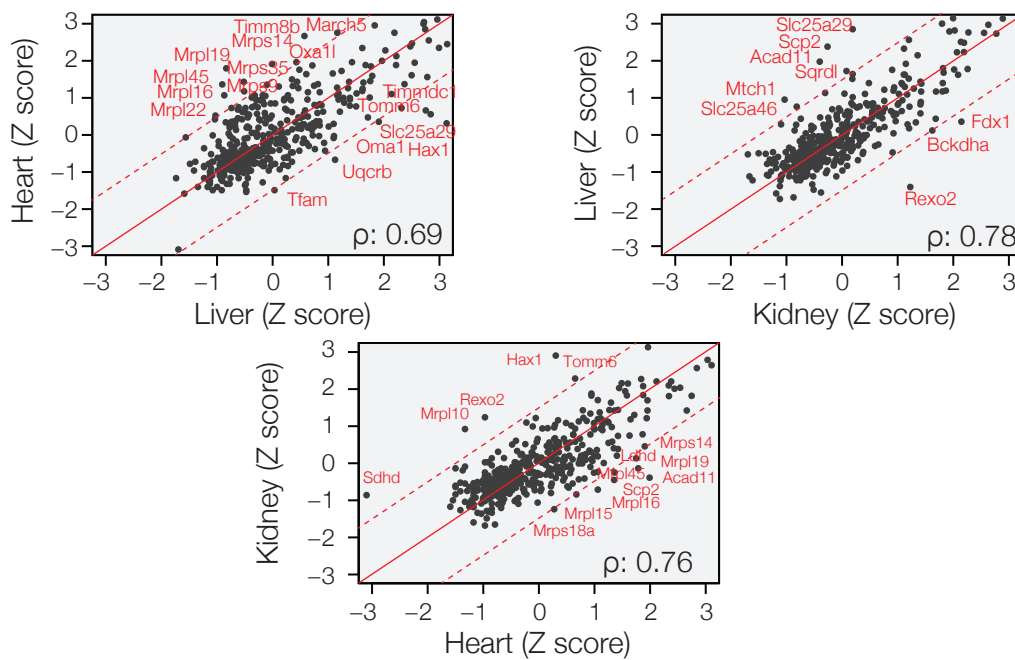
FIGURE 1.16   Heterogeneity of protein turnover in different tissues

FIGURE 1.16 shows three scatter plots of standardized log turnover rates (Z score) of 444 mitochondrial proteins commonly measured in the mouse heart, liver, and kidney. Comparisons between (Left) heart and liver; (Right) liver and kidney; and (Bottom) kidney and heart are shown in each plot. Each data point represents a distinct protein, and the red diagonal line

represents 1:1 in standardized turnover rates in two respective tissues, whereas the dashed lines represent the positions of data points where a protein turns over markedly faster or slower in one tissue (+1.5 or -1.5 standard deviations from the mean); ρ: Spearman's correlation coefficient. Proteins that differ markedly in turnover rates between two tissues are labeled, for example, a number of mitochondrial ribosome subunits can be seen that turn over relatively faster in the heart than in the liver or the kidney. The highlight of mitochondrial ribosomal subunits is of interest because they are thought to control respiratory rate and the stoichiometric balance between mitochondrial and nuclear encoded proteins (Houtkooper et al., 2013); their differential turnover between the heart and liver may therefore have implications on the proteome organization of the cardiac mitochondrion with its predominantly energetics functions vs. that of liver mitochondria. In contrast, several inner membrane carriers, e.g., for arginine and amino acid precursors (SLC25A29) turn over relatively faster in the liver (in Z score) than would be expected in the kidney. Taken together, these differences suggest that the heterogeneity in the regulation of protein turnover rates may reflect differences in mitochondrial biology in different tissues or system.

The diverse turnover rates of individual mitochondrial proteins hint at regulatory mechanisms that are capable of fine-tuning individual protein turnover rates. Hence, we considered whether there are discernible rules that may govern the turnover rates of particular proteins from the dataset, and conversely whether one may discern biological significance from the measured distribution of protein turnover rates. There have been numerous literature reports that link the in vivo half-life of mammalian proteins to simple biophysical parameters. Hence we decided to first analyze whether the acquired turnover rate distributions replicate these findings, i.e., whether a protein may have longer half-life simply because it is more hydrophobic, as opposed to its being under more complex physiological regulations.
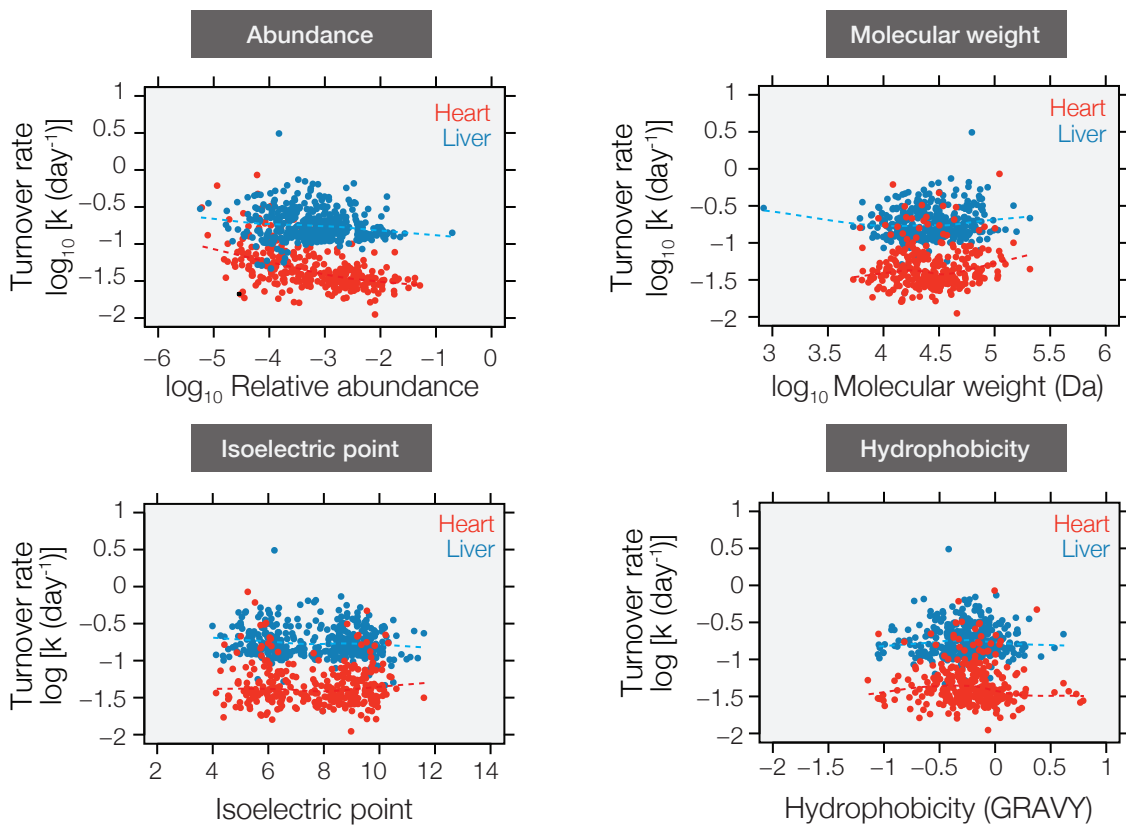
FIGURE 1.17   Correlation between protein turnover and biophysical properties

FIGURE 1.17 displays four scatterplots that correlate individual mitochondrial protein turnover rates to four biophysical or biochemical parameters: the abundance (upper left), molecular weight (upper right), isoelectric point (lower left), and hydrophobicity (lower right) of a protein. A modest inverse correlation was observed between protein turnover rate and the relative abundance of the protein (heart: Spearman's correlation coefficient $\rho = -0.46$, $P < 2.2 \times 10^{-16}$ and liver: $\rho = -0.19$, $P = 7.95 \times 10^{-3}$), corroborating that abundant proteins turn over more slowly in general. This trend has also been observed from limited data in other systems such as the human plasma, where the most abundant protein, serum albumin, has one of the slowest turnover rates among plasma proteins. As discussed above, this may reflect a possible adaptation given the prohibitive energy expenditure that would result from constantly replacing such a massive protein pool. By contrast, we observed no significant correlations in either the heart or the liver between protein turnover rates and their molecular weights. It was reported in the

1970's from small-scale studies of few proteins (33 or less) that larger polypeptide subunits may turnover faster (Dehlinger and Schimke, 1970; Dice and Goldberg, 1975a), but our large-scale investigation failed to replicate this observation, at least within cardiac mitochondria. It was further reported in 1975 from a study of 22 proteins that proteins with lower isoelectric points tended to also exhibit shorter half-life in rats (Dice and Goldberg, 1975b), which was interpreted to suggest a potential degradation mechanism. However, when it was examined whether any systematic relationship existed between isoelectric points and turnover rate in our sample, no significant correlation was shown in the mitochondria. Likewise, no significant correlation was observed between protein turnover and hydrophobicity, as estimated using the GRAVY index (Grand Average of Hydropathicity) (Kyte and Doolittle, 1982) with the ProtParam programon ExPASy (Artimo et al., 2012), which is a function of the empirical hydropathicity of the constituent amino acid residue of the protein.

The data further presented an opportunity to examine the effect of the primary structure of the proteins on their turnover rates. In vivo protein half-life has been proposed to be governed in part by specific sequences on the protein that may target them for proteasomal or lysosomal degradation. A number of these sequences have been discovered that include the N-end rule sequences and the PEST motif. The N-end rule has since been worked out extensively and is attributable to N-terminal degrons recognized by E3 ubiquitin ligases. The PEST motifs are sequences rich in proline (P), glutamic acid (E), serine (S), and threonine (T) that are thought to be signals for proteasomal and calpain degradation and have been associated with short protein half-life (Rogers et al., 1986). In at least some important cardiac proteins including annexins, PEST motifs have been shown to be proteolytic signals for calpain-mediated degradation that govern protein stability (Barnes and Gomes, 2002). Likewise, the intrinsic instability of the protein sequence has also been proposed to confer short protein half-life, in part because the proteasome is thought to require an unstructured region on the substrate to initiate degradation (Prakash et al., 2004). Relatively few studies have examined whether PEST

sequences or protein sequence disorders act as a global predictor of overall protein half-life in unbiased manners, although a recent large-scale study in vitro suggest that fast-turnover proteins in HeLa cells tend to have higher frequency of PEST motifs (Boisvert et al., 2012). Hence we examined whether the observation is recapitulated in our in vivo dataset.
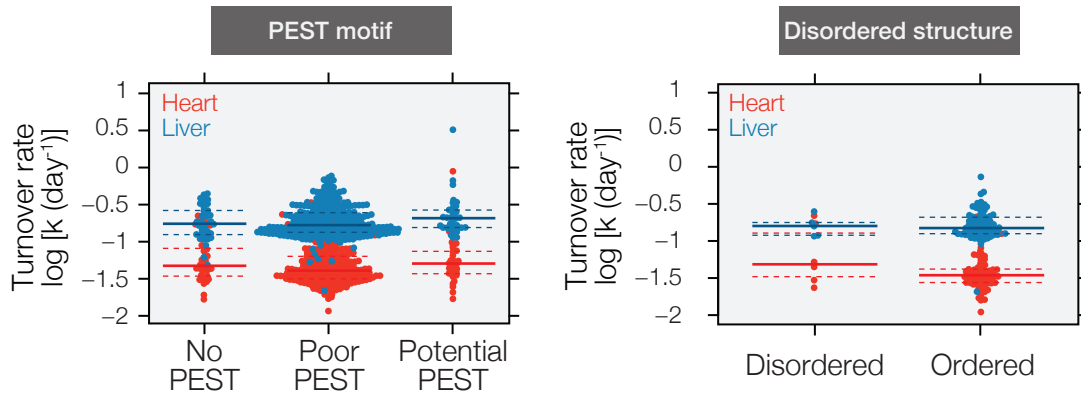
FIGURE 1.18   Correlation between protein turnover and sequence features

FIGURE 1.18 compares the turnover rates of proteins with or without PEST motifs (left) and with or without intrinsically disordered structures based. Each data point represents one proteins. Solid line represents median; dashed lines represent the interquartile range. The presence of PEST motifs on the mitochondrial proteins was queried using the ePESTfind algorithm (Rogers et al., 1986; Schuster and Grabner, 1986) hosted on ExPASy (Artimo et al., 2012), which analyzes protein sequence we submitted in batch through Taverna (Wolstencroft et al., 2013) and categorizes protein and scores for potential PEST motifs and whether a protein contains a potential, poor, or none predicted PEST sequence. We found that at least within the mitochondria, proteins that contain at least one potential PEST motif did not appear to have a prominent difference on in vivo protein half-life than those without (Mann-Whitney U test, $P >$ 0.10). Our result corroborates a recent observation which found no evidence that they affect protein age/ isotope incorporation in vivo (Doherty et al., 2009). However, these data should be

interpreted with caution because the lack of correlation in this particular experiment does not necessarily suggest that the PEST motif does not influence protein half-life in any way. It is possible that the degradation signal may not exist inside mitochondria, or may be cell type and stimulus dependent. The result also depends heavily upon how the PEST motifs are defined, and it may be that very many number of degradation mediators would recognize variations of PEST motif to promote or suppress degradation, such that the overall effect is hard to discern on the global scale. Nevertheless, for the time being the data conclude that there is no systematic bias introduced by the presence of PEST motifs to the turnover rates of mitochondrial proteins. When we queried the presence of potential unfoldability in the protein list using the FoldIndex algorithm (Prilusky et al., 2005), which analyzes the linear protein sequence and look for local unfoldability and the number of potential disordered region, again no global difference in turnover rates was apparent between proteins that contain disordered regions vs. no disordered regions (Mann-Whitney U test, $P > 0.10$).

Lastly, mitochondria are suggested to have inherited Arg/N-end rule and Leu/N-end rule pathways (Varshavsky, 2011; Vögtle et al., 2009), although major components of the degron recognition system are pooly understood. A recent study by William Stanley and colleagues found a significant difference between proteins with stabilizing or destabilizing N-terminal amino acids among the 47 proteins considered (Shekar et al., 2014). However, we found no significant correlation between our turnover rate data and the proteins' predicted in vitro half-life from ProtParam (Artimo et al., 2012), which is based on the N-end rule (Varshavsky, 1996, 2011). A possible explanation for this discrepancy may be differences in the scales of the study, or the accuracy of the N-terminal amino acid in the mature protein chain after specific cleavage of N-terminal pre-sequences.

Taken together, these analyses suggest that primary structure is a poor predictor of in-vivo protein half-life, at least insofar as cardiac mitochondrial proteins are considered.
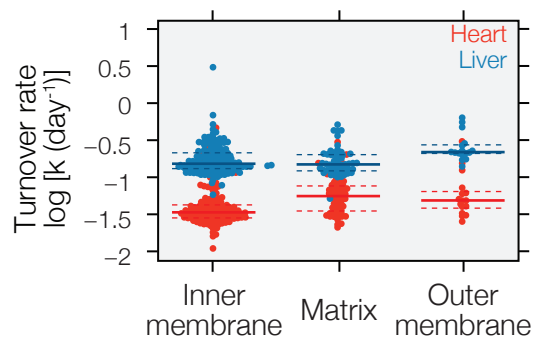
FIGURE 1.19   Correlation between turnover and sub-organelle localization

FIGURE 1.19 compares the turnover rates of proteins assigned to different sub-organellar compartments according to Swissprot/ Protein Information Resource (SP/PIR). Each data point represents a distinct protein. The solid horizontal line represents the sample median; dashed lines represent the interquartile range. Inner membrane proteins have similar median half-life as matrix proteins, whereas the outer membrane proteins have significantly shorter half-life than those on the inner membrane (Mann-Whitney U test, Heart: $P = 5.55 \times 10^{-3}$, Liver: $P = 5.21 \times 10^{-4}$). This observation corroborates previous observations in bulk tissue components that measured total protein turnover in inner membrane extracts vs. outer membrane extracts (Brunner and Neupert, 1968; Lipsky and Pedersen, 1981). Although the data also revealed additional variability within each component, we interpret the data as suggesting the two sub-organellar compartments to be under influence from different protein degradation mechanisms, with the cytosolic-facing outer membrane having additional access to proteasomal, and other, degradation.

We next considered some of the implications that may be drawn from the data on mitochondrial biology, such as whether protein turnover informs on the sequence of protein complex assembly. This is a relevant question because whether protein complexes turn over synchronously, i.e., most constituent subunits are produced and degraded in coordinated fashion, remains an open question under debate. In a large-scale study by Price et al., subunits of multiprotein complexes have been suggested to have coordinated turnover (Cambridge et al.,

50

2011; Price et al., 2010), whereas other studies have reported notable exceptions of asynchronous turnover (Doherty et al., 2009; Savas et al., 2012). In our datasets presented earlier in this chapter and in the next chapter, we found a general observation where the subunits of well-defined, stable protein complexes are indeed more clustered in terms of protein turnover over the whole proteome. Nevertheless, considerable variability in turnover exists within each cluster, and indeed particular members of intermediate subcomplexes may turn over more tightly synchronously than the other subunits at large. This observation was most apparent in the case of the respiratory chain complex I, in which the transiently associated assembly factors turned over considerably faster than the median of the entire protein complex. In cardiac mitochondria, the assembly factors NDUAFAF2 and NDUAFAF3 had turnover rates of $k = 0.053$ d^{-1} and 0.078 d^{-1} respectively, as compared to the complex median value of 0.036 +/- 0.007 d^{-1}. The assembly factors are integral to complex I topogenesis but dissociate from the mature protein complex; in contrast, the core subunits of the Q subcomplex, NDUFS2, NDUFS3, NDUFS7, and NDUFS8 turned over almost synchronously (heart: $k = 0.039$ d^{-1}, 0.036 d^{-1}, 0.042 d^{-1}, 0.039 d^{-1}, respectively). A possible explanation is that the subunits with higher turnover rates may owe it to their more frequent exposure to proteolytic mechanisms, or may exist more frequently as dissociated monomers owing to the complex assembly sequence and/or topology.

This hypothesis suggests that turnover rates are influenced by the stability with which a protein subunit associates with the final assemblage. This is in opposition to the synchronized complex turnover model, wherein all constitutive subunits would have synchronized turnover kinetics. In attempt to differentiate between the two models, we further exampled the data on the subunit NDUFA9, which has a relatively high turnover compared to other complex I subunits in the liver ($k = 0.27$ d^{-1}) but not the heart ($k = 0.035$ d^{-1}). During the biogenesis of complex I, the Q subunit is the first to assemble before the NDUFA9 protein associates with the mitochondria-encoded MT-ND1 subunit to initiate the next intermediate step in the assembly sequence

(Janssen et al., 2006). Incidentally, MT-ND1 has a considerably lower abundance in the liver than in the heart relative to other subunits, which would be consistent with an increased surplus of NDUFA9 free subunits and may explain why NDUFA9 has a faster turnover. In a second example, the NDUFA4 and NDUFS7 subunits have above-median turnover rates in both the liver and the heart (NDUFA4: k = 0.047 d^{-1} in the heart, k = 0.30 d^{-1} in the liver; NDHFS7: k = 0.042 d^{-1} in the heart; k = 0.028 d^{-1} in the liver). Both subunits are incorporated into complex I relatively late in the assembly sequence and only after other stable intermediates are formed (Janssen et al., 2006), which is consistent with their increased exposure to proteolytic mechanisms.

To determine whether the measured turnover rates from the subunits in whole-mitochondrial lysate may differ from the native complexes, we conducted blue native (BN)-PAGE separation of mitochondria followed by in-gel digestion of large supramolecular complexes and analyzed protein turnover rates by mass spectrometry.
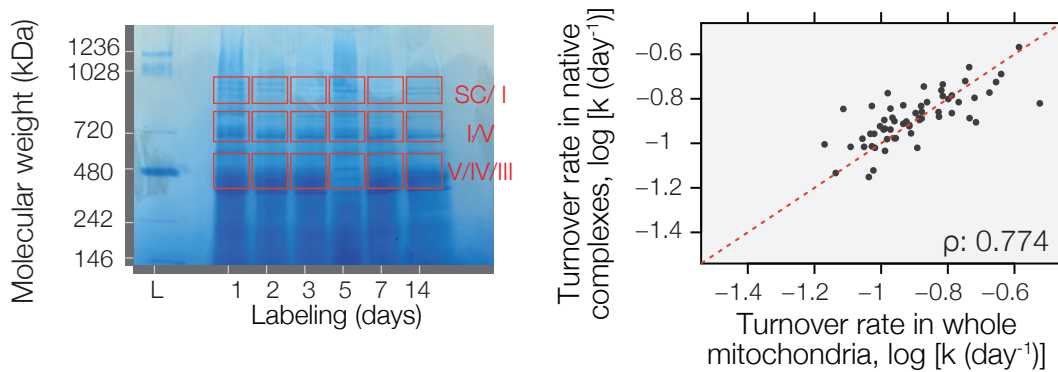
FIGURE 1.20   Turnover rates of intact protein complexes

FIGURE 1.20 shows the measurements of turnover rates in native complexes. (Left) Mouse liver mitochondrial proteins from day 1, 2, 3, 5, 7, and 14 of ^2H_2O labeling were resolved with BN-PAGE under gentle conditions to isolate large supramolecular complexes. Gel bands that correspond to complexes I, III, IV, and V, as well as supercomplexes (SC) based on previous experience were excised for in-gel digestion and MS analysis. L: size ladder. (Right) Scatterplot showing the comparison of the turnover rates of 62 respiratory complex subunits measured from BN-PAGE excisions and whole mitochondrial lysate. Overall, we observed no systematic bias in turnover rates, with the median ratios of BN-PAGE over whole-mitochondrial lysate of 1.04 [0.92 – 1.18]. Only two respiratory complex subunits exhibited significant differences in turnover rates. Both showed modestly faster turnover in the BN-PAGE-resolved samples – ATP5D: ratio: 1.13, Mann-Whitney U test P: 3.6×10^{-2}; and ATP5B: 1.1, Mann-Whitney U test P: 2.8×10^{-3}. Thus although some variability exists between the turnover of free subunits and complex-associated subunits, overall we did not observe compelling evidence to suggest that the assembled complexes are in disequilibrium from the whole-mitochondrial lysates, or that the subunits isolated from assembled complexes exhibited more tightly clustered turnover.

Although further investigations are necessary to determine whether protein turnover rates can be used to derive mechanistic insights on protein assembly, the presented observations are consistent with finer regulations of protein turnover within a stable protein complex. It is entire-

ly possible that a combination of abundance and turnover may in fact be one regulatory mechanism on the level of functional protein complexes in the cell. In fact, it may be reasonably expected that respiratory complex I subunits ought not to turn over completely synchronously given the vast differences in the relative abundance of the subunits themselves. This is as opposed to the 20S proteasome, where data we acquired show that the core subunits have relatively uniform abundance as well as turnover rates.

The variable turnover dynamics of the mitochondrial proteome also hint at the types of proteolytic mechanisms that may govern protein degradation in cardiac mitochondria. When induced, macroautophagy of the mitochondria, whether through PINK1/Parkin-mediated canonical mitophagy or otherwise, is known to engulf and remove entire mitochondria simultaneously (Kubli and Gustafsson, 2012). In theory, the assumption of steady-state protein abundance in inferring turnover from synthesis may be transiently offset by bouts of occasional mitophagy on selected organelle units and still remain valid over the labeling period. By removing all mitochondrial proteins from the cell at a fixed rate, this process would act as a synchronizing mechanism for protein dynamics inside the organelle. Indeed, the overall range of mitochondrial protein turnover rates that was observed in the experiment is a much narrower than that for the entire heart, both in literature reports and in our experiments as reported in the next chapter, indicating that mitochondrial proteins do share similar turnover rates insofar as the entire cardiac proteome is concerned.

Nevertheless, the diverse turnover rates of mitochondrial proteins dispute the indispensability of indiscriminate mitophagy in individual protein homeostasis. In other words, the mitochondrial proteome does not only turn over as a single unit. Since the synthesis rates of mitochondrial proteins span over an order of magnitude in the heart, at any moment each mitochondrion must contain certain proteins that on average have been synthesized more recently than others. If mitophagy were indeed the predominant process of mitochondrial protein removal in the

heart, then it would follow that many mitochondria would be missing critical components. To resolve this paradox, a mechanism is necessary that would allow mitochondria with new and old proteins to preserve homeostasis under mitophagy. For example, mitochondrial proteins may be synthesized in excess in the cytosol at variable rates before simultaneous import. Alternatively, a sorting mechanism prior to autophagy must exist such that some protein species would be preferentially recycled during fusion-fission cycle. At present, evidence is scarce to support the existence of either scenario in the heart, although recent evidences suggest that some outer membrane proteins may escape mitophagy by translocation to the ER (Saita et al., 2013), and that mitochondria may derive mitochondria-derived vesicles to the lysosome (McLelland et al., 2014; Soubannier et al., 2012). Such vesicles may contain a specific subset of the mitochondrial proteome. Notwithstanding, the data are consistent with substrate-level proteolysis playing significant roles in mitochondrial dynamics, as would be consistent with the various intra-mitochondrial protease complexes expressed by cardiac cells. The data highlight the potential of a proteome dynamics map at individual protein resolution for uncovering signatures of protein quality control dysfunctions, such as in aging and metabolic perturbation studies, where measuring bulk organellar protein synthesis as a proxy for mitochondrial homeostasis would be an inadequate means of capturing the details of mitochondrial protein turnover.

Materials and methods

Method Summary: The data shown in this chapter were acquired by performing ^2H_2O labeling on healthy adult Hsd:ICR mice and analyzing protein isotope incorporation with mass spectrometry and bioinformatics tools. Experimental details are given below:

Reagents: ^2H_2O (70% and 99.9% molar ratio) was purchased from Cambridge Isotope Laboratories and filtered through 0.1-μm polyethersulfone membranes (VWR). Other chemical reagents were from Sigma-Aldrich unless specified. Milli-Q (Millipore) filtered water (18.2 MΩ) was used.

Study approval: Mouse experiments were conducted in accordance with the Guide for the Care and Use of Laboratory Animals by the National Research Council and approved by University of California, Los Angeles.

Introduction of stable isotope labels: Male Hsd:ICR (CD-1) outbred mice (Harlan laboratories, 8 – 10 weeks of age) were used in the study. The animals were housed upon arrival in a 12-hour/12-hour light-dark cycle with controlled temperature and humidity, free access to standard chow and water. To initiate labeling, we gave each animal two intraperitoneal (i.p.) injections of 500-μL 99.9% molar ratio ^2H_2O-saline 4 hours apart. The mice were then allowed access to 8% (v/v; 7.25% molar ratio) ^2H_2O in the drinking water supply ad libitum. We euthanized the animals at up to 13 time points (0, 0.5, 1, 2, 4, 7, 12, 17, 22, 27, 32, 37, 90 days following the second ^2H_2O injection for sample collection) to collect heart, liver, and blood samples to determine ^2H_2O enrichment in body water and protein turnover rates. We did not observe significant change in body weights of mice ($\approx$ 40 g) during the labeling period.

Measurement of body water label enrichment: To measure the amount of ^2H_2O that is incorporated into the animal's body water throughput the labeling period, mouse and human plasma samples were used directly for gas chromatography MS analyses. For each sample, 20 μL of plasma was mixed with 2 μL of 10 N NaOH and 4 μL of 5% (v/v) acetone in acetonitrile. The standard curves were created by adding 0% to 20% molar ratio of ^2H_2O at 11 regular intervals in 1× PBS in place of the plasma sample to the acetone. The sample mixtures were incubated at ambient temperature overnight. Acetone was extracted by adding 500 μL of chloroform and

0.5 g of anhydrous sodium sulfate. One µL of the extracted solution was analyzed on a GC-mass spectrometer (Agilent 6890/5975) with a J&W DB17-MS capillary column (Agilent, 30 m × 0.25 mm × 0.25 µm) at the UCLA Molecular Instrumentation Center. The column temperature gradient was as follows: 60 °C initial, 20 °C·min^{-1} increase to 100 °C, 50 °C·min^{-1} increase to 220 °C, 1 min hold. The mass spectrometer operated in the electron impact mode (70 eV) and selective ion monitoring at m/z 58 and 59 with 10 ms dwell time.

Isolation of cardiac and hepatic mitochondria: To isolate mitochondria, we excised the heart and liver from each mouse, and homogenized the tissues using a 7-mL Dounce homogenizer (Pyrex) (20 strokes) in an extraction buffer (250 mmol·L^{-1} sucrose, 10 mmol·L^{-1} HEPES, 10 mmol·L^{-1} Tris, 1 mmol·L^{-1} EGTA, 10 mmol·L^{-1} dithiothreitol, protease and phosphatase inhibitors (Pierce Halt), pH 7.4) at 4 °C. The homogenate was then centrifuged (800 rcf, 4 °C, 7 min). The supernatant from the first spin was taken and further centrifuged (4,000 rcf, 4 °C, 30 min) to collect as the organelle-depleted cytosolic fraction. The pellet from the second spin was washed once with 1 mL of the extraction buffer, centrifuged again (4,000 rcf, 4 °C, 30 min), then overlaid on a 19%/30%/60% discrete Percoll gradient. The mitochondria were then sedimented by ultracentrifugation (12,000 rcf, 4 °C, 10 min). Purified mitochondria were collected from the 30%/60% interface layer and washed twice with 1 mL of the extraction buffer followed with centrifugation (4,000 rcf, 4 °C, 15 min). We then lysed the purified mitochondria by sonication in 10 mmol·L^{-1} Tris-HCl. Protein concentrations were measured by bicinchoninic acid assays (Smith et al., 1985) using pure bovine serum albumins as standards (Thermo Pierce).

Fractionation and digestion of mitochondrial proteins: To prepare the isolated mitochondrial proteins for MS analysis, we fractionated the total protein using polyacrylamide gel electrophoresis and performed in-gel trypsin digestion. Two hundred µg of proteins were denatured at 70 °C in Laemmli sample buffer for 5 minutes and then separated on a 12% Tris-glycine

57

acrylamide gel with 6% stacking gel, at 80 V, at ambient temperature for 19 hours. The gel was Coomassie-stained and cut into 21 fractions. Each fraction was minced into ~1 mm^3 cubes and destained with 300 µL of 50 mmol·L^{-1} NH$_4$HCO$_3$ and 25% acetonitrile. The gel cubes were dehydrated with 300 µL of acetonitrile, then rehydrated in 300 µL of 10 mM dithiothreitol, washed and dehydrated, then alkylated in 100 mM of iodoacetamide, and digested with 30:1 (w/w) sequencing-grade trypsin (Promega) at 37°C overnight.

Measurement of protein isotope incorporation: To acquire information on protein identity and the amount of incorporated heavy isotope at each time point, we analyzed the proteolytic peptides using a LTQ Orbitrap XL mass spectrometer (Thermo Fisher Scientific), coupled to a nanoACQUITY UPLC system (Waters). The trapping (30 mm in length) and analytical (200 mm in length) columns for peptide separation were packed in-house in an IntegraFrit columns (New Objective) (360-µm outer diameter, 75-µm inner diameter) with Jupiter Proteo C$_{12}$ resin (Phenomenex) (90-Å pore, 4-µm particle) using a NanoBaume pressure bomb (Western Analytical Products). To fractionate the peptide species on the LC column, we used a binary buffer system consisting of 0.1% (v/v) formic acid in 2% (v/v) acetonitrile (buffer A) and 0.1% formic acid in 80% acetonitrile (buffer B). The separation gradient was made by changing buffer B as follows: 0 minute, 2% B; 0.1 minute, 5% B; 70 minute, 40% B; 90 minute, 98% B; 100 minute, 98% B; and 105 minute, 2% B, with subsequent equilibrium at 2% B for 5 minutes. Mass spectra were obtained in profile mode for MS survey scan in the Orbitrap at a resolution of 7,500 and in centroid mode for MS/MS scan in the LTQ ion trap. The top five intense peaks in the MS scan were subjected to CID with an isolation window of 3 m/z and a dynamic exclusion of 25 seconds.

Database search for protein identification from mass spectra: To identify the protein species present in the sample, we matched the acquired spectra against a protein database using a search engine. The raw spectral data were processed by BioWorks (ThermoFisher Scientific,

version 3.3.1 SP1) into a searchable format, then matched using SEQUEST (ThermoFisher Scientific, version 3.3.1) against the UniProt mouse database (2011-07-27; 55,744 entries). The SEQUEST search parameters included fixed cysteine carbamidomethylation and variable methionine oxidation, with enzymatic specificity set to trypsin, and two missed cleavages. The mass tolerances for the precursor and the product ions were 100 ppm and 1 Th, respectively. The minimum redundancy set of proteins was filtered with Scaffold (Proteome Software, version 3.3.3), requiring at least two peptides and 99.0% protein confidence for affirmation. The global false discovery rate was set to 0.1% in Scaffold. Because they may be shared by proteins with different turnover rates, all peptides shared by multiple proteins or protein isoforms were excluded from downstream turnover rate calculations.

Analysis of protein isotope incorporation patterns: To input into the in-house analysis program, [.raw] mass spectra were first converted into [.mzML] format using ProteoWizard (version 2.2.2913). The relative abundance of a protein was determined by the summation of total chromatographic areas of the constituent peptide ion peaks divided by the areas of all identified peptide ions in the experimental dataset using Progenesis LC-MS (Ver. 4.0.4441.29989, Nonlinear Dynamics).

Statistical analyses: Uncertainties in rate constants were estimated using the Monte Carlo method. The distribution of the relative abundance was approximated using the absolute value of the residues. At each measured time point, a single point was synthetically generated using random numbers from a Gaussian distribution with the same width as the distribution of the absolute values of the residuals and a mean of the model value. New rate constants were determined for the 10,000 synthetic datasets, and the distribution of rates was observed to converge approximately to a Gaussian distribution. The width of this distribution (1σ) was reported as the standard error of the rate constant. Quantile-quantile plots suggest that the turnover rates of proteins within a tissue homogenate are not normally distributed. Significanc-

es of difference between groups were thus assessed by rank-based, non-parametric Mann-Whitney U tests using R (v.3.0.3). Correlations between variables were denoted by Spearman's rank-correlation coefficient (ρ).

II. Proteome dynamics of cardiac remodeling

Following the development of a large-scale method to study protein half-life in vivo, our next objective was to measure how protein expression and turnover may alter during the development of heart diseases. Using ^2H_2O labeling and an isoproterenol-challenge model of cardiac remodeling in mice, we measured the turnover rates of approximately 3,000 cardiac proteins, and observed widespread and specific changes in turnover during cardiac remodeling and reverse remodeling. The data suggest that proteins with highly elevated protein turnover rates during disease may represent a new class of candidate disease drives that elude detection by experiments that measure only steady-state protein abundance, which include mitochondrial proteins such as HK1, ALDH1B1, and PHB, as well as a number of cytosolic proteins. We further describe some features of protein dynamics changes in relation to expected physiological and proteomic changes. The material composing this chapter was published and can be found in our publication (Lam et al., 2014).

Mitochondrial dysfunctions in cardiac remodeling

Heart failure afflicts oppressive societal and human loss, affecting 5.1 million Americans and contributing to one in nine deaths per year (Go et al., 2013). During the development of heart failure, the myocardium undergoes massive and progressive remodeling, characterized at the cellular level by changes to multiple subsystems including calcium signaling, adrenergic signaling, metabolic changes, cell death signaling, and redox balance. At the molecular level, the dynamic equilibria of multiple biomolecules are simultaneously shifting towards pathological steady states during disease development. Despite decades of research, important knowledge gaps persist on the cardiac remodeling process, which can in part be attributed to an incomplete description on how molecular events interact to orchestrate complex, multifactorial etiologies. Identifying the participants and sequences of the remodeling process is thus an important of cardiac research that could lead to general principles that explain the pathogenic mechanism and time-evolution of heart diseases.

Mitochondrial dysfunction is a hallmark of the failing heart. (Abel and Doenst, 2011; Marin-Garcia et al., 2001; Neubauer, 2007; Rabinowitz and Zak, 1975; Rosca and Hoppel, 2010; Tokoro et al., 1995). Functional abnormalities of the mitochondrion typically present during the onset of pathological remodeling, and may develop progressively parallel to left ventricular dysfunctions (Abel and Doenst, 2011; Marin-Garcia et al., 2001; Neubauer, 2007; Rosca and Hoppel, 2010). Whilst these changes can in part be attributed to a general decrease in mitochondrial biogenesis, different mitochondrial components often present different injuries, suggesting that alterations of distinct sub-proteomes or individual proteins are crucial to overall disease development.
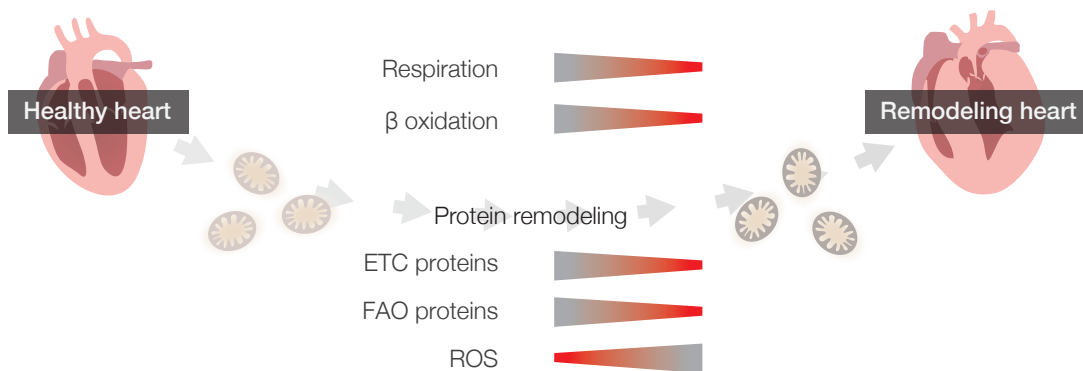
FIGURE 2.1   Typical mitochondrial derangements in cardiac remodeling

FIGURE 2.1 summarizes some mitochondrial alterations that occur during cardiac remodeling. Common mitochondrial ultrastructural abnormalities may be observed under the microscope and include disarrayed organelle arrangements along myofibrils and disrupted cristae. Physiological perturbations include diminished adenosine triphosphate (ATP) production, phosphocreatine levels, and fatty acid utilization (Abel and Doenst, 2011; Lin et al., 2003; Marin-Garcia et al., 2001; Tokoro et al., 1995). Changes in gross phenotypes are paralleled by a remodeling of the mitochondrial proteome into a pathological state that reflects a decrease in substrate metabolism and energy conversion (Neubauer, 2007; Rabinowitz and Zak, 1975; Rosca and Hoppel, 2010). Known components of proteome remodeling include the decrease of fatty acid oxidation (FAO) enzymes including CPT1B, MCAD, and ACADVL (Bugger et al., 2010); repressed expression of electron transport chain (ETC) subunits including NDUFA9, SDHB, and COX5B (Bugger et al., 2010); the disassembly of respiratory chain supercomplexes (Rosca et al., 2008); and widespread alterations of other metabolic protein expression (Dai et al., 2013; Kato et al., 2010; Meng et al., 2009). The proteome changes are thought to be harbingers of higher metabolic and energetic disorders including decreased ATP production and respiratory capacity. Hence an objective of understanding cardiac hypertrophy is to establish how mitochondrial remodeling is initiated, i.e., to define the sequence of alterations in proteome anatomy, and to ascertain whether certain events consistently lead to irreversible mitochondrial

damage. Proteome changes coincide with the elevated ROS (Tsutsui et al., 2009), and it is thought that the promotion of protein damage may underlie some pathological phenotypes. Because of the proximity of mitochondria with ROS and the general decrease of protein quality control in the failing heart, increased ROS encountered by mitochondrial proteins in the diseased heart in particular (Giordano, 2005) would render proteins more susceptible to misfolding, aggregation, and chemical modifications.

In parallel, malfunctions of protein turnover are increasingly recognized in numerous human disorders, including cystic fibrosis, neurodegenerative diseases, and heart diseases (Balch et al., 2008; Hinkson and Elias, 2011). In the normal heart, protein turnover helps maintain the protein pool in homeostasis through continual synthesis and degradation. The turnover cycle becomes perturbed during cardiac injury and heart failure, by factors including hypertrophic signaling calcium regulation and proteolytic stress (Giordano, 2005; Goonasekera et al., 2012; Katz, 2010; Tsutsui et al., 2009). Hypertrophy is associated with increased overall protein synthesis, which at the same time creates increased protein misfolding which stresses cellular protein quality control system to maintain homeostasis (Doroudgar and Glembotski, 2013). Altogether, changes to protein degradation and synthesis instigate a remodeling of the cardiac proteome that parallel, at the molecular level, the progressive deterioration of cardiac structure and functions (Abel and Doenst, 2011; Dai et al., 2012; Drews et al., 2010; Katz, 2010). Multiple pharmacological interventions that target protein kinetics are also known to modulate the outcome of isoproterenol-induced cardiac remodeling markedly. Rapamycin, which inhibits mTOR-mediated protein synthesis and promotes autophagy, is known to ameliorate heart failure. On the other hand, proteasome inhibition, which decreases the amount of proteins being degraded, has complex and sometimes dichotomous outcomes on cardiac disease phenotypes (Glembotski, 2012; Hedhli and Depre, 2010; Stansfield et al., 2008). In at least one study, inhibition of proteasomes has been found to exacerbate and even been sufficient to reproduce the phenotypes of isoproterenol stimulation (Tang et al., 2010).

Because either the rate of protein synthesis or degradation (i.e., protein turnover) must deviate from normal values in order for the protein pool size to adjust to a new level, any permutation of proteome states leaves behind a kinetic signature, in the form of the fraction of newly synthesized proteins in the protein pool (Claydon et al., 2012; Doherty and Beynon, 2006). This kinetic signature can be measured through the incorporation of isotopes into protein over time, and may be exploited to identify unexpected disease proteins and their pathological implications independently of abundance measurements. For instance, the increased abundance of a protein may originate from elevated protein synthesis or decreased proteolysis, two scenarios which can be distinguished by the replacement kinetics of the protein pool, i.e., protein half-life. Alternatively, cellular signaling may accelerate synthesis and degradation to shorten protein half-life without altering protein abundance, which has been hypothesized to facilitate the generation of spatial gradients (Varshavsky, 2011). Since abundance measurement per se conflates disparate kinetic scenarios, investigations restricted to steady-state measurements have limited power to discern certain time-dimensional features of disease progression. The overall protein pool abundance conflates a number of disparate biological realities – a protein of increased abundance could owe it to increased synthesis or decreased degradation; a protein with shortened half-life may show no abundance change. These kinetic scenarios would be indicative of relevant pathologies, e.g., a drastic increase in turnover in early hypertrophy would signify functional activation in relation to remodeling, whereas prolonged half-life amid elevated ROS in the decompensated heart would be symptomatic of impaired proteolysis, because the previously existing protein pool accumulates. These and further pathologic scenarios present only in the time dimension and are obscured from instantaneous protein abundance measurements.

This limitation has perhaps hindered the identification of causal events during hypertrophic responses, because potential drug target proteins for which abundance is not the correlating

parameter in its disease association may be obscured. The dynamic process of cardiac re-modeling is inadequately captured by our static conceptualization of proteins: current techniques produce fragmented snapshots of protein expression that are difficult to connect in a coherent sequence or relate to other cellular processes. Assessing global protein turnover kinetics in the remodeling heart therefore provides new opportunities to understand cardiac remodeling and identify molecular changes that presage functional debilitations.

Although disrupted protein homeostasis, or proteostasis, is a hallmark of the remodeling heart, the technologies to quantify its effects on protein turnover have been under-developed. It remains to be established how the disruption of protein quality control may lead to the observed molecular dysfunctions in cardiac diseases, and the disruption of which proteins may constitute important disease drivers. Hence, to understand the remodeling process at the molecular level, we wish to explore proteostasis in the heart through the measurement protein turnover – the continual replacement of protein pools by protein synthesis and degradation – and how it is disrupted during disease progression. We ask two specific questions – first, what the nature of cardiac mitochondrial dynamics at the individual protein level is in disease, and second, how might the regulatory mechanisms of protein homeostasis permute to contribute to cardiac remodeling.

As described in Chapter I, measuring protein turnover in vivo entails additional technical challenges including label delivery and tolerance, determination of precursor enrichment, and data interpretation. Stable isotope labeling using deuterium oxide (^2H_2O) tracers has shown great potential for tracing protein turnover in mammals (Fanara et al., 2012; Kasumov et al., 2013; Rachdaoui et al., 2009). Widespread applications to studying diseases have been hindered by the lack of necessary computational workflow for large-dataset analysis and translatable methods for human clinical studies.

To address these challenges, we combine animal disease models, ^2H_2O labeling, mass spectrometry analysis to interrogate large-scale temporal dynamics in a mouse β-adrenergic stimulation model of cardiac remodeling. We first implemented a mouse model of cardiac remodeling through chronic isoproterenol challenge. Many aspects of adverse cardiac remodeling can be recapitulated in the laboratory using a number of animal models (Balakumar et al., 2007; Houser et al., 2012). The induction of chronic β-adrenergic stimulation through isoproterenol, a high-affinity $β_1/β_2$-adrenergic receptor agonist (Drews et al., 2010; Rockman et al., 1998), was chosen based on the considerations that the model is well established in the literature, considered to be relatively simple to perform and reproduce, and consistently produces well-defined pathological stimuli in our hands. As with most animal models of complex diseases, isoproterenol challenge does not necessarily recapitulate every aspect of human disease etiology, but for our purpose it mimics the pathological traits of interest, namely, the gradual reorganization of the mammalian heart from a healthy makeup, through initially compensatory enlargement or hypertrophy, to a decompensated state and dilated cardiomyopathy and reduction of contractility.

Isoproterenol stimulation causes positive inotropic and chronotropic responses in the mouse heart. Prolonged stimulation over a period of 7 to 21 days induces cardiac dysfunctions and decreases in cardiac outputs. Cardiac remodeling and failure in this model is thought to occur through multiple, incompletely defined pathways including direct G protein-coupled receptor (GPCR)-mediated signaling, G protein-independent signaling, or complex interactions thereof. GPCR-dependent effects of β-adrenergic stimulation include $Gα_s$-cAMP-PKA stimulation and MAPK activation, leading to induction of transcriptional changes (Noor et al., 2011; Salazar et al., 2007), whereas G-protein-independent signaling include the increased calcium entry that can impinge upon Ca^{2+}/calmodulin-dependent kinase (CamKII), calcineurin, and nuclear factor of activated T-cell (NFAT) signaling (Anderson et al., 2011; Molkentin, 2004). Chronic β-adrenergic stimulation also causes an increase in ROS production, increased apoptotic signal-

ing, and proteasomal alterations (Drews et al., 2010; Salazar et al., 2007; Zhang et al., 2005) that coincide with and may be causally linked to functional deteriorations of the mitochondrion. Collectively, prolonged signals in both GPCR-dependent and G protein-independent arms are thought to elicit hypertrophy as well as a switch to the fetal gene expression profile (ANP, β-MHC, Glut-1, etc.) (Gaussin et al., 2003; Razeghi et al., 2001), which is thought to be initially stress-protective in compensatory hypertrophy but ultimately detrimental toward adverse cardiac remodeling.

As introduced in Chapter I, the turnover rates of proteins can be measured by stable isotope labeling techniques that distinguish new and pre-existing proteins at a given time, but a current hindrance in their usage is the lack of analytical methods that are compatible with large-scale studies in animal models. The development of the described ^2H_2O labeling method and an in-house software program created a unique opportunity to assay time-dimension features of protein remodeling and measure how mitochondrial proteins are replaced over the course of time.
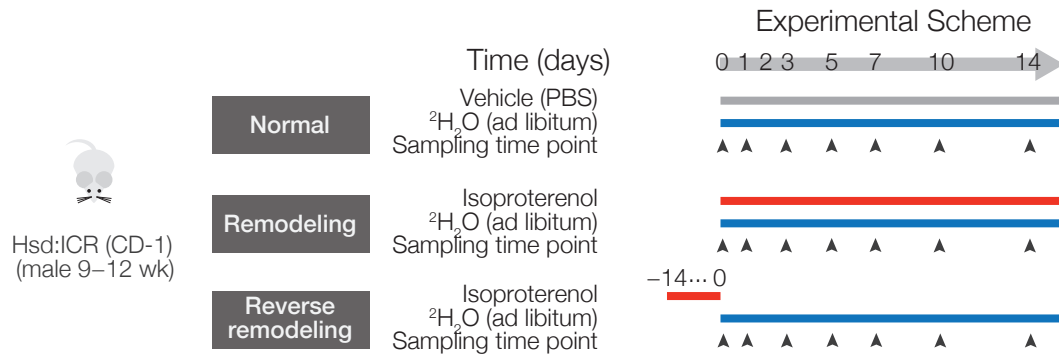
FIGURE 2.2   Mouse model of cardiac remodeling and reverse remodeling

FIGURE 2.2 shows the experimental scheme to measure protein turnover dynamics in normal and diseased mouse hearts through metabolic labeling. Sixty-three male Hsd:ICR (CD-1) mice, nine to 12 weeks of age, were randomized into three separate experimental groups. The first group of mice (Normal) received subcutaneous implantation of micro-osmotic pumps (Aztec) calibrated to deliver PBS over the course of 14 days and acted as baseline control. ^2H_2O labeling was initiated as described in Chapter I at the same time as the implantation surgery for 14 days. A second group of mice (Remodeling) were implanted with micro-osmotic pumps calibrated to deliver 15 mg·kg·d^{-1} of isoproterenol for 14 days to effect gradual cardiac remodeling. A third group of mice received 15 mg·kg·d^{-1} of isoproterenol via micro-osmotic pumps for 14 days prior to the initiation of ^2H_2O labeling (day -14 to day 0) to model the reverse remodeling process following isoproterenol withdrawal. ^2H_2O labeling then proceeded for 14 days in identical manners with the other group.
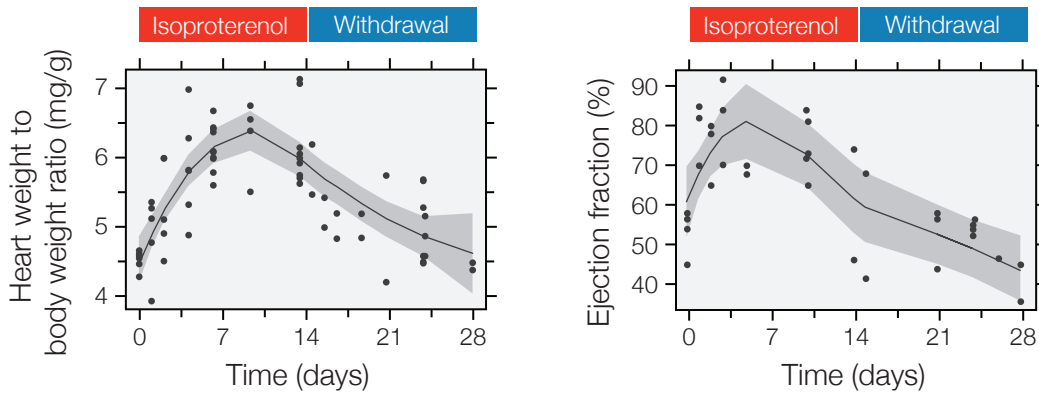
FIGURE 2.3   Isoproterenol challenge model of cardiac remodeling

FIGURE 2.3 depicts the changes in normalized heart weight (left) and in cardiac ejection fraction (right) during 14 days of 15 mg·kg^{-1}·d^{-1} isoproterenol stimulation in Hsd:ICR (CD-1) mice. Each data point represents one individual mouse and/or measurement. The line and shading represents local regression and 95% confidence intervals of the trend over time. We performed ^{2}H$_2$O-labeling on 24 additional mice that were simultaneously administered isoproterenol to induce pathological hypertrophy and remodeling (Drews et al., 2010; Rockman et al., 1998). It can be seen that during the isoproterenol delivery (red), heart weight over body weight ratio increased, signifying hypertrophy. Following the withdrawal of isoproterenol, a reverse remodeling phase occurred as the ratio of cardiac and total body mass reverted to the normal pre-isoproterenol values of approximately 4 mg·g^{-1}. Hence our isoproterenol stimulation model causes cardiac hypertrophy and alterations in contractility as expected.
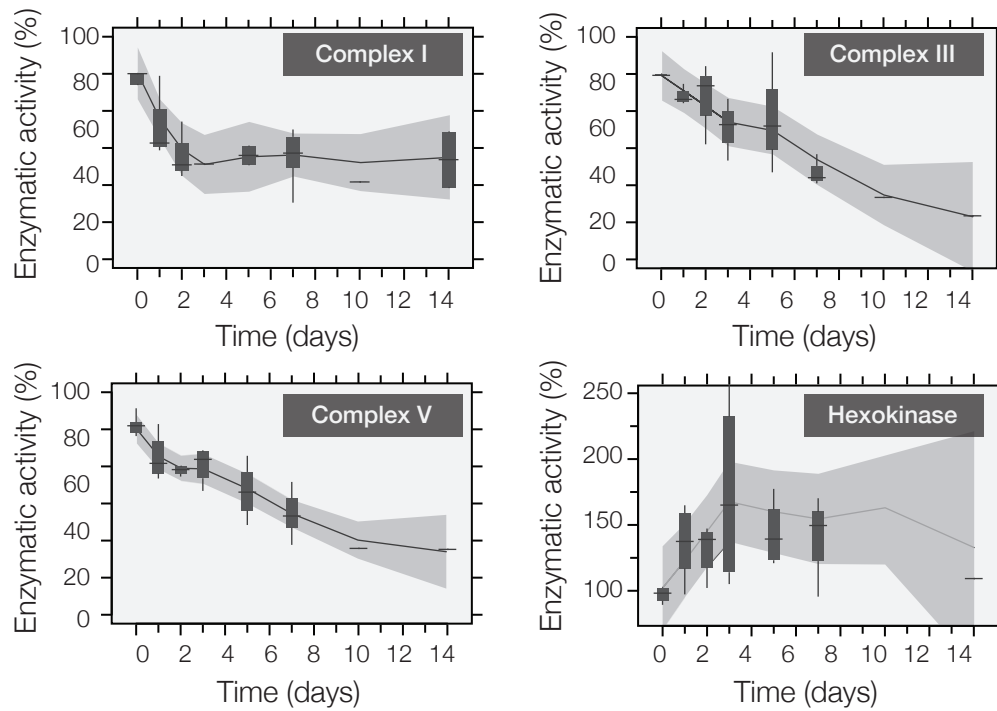
FIGURE 2.4   Metabolic changes during cardiac remodeling

FIGURE 2.4 illustrates some examples of energetic changes in the mouse model. The graphs illustrate the in-vitro enzymatic activities of respiratory chain complex I (NADH:ubiquinone oxidoreductase) (upper left) , complex III (ubiquinol:cytochrome c oxidoreductase) (upper right) and complex V (ATP synthase) (lower left); and hexokinase (lower right), normalized to mitochondrial protein amount input and represented as ratio of the activity in the normal heart (%). Vertical box and whiskers denote interquartile range and 1.5× interquartile range of readings at a particular time point. Horizontal lines and grey area denote local regression fitting and 95% confidence interval. It could be seen that the in vitro respiratory complex activities gradually decreased over the course of cardiac remodeling, due to lowering amount of assembled enzyme complexes and/or allosteric control, whereas glycolytic activities surged. Taken together, the data indicate that following isoproterenol, myocardium remodeling is also evident in terms of energetics, and the individual mitochondrial complexes exhibit differential regulations.
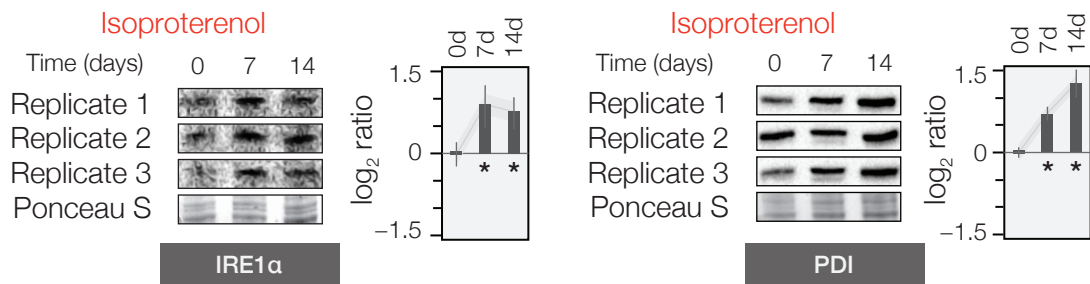
FIGURE 2.5   Proteostatic changes in cardiac remodeling

FIGURE 2.5 illustrates some example markers of ER stress in the remodeling hearts at day 7 and day 14 following isoproterenol challenges. During hypertrophy, the increased burden of protein production and folding exceeds the capacity of the cardiac ER/SR. The resulting ER stress is a hallmark of multiple cardiac etiologies and is indicative of increased protein production and protein folding stress after isoproterenol challenge. Immunoblots for the increased expression of two ER stress markers, IRE1α and PDI, are shown, along with densitometry quantification of immunoreactivity.
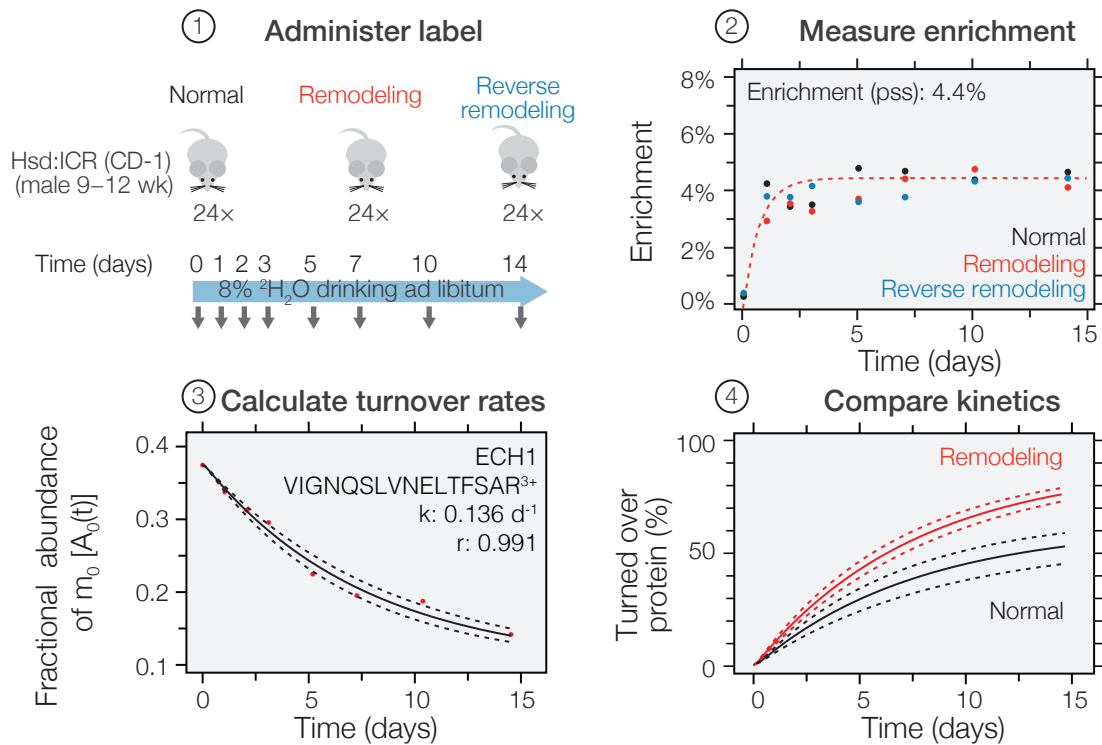
FIGURE 2.6 Strategy to compare turnover rates in health and disease

FIGURE 2.6 illustrates the overall strategy to investigate the protein dynamics of cardiac re-modeling by comparing the turnover rates of proteins measured from normal mice and mice undergoing adverse cardiac remodeling or reverse remodeling. (Step 1) At eight separate time points, we serially harvested mouse heart and blood from three mice of each group. The cardiac lysate was fractionated mitochondrial and cytosolic fractions, and the extracted protein samples were analyzed with high-resolution Orbitrap MS. (Step 2) GC-MS data demonstrating that the labeling protocol resulted in fast and steady ^2H_2O enrichment of ≈4.4% of total body water in the mice. Each data point represents one individual animal in each group (Step 3). The incorporation of ^2H_2O labels into newly-synthesized proteins increases the proportion of proteins with heavier isotope compositions as described in Chapter I. The gradual shifts in peptide isotopomer patterns could then be distinguished by MS, and the rate of shift can be modeled to deduce the rate of turnover of the protein pool given the appropriate analytical software.

(Step 4) The turnover rates of a protein in normal and diseased states are compared to identify proteins with significant differences in turnover during disease development.
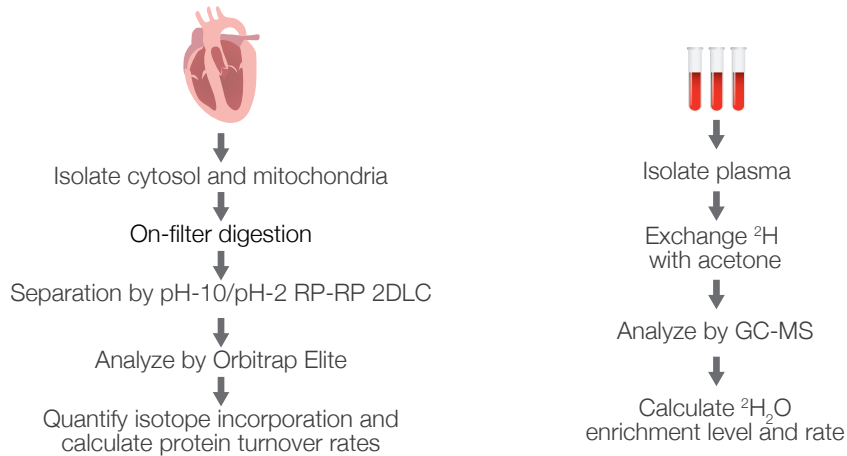
FIGURE 2.7   Sample processing scheme (normal and remodeling hearts)

FIGURE 2.7 illustrates the sample processing workflow to measure protein turnover in normal and remodeling hearts. From each time point, plasma samples were collected for GC-MS analysis of body water ^2H_2O enrichment, whereas cardiac proteins were separated into cytosolic and mitochondrial fractions and analyzed by mass spectrometry.

Protein kinetic signatures of remodeling hearts

From the normal, remodeling, and reverse-remodeling mouse hearts, the MS experiments discovered the in vivo half-life of approximately 3,000 distinct cardiac proteins from over 10,000 distinct peptides.
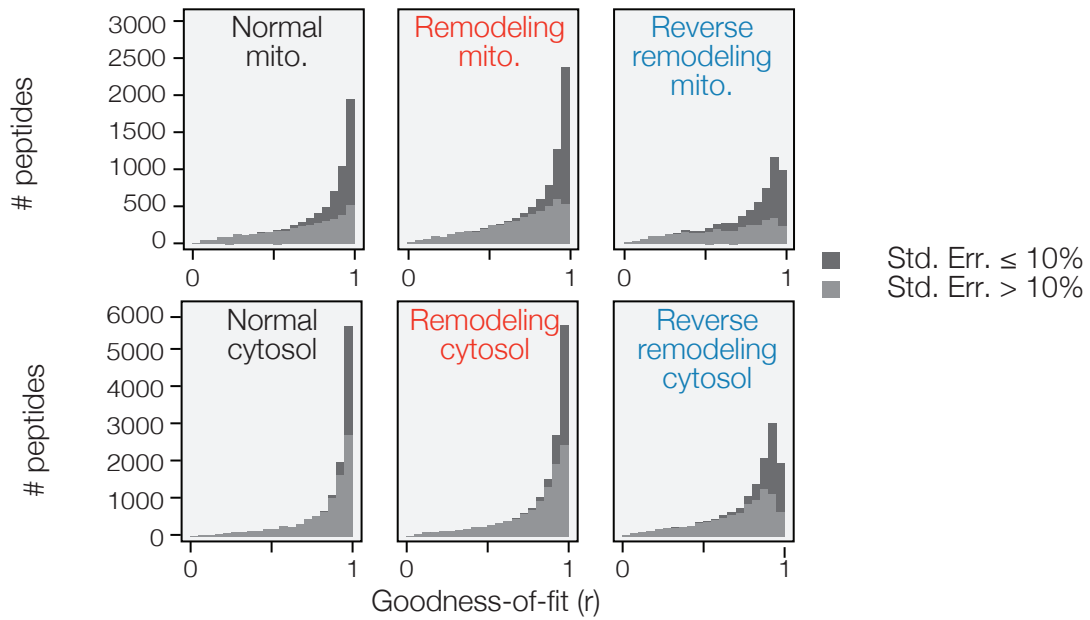
FIGURE 2.8   Peptide kinetic curve fitting quality (r value)

FIGURE 2.8 demonstrates the quality of fitting of peptide data from the normal and remodeling mouse hearts using the described workflow, as estimated by the goodness-of-fit (r) of the nonlinear kinetic model to the acquired data points. Data from both mitochondrial proteins (top) and cytosolic proteins (bottom) are shown. A goodness-of-fit of 0.9 is considered acceptable (see Materials and Methods). Approximately 10,000 peptides passed the quality filter in both normal and remodeling hearts, with the precision of the model in predicting protein data points suggesting that most proteins changed in gradual manners during cardiac remodeling. In contrast, a decrease in the proportion of fitted peptides was apparently during reverse remodeling following isoproterenol withdrawal. In each histogram, the dark gray shading represents the proteins which also exhibited low standard errors of estimate (Std. Err.) of the fitting of the peptide time series as an alternative means of estimating fitting fidelity. In general, peptides with good goodness-of-fit generally also exhibited low standard errors of fitting.
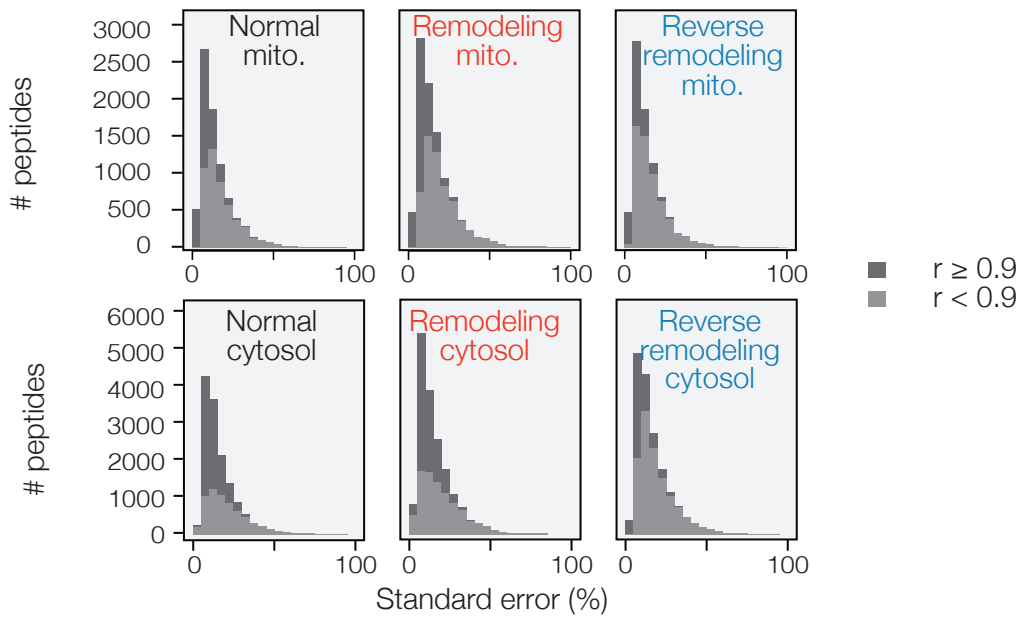
FIGURE 2.9   Peptide kinetic curve fitting quality (standard error)

FIGURE 2.9 shows the quality of fitting seen from standard error of estimate. The second quality filter was introduced because peptides with slow turnover will invariably exhibit poor r values even if they were fitted to the kinetic model reasonably well, since the variance of the data point approaches the variance of the residuals. The inclusion of this alternative criterion boosted the number of confidently quantified peptides by ~5%, as can be seen in the graphs. In each histogram, the dark grey shading represents the corresponding goodness-of-fit of the peptide.
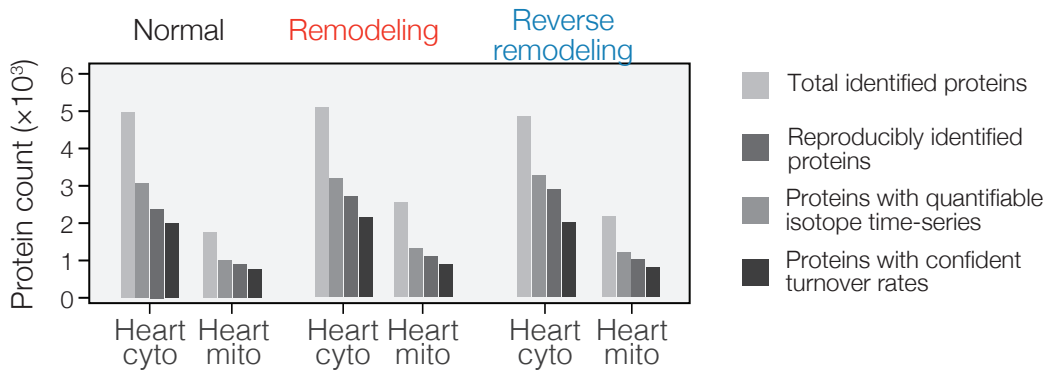
FIGURE 2.10   Number of proteins identified and quantified

FIGURE 2.10 enumerates the total counts of cardiac proteins in the mitochondria and the cytosol for which confident identification and quantification information was acquired. In total, we identified over 5,000 proteins from all three samples, or ~62.5% of the total estimated cardiac proteome (gray tone 1). This number was calculated based on previous detection of approximately 8,000 cardiac transcript with significant expression levels in the mouse heart. Approximately 4,200 total proteins were reproducibly identified independently in at least four time points, which is a prerequisite for kinetic curve-fitting under our quality control filter (gray tone 2). The majority of these proteins were quantified with isotopomer fractional abundance time-series from at least four time points (gray tone 3). The ^2H_2O-labeling MS experiments discovered the in vivo half-life of approximately 3,000 distinct cardiac proteins, including at least 1,078 proteins in the mitochondrial samples, which passed the quality control filters (gray tone 4). This dataset represents the largest collection of protein turnover information in a mammalian organ at the time of writing.
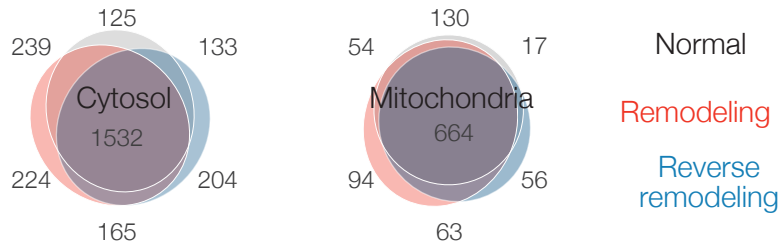
FIGURE 2.11 Venn diagrams of quantified proteins

FIGURE 2.11 depicts two proportional Venn diagrams of proteins with quantified turnover rates in the cytosol (Left) and the mitochondria (Right). In each Venn diagram, in the middle interaction lies the subset of proteins that were quantified across normal (gray), remodeling (red), and reverse remodeling (blue) heart samples. In total, 1,532 proteins were commonly quantified in all three mouse heart samples in the cytosol, and 664 proteins were commonly quantified in the mitochondrial samples. A number of confirmed mitochondrial proteins were also quantified in the mitochondria-depleted cytosol sample.
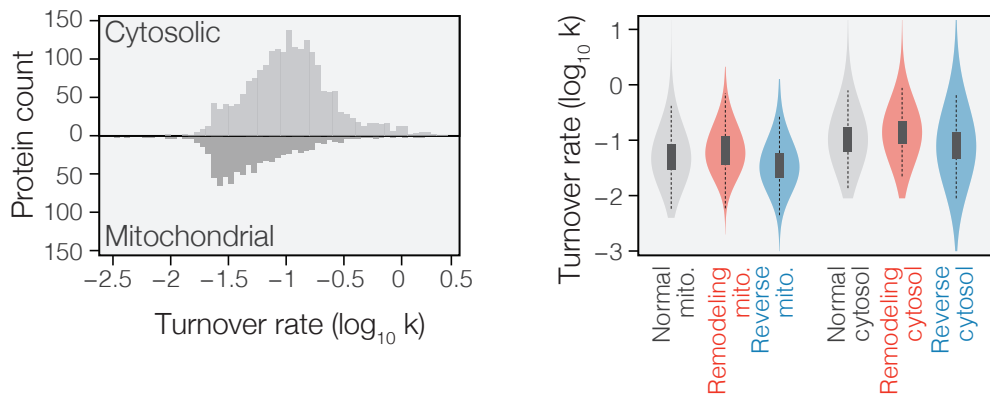
FIGURE 2.12 Range of turnover rates in cardiac cytosol and mitochondria

FIGURE 2.12 portrays the range of measured protein turnover rates in cytosolic and mitochondrial proteins in the normal heart (Left) and in remodeling and reverse-remodeling hearts (Right). (Left) The observed turnover rates were highly diverse and spanned a range >100-fold,

with half-life ranging from less than one day to more than three weeks. Cardiac mitochondria appear to be correlated with additional protein stability. In the normal heart, the average mitochondrial protein pool turned over ≈5% per day (k = 0.045 [0.021 – 0.230] d^{-1}), translating into half-life of ~15 days, in contrast to the average cytosolic protein species, which turned over ~10% per day (turnover rate, k = 0.107 [0.028–0.553] d^{-1}, or half-life of ~6.5 days). (Right) It can be seen that isoproterenol stimulation increases overall protein turnover in the heart. Among the 2,034 protein-pairs we compared between normal and remodeling (isoproterenol-stimulated) hearts, turnover rates during remodeling were on average +1.23-fold of that in the normal heart (5th – 95th percentile: −1.5-fold to +2.9-fold, Mann-Whitney U test P < 2.2 × 10^{-16}), reflecting an increased synthesis and replacement of protein pools during remodeling. Isoproterenol led to increased turnover of 972 proteins (> +1.25-fold), as compared to the decreased turnover of only 216 proteins. Thus isoproterenol treatment largely led to widespread acceleration of protein turnover in the heart. This is in contrast to protein turnover in response to isoproterenol withdrawal, where turnover rates decreased by 1.3-fold compared to normal (5th – 95th percentile: −2.3-fold to +1.3-fold, Mann-Whitney U test P < 2.2 × 10^{-16}).

Although the quartiles of turnover rates in each sample were conclusively measured, it should be noted that the absolute range of protein turnover detected in the organelles depends to a certain extent on the range of sampling time points, for example, if the first designed time point is at 3 days following the start of labeling, then it follows that any protein with a half-life of 15 hours or below would have already plateaued in labels by the time the first sample is collected, and no information regarding its turnover may be discerned other than the minimal limit of its turnover rate. Conversely, if a protein has a half-life in the order of months, then it follows that by 14 days of labeling, the protein pool may not have acquired sufficient label for the MS experiments to differentiate the differences between labeled and unlabeled, or between control and disease. In order to balance the coverage of proteins with the time-scale of the cardiac remodeling model in a 14-day period, preferentially one would wish to complete sample collec-

tion within a particular period of remodeling such that the system has not changed such drastically during labeling to complicate anyalysis.

Nevertheless, the quantitation data provided much expanded coverage of major protein pathways in the cardiac cytosol and the mitochondria. For instance, we discovered the turnover rate of 80 out of 95 respiratory chain subunits, 63 out of 79 eukaryotic ribosome subunits, and all core 20S proteasome subunits in at least one experimental condition. Heterogeneous temporal kinetics could be observed across molecular weight, isoelectric points, and other biophysical parameters, consistent with previous results presented in Chapter II.

As was described in Chapter II, we observed that turnover rates clustered with protein localizations and complex associations, which further underscores the regulation of protein turnover cellular parameter.
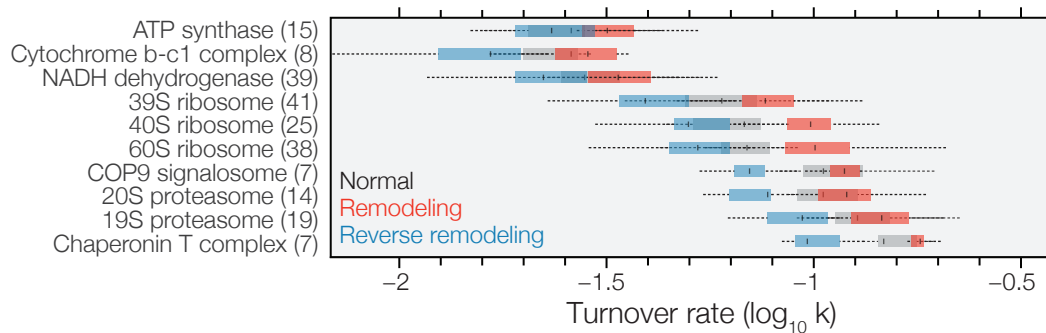
FIGURE 2.13   Turnover dynamics of protein categories

FIGURE 2.13 is a box-and-whisker graph of the distribution of protein turnover rates of a number of established protein complexes both in the mitochondria (ATP synthase, cytochrome b-c1 complex, NADH dehydrogenase, 39S ribosome) and in the cytosol (COP9 signalosome, 20S/19S proteasome, 40S/60S ribosomes, chaperonin T complex). It can be seen that proteins forming a single complex tend to have clustered turnover rates, and, also react to isoproterenol

challenge in characteristic manners. Mitochondrial ribosomes exhibited particularly elevated turnover during remodeling (red boxes) over normal hearts (gray boxes). All protein complexes exhibited decreased turnover during reverse remodeling following isoproterenol withdrawal (blue boxes). Box: interquartile; whiskers: 1.5× interquartiles.

The proteins with significant changes after isoproterenol treatment belong to at least 35 over-lapping biological processes that present promising targets for further studies.

GO Biological Process	Protein count	% of proteome	Fisher's Exact test P	Benjamini-Hochberg P
Monosaccharide metabolic process	23	5.2	9.2E-10	1.1E-6
Generation of precursor metabolites and energy	27	6.1	9.8E-10	1.9E-6
Regulation of cellular component organization	28	6.3	3.9E-8	2.1E-5
Protein metabolic process	108	24.3	1.6E-7	3.0E-5
Cellular carbohydrate metabolic process	27	6.1	1.2E-7	3.7E-5
Alcohol catabolic process	12	2.7	9.3E-8	6.0E-5
Carbohydrate catabolic process	13	2.9	1.5E-7	7.1E-5
Intracellular transport	30	6.7	9.6E-7	1.4E-4
Regulation of organelle organization	17	3.8	5.3E-7	1.4E-4
Negative regulation of cellular component organization	13	2.9	8.0E-7	2.2E-4
Regulation of protein complex assembly	11	2.5	8.1E-7	2.5E-4
Carbohydrate metabolic process	30	6.7	2.8E-6	2.8E-4
Regulation of protein complex disassembly	9	2	1.3E-6	4.4E-4
Cofactor metabolic process	17	3.8	5.4E-6	6.9E-4
Regulation of actin filament-based process	10	2.2	3.5E-6	7.7E-4
Complement activation	8	1.8	3.1E-6	9.3E-4
Negative regulation of protein complex assembly	7	1.6	4.3E-6	1.5E-3
Protein localization	39	8.8	3.1E-5	1.6E-3
Regulation of cellular component biogenesis	11	2.5	1.9E-5	2.4E-3
Heterocycle metabolic process	20	4.5	6.3E-5	4.1E-3
Transport	88	19.8	1.4E-4	4.6E-3
Negative regulation of protein complex disassembly	7	1.6	2.7E-5	5.2E-3
Establishment of localization in cell	32	7.2	1.3E-4	5.3E-3
Protein transport	33	7.4	1.9E-4	7.5E-3
Humoral immune response	8	1.8	7.1E-5	8.1E-3
Establishment of protein localization	33	7.4	2.3E-4	8.4E-3
Cellular macromolecule localization	19	4.3	3.4E-4	1.5E-2
Regulation of cellular component size	13	2.9	3.0E-4	1.6E-2
Negative regulation of organelle organization	8	1.8	1.9E-4	1.7E-2
Cytoskeleton organization	19	4.3	9.1E-4	3.1E-2
Positive regulation of organelle organization	7	1.6	3.7E-4	3.2E-2
Regulation of localization	22	4.9	9.7E-4	3.2E-2
Homeostatic process	28	6.3	1.4E-3	3.7E-2
Positive regulation of immune response	11	2.5	8.5E-4	3.8E-2
Positive regulation of response to stimulus	13	2.9	1.2E-3	4.3E-2

TABLE 2.1   **Biological processes with altered turnover in remodeling**

TABLE 2.1 lists 35 biological processes (Gene Ontology Biological Processes level 3) that are enriched with proteins exhibiting significant changes in protein turnover during cardiac remodeling. The number of proteins with each category and the significance of the enrichment (Fisher's exact test P and Benjamini-Hochberg adjustment P) are shown. Among the enriched biological processes are many that are associated with cardiac mitochondria including protein metabolic processes and organelle organization, including protein metabolic process, co-factor metabolic process, and organelle organization. The broad range of processes involved indicates that the remodeling heart is associated with widespread changes in protein kinetics.

Altogether, these results widen the existing catalog of in vivo protein kinetics information considerably. Despite that the cardiac proteome does not remain constant during remodeling, the nonlinear kinetic model employed here to calculate turnover rates precisely represented the majority of protein turnover behaviors, suggesting the changes in protein pools occurred gradually and was amenable to longitudinal modeling. The global increases in turnover were specific and could not be explained by sample bias, because global plasma protein turnover from the same animals did not elevate after adrenergic stimulation, and there were also proteins that exhibited retarded turnover in the remodeling heart (< -1.25-fold).

We then analyzed the turnover data to determine what implications they may have for overall mitochondrial dynamics in the remodeling heart. Notably, the ratio of changes in mitochondrial protein turnover in remodeling vs. normal hearts were overall quite similar in magnitude and distribution to changes in cytosolic proteins. Continuing on the discussion in Chapter I regarding the observations that the mitochondrial proteome do not turn over only as a unit, autophagy can remove whole mitochondria and synchronize turnover, and alterations in the rate of autophagy could have a drastic effect on the turnover rates of all mitochondrial proteins. Certain specific impairments of proteolysis could also lead to such global effects, e.g., if proteasomal removal of mitofusin is inhibited. Nevertheless, the data appear to continue to support the idea that regulatory mechanisms of individual protein turnover predominate. If protein dynamics were purely driven by increased mitophagy and/or mitochondrial biogenesis, one may expect that all mitochondrial proteins would simply shift linearly, elevating in their turnover rates by the same ratio. In reality, the impact of remodeling on individual-protein turnover can be distinguished as individual deviations from the population average.

One important consideration is whether the measured mitochondrial protein turnover rates reflect any "bottleneck" effect due to slow import of proteins into the mitochondria or incomplete equilibrium between cellular compartments. Previous investigations in HeLa cells in vitro

suggest that variations may exist between the turnover rates of identical protein species in different subcompartments, which may be due to non-exchanging subpopulations. For example, in HeLa cells certain ribosomal subunits have half-life of ~6 hours in the nucleolus but >30 hours in the cytosol (Boisvert et al., 2012). Hence to evaluate whether the rates of protein import into cardiac mitochondria may present a bottleneck for isotope incorporation and lead to inaccurate measurements of protein replacement inside mitochondria, I first compared the turnover rates of mitochondria-targeted proteins measured in the mitochondria and their cytosolic milieu. Such analysis is predicated on the precise isolation of compartment. Our differential centrifugation protocol has been well validated in the Ping lab over the last decade and the purity of isolated mitochondria have been verified using protein compartment markers and electron microscopy, as reviewed in (Zhang et al., 2012).
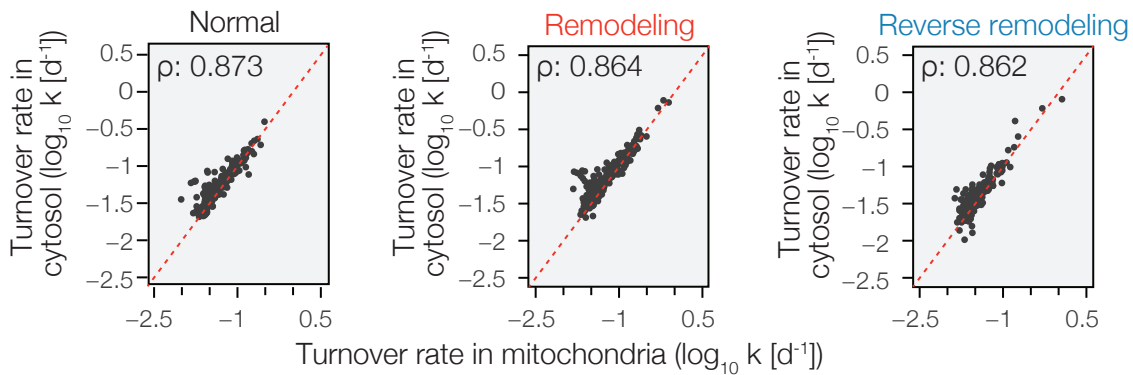
FIGURE 2.14   Mitochondrial protein turnover in mitochondria vs. cytosol

FIGURE 2.14 plots the turnover rates of mitochondrial-targeted proteins measured in purified mitochondrial samples, against the turnover rates of the same proteins measured in mitochondria-depleted cytosolic samples. Data from normal hearts (left), remodeling hearts (middle), and reverse remodeling hearts (right) are shown. Each data point represents a distinct protein. Abscissae represent turnover rates in the mitochondrial samples; ordinates represent turnover rates measured in cytosolic samples. ρ: Spearman's correlation coefficient. In most cases, the proteins shared similar turnover rates when detected from either localization. Although isopro-

84

terenol stimulus exerted differential effects on the turnover rates of a small number of proteins in the cytosol versus the mitochondria (Kolmogorov-Smirnov test $P \leq 7.3 \times 10^{-4}$), as a whole there is limited evidence to suggest a disequilibrium between the mitochondrial-targeted protein populations inside and outside of mitochondria, or that lapses in import would constrain mitochondrial protein pool replacement within the measured time period.

In contrast to proteins that are conventionally assumed to be primarily mitochondrial in target localization (e.g., most respiratory complexes), some proteins that are known to reside in multiple compartments do in fact show differential turnover rates from the cytosolic and mitochondrial preparations, which may reflect their compartment-specific turnover. For instance, in addition to forming the gap junctions at the intercalated disks between two adjacent cardiomyocytes, connexin 43 (Cx43/GJA1) also localizes to cardiac mitochondria where the protein forms hemichannels on the mitochondrial inner membrane and potentially contributes to mitochondriak K^+ influx (Miro-Casas et al., 2009). From our dataset, we observed that the cytosolic population of Cx43 turns over significantly faster (k: 0.127 +/- 0.025 d^{-1}) than the mitochondrial population (k: 0.069 +/- 0.013 d^{-1}). The mitochondrial and cytosolic populations also respond to isoproterenol differently, being up-regulated at 1.22-fold in the cytosol (Mann-Whitney U test P: 0.03) but 1.60-fold in the mitochondria (Mann-Whitney U test P: 7.0×10^{-6}), respectively. A similar observation was made for fatty acid transport protein 1 (FATP1/SLC27A1), a long-chain fatty acid transporter with potentially multiple subcellular localizations (Guitart et al., 2014), from which we measured cytosolic k: 0.130 +/- 0.062 d^{-1}, and mitochondrial k: 0.068 +/- 0.021 d^{-1}.

Interestingly, the data also suggest that the cytosolic and mitochondrial populations of Cx43 are not in equilibrium with one another (and likewise cytosolic and mitochondrial FATP1). To illustrate, contrast the differences in measured turnover rates with the cases of hexokinase I (HK1) and hexokinase II (HK2). HK1 is thought to be stably located on the mitochondrial outer

membrane surface, and has turnover rates that are typical of a mitochondrial protein when measured from either mitochondrial or cytosolic preparations (k: 0.032 +/- 0.006 d^{-1} and 0.042 +/- 0.006 d^{-1}, respectively). HK2, on the other hand, translocates dynamically between the mitochondrial surface and cytosol according to glucose metabolic status (John et al., 2011). Consistently, we observed that HK2 has turnover rates that are typical of a cytosolic protein when measured from either mitochondrial or cytosolic preparations (k: 0.137 +/- 0.037 d^{-1} and 0.120 +/- 0.018 d^{-1}, respectively).

Mitochondrial dynamics, including biogenesis, fusion-fission cycles, and autophagy play critical roles in cardiac functions (Dorn 2nd, 2013; Gottlieb and Gustafsson, 2011). We previously observed diverse and asynchronous mitochondrial protein turnover in the normal mouse heart that led us to conclude that the turnover of individual proteins can influence the homeostasis and dynamics of mitochondria (Kim et al., 2012; Lau et al., 2012). Consistent with this notion, we found complex and bidirectional kinetic responses among individual mitochondrial proteins in the remodeling heart. Whereas some proteins related to mitochondrial dynamics exhibited accelerated turnover (MIRO1/2, LONP1, PHB), others remained unchanged (MFN1/2, FIS1). The case of MIRO1 and MIRO2 are particularly noteworthy; both are atypical rho GTPases best known to be involved in anterograde mitochondrial transport along microtubules in neurons via their association through Milton/TRAK1 to kinesin. Transcript profiling experiments suggest that MIRO1/2 are highly expressed in the heart, but their functions are unclear. Our data show that they are prominently and significantly altered in protein turnover after isoproterenol, suggesting they may function in orchestrating cardiac remodeling through unknown mechanisms.

In general, we observed differential response amongst distinct proteins to cardiac remodeling. This heterogeneity is apparent on individual protein level, and applies to the subunits of supramolecular complexes. Although most respiratory chain components exhibited modestly

elevated turnover, we observed heterogeneity in turnover rates among subunits and sub-complexes.
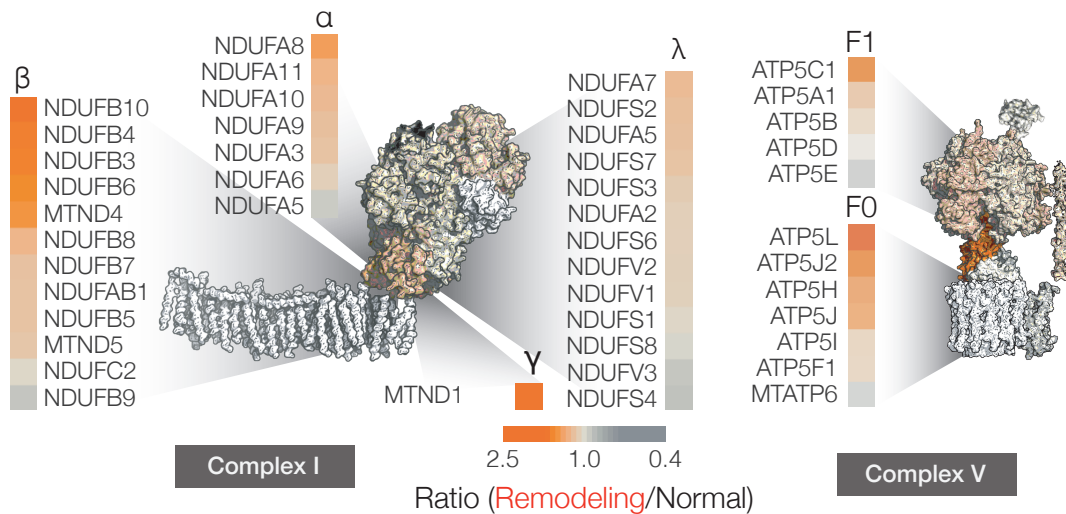
FIGURE 2.15   Protein dynamics of respiratory subunits

FIGURE 2.15 demonstrates how particular subunits of mitochondrial proteins respond preferentially to cardiac remodeling. (Left) In complex I, the membrane-embedded β sub-complex was independently influenced by remodeling than the rest, whereas the F_0 subunits of the complex V were similarly enriched for elevated turnover. The color of the box each subunit corresponds to heat map representations of turnover ratios in remodeling hearts over normal he arts. The structure of each subunit was colored identically when applicable; some subunits were not quantified or were not present in the crystal structure. In ETC complex I, the membrane-embedded beta sub-complex was particularly elevated in turnover when compared to the other sub-complexes, whereas in ATP synthase, the F_0 subunit was similarly enriched for elevated turnover. The results further demonstrate that mitochondrial proteins are under independent control of different regulatory elements during proteome remodeling, highlighting the added insights to organelle dynamics from the analysis of protein kinetics at individual-protein resolution.

The heterogeneity of turnover response to cardiac remodeling was also evident on pathway levels, in particular among metabolic and proteostatic proteins. I examined the alterations in turnover rates among three metabolic pathways in and out of mitochondria (fatty oxidation, branched-chain amino acid metabolism, and glycolysis).
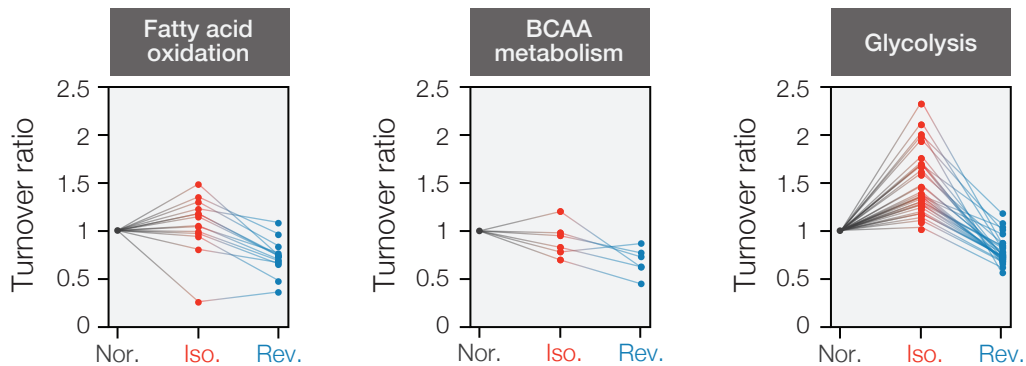
FIGURE 2.16   Protein dynamics in cardiac metabolic pathways

FIGURE 2.16 shows parallel plots of protein dynamics behaviors of a number proteins belonging to three metabolic pathways (fatty acid oxidation, branched-chain amino acid (BCAA) metabolism, and glycolysis) both within and without cardiac mitochondria. Each data series (line) represents the behavior of a distinct protein in normal, remodeling, and reverse remodeling hearts; ordinates represent the ratio of turnover rates when compared with the normal heart. It can be seen that unlike proteins belonging to fatty acid oxidation and branched-chain amino acid metabolism, glycolytic enzymes were highly and significantly elevated in turnover dynamics in adverse cardiac remodeling. The accelerated turnover reverted to normal in reverse remodeling following isoproterenol withdrawal.

To some extent, changes in turnover of these pathways paralleled the molecular phenotypes of the remodeling heart, which increases in glycolytic usage. It has long been known that the rate of glycolysis is accelerated early in cardiac remodeling (Allard et al., 1994; Kolwicz Jr. and Tian, 2011) as the heart shifts its fuel consumption from primarily fatty acid to primarily carbohydrates. However, a large number of protein and transcript expression studies have failed to convincingly show that there is a concomitant increase in protein abundance of glycolytic enzymes in the remodeling heart (van Bilsen et al., 2004; Dai et al., 2013; Kolwicz Jr. and Tian, 2011; Petrak et al., 2011), which has led to speculations that additional regulations than expression level may be responsible for the increased glycolysis (e.g., glucose import, allosteric regulation, post-translational modification). Our data demonstrate a highly and significantly accelerated turnover in glycolytic enzymes in the isoproterenol-challenge model, indicating accelerated replacement of glycolytic enzymes may constitute one level of regulation. The observed kinetic changes were not confined to a few rate-limiting enzymes but were virtually ubiquitous along the glycolytic pathway, e.g., the half-life of hexokinase 1 (HK1) decreased from 16.7 to 9.8 days in the remodeling heart (measured in the cytosolic sample), that of glyceraldehyde-3-phosphate dehydrogenase (GAPDH) decreased from 10.8 to 6.7 days, and that of phosphoglycerate mutase 1 (PGAM1) decreased from 12.2 days to 6.9 days. Mass spectrometry quantitation and immunoblotting data suggest that the abundances of these proteins are relatively unchanged (vide infra). Assuming increased turnover but unchanged abundance, it could be deduced that proteome remodeling increased both synthesis and degradation of glycolytic enzymes, replacing the protein pools at a higher rate.

The data indicate that concomitant with increased glycolysis, the remodeling heart exhibits higher turnover of glycolytic enzymes. We postulate that may explain the higher turnover rate is that faster protein pool replacement is necessary to remove damaged proteins and maintain enzyme pool efficiency. It is known that certain glycolysis enzymes including triosephosphate isomerase (TPI) are irreversibly damaged during catalysis through arginine deamidation and

possible racemization of the reaction center (Hipkiss, 2011). The turnover rates of the enzyme pools could therefore place an indirect limit on fuel consumption in the diseased heart by regulating the proportion of functional glycolytic enzymes in the protein pool. Faster replacement of enzymes may constitute a new type of cardiac response to metabolic demands. Future experiments may test this hypothesis by examining in vitro enzyme function and modifications; for example, it will predict higher in-vitro glycolytic rates in systems where the enzymes are artificially replaced periodically, and that higher arginine deamidation may be observable in other systems with high glycolytic rates if turnover is not accelerated in compensation. Several potential reasons may be conjectured as to why the remodeling cardiac cell may prefer to increase protein turnover over simply producing a larger enzyme pool. Maintaining a moderate total enzyme pools may allow higher speed and finesse in controlling maximal reaction rates. How this system may exert its effect alongside the well characterized allosteric control of glycolytic enzymes will be an interesting topic, given that metabolite binding may in turn also modulate the rate of protein degradation and turnover, as has been witnessed in the cases of ferritin and tryptophan oxygenases.

In contrast to glycolytic enzymes, mitochondrial metabolic pathways behaved quite differently. Fatty acid oxidation proteins had much more subdued changes following isoproterenol. In conjunction with the commonly observed decrease in their abundance in the remodeling heart, the protein dynamics data are consistent with a scenario where decreased synthesis of the fatty acid enzyme drove the decrease in fatty acid oxidation capacity. A notable exception is that of the fatty acid importer CD36, where increased turnover (+1.5-fold) in the remodeling heart instead suggests it may be regulated primarily by proteolysis. Branched-chain amino acid metabolism proteins exhibited lower turnover relative to the proteome, again illustrating that isoproterenol stimulus exerts differential kinetic regulations on multiple metabolic pathways.

Overall, widespread alterations to individual protein turnover can be observed in both the cytosol and the mitochondria. One possible treatment of these data is that one can embark on a search of proteins that show exceptional changes in protein turnover, which may be inferred to be particularly associated with disease progression because their behaviors are specifically modified during remodeling. This is the same interpretation that underlies many experiments aimed at the measurements of transcript and protein abundance (most up-regulated or down-regulated proteins within a system may be associated with disease). We found that in particular protein species indeed displayed much more elevated turnover rates than the population average. Some proteins were turned over up to 3 times as fast as in the normal heart, whereas other proteins turned over as much as 50% slower.

Cytosolic proteins		k	FC	*P*	Pct	Function/ disease association
FBN1	Fibrillin-1	0.009	6.89	5.0E-3	99	Mut. in Marfan syndrome
FHL1	Four-and-a-half LIM domains 1	0.078	3.56	1.0E-3	99	Mut. in heart failure
ANXA2	Annexin II	0.042	3.01	4.0E-5	98	Membrane remodeling
VIM	Vimentin	0.091	2.50	1.8E-2	97	Stabilization of intracellular architecture
DES	Desmin	0.100	2.50	1.0E-2	97	Mut. in familial ventricular myopathy
TGM2	Transglutaminase 2	0.066	2.06	4.0E-3	94	Apoptosis; overexpressed in heart failure
COL15A1	Collagen XV/ endostatin	0.047	2.00	4.0E-3	93	Extracellular matrix remodeling
TPM4	Tropomyosin 4	0.143	1.94	2.0E-3	92	Contractility
ANXA5	Annexin V	0.065	1.89	1.0E-3	91	Membrane remodeling
ATP1A1	Na+/K+ ATPase alpha-1	0.052	1.82	1.0E-4	90	Contractility; Mut. in hypertension
XIRP1	Xin actin-binding repeat 1	0.252	1.69	4.0E-2	85	Cardiac myogenesis
Mitochondrial proteins						
HK1	Hexokinase-1	0.032	2.08	1.0E-6	96	Glycolysis
ALDH1B1	Aldehyde dehydrogenase X	0.038	1.83	6.0E-3	93	Aldehyde catabolism
PHB	Prohibitin	0.024	1.79	6.0E-3	92	Mitochondrial remodeling
MRPL40	39S ribosomal protein L40	0.049	1.57	1.0E-2	87	Mut. in Velo-Cardiao-Facial Syndrome

TABLE 2.2   Example proteins with conspicuous turnover changes

TABLE 2.2 lists a number of representative proteins with conspicuous turnover behaviors that may be identified as candidate markers of disease association in the cytosol and in the mitochondria. Selected proteins and their turnover rates (k), fold-change in turnover during remodeling vs. in the normal heart (FC), Mann-Whitney U test significance between turnover in normal

and remodeling hearts (*P*), rank percentile amongst all turnover changes within a sample (Pct), and known disease associations are shown. In the mitochondria, change in hexokinase-1 turnover was particularly pronounced as discussed, as was that of the mitochondrial 39S ribosome subunit MRPL40. Outside the mitochondria, the turnover elevations were notably pronounced in the calcium-dependent membrane-binding proteins in the annexin family. Among the eight annexins quantified, all but two displayed significantly accelerated replacement in the protein pool. ANXA2/3/4/5 changed most prominently in the remodeling heart cytosol (+1.7 to +3.0 fold, 86th – 98th percentile rank), translating for example into a decrease of ANXA2 half-life from 16.7 to 5.5 days, whereas ANXA6 and ANXA7 were also significantly elevated (+1.4-fold). ANXA2 and ANXA5 are widely known to have elevated transcript and protein levels in heart failure patients (Benevolensky et al., 2000; Song et al., 1998), but consensus is lacking on the other isoforms. The broadly increased kinetics among six isoforms provides new evidence that annexins may be generally associated with cardiac remodeling and hypertrophy. Importantly, the data also revealed proteins with significantly elevated turnover that were not previously associated with cardiac remodeling, both within mitochondria and in the cytosol. These putative remodeling proteins belong to diverse functional processes, including extracellular matrix remodeling (e.g., VIM1, COL15A1), mitochondrial remodeling (PHB), and excitation-contraction coupling (e.g., TNNC1, ATP1A1, RYR2). Several proteins (e.g. FHL1, XIRP1, MRPL40) are known to be mutated or deleted in congenital heart diseases, and thus may be promising candidate hypertrophy drivers (Gaussin et al., 2003; Sheikh et al., 2008).

With validation experiments that will be proposed in Chapter IV, it will be of interest to determine whether these proteins are novel disease drivers discovered via their temporal behavior. Prior to that, however, we first determined whether some of the proteins revert in turnover changes during isoproterenol-withdrawal, as a differential to shortlist our list of potential disease proteins, i.e., a bona fide disease driver with elevated turnover during remodeling is more likely to show decreased protein turnover following the withdrawal of isoproterenol stimulus,

when the mouse hearts undergo recuperative reverse remodeling accompanied by reversed changes in cardiac functions and reduced hypertrophy. The biomolecular changes of reverse remodeling per se are also of broad interest to cardiac research, as they are considered more clinically relevant targets for interventions that are aimed at halting or reversing human heart failure. Understanding how molecular dynamics changes in reverse remodeling such as during LVAD-mediated mechanical unloading in human patient is also being investigated for its potential to identify a new generation of therapeutic targets, understand the recuperative mechanism of mechanical unloading, and justify the use of LVAD as a destination therapy. We therefore examined whether the reverse remodeling process is indeed a passive reversal of the remodeling process, i.e., whether elevated protein turnover during remodeling exhibited the a commensurate but opposite change in turnover rates during reverse remodeling.
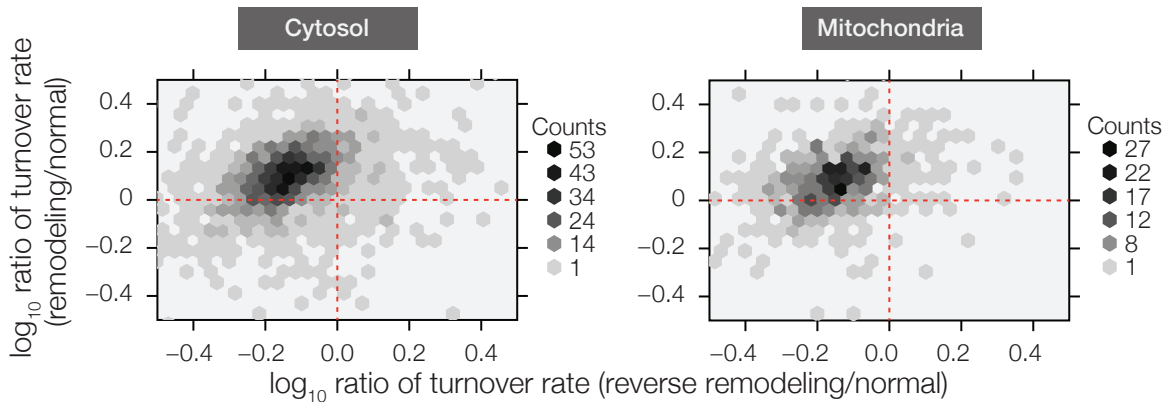
FIGURE 2.17   Protein dynamics in reverse remodeling

FIGURE 2.17 plots the changes in protein turnover during remodeling and reverse remodeling over all compared protein-pairs. Data from cytosolic (Left) and mitochondrial (Right) proteins are shown. The color of each bin represents the density of individual protein data points in a particular area in the Cartesian coordinate, with the abscissae being the ratios of turnover rates of proteins in reverse remodeling when compared to their turnover in the normal heart, and the ordinate comparing remodeling and normal hearts. It can be seen that not all changes in pro-

tein dynamics simply reverted towards that of the normal heart. Based on the directions of kinetic changes following chronic β-adrenergic stimulation and its subsequent withdrawal, the kinetic behaviors of proteins can be categorized into four quadrants. For the most part, proteins with elevated turnover during remodeling exhibited lower turnover during reverse remodeling (upper left quadrant). However, proteins which showed decreased turnover during remodeling for the most part did not exhibit any compensatory increase in turnover during revere remodeling (lower left quadrant). Some proteins appeared to have increased turnover in both remodeling and reverse remodeling (upper right quadrant). This trend was observed in both mitochondrial and cytosolic proteins, which may be interpreted to suggest that total mitochondrial protein dynamics did not deviate from the whole-heart average significantly during reverse remodeling, as might have been expected if reverse remodeling were associated with massive alterations in mitochondrial biogenesis or mitophagy. (Right) Mitochondrial proteins likewise showed the diverse changes during in remodeling and reverse remodeling, and did not cluster to any single quadrants.
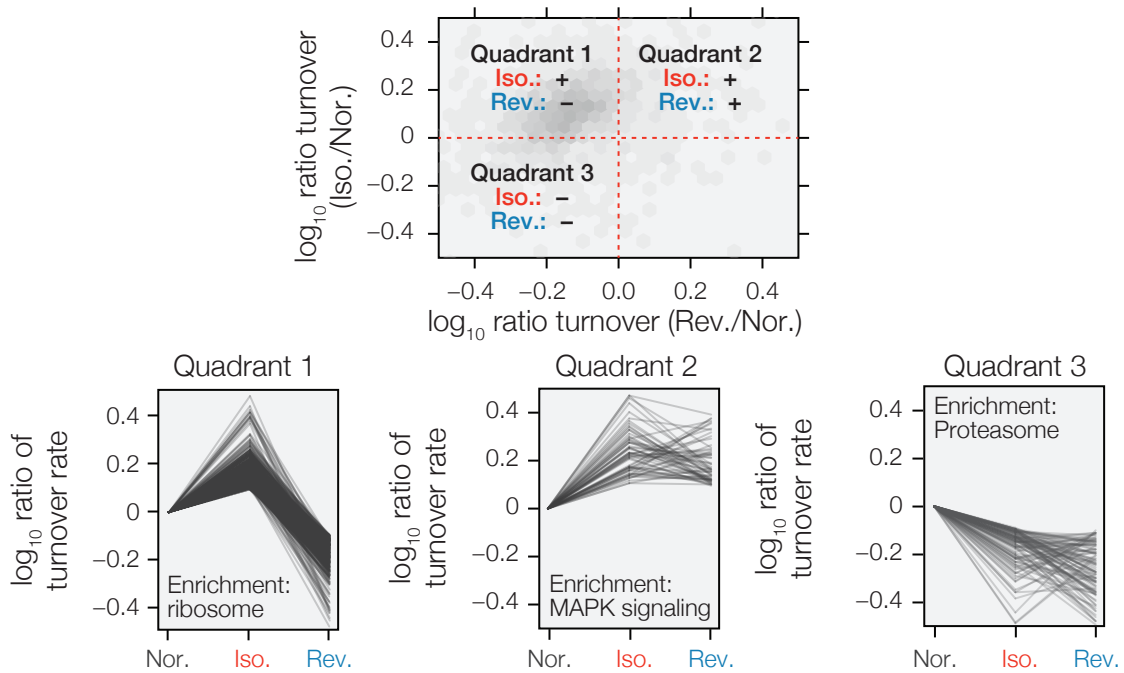
FIGURE 2.18   Protein dynamics in reverse remodeling (continued)

94

FIGURE 2.18 shows the functional enrichment of proteins with different behaviors in remodeling and reverse remodeling. (Top) The quantified proteins were separated into three groups corresponding to the shown quadrants. (Bottle left) In the first group, reverse cardiac remodeling largely overturned the elevated kinetics of proteins observed during remodeling, in synchrony with the increase and subsequent decrease in heart weight. This group encompasses most proteins including the glycolytic enzymes, but was most prominently enriched for ribosome subunits (Fisher's exact test, $P \leq 8.6 \times 10^{-7}$; Benjamini-Hochberg adjustment $P \leq 6.9 \times 10^{-4}$). (Bottom center) The second group of proteins displayed elevated kinetics in β-adrenergic stimulation that were sustained in reverse remodeling. This group can be functionally distinguished from the first by its significant enrichment of MAPK signaling proteins (Fisher's exact test $P \leq 6.3 \times 10^{-5}$; Benhamini-Hochberg adjustment $P \leq 0.039$), including RAC1, MAPK1, MAP2K2, MAP2K3, and STAT1. (Bottom right) Relatively few proteins showed decreased turnover throughout both remodeling and reverse remodeling, a group suggestively enriched for proteolysis pathway proteins ($P \leq 9.2 \times 10^{-4}$, Fisher's exact test). Other notable proteins in this uncommon category include the nicotinamide nucleotide metabolism enzymes NNT and NAMPT, which participate in mitochondrial NAD^+-mediated protein acetylation and metabolic regulations. Only nine proteins had decreased turnover in isoproterenol treatment but increased turnover in reverse remodeling, including some likely plasma contaminants but also thioredoxin-interacting protein (TXNIP) (remodeling: −3.03-fold, reverse remodeling: +2.08-fold), a protein involved in regulating glucose mechanism and not quantified in the plasma sample. The statistical enrichments underline that imbalance between protein synthesis and degradation is a prominent feature of cardiac remodeling, and that recovery may involve the sustained elevation of particular branches of MAPK signaling. Altogether, these results demonstrate the insights that may be acquired from turnover studies to support new hypotheses and investigations regarding recovery from adverse remodeling.

A relevant question is what may cause changes in turnover rate of a particular protein in disease. During disease development, where cellular components change from one state to another that is defined by different compositions, many substrate-level mechanisms can modulate the commitment step of protein degradation for a particular proteins; e.g., enzyme-substrate interactions, post-translational modification of degron sequences, and other modulations of E3 ligase binding, etc.; and many more mechanisms for protein synthesis. At the minimum, however, it would be of interest to determine whether alterations of protein turnover are driven primarily by alterations in synthesis or degradation.

Orthogonality of protein expression and dynamics

Protein synthesis is commonly explored via microarray studies, which makes the assumption that transcript abundance indirectly represents protein synthesis. However, data interpretation is often made ambiguous by the imperfect correlation between mRNA and protein abundance (Ideker et al., 2001; Maier et al., 2009; Taniguchi et al., 2010). As it is thought that such discrepancy could in part be reconciled by supplying the altered rates of proteolysis (Vogel and Marcotte, 2012), we first examined whether protein abundance and protein expression are themselves inter-correlated parameters. As discussed, a measurable change in protein turnover may be indicative of a number of possible pathophysiological scenarios. In the most straightforward scenario, one may expect the particular protein to have changed in abundance correspondingly, such that the increase in isotope incorporation simply reflects the outcome of increased protein expression and synthesis. Ample scenarios also exist, however, where the turnover cycle can permute without conspicuous net differences in protein abundance, such as when increased degradation counterpoises increased synthesis, as is likely for a number of glycolytic enzymes as presented earlier in this chapter. This point is also consistent with the poor overlap between the list of kinetically regulated proteins discovered here and the differen-

tially expressed proteins from large-scale protein abundance profiles of the failing heart in the literature, e.g., in References (Lindsey et al., 2006; Petrak et al., 2011).

In theory, a disease sample in which both abundance and dynamics alters violates the assumption of the steady state protein pool for inferring protein turnover rates from isotope incorporation. To circumvent this problem, one may opt to forego the parametrization of the turnover rate constant, and simply look for proteins that differ significantly in their isotope incorporation at different time points. This approach was employed by Marc Hellerstein and colleagues to examine axonal transport kinetics in the cerebrospinal fluid of neurodegenerative disease patients (Fanara et al., 2012). An obvious advantage of this method is that one may identify proteins whose turnover conforms to first-order kinetics in the normal sample but no longer does so in disease. The lack of turnover rate constant results, however, makes quantitative comparisons across datasets problematic.

Alternatively, analytical methods that take into account changes in both protein abundance and protein turnover may be employed to differentiate changes in protein synthesis from the total turnover changes. For example, Jayapal et al. made use of an additional chemical labeling step with isobaric tags for more accurate quantification of overall protein abundance at different time points of development (Jayapal et al., 2010). The true fractional synthesis of the protein pool could thus be calculated by considering both the raw amount of label that has been incorporated into the protein pool with the final proportion of labeled proteins at a time point. However, the use of isobaric tags tends to lower the coverage protein identification and quantification and thus was not considered here.

Our solution is to simply search for proteins that exhibit altered protein turnover rate constants when considering only proteins to which a kinetic curve continues to fit well even during disease development, whilst acknowledging that some inaccuracies may result. This is the prima-

ry approach we have taken here. A potential drawback of this approach is that some proteins of interest will be excluded from the filtered dataset that may exhibit abrupt changes in isotope incorporation during disease development that no longer conforms to the expected first-order kinetic curve. It may be possible to re-analyze the data to search for such proteins that do not conform to the first-order kinetics curve in specific manners when more sophisticated analytical workflows become available.

To compare the protein dynamics data with the changes in protein expression over the course of isoproterenol challenge, we acquired of both protein expression and protein dynamics information from the same mass spectrometry data without additional experimentation. Changes in protein abundance were acquired by comparing relative abundance level between day 14 of isoproterenol treatment and the day 0 (normal) sample using two common label-free quantitative MS methods: spectral counting (Huttlin et al., 2010; Xu et al., 2006) as implemented in ProLuCID and DTASelect, and iBAQ-normalized peptide area-under-peak intensity quantification (Nagaraj et al., 2011; Schwanhausser et al., 2011) as implemented in ProTurn. Spectral counting quantification assumes that a protein species with higher natural abundance in a protein mixture will result in more identifiable peptides in an MS experiment after normalizing for the protein sequence length, assuming the observability differences between peptides of different proteins cancel each other on a large scale. The iBAQ-based peak area intensity comparison method calculates protein abundance based on the sum of integrated peak areas of all the peptides identified to the protein species, after normalizing for the theoretical number of observable tryptic peptide sequences (with lengths between six and twenty-five amino acids) of each protein. Although dual labeling experiments using ^2H_2O and SILAC mice, three-label SILAC amino acids, or post-extraction chemical labeling have been demonstrated (Jayapal et al., 2010; Kristensen et al., 2013; Price et al., 2012b), after careful considerations we have decided upon label-free quantification to balance accuracy with coverage and throughput. Although an isotope-labeled approach may have improved the accuracy of label-

ing, isotope tags could create separate isotope clusters and thus essentially double the complexity of the sample and reduce protein identification coverage. In some cases such as using isobaric tags or $H_2^{18}O$ labels, the resulting isotope signatures would alter or overlap with the first isotope cluster after ^2H_2O labeling and is incompatible with the objective of measuring fractional synthesis from isotope abundance, necessitating two individual sets of mass spectrometry analysis and thus doubling the amount of time required for experimentation. The ability to quantify a tagged peptide is also stochastic to some degree, leaving only the overlapping set of proteins with quantified abundance and turnover as useful results. Lastly, it is unclear if an isotope tagging approach does outperform label-free quantification in detecting subtle changes in quantity, as it is unusual for proteins with subtle changes in abundance to reach statistical significance without high numbers of replicates in most protein quantification studies.

The results showed that data spectral counting and area-under-peak intensity quantification generally correlated with one another, though not without significant variability between the two methods. Here only comparisons against area-under-peak quantification datasets are shown, with the consideration that the quantification data are based on the identical integration results used by ProTurn to calculate protein isotope incorporation and turnover, and so the two ought to be more directly comparable.
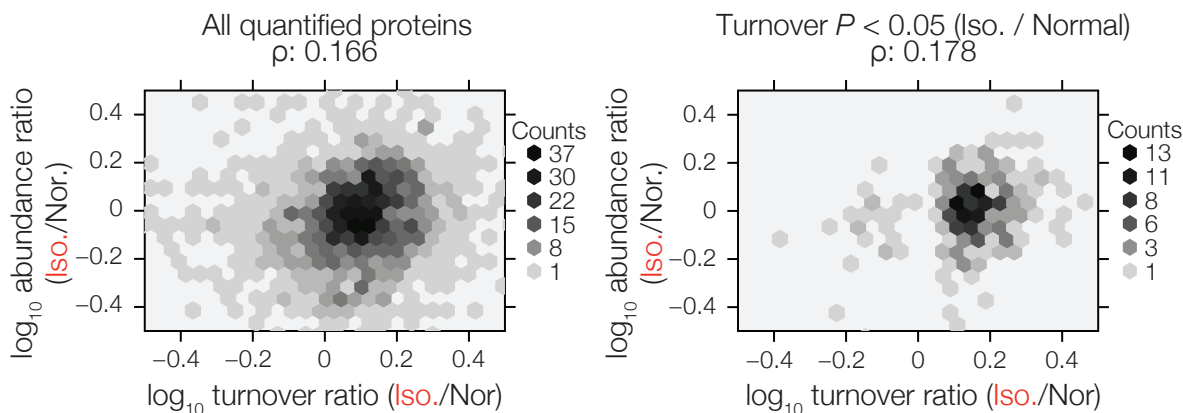
FIGURE 2.19   Non-correlation between protein abundance and dynamics

FIGURE 2.19 is a hexagonal bin plot that describes the relationship between the changes in expression and temporal dynamics of cardiac proteins following isoproterenol challenge. On the left panel, results from 1,771 quantified cardiac proteins are shown, whereas the right panel shows the results from only 232 of the proteins with the most significant differences in protein dynamics between isoproterenol-challenged and control mice. Data points that appear in proximity to each other on Cartesian coordinates are binned together into a hexagonal region, the data density of which are represented by the fill saturation scale (darker equals more data points). It can be seen that in both panels, significant, comparable data point densities are scatted in both the upper right and lower right quadrants, demonstrating that proteins with increased turnover dynamics after isoproterenol challenge could either show increased or decreased overall abundance. To illustrate, we observed higher turnover coincided with congruent abundance increases in some proteins (e.g., ANXA5 and FHL1) but not others (e.g. DES and HK1). Overall, only a very modest correlation existed between abundance and half-life changes (Spearman's correlation coefficient $\rho < 0.2$), indicating a large number of proteins with increased turnover did not in fact increase in steady-state abundance, and vice versa. This result held true even when considering only the proteins with the greatest and most significant

changes in turnover (Right). Similar results were observed when we compared the data with the cardiac transcript profile following isoproterenol stimulation in mice (NCBI Gene Expression Omnibus GSE48670), which we will consider in further details below.

As an orthogonal technique to validate the mass spectrometry abundance measurements, we performed immunoblotting experiments on 14 proteins of particular interest in our dataset to compare their expression in normal and remodeling hearts.

| | Isoproterenol | | | | | | | Isoproterenol | | |
| Normal | (7 d) | (14 d) | | Immunoblot: | | Normal | (7 d) | (14 d) | | Immunoblot: |

ANXA2 (38 kDa) k_{iso}/k: +3.01

ANXA5 (30 kDa) k_{iso}/k: +1.89

ALDOA (40 kDa) k_{iso}/k: +1.33

ATP1A1 (100 kDa) k_{iso}/k: +1.83

GAPDH (37 kDa) k_{iso}/k: +1.63

HK1 (102 kDa) k_{iso}/k: +1.71

HK2 (102 kDa) k_{iso}/k: +1.27

LDHA (37 kDa) k_{iso}/k: +1.69

MSN (78 kDa) k_{iso}/k: +1.88

PDH (43 kDa) k_{iso}/k: +1.23

PGAM1 (28 kDa) k_{iso}/k: +1.77

PKM1/2 (60 kDa) k_{iso}/k: +1.38

TGM2 (78 kDa) k_{iso}/k: +2.06

VIM (57 kDa) k_{iso}/k: +2.51
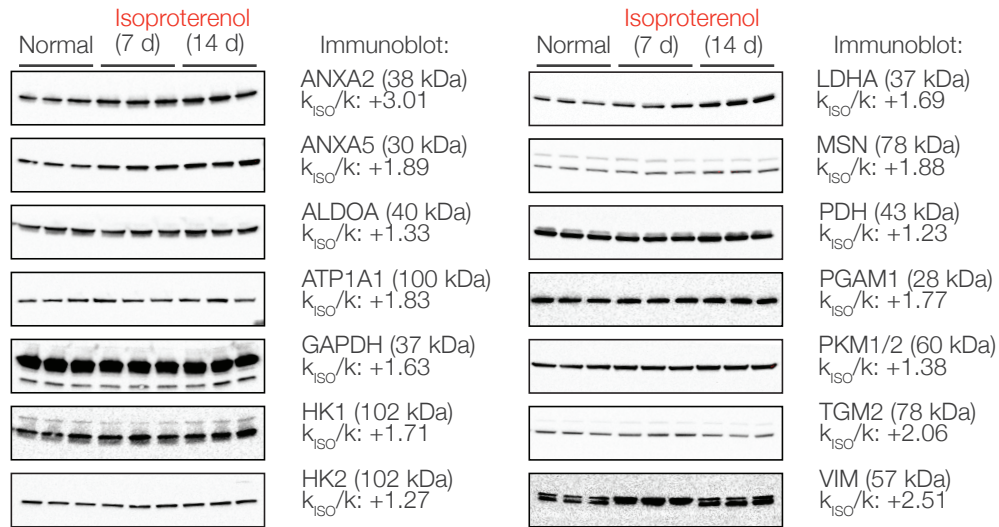
FIGURE 2.20   Immunoblot validations of abundance changes

FIGURE 2.20 displays the immunoblot results that compared the abundance of 14 selected proteins (both mitochondrial and cytosolic) in normal hearts and hearts stimulated by isoproterenol for 7 or 14 days. It can be seen from the figure that whilst some proteins with elevated turnover (shortened half-life) also demonstrated concomitant increase in abundance, many more were not changed in expression level after isoproterenol treatment. For example, annexin II (ANXA2) and annexin V (ANXA5) both exhibited an increase in protein abundance in the remodeling heart, consistent with previous reports (Benevolensky et al., 2000; Song et al., 1998). However, immunoblots failed to detect evidence for increased expression among the tested glycolysis or glycolysis-related enzymes, including fructose-bisphosphate aldolase A (ALDOA), glyceraldehyde-3-phosphate dehydrogenase (GAPDH), hexokinase I (HK1), hexokinase II (HK2), pyruvate dehydrogenase E1 subunit α (PDHA) and pyruvate kinase (PKM1); with the exception of L-lactate dehydrogenase A chain (LDHA).

Taken together, the immunoblotting data support that changes in protein turnover and protein abundance in a system are largely independent parameters, an observation that is further consistent with a recent study in ^2H_2O and SILAC doubly-labeled mice (Price et al., 2012b). The

study further suggested that the changes in total protein synthesis flux are correlated with the changes in protein concentration, but such relationship may have been largely explainable by the transformation of the data by a common factor.

The discordance between increases in synthesis and increases in expression may seem counterintuitive if one considers that cardiac hypertrophy is strongly associated with global increase in both protein synthesis and abundance. However, even under global increases in protein synthesis, individual proteins may expand or contract to different degrees. Because both protein synthesis and protein degradation contribute to the protein pool size, a protein may increase in abundance either through increased synthesis or decreased degradation. The former would result in a higher increase of turnover than the latter, which may in fact exhibit lower apparent turnover because the protein pool consists primarily of unlabeled species. In other words, a protein may exhibit a prominent five-fold increase in abundance but only a modest 20% increase in turnover, whereas another protein may have a five-fold increase in both abundance and turnover. A poor overall correlation between abundance and turnover changes would result when all protein species are considered. Indeed, the data suggest that these and numerous other scenarios exist and collectively contribute to the overall hypertrophic response.

Furthermore, it is possible that a protein may also show increased turnover without apparent abundance change if the elevation of abundance was transient and the protein level had already returned to normal at the time point it was measured. I observed subtle examples of this scenario in the immunoblotting data; for example, the abundance of vimentin (VIM) was elevated seven days following the onset of isoproterenol challenge, but had reverted to the baseline by day 14. In contrast, even transient increases in synthesis during labeling will permanently increase the proportion of labeled vs. unlabeled proteins. The resulting isotope pattern is a

signature of protein turnover that remains imprinted in a mixed protein pool, even if some of the proteins later become exported or aggregated.

Lastly, the contribution of the different sources of experimental variation between abundance measurements and turnover measurements cannot be completely ruled out, although we do not believe it to be a major source of the non-correlation. This variability may arise because whereas turnover errors may come from kinetic curve-fitting and data variance at the informative parts of the kinetic curve, intrinsic variations in protein abundance measurements could come from other sources including sample adulteration and loss during handling. In addition, protein abundance measurements quantify the amount of proteins present in a sample, and are thus sensitive to fluctuations in sample loading and MS signal intensity. Complex proteome-wide changes especially impose formidable challenges on data normalization in quantitative experiments. On the other hand, the kinetic signature of protein pool replacement following labeling, i.e., the proportion of protein light and heavy isotopes, is self-normalized within an individual sample and not subjected to adulteration during sample preparation.

Several interpretations can be drawn from the effective independence between the pool size of the protein population, the average life-span of its individual members, and transcript abundance. Firstly, the data lend credence to the idea that proteome dynamics may better reflect the changes in some aspects of the diseased heart, again due to the degeneracy of protein abundance with regard to the protein turnover cycle. To risk belaboring this point, in order for the protein abundance level to alter, the turnover cycle (i.e. proportion of new vs. old proteins) must change. Since label incorporation is history-dependent, even transient increases in protein synthesis will be recorded in a fingerprint of increased proportion of labeled vs. unlabeled proteins. In contrast, ample scenarios exist where the turnover cycle permutes without conspicuous net differences in protein abundance, such as when increased degradation counteracts increased synthesis, as is likely for a number of glycolytic enzymes in this study.

Irrespective of their abundance change, our data provide concrete evidence that protein kinetics per se constitutes a sensitive and specific discriminator of stress-induced responses in a disease model in a number of instances. Although future experiments are needed to fully integrate all relevant protein properties, these endeavors will be facilitated by the technique and quantitative kinetic data first reported here.

To summarize, it may be surmised from the data that alterations in protein dynamics are largely independent from alterations in protein abundance at least in the specific scenario of cardiac remodeling. Importantly, we demonstrated that changes in protein dynamics are effectively orthogonal to changes in protein expression or RNA expression with each parameter reflecting specific aspects of cardiac physiology and indicating distinct disease protein candidates. The next chapter will further integrate mRNA abundance, protein abundance, and turnover parameters with transcript data to draw systems-level inference of proteostasis.

Materials and Methods

Method summary: Adverse cardiac remodeling in mice was induced by implantation of micro-osmotic pumps delivering isoproterenol over 14 days. The animals were labeled with ^2H_2O concurrently. Protein isotope incorporation was analyzed with mass spectrometry and the ProTurn data analysis workflow to determine protein turnover dynamics in the remodeling heart. Experimental details are given below:

Reagents: ^2H_2O (70% and 99.9% molar ratio) was purchased from Cambridge Isotope Laboratories and filtered through 0.1-μm polyethersulfone membranes (VWR). Other chemical reagents were from Sigma-Aldrich unless specified. Milli-Q (Millipore) filtered water (18.2 MΩ) was used.

Study approval: Mouse experiments were performed in accordance with the Guide of the Care and Use of Laboratory Animals by the National Research Council and approved by UCLA.

Animal models and ^2H_2O labeling: Male Hsd:ICR (CD-1) mice (Harlan Laboratories) 9–12 weeks of age were housed in a 12 hour/12 hour light-dark cycle with controlled temperature, humidity, and free access to standard chow and water. Labeling was initiated by two intraperitoneal injections of 500-µL 99.9% molar ratio ^2H_2O-saline 4 hours apart. Mice were then given free access to 8% (v/v; 7.25% molar ratio) ^2H_2O in the drinking water supply. Groups of 3 mice each were euthanized at 0, 1, 2, 3, 5, 7, 10, 14 days following the first ^2H_2O injection at 12:00 noon for sample collection. Remodeling and reverse remodeling mice were surgically implanted with subcutaneous micro-osmotic pumps (Alzet) delivering 15 mg·kg^{-1}·d^{-1} isoproterenol over 14 days. ^2H_2O labeling was initiated as above, either immediately or 14 days after pump implantation.

Measurement of the physiological and molecular impacts of isoproterenol: Heart weights and body weights were measured at the time of euthanasia of each animal to record hypertrophy of the myocardium. Echocardiography were conducted by David Liem and our collaborator Yibin Wang on a Velvo 700 system equipped with a 45MHz transducer (Visualsonics, Toronto) and cardiac function analysis suite. Detailed cardiac function and chamber morphology was studied by ECG gated recording (EKV). M-mode of short-axis cross-section and Doppler at mitral valve can be recorded. Parameters, including wall thickness, chamber size and blood flow velocity were measured and calculated from stored images using the Visualsonic software package. The enzymatic activities of respiratory chain complexes I to V were measured from 10 µg of isolated mitochondrial proteins by spectrophotometric methods. Briefly, complex I activity was measured by the rate of electron transfer onto nitro blue tetrazolium when given the complex I substrate NADH and when the other complexes are inhibited with specific inhibitors.

The specific activity of complex I was deduced by comparing the rate with or without the specific complex I inhibitor diphenyleneiodonium. Activities for other complexes were measured similarly and compared to their respective specific inhibitors, as previously described (Lotz et al., 2013).

Measurement of body water label enrichment: To measure the amount of ^2H_2O that is incorporated into the animal's body water throughput the labeling period, mouse plasma samples were used directly for gas chromatography MS analyses. For each sample, 20 µL of plasma was mixed with 2 µL of 10 N NaOH and 4 µL of 5% (v/v) acetone in acetonitrile. The standard curves were created by adding 0% to 20% molar ratio of ^2H_2O at 11 regular intervals in 1× PBS in place of the plasma sample to the acetone. The sample mixtures were incubated at ambient temperature overnight. Acetone was extracted by adding 500 µL of chloroform and 0.5 g of anhydrous sodium sulfate. One µL of the extracted solution was analyzed on a GC-mass spectrometer (Agilent 6890/5975) with a J&W DB17-MS capillary column (Agilent, 30 m × 0.25 mm × 0.25 µm) at the UCLA Molecular Instrumentation Center. The column temperature gradient was as follows: 60 °C initial, 20 °C·min^{-1} increase to 100 °C, 50 °C·min^{-1} increase to 220 °C, 1 min hold. The mass spectrometer operated in the electron impact mode (70 eV) and selective ion monitoring at m/z 58 and 59 with 10 ms dwell time.

Protein sample preparation: Mouse hearts were excised and homogenized by a 7-mL Dounce homogenizer (Pyrex) (20 strokes) in an extraction buffer (250 mmol·L^{-1} sucrose, 10 mmol·L^{-1} HEPES, 10 mmol·L^{-1} Tris, 1 mmol·L^{-1} EGTA, 10 mmol·L^{-1} dithiothreitol, protease and phosphatase inhibitors, pH 7.4) at 4 °C, then centrifuged (800 g, 4 °C, 7 min). The pellet was collected as the total debris fraction. The supernatant was centrifuged (4,000 g, 4 °C, 30 min) and collected as the organelle-depleted cytosolic fraction. The pellet was washed, then overlaid on a 19%/30%/60% discrete Percoll gradient pellet, and sedimented by ultracentrifugation (12,000 g, 4 °C, 10 min). Purified mitochondria were collected from the 30%/60% interface

layer and washed twice. Protein concentrations were measured by bicinchoninic acid assays using pure bovine serum albumins as standards (Thermo Pierce).

Mouse plasma, heart, and human erythrocyte protein samples were separately digested in-solution; 200 μg proteins were heated at 80 °C with 0.2% (w/v) Rapigest (Waters) for 5 min, then heated at 70 °C with 3 mmol·L^{-1} dithiothreitol for 5 min, followed by alkylation with 9 mmol·L^{-1} iodoacetamide in the dark at ambient temperature. Proteins were digested with 50:1 sequencing grade trypsin (Promega) for 16 h at 37 °C, then acidified with 1% trifluoroacetic acid (Thermo Pierce). Depleted human plasma samples were digested on-filter using 10,000 Da filters (Pall Life Sciences). Sample buffer was exchanged on-filter with 100 mmol·L^{-1} ammonium bicarbonate. The samples were then heated on-filter at 70 °C with 3 mmol·L^{-1} dithiothreitol for 5 min, followed by alkylation with 9 mmol·L^{-1} iodoacetamide in the dark at ambient temperature. Proteins were digested with 50:1 sequencing grade trypsin (Promega) for 16 h at 37 °C.

Separation of peptides by two-dimensional liquid chromatography. To reduce sample complexity and improve sample coverage, we separated the digested peptide with two-dimensional reversed-phase/reversed-phase LC prior to MS analysis (Lam et al., 2011; Lau et al., 2011). First-dimension (high-pH) separation for mouse (heart cytosol and mitochondria, nucleus, plasma) and human (subject 4 and 6) samples was conducted on a Phenomenex C_{12} reversed-phase column (Jupiter Proteo C_{12}, 4 μm particle, 90 Å pore, 100 mm length × 1 mm inner diameter) at high pH using a Finnigan Surveyor LC system. The solvent gradient was as follows: 0th – 2nd minute, 0 – 5% B; 3rd – 32nd minute, 5 – 35% B; 32nd – 37th minute, 80% B; 50 μL·min^{-1}; A: 20 mM ammonium formate, pH 10; B: 20 mM ammonium formate, 90% (v/v) acetonitrile, pH 10. We then injected 50 μg of proteolytic peptides with a syringe into a manual 6-port/2-position switch valve. Twelve fractions from 16 – 40 minute were collected, lyophilized and re-dissolved in 20 μL of 0.5% (v/v) formic acid with 2% (v/v) acetonitrile prior to low-pH reversed-phase separation.

We then performed second-dimension (low-pH) reversed-phase chromatography using an Easy-nLC 1000 nano-UPLC system (Thermo Scientific) on an EasySpray C_{18} reversed-phase column (PepMap, 3-μm particle, 100-Å pore; 150 mm length × 75 μm dimension; Thermo Scientific) held at 50 °C. The solvent gradient was 0–110 minute: 0–40% B; 110–117 minute: 40–80% B; 117–120 minute: 80% B; 300 nL·min^{-1}; A: 0.1% (v/v) formic acid, 2% (v/v) acetonitrile; B: 0.1% (v/v) formic acid, 80% (v/v) acetonitrile. The autosampler on the Easy-nLC 1000 nano-UPLC system then injected 10 μL of each high-pH fraction into the solvent flow path. High-performance liquid chromatography-grade water (J.T.Baker) was used for all analytical solvent preparations.

Protein identification and quantification using mass spectrometry. Mass spectrometry was performed on an LTQ Orbitrap Elite mass spectrometer (Thermo Fisher Scientific) controlled by XCalibur (v.2.1.0) coupled to the Easy-nLC 1000 nano-UPLC system through a Thermo EasySpray interface. Each survey scan was analyzed inside the Orbitrap at 60,000 resolving power in profile mode, followed by data-dependent collision-induced dissociation MS2 scans on the top 15 ions inside the ion trap. MS1 and MS2 target ion accumulations were 1×10^4 and 1×10^6, respectively. We set dynamic exclusion to 90 seconds to avoid acquisition of redundant spectra. We further used an MS1 scan lock mass of m/z 425.120025 for internal mass calibration. Protein identification was performed with ProLuCID (Xu et al., 2006) against a reverse-decoyed database (Uniprot mouse Reference Proteome Reviewed, February 19th, 2013, 16,590 entries). The search allowed for static cysteine carbamidomethylation (+57.02146 Da) modification and up to 3 variable modifications, including methionine oxidation (+15.9949 Da), lysine acetylation (+42.0106 Da), serine/threonine/tyrosine phosphorylation (+79.9663 Da), or lysine ubiquitylation (+114.0403 Da). Tryptic, semi-tryptic, and non-tryptic peptides within a 20-ppm mass window surrounding the candidate precursor mass were searched under separate confidence calculation. Protein identifications were filtered by DTASelect (Tabb et al.,

2002), requiring ≤ 1% global peptide false discovery rate and two unique peptides per protein. ProLuCID performs multiple iterations of database search for every spectrum, first to identify only unmodified peptides and then to assume variable mass shifts of unmodified peptides (Wong et al., 2007). DTASelect, with the –modstat parameter specified, then applies separate statistical filters to the modified and unmodified peptides to identify variable modifications using separate protein identification confidence calculations (Tabb et al., 2002), which would explain why searching with variable modifications in our typical workflow did not negatively impact protein identification performance. Note that modified peptides (other than methionine oxidation) were not considered for comparative analyses as we await rigorous validations of the number of label-accessible atoms on the modification moieties. However, scenarios exist where performing database search with modifications would nevertheless improve coverage – because a protein may be confidently identified by an unmodified and a modified peptide at two different sites to satisfy the two-peptide rule, and the unmodified peptide could go on to yield confident information on protein dynamics. On a related note, so far in our unpublished data we have not observed any systematic difference in turnover rates between modified and unmodified peptides of the same proteins.

Computational workflow for protein kinetics analysis: Proteins were identified from the acquired mass spectra using ProLuCID (Xu et al., 2006) Protein functional information and Gene Ontology entries were queried through NCBI DAVID (Huang da et al., 2009) and COPaKB (Zong et al., 2013). Protein turnover kinetics was quantified with ProTurn.

The nonlinear fitting parameters utilized to deduce protein turnover rates were as follows. Orbitrap spectra were input to ProTurn after conversion into the open [.mzML] format using MSConvert (Chambers et al., 2012). ProTurn was then instructed to select only confidently identified peptides that were uniquely assigned to a protein from the ProLuCID search result [.dta] file.

For each identified peptide, all isotopomer areas-under-curves over a 60-ppm window of the peptide mass were integrated from the raw mass spectra, at the retention time in the MS1 extracted ion chromatograph as indicated by the scan number in the protein identification list. Savizky-Golay filters over 7 data points were applied to the MS1 chromatograph prior to it-negration (Savitzky and Golay, 1964). False positive identifications were further controlled by the requirement of a peptide to be explicitly identified in at least 4 time points before it is considered for kinetics calculation. Turnover rates were extracted by multivariate optimization to a nonlinear function. The optimization results were independently verified by two data-fitting scripts, written in R and in MATLAB. Peptide isotopomer time-series were accepted if they fit to the model with r ≥ 0.9, or alternatively with standard error of estimate of ≤ 10%.

For iBAQ-based label-free quantification in ProTurn, the integrated isotopomer peak areas were summed up as the peptide cluster area. Protein areas were defined as the sum of all peptide areas from identified peptides, normalized to the total spectral intensity, then normalized to the potential number of peptides (six or more amino acids in length) that may be produced from the protein sequence in an in silico tryptic digest.

Statistical analysis. Non-parametric Mann-Whitney-Wilcoxon statistics were calculated in R (v.3.0.3) to estimate the significance of difference in turnover rates. Fisher's exact test with the Benjamini-Hochberg procedure was performed through NCBI DAVID (Huang da et al., 2009) to estimate the significance of enrichment of functional categories. Results with $P < 0.05$ after multiple testing correction were considered significant.

Validation of protein abundance changes. To corroborate the mass spectrometry data on protein abundance, we measured protein abundance in the heart before and after isoproterenol challenge with immunoblotting. Equal amounts of cardiac proteins (40 µg) were heated with

Laemmli loading buffer with 100 mM dithiothreitol at 70 °C for 10 minutes. The proteins were separated using SDS-PAGE on a Bio-Rad Mini-Protean 10–200 kDa Tris-glycine gel (Weber and Osborn, 1969), then transferred onto a polyvinylidene difluoride membrane (Bio-Rad TransBlot Turbo). Protein loading and transfer was verified with Ponceau S staining. The blots were blocked in the blocking buffer (5% bovine serum albumin, 0.005% sodium azide, in 1× Tris-buffered saline/ Tween 20 (TBST) (Cell Signaling)), reacted with primary antibodies at 4 °C overnight, washed with 1× TBST, reacted with secondary antibodies at ambient temperature for 1 hr, washed with 16y× TBST, then detected by chemiluminescence. All antibodies were purchased from Cell Signaling, including rabbit monoclonal IgG against GAPDH (#5174), HK1 (#2024), HK2 (#2867), ANXA2 (#8235), VIM (#5741), TGM2 (#3557), PGAM1 (#12098), LDHA/C (#3558), ALDOA (#8060), PKM1/2 (#3190), PDH (#3205); and rabbit polyclonal antibodies against ANXA5 (#8555), MSN (#3146), ATP1A1 (#3010). Primary antibodies were diluted in 1:1000 in the blocking buffer. Secondary antibodies were 1:3000 goat anti-rabbit IgG conjugated to horseradish peroxidase (#7074) in the blocking buffer.

III. Mechanisms of proteolysis in cardiac mitochondria

In this chapter, we integrate mRNA, protein, and turnover data to identify a class of proteins with impaired proteolysis during cardiac remodeling. Using this method, we found a number of mitochondrial proteins with decreased degradation during disease development, including FXN, LTEM1, CYC1, and others. To characterize the potential mechanisms by which the implicated proteins are degraded in the cardiac mitochondrion, we developed a 2D-DIGE based method to quantify the rate of proteolysis under experimental perturbations in vitro. Intramitochondrial proteases including Lon exhibited different proteolytic activities and specificities than the 20S proteasome, which was also found to retard the turnover of mitochondrial proteins in vivo. The described methods should be applicable to other systems where the rate and target of protein degradation in the mitochondria are of interest. The material composing this chapter was published and can be found in our publication (Lau et al., 2012).

Impaired degradation of mitochondrial proteins in remodeling hearts

Protein degradation stress and abnormal protein accumulation is a hallmark of multiple heart diseases (Divald et al., 2010; Gomes et al., 2006; Papa et al., 2007). In end-stage heart failure, several lines of evidence indicate impairments of the ubiquitin-proteasome system and the accumulation of poly-ubiquitinated protein, as reviewed in (Day, 2013). In human patients with hypertrophic and dilated cardiomyopathies, where proteasome activities markedly decrease in the failing heart but partially recover after mechanical unloading by LVAD (Predmore et al., 2010). The capacity of protein quality control decreases in the diseased heart in human and

113

rodents (Gianni et al., 2010; Wang et al., 2011b), whereas in a mouse transverse aortic con-striction model, proteasome activities decrease and ubiquitinated proteins accumulate as heart failure develops (Tsukamoto et al., 2006). The heart appears to be particularly prone to protein degradation stress compared to other cell and tissue types in the body, possibly because of the large amount of sarcomeric proteins that need to be degraded. Several protein misfolding models can lead to heart failure without other overt phenotypes (Hamada et al., 2004; Wang and Robbins, 2006). Activation of proteasomes decrease hypertrophy and increases lifespan in a desmin-related cardiomyopathy model (Li et al., 2011). Hence disrupted protein quality con-trol may act both as an initiator of disease and as a cellular response to insults (Gianni et al., 2010; Wang et al., 2011b).

In the early-remodeling mouse model we employed here, we do not expect a decrease in global proteolytic activity. Indeed, peptidase activities in both 26S (ATP-dependent) and 20S (ATP-independent) proteasomes were augmented after isoproterenol and before the transition into heart failure (Drews et al., 2010). Hence our studies were not designed to examine pro-teasome functional insufficiency, a term reserved for global dysfunction of proteasome enzy-matic activity, in our current model, as it manifests only in later stages of cardiac disease when protein aggregates and proteotoxicity are observed. Nevertheless, altered degradation may contribute to disease development by altering the state of the proteome in heart diseases. Examples abound for proteins whose expression level is primarily controlled by degradation, notably p53 and PINK1, where both proteins are continuously synthesized in the cell but their steady-state levels are kept low due to rapid, continuous degradation under normal cellular conditions (Jin et al., 2010; Lukashchuk and Vousden, 2007). When cellular conditions call for protein activation (replication errors for p53 and mitochondrial depolarization for PINK1), spe-cific proteolysis is suppressed, leading to an increase in steady-state level.

Accordingly, we hypothesize that a target subset of proteins in the heart exhibit impairment of selective degradation during cardiac remodeling, either through post-translational modifications or interactions with proteolytic mechanisms. Our goal was to identify a particular class of proteins based on kinetic and abundance behaviors, which may represent a class of candidate disease drivers. This paradigm is distinct from the identification and rescuing of global proteolytic impairment that affects a broad swath of proteome substrates, as may be expected in late-stage heart failure. In this chapter, we will explore the combinatorial use of mRNA, protein expression, and protein turnover data to identify proteins with impaired proteolysis.

Given that mRNA and protein expression are well known to be poorly correlated, we explored whether protein turnover rate information can be used to disambiguate the discrepancy between mRNA and protein abundance, I computed the degree of concordance between changes in mRNA and protein levels following isoproterenol-induced remodeling, defined here as an mRNA exhibiting appreciable unidirectional changes of more than 10% in magnitude as its cognate protein in the isoproterenol vs. control sample. Proteins and mRNA changes were poorly correlated, exhibiting concordant behaviors (co-directional changes) in 19% of all the examined mRNA/protein species (Spearman's correlation coefficient: 0.07). The poor correlation between abundance and turnover changes, however, did not translate into considerably higher proportions of concordant changes (24%) when mRNA abundance was matched toward either unidirectional protein abundance change or unidirectional protein turnover change. Taken together, the poor correlation between turnover and abundance suggests that protein turnover data alone explain only a small degree of the discrepancy between mRNA and protein abundance. Rather, it provides strong evidence that protein turnover measurements can be leveraged to provide additional discriminatory power to study the plasticity of the pathological proteome in parallel to commonly pursued protein expression profiling.
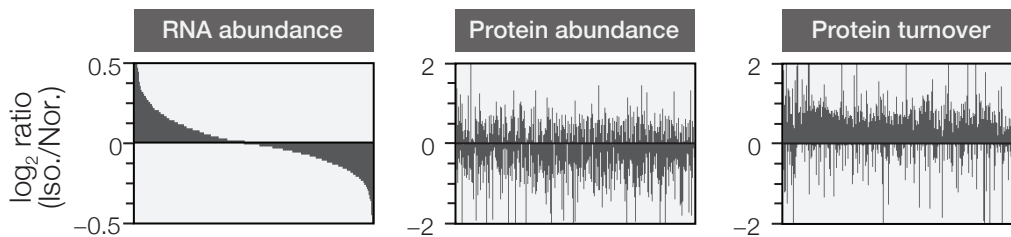
FIGURE 3.1   RNA, protein abundance, and protein dynamics

FIGURE 3.1 illustrates the discordant changes amongst RNA abundance, protein abundance, and protein dynamics in the remodeling heart. The changes in each parameter of 1,300 genes or proteins are shown. In each graph, the genes/proteins are ranked in descending order from the gene/protein with highest ratio in RNA abundance in remodeling over normal hearts to the one with the lowest (Left). It can be seen that neither the changes in protein abundance nor protein turnover had any obvious correlation with changes in RNA level either globally or when a specific protein is concerned, i.e., a gene/protein species with severely down-regulated RNA levels in disease may nevertheless exhibit highly increased protein abundance or turnover, and vice versa.

Hence we conclude that changes in mRNA, protein abundance, and protein turnover in the diseased heart were effectively orthogonal to one another. The independence of RNA expression, protein expression, and protein dynamics suggest that these multi-scale data types may be synthesized to generate new hypotheses and may thus be harnessed collectively to describe the state of homeostasis of cardiac proteins. Such analysis could provide intrinsically mechanistic information regarding how mitochondrial protein abundance occurs (increased abundance due to increased synthesis or decreased degradation). Our method thus provides a novel method to detect selective impairments of protein degradation at the target substrate level, prior to severe protein aggregation formation, as opposed to commonplace measure-

ments of global decreases in proteolytic capacity, which would affect the degradation of multiple proteins on a large-scale.

	RNA abundance	Protein abundance	Protein turnover	Possible interpretation
1	Increased	Increased	Increased	Increased transcription
2	Decreased	Decreased	Decreased/No change	Decreased transcription
3	Decreased/No change	Increased	Increased	Post-transcriptional control
4	Decreased/No change	Increased	Decreased/No change	Impaired degradation

TABLE 3.1   Possible scenarios of protein dynamic changes in disease

TABLE 3.1 explores some potential combinations of changes in RNA abundance, protein abundance, and protein turnover in disease development. The three parameters can be pursued combinatorially to identify proteins associated with impaired degradation in disease, which would show decreased/unchanged RNA abundance, decreased/unchanged protein turnover (isotope incorporation normalized by the entire protein pool), but increased protein abundance. It should be noted that these interpretations are not definitive. For example, the characteristic profile of decreased/unchanged RNA level, decreased/unchanged protein turnover and increased protein abundance does not definitively indicate only impaired degradation of proteins. It is possible for increased synthesis (due to post-transcriptional mechanisms) and attenuated degradation to simultaneously occur, which would be reflected as decreased turnover and RNA level. Nevertheless, by comparing these three independent parameters, we now have a tool at hand that allows us to detect proteins with inhibited proteolysis in the heart before the onset of aggregate formation. This provides an important differential that may lead to more actionable findings. For example, although we observed from the data that the mitochondrial protein prohibitin (PHB) turns over faster in the remodeling heart, at present we do not know whether it turns over faster due to increased synthesis alone, or increased degradation, information that is needed if we are to modulate its turnover.

At this point it may be apposite to revisit how the protein turnover cycle serves as an underlying mechanism of protein expression as alluded to in the previous chapter. The collection of both protein expression and protein turnover data allows us to, at least in principle, solve the quantitative changes of the protein pool over time (Claydon and Beynon, 2012):

$$d[P]/dt = (k_s - k_d) \cdot [P]$$

where [P] denotes the size of the protein pool and k_s and k_d denote the rate constant of protein synthesis and protein degradation, respectively. It is further noted that as synthesis is assumed to be a zero-order process, k_s takes the form of raw number of molecules entering the protein pool per unit of time; whereas given protein degradation is assumed to be a first-order process, k_d is expressed as the flux of the protein pool and takes the form of the proportion of the pool removed from the pool per unit of time. If we assume that changes in the proteome over physiologically relevant periods occur gradually, then over an instantaneous period of time being considered the protein pool would approach steady state, such that the rate of synthesis (protein molecules entering the protein pool) is roughly balanced by the rate of degradation (protein molecules exiting the protein pool). In other words, given that $d[P]/dt \cong 0$, it follows that the raw number of molecules coming in to the protein pool per unit time (k_s) and the raw number of molecules leaving the pool ([P] · k_d) would be equal, such that:

$$[P] = k_s/k_d$$

With this model, one can describe changes in particular proteins during hypertrophy in further details, and the following two, albeit very approximate, calculations are given here for discussion purpose, with the intention to illustrate this general concept, and should be interpreted with the caveat in mind that the protein expression values originate from relative quantification experiments.

We first consider four-and-a-half LIM domain protein 1 (FHL1), which in the previous chapter we described as being one of the proteins with the most drastic changes in protein turnover in cardiac remodeling, which also showed a congruent increase in protein abundance. From our experimental data, FHL1 has a relative expression level of 6.7×10^{-4} and $k = 0.078$ d^{-1}. Given that k is a first-order rate constant that is expressed as the flux of isotopes through the protein pool, we assume that the experimentally measured k approximates k_d in the model. Further assuming a weighted average molecular weight of 46 kDa in the cardiac proteome, one can surmise that there are approximately 9.0×10^{10} FHL1 molecules per 1 µg of injected cardiac protein samples, and that 7.0×10^8 FHL1 molecules are being synthesized per day. In the remodeling heart, the relative expression level of FHL1 is 1.3×10^{-3} and k_d is 0.278 d^{-1}. Hence there are 1.8×10^{10} FHL1 molecules per 1 µg of protein samples, and that 5.0×10^9 molecules are being introduced into the protein pool per 1 µg of protein samples per day. Hence in the remodeling heart, the synthesis of FHL1 increases at least 7-fold, the degradation of FHL1 increases ~ 3.5 fold, and the expression level of FHL1 increases by twofold.

Next, consider cardiac troponin T (TNNT2), which encodes part of the troponin complex and is a major component of the cardiac contractile machinery. As the heart undergoes hypertrophy and increases in mass, TNNT2 expression would be expected to increase over the entire organ. However, given that muscle fibers occupy a high proportion of cardiac mass, its changes will dominate the changes in cardiac mass in the absence of drastic changes in the composition of cardiac cells, so one may expect minor changes in overall abundance of TNNT2 per unit mass of heart. From our experimental data, TNNT2 has a relative expression level of 2.3×10^{-3} and $k = 0.091$ d^{-1}. Again if we assume that the experimental k approximates k_d, there are approximately 3.1×10^{10} cardiac troponin T molecules per 1 µg of injected cardiac protein samples, and 2.7×10^9 molecules are being synthesized per 1 µg of samples per day. In the remodeling heart, relative expression of TNNT2 is 1.8×10^{-3}, k_d is 0.108 d^{-1}, and the synthesis

rate is 2.6×10^9 molecules per day. It may be surmised that any potential increase in TNNT2 over the entire organ is due largely to increased synthesis.

Because of the potential variability in these calculations, they will not be further considered in detail in the following analysis. Instead, we attempted to differentiate the directions of change of each gene/protein in multiple parameters, in order to categorize different types of behaviors in turnover and expression. To do so, we performed unsupervised agglomerative hierarchical clustering to categorize the quantified cardiac proteins according to their changes in RNA abundance, protein abundance, and protein turnover, in order to describe their state of home-ostasis in transcriptional and translational spaces. Under such clustering analysis, proteins that behave closely in both expression and dynamics in the remodeling hearts would be grouped together, and may be enriched for functional annotations that would allow inference of in-volvement of particular pathways.
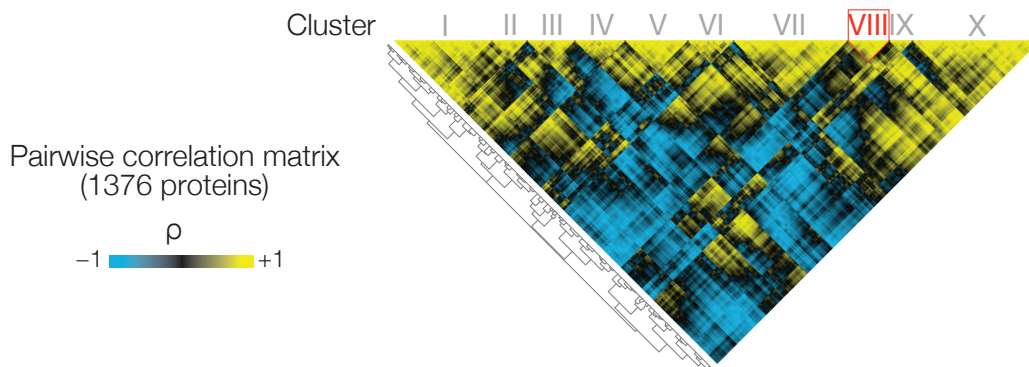
FIGURE 3.2 Hierarchical clustering of RNA, protein, and turnover data

FIGURE 3.2 is a heat map representation of the results of the agglomerative hierarchical clustering analysis. A total of 1,376 proteins (or their cognate mRNA) in normal and remodeling hearts, as described in Chapter II, were analyzed. From each gene or protein, the RNA abun-

dance, protein abundance, and protein turnover data during disease development as collected from the previous chapter were standardized, which were then used to calculate the Spearman's correlation coefficients between every protein pair combination. The data were used to generate a 1,376 x 1,376 protein correlation matrix for hierarchical clustering analysis.

The clustered protein data are here represented as a heat map, in which blue-colored cells represent strong negative correlations between the two proteins that the cells represent along the diagonal axes, whereas yellow represents strong positive correlation. Due to the low dimensionality of the data, the selection of clusters was intended to be exploratory in nature in order to help identify potential proteins of interest, and no test of significance of clustering was carried out. Nevertheless, a number of principal protein clusters can be observed (yellow blocks), each containing proteins with inter-correlated kinetic behaviors during cardiac remodeling. Cluster VIII (outlined in red) in particular contained proteins which showed characteristic profiles of impaired degradation, as shown below.
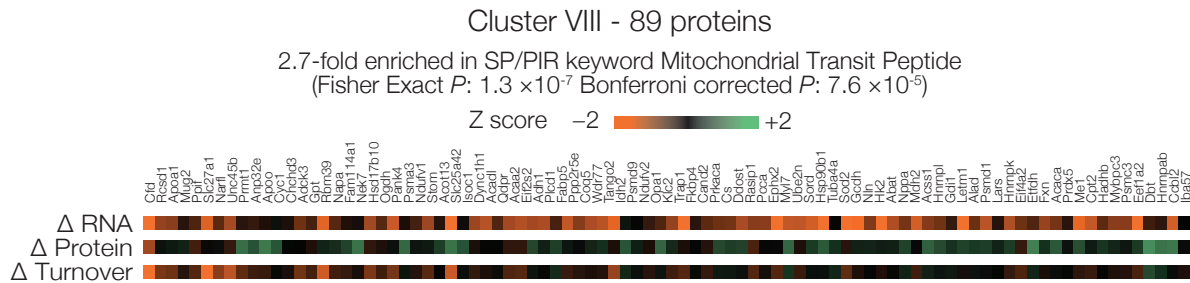
FIGURE 3.3   Cluster of mitochondrial proteins with impaired proteolysis

FIGURE 3.3 examines Cluster VIII of cardiac proteins from the unsupervised clustering experiments above. Cluster VIII contains 89 cardiac proteins, which are here represented by a heat map of their standardized Z score within a particular parameter (number of standard deviations from the population average). Green color denotes two positive standard deviations from the mean (i.e., the protein is highly up-regulated in that particular parameter), whereas red denotes two negative standard deviations from the mean (highly down-regulated).

It can be seen that the 89 proteins generally exhibit decreased/unchanged mRNA abundance (red color), increased/unchanged protein abundance (green color), but decreased/unchanged protein turnover (red color) in cardiac remodeling. This cluster is significantly enriched for mitochondria-located proteins (Swissprot/Protein Information Resource SP/PIR keyword Mitochondrial Transit Peptide; 2.7-fold enriched; Fisher's Exact test P: 1.3 x 10^{-7}; Benjamini-Hochberg adjusted P: 1.2 $\times$ 10^{-4}). This was an unusual and conspicuous pattern within the sample, as it was inconsistent with the global trend of increased turnover and synthesis one expects during the course of cardiac hypertrophy. Since neither RNA abundance nor protein turnover increased, the data indicated a post-transcriptional and post-translational mechanism whereby these proteins are perturbed in disease (e.g., impaired degradation).
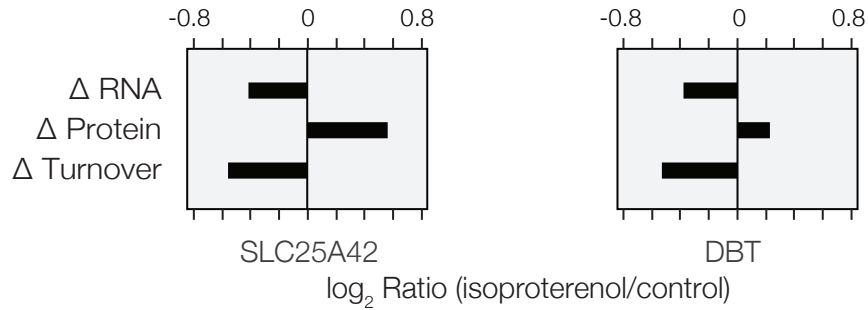
FIGURE 3.4   Mitochondrial proteins with impaired proteolysis (continued)

FIGURE 3.4 is an alternative representation of the profiles of two proteins in the cluster (SLC25A42 and DBT), intended to illustrate the general patterns of changes in RNA, protein expression, and protein turnover during remodeling amongst proteins in the cluster.

The cluster could be further subdivided using the change in protein turnover during reverse remodeling as a differential factor, i.e., by following the assumption that a bona fide disease protein is likely to recover in molecular profiles during recuperative reverse remodeling where decreases in hypertrophy is observed.
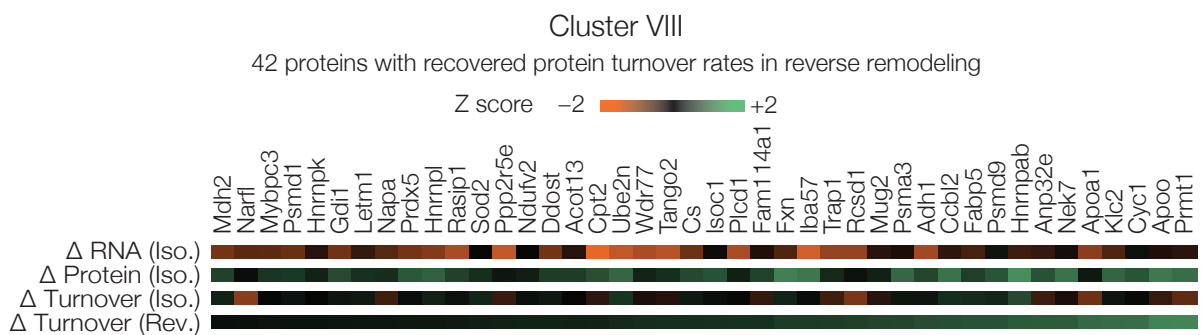
FIGURE 3.5   Mitochondrial proteins with impaired proteolysis (continued)

FIGURE 3.5 shows a subset of proteins in Cluster VIII which showed increased protein turnover during reverse remodeling (Rev.). The heat map is as in above, with the addition of reverse remodeling (Rev.) data being displayed in addition to remodeling (Iso.) data. The 42 shown proteins exhibit impaired degradation that are recovered during isoproterenol withdrawal and are interpreted here as potential disease proteins associated with the pathogenesis of cardiac remodeling. A number of proteins in this protein set have previous been implicated in cardiac hypertrophy and heart failure. Frataxin (FXN) is a mitochondrial matrix protein that is mutated in Friedreich's ataxia, a devastating mitochondrial disease associated with cardiac degeneration, cardiac hypertrophy, and heart failure (Lane et al., 2013). Leucine-zipper-EF hand-containing transmembrane region (LETM1) is a mitochondrial protein involved in respiratory chain biogenesis that is deleted in Wolf-Hirschhorn syndrome, a developmental disorder that affects multiple systems including the heart. Apolipoprotein O (APOO) is a non-mitochondrial proteoglycan in the cluster, which has been shown to be up-regulated in the heart in obesity and diabetes (Lamant et al., 2006). PRMT1 is an arginine methyltransferase that is required for mitochondrial localization of BAD (Sakamaki et al., 2011), required for PGC-1alpha activation, and that is associated with coronary heart diseases. The present dataset suggest a potential mechanism (impaired degradation) whereby these proteins may participate in the disease process. Furthermore, a number of proteins in the cluster were previously not associated with cardiac remodeling, and thus present new candidate disease drivers. Tumor necrosis factor receptor-associated protein-1 (TRAP1) is a pleiotropic mitochondrial-specific heat shock protein-90 (HSP90)-like chaperone, which is involved in mitochondrial redox and cell death pathways and in neurodegenerative diseases (Altieri et al., 2012).

Though not every protein in this cluster is mitochondrial, the enrichment of mitochondrial proteins such as FXN, LETM1, CYC1, and others in this cluster of proteins with distinct turnover characteristic is intriguing. Based on the data, I hypothesized that cardiac remodeling stimuli contributes to heart disease in part by disrupting the expression and turnover dynamics of

specific mitochondrial proteins in the heart; more specifically, the disruption of mitochondrial protein degradation mechanisms lead to decreased proteolysis, accumulation of specific protein species, and disease development. If this hypothesis proves to be useful in predicting disease proteins, one may envision that protein dynamics studies can provide a more informative route to future interventions than protein expression analysis alone, in that the half-life of particular constituents of the mitochondrial proteome may be individually modulated through suppressing or activating targeted protein synthesis or degradation pathways.

Substrates and activities of intra-mitochondrial proteases

The route to translatable findings will additionally require understanding the mechanism of degradation of individual mitochondrial proteins. To illustrate this point, although the turnover data indicate that the degradation of frataxin may be altered in the failing heart, at present there are limited clues as to the mechanisms through which the protein may be degraded in health or disease that may serve as potential intervention targets. Finding out the degradation mechanism of mitochondrial proteins is therefore an important objective, to which we considered two available strategies that may be employed. Firstly, an in vitro method to detect protease substrates may be pursued, where the protein substrates are introduced to proteolytic agents of choice and proteolysis allowed to take place in vitro under controlled conditions. The degree of proteolysis may then be measured by the residual protein abundance in the absence of interfering protein synthesis. This method allows more experimental perturbations to be applied to test various hypotheses. Secondly, an in vivo study may be employed where a particular protein degradation pathway is inhibited, possibly pharmacologically, and the resulting half-life of proteins is measured, and an increase in half-life for a protein may be inferred as evidence of its normally being degraded by the suppressed pathway. This method has proven useful to measure single targeted protein degradation mechanisms in the adult heart in the

past (Beardslee et al., 1998). Both methods were attempted here in order to address whether the mitochondrial protein turnover changes were impacted by their differential degradation in vitro and in vivo. We will investigate both the proteolytic agent, and the availability of substrates, both of which will modulate protein degradation rates. We show that mitochondrial proteases degrade proteins in isolated cardiac mitochondria minimally, but show preferences for selected protein charge variants.

Protease systems that exist inside mitochondria include several ATP-dependent protease complexes: the Lon protease homolog, Clp, and the m-AAA and i-AAA metalloprotease complexes, among which the Lon protease homolog is the best characterized. The Lon protease is a homoheptameric complex of LONP1 monomers conserved in all domains of life, and contains distinct domains for ATP binding, substrate recognition, and proteolysis. The substrate-recognition domain is thought to bind to exposed hydrophobic domains from potential protein substrates (Smith et al., 1999). Indeed, Lon has been shown to promote the degradation mildly oxidized proteins (Bota and Davies, 2002; Bota et al., 2002; Kaser and Langer, 2000) and impede protein carbonyl accumulation in vitro (Ngo and Davies, 2009; Ngo et al., 2011). Nevertheless, in vivo data on the physiological significance of these targets have been inconclusive (Bender et al., 2011; Major et al., 2006). Thus far only a few proteins have been conclusively demonstrated to be Lon substrates in vivo (Bezawork-Geleta et al., 2014; Matsushima et al., 2010), most notable of which is the mitochondrial transcription factor A (TFAM), through the action on which Lon may modulate mitochondrial DNA copy number (Matsushima et al., 2010). Curiously, genetic ablation of the LONP1 homolog in yeast (Pim1) causes impairments in respiration and mitochondrial functions (Suzuki et al., 1994) but results in the accumulation of only very few proteins in the yeast mitochondrion (14 out of > 200 spots) (Bayot et al., 2010), an observation potentially attributable to compensatory effects from decreased protein synthesis of the Pim1 substrates in Pim1Δ strains. Hence the general repertoire of Lon protease substrates remains poorly defined.

126
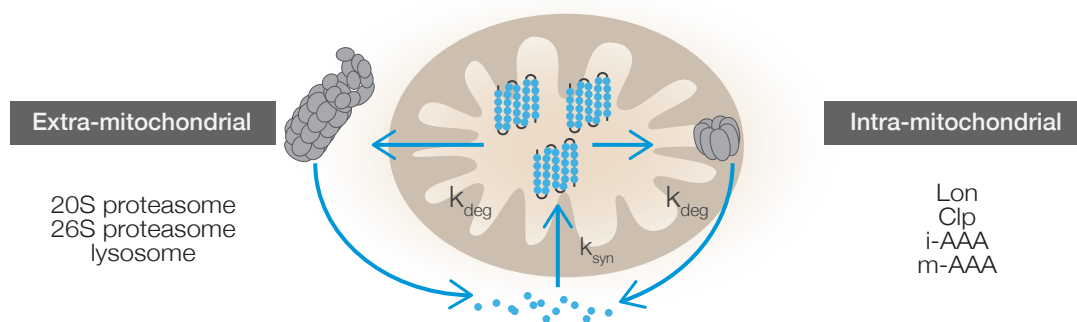
FIGURE 3.6   Overview of mitochondrial protein degradation mechanisms

FIGURE 3.6 illustrates two potential routes of degradation that a hypothetical intra-mitochondrial protein may go through. Extra-mitochondrial proteolysis is shown on the left, which may occur via PINK1/Parkin mitophagy, general macroautophagy, or cytosolic pro-teasomes, which have been theorized to destroy mitochondrial proteins either through mito-chondrial assisted degradation, or export of mitochondrial proteins into the cytosol.

Gene name	Protein name	Spectral abundance	Rank	SYPRO Ruby
LONP1	Lon protease homolog	0.10% ± 0.01%	166	~0.10%
CLPP	Clp protease (proteolytic subunit)	0.03% ± 0.00%	293	ND
CLPX	Clp protease (ATP-binding subunit)	0.03% ± 0.00%	431	ND
AFG3L2	m-AAA AFG3-like protein 2	0.04% ± 0.00%	266	ND
SPG7	m-AAA Paraplegin	0.01% ± 0.00%	557	ND
YME1L1	i-AAA FtsH homolog	0.01% ± 0.00%	558	ND

TABLE 3.2   Endogenous protease complexes in cardiac mitochondria

TABLE 3.2 lists the endogenous AAA$^+$ protease complexes we identified from the cardiac mitochondrion. A number of detected protein subunits belonging to the AAA$^+$ family of intra-mitochondrial proteases are shown, Including the Lon homolog, Clp protease, m-AAA, and i-AAA metalloproteases. The Spectral abundance column shows the abundance of the protease expressed as the proportion of all proteins in the mitochondrial proteome, as measured from

label-free spectral count technique. The Rank column shows the abundance rank of the protease in descending abundance in the mitochondrial proteome. The SYPRO Ruby column shows the results when we measured the relative abundances of cardiac mitochondrial proteins with the ruthenium-based fluorescent dye SYPRO Ruby, following two-dimensional isoelectric focusing (IEF)-polyacrylamide gel electrophoresis (PAGE) separation. Both independent methods indicated that AAA^+ proteases were minute in abundance in cardiac mitochondria. The Lon homolog LONP1 was the only species with appreciable concentration, representing ~0.1% of total detected cardiac mitochondrial proteins. These quantification results were reaffirmed by a recent investigation in the Ping laboratory (Lotz et al., 2013).

The relative abundance of LONP1 in the mitochondrion is comparable to the expression of its bacterial homolog as quantified in *Mycoplasma pneumonia* (0.2%) (Maier et al., 2011), but both are dwarfed by the content of proteasomes in the cytosol, which may be as abundant as accounting for 0.9% of liver proteins (Tanaka et al., 1986). Given the proximity of mitochondrial proteins to ROS-mediated protein damage, the low abundance of proteases in cardiac mitochondria is remarkable. To determine the potential activity of the intra-mitochondrial mitochondrial proteases in degrading protein substrates, we measured their endogenous enzymatic activity using an in vitro fluorescent substrate. The method is based on the introduction of fluorescence tagged casein to the proteases of interest for a period of time, followed by precipitation of undigested proteins and measurement of fluorescence in the supernatant.
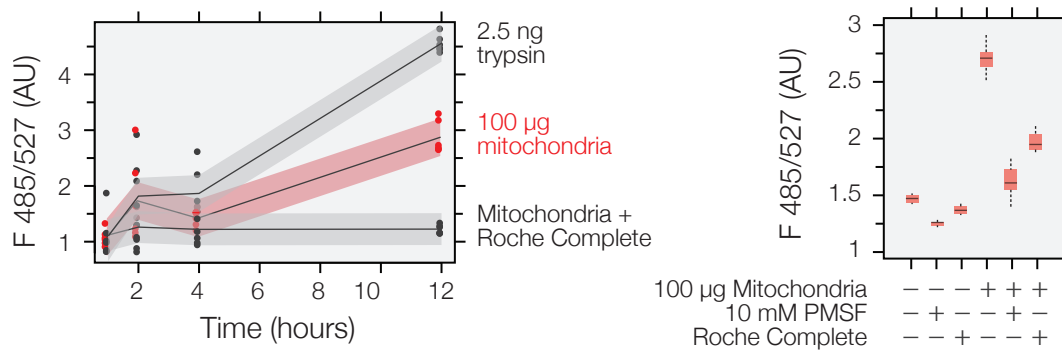
FIGURE 3.7 Enzymatic activities of intra-mitochondrial proteases

FIGURE 3.5 shows the activity of intra-mitochondrial proteases in digesting a fluorescent substrate. (Left) Activity over protease inhibitor control (gray) can be differentiated after 12 hours of incubation from 100 μg of mitochondrial proteins (red) (3 arbitrary units (AU) vs. 1 AU), which was equivalent to approximately 50% the activity of 2.5 ng of bovine trypsin (green). Each data point represents reading from one experimental replicate. Lines and shaded areas represent local regression and 95% confidence intervals of the trend over time. (Right) We sought to differentiate the nature of proteolytic activities by using inhibitors that show specific preference to different protease classes based on their catalytic mechanism. In total, we tested the effects of the serine protease inhibitor phenylmethanesufonyl fluoride (PMSF; 1 mmol·L^{-1}); the cysteine protease inhibitor E-64 (0.35 g·L^{-1}); the aspartate protease inhibitor pepstatin (1 μmol·L^{-1}); the metalloproteinase inhibitor 1,10-phenanthroline (2 g·L^{-1}); and a protease inhibitor cocktail (Roche Complete), which contains serine protease, cysteine protease, and metalloprotease inhibitors. A minimal and variable response towards E-64, pepstatin, and 1,10-phenanthroline was observed, which in three separate experiments not shown here only marginally reduced the proteolytic activities of mitochondria to 90% ± 20% of normal. By contrast, both PMSF and, to a higher degree, Roche Complete abolished the majority (~60 – 80%) of the observed activities in the shown experiment.

Thus, cardiac mitochondria exhibit proteolytic capacity in vitro, which appear to be largely in serine protease type despite the various numbers of proteases present, consistent with LONP1 being the predominant proteolytic system inside mitochondria, which agree with its predominant abundance. We next determined whether the measured proteolytic activity is impacted by the presence of oxidative stress as may be encountered by the cardiac mitochondrion during remodeling, and to contrast it to changes in 20S proteasome activity under identical conditions.
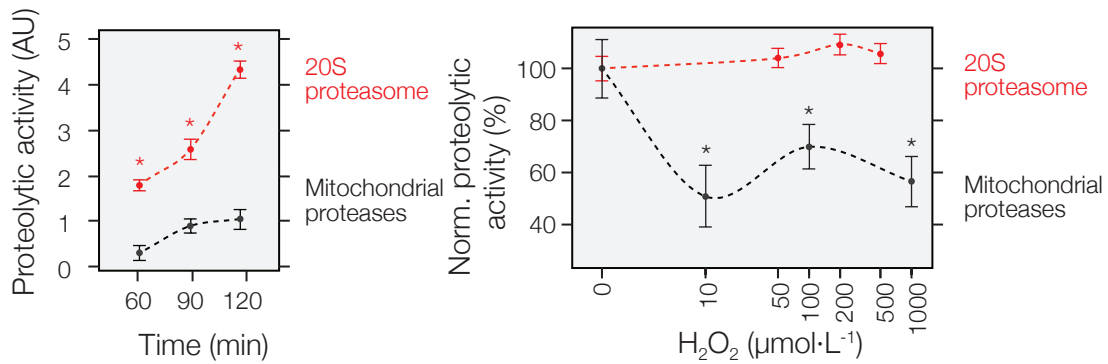
FIGURE 3.8   Proteolytic activities under oxidative insult

FIGURE 3.8 shows the activities of mitochondrial proteases and 20S proteasome under various concentrations of H_2O_2 in vitro. (Left) Comparisons of baseline proteolytic activity using the in vitro casein assay between 100 µg of cardiac mitochondrial proteases and 1 µg of 20S proteasome isolated from the mouse heart. Error bars: standard errors of means; n=6; asterisks: $P < 0.05$, Student's t test. (Right) The effects of H_2O_2 on the proteolytic activity of 20S proteasome (20S) and mitochondrial proteases (Mito) are shown. The introduction of as little as 10 µmol·L^{-1} of H_2O_2 was found to be sufficient to reduce the normalized activity of mitochondrial lysates to roughly half of normal levels. On the other hand, 20S proteasomes were resistant to up to 1 mM Error bar: SEM; asterisks: $P < 0.05$ vs. no H_2O_2, Student's t test; n = 4 for 20S proteasome, n = 10 for mitochondrial proteases.

The observation that oxidative insults may deactivate LONP1 is corroborated by a recent report, which found that oxidative modifications induced by H_2O_2 suppresses its proteolytic activity reversibly (Hoshino et al., 2014). Accordingly, we determined whether in vivo modulation of oxidation could also alter the proteolytic activity of LONP1 in the mouse heart. A pilot experiment was conducted that compared normal Hsd:ICR (CD-1) mice, to mice treated with 10 mg·kg^{-1}·wk^{-1} of the pro-oxidant herbicide paraquat, and to mice treated with paraquat plus 0.7 mg·kg^{-1}·d^{-1}MitoTEMPO, a mitochondrial-targeted antioxidant (Trnka et al., 2009). The mice were labeled with ^2H_2O as described in the previous chapters and samples were taken at day 3, 7, 10, and 14 to generate a preliminary overview of protein turnover distributions. Among the mitochondrial proteins with statistically significant differences in turnover rates between paraquat and normal samples, the median turnover rate upon paraquat treatment was 84% of that in a normal mouse (5th to 95th percentile: 71% to 92%). Simultaneous administration of Mito-TEMPO reverted the effect of paraquat, in that the median turnover rate of the proteins was 102% of that in a normal mouse (5th to 95th percentile: 95% to 111%). Hence, preliminary analyses suggest that the introduction of oxidative stress appears to slow down the turnover of mitochondrial proteins in vivo, which is consistent with, though not diagnostic of, an inhibition of mitochondrial proteases causing an impairment of degradation.

Although our initial plan was to differentiate how different proteases may permute in the disease heart, the current experimental design will mostly discern the contributions from LONP1. The other protease complexes are known to serve other physiological functions, but as they are less amenable to large-scale biochemical investigations, we shifted our focus to determining which substrates are being degraded by the observed intrinsic proteolytic activity of cardiac mitochondria.

To elucidate how mitochondrial protein degradation is regulated at the individual protein level, we examined the substrate pool of intra-mitochondrial proteases. Our approach was to use two-dimensional differential gel electrophoresis (2D-DIGE) – a combination of fluorescent Cy dye labeling and IEF SDS-PAGE two-dimensional separation (Wang et al., 2011a) – to resolve and quantify individual mitochondrial proteins. These experiments were performed in vitro by design, in order to avoid the confounding influence of synthesis and to complement the in vivo half-life data described in the previous two chapters. Although in vivo isotope labeling may be used to quantify protein turnover as a summation of protein synthesis, translocation, and degradation, such methods cannot easily differentiate the contributions and activities of different degradation mechanisms. Furthermore, they cannot easily distinguish intact protein substrates from proteolytic fragments, whereas the use of in vitro fluorescence labeling followed by two-dimensional electrophoretic separation allowed us to directly assess proteolytic changes of individual substrates and isoforms.
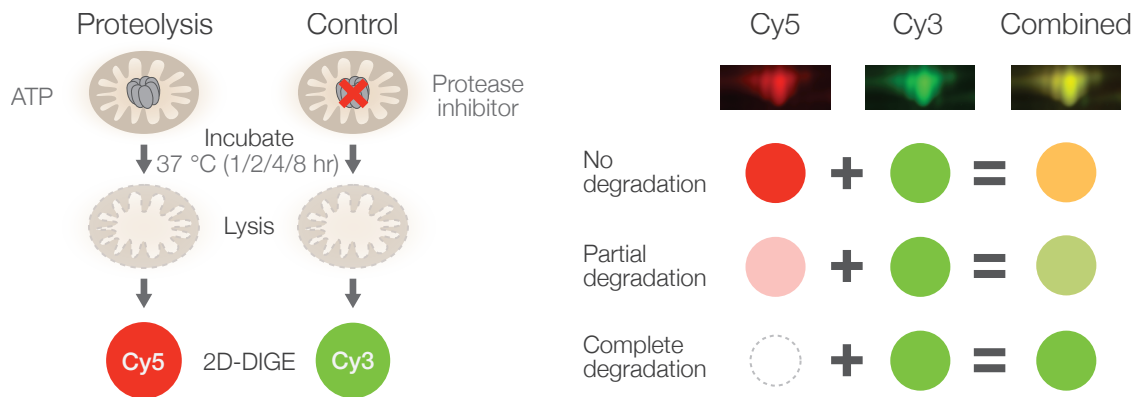
FIGURE 3.9   2D-DIGE strategy to identify mitochondrial protease targets

FIGURE 3.9 illustrates the principle of the 2D-DIGE strategy to measure the degree of in vitro proteolysis in the cardiac mitochondrion. Equal amounts (100 μg) of cardiac mitochondrial proteins were permitted either to degrade by the present proteolytic agents, or were protected

by protease inhibitors throughout incubation. The residual proteins from the proteolyzed samples were labeled with Cy5 dyes, which fluoresces in red. The un-degraded control sample was labeled with Cy3 dye, which fluoresces in green. The two samples were mixed and resolved on two-dimensional gels then scanned for quantity comparison of each resolved protein spot. A protein that is not degraded by the present proteases appears as yellow in the combined fluorescence image (equal intensity of red and green), whereas a protein that is susceptible to degradation appears as green (present only in the un-degraded sample).

Hence to discover the in vitro targets of mitochondrial proteases, we incubated isolated mouse heart mitochondria either in the presence of either ATP or protease inhibitor, after which the 2D-DIGE approach was utilized to determine which proteins remain to be present in the mitochondrial extract.
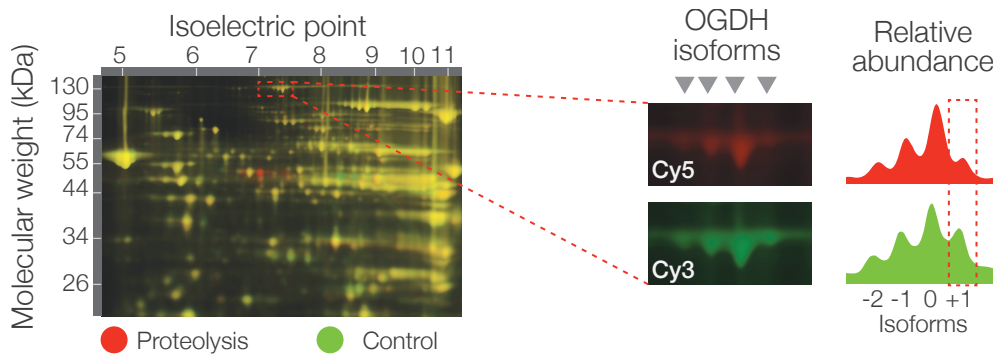
FIGURE 3.10   In vitro proteolytic maps of mitochondrial proteases

FIGURE 3.10 displays the result of one representative gel from triplicate 2D-DIGE experiments. Each gel spot represents one protein species (a gene product or charge/size isoform thereof) as separated by charge and molecular weight. Following incubation of cardiac mitochondria in isolation to promote endogenous proteolysis, 111 unique proteins were identified by liquid

chromatography-tandem mass spectrometry (LC-MS/MS) to yield a protein-specific in vitro degradation map. It can be seen from the map on the left that the majority of the proteins exhibited a modest decrement in abundance in the proteolysis-enabled sample. On average, over 80% of each protein species remained intact after incubation, but specific spots with degraded proteins were nevertheless detected (Right), altogether indicating that the mitochondrial proteome was relatively stable in isolation in vitro. This observation corroborates similar reports in the literature from experiments performed in yeast (Augustin et al., 2005; Bender et al., 2010) and suggests that mitochondrial proteases have highly specific substrate preferences. This is further consistent with the observation that functional ablation of the yeast Lon homolog PIM1 resulted in the accumulation of few detectable proteins (Major et al., 2006) and proteolysis assays generally did not indicate the respiratory complexes to be efficient substrates of mitochondrial proteases (Bender et al., 2010; Major et al., 2006).

However, the in vivo data from the previous chapters unequivocally indicated that mitochondrial proteins do turn over at appreciable rates in the heart, whereas in the in vitro experiments, a number of proteins susceptible to oxidative damage including the NADH:ubiquinone oxidoreductase iron-sulfur cluster subunits did not appear to be efficient substrates of mitochondrial proteases. A possible explanation for the modest degrees of in vitro degradation is that a missing degradation signal is not present in the experimental system, or that the mitochondrial proteases have a limited intrinsic capacity to degrade mitochondrial proteins under basal conditions. Another possibility, which we will consider later, is that these proteins could conceivably be degraded by extra-mitochondrial factors, provided there is accessibility between the proteolytic agent and its substrates.

Despite the overall stability of the proteome, different degrees of degradation were clearly discernible from selected individual protein spots, which may be used to infer substrate selectivity. A number of mitochondrial proteins exist in charge variants that were readily resolved by

isoelectric focusing. It can be seen from the zoomed-in view on the right that the mitochondrial proteases favor the degradation of the more basic isoforms of selected proteins, suggesting a possible recognition mechanism for proteolysis that would be otherwise masked by other means of detection. This isoform preference was repeatedly observed in multiple mitochondrial protein species.
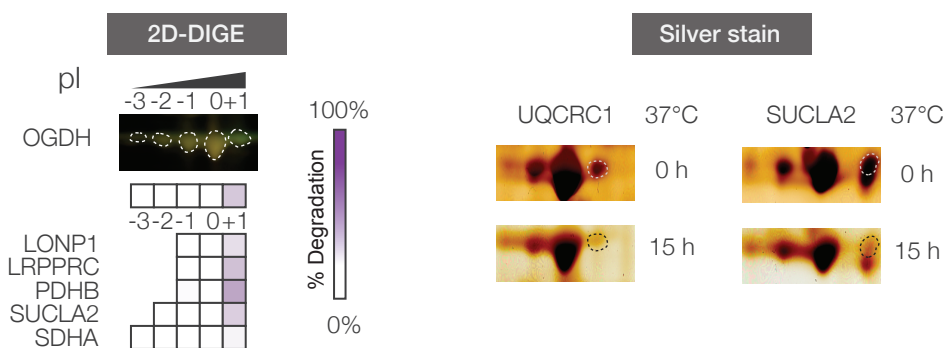
FIGURE 3.11 Isoform preference of mitochondrial proteases

FIGURE 3.11 shows the similar 2D-DIGE patterns we observed from a number of mitochondrial proteins. (Left) The 2D-DIGE image shows an example of such basic isoform preference on the mitochondrial 2-oxoglutarate dehydrogensase (OGDH), with its five charge variants outlined in white. The isoforms were numbered with the most abundant isoform arbitrarily numbered as 0, and its more basic number as +1, and so on. The heat maps below show the degree of degradation (measured as the percentage of decreased abundance vs. control samples) in several other mitochondrial proteins including the Lon protease itself (LONP1), leucine-rich PPR motif-containing protein (LRPPRC), pyruvate dehydrogenase E1 beta subunit (PDHB), succinyl-CoA ligase [ADP-forming] subunit beta (SUCLA2), and succinate dehydrogenase subunit A (SDHA); where the basic isoform (the high-pI end of the IEF-PAGE map from the most prominent isoform) was conspicuously more prone to experimental degradation. This specificity was absent

from proteolysis conducted by proteasomes, as we will consider below. To confirm this result, we conducted reverse labeling experiments (data not reproduced here from our publication (Lau et al., 2012)) as well as detection with silver staining in lieu of 2D-DIGE (Right), and found that the charge specificity remained observable.

It is known that many proteins contain isoform series that can be separated by their horizontal migration patterns in two-dimensional electrophoresis (Claydon et al., 2012). These "trains" of charge variants were proposed to reflect protein lifetime-dependent progression (e.g., chemical asparagine deamidation) (Lindner and Helliger, 2001; Weintraub and Deverman, 2007), but recent proteomics evidence suggests the variants have similar isotope incorporation rates and thus are of the same molecular age (Claydon et al., 2012). There are also some other discrepancies between this hypothesis and the 2D-DIGE data. Because asparagine reduces the pI of the residue (Yang and Zubarev, 2010), the charge variants would be expected to rank from oldest to newest from the most acidic (left) to the most basic (right). The data would suggest that only newly synthesized proteins are capable of being degraded by the mitochondrial proteases, which is clearly not what one would expect in a protein degradation system in homeostasis. Lastly, if the chance of protein degradation is not orthogonal to molecular age, one might expect that total protein pool replacement would be more linear than the observed first-order kinetics.

An alternative hypothesis for the specificity for charge variants is that they may represent post-translational modification that designate proteins for degradation but are independent of their molecular age. Substrate presentation, which governs substrate recognition and recruitment, is finely tuned in the major proteolytic system of the cell, where recruitment to proteasomes by E3 ligases and ubiquitin receptors work with proteins with degradation signals (degrons) that are exposed to the ubiquitin-proteasome system under various cell states to orchestrate individual protein degradation rates and thus individual protein steady-state expression.

We postulate that similar cytochemical or enzymatic post-translational modification signals may be recognized by intra-mitochondrial proteases directly or indirectly (such as by promoting misfolding or as a degron for intermediate signals) (Bota and Davies, 2002; Leonhard et al., 2000; Marcillat et al., 1988). To assay the identity of the charge variants, we performed a series of biochemistry and gel staining experiments designed to look for several different post-translational modifications in the mitochondria. Although the results did not provide support to the hypotheses, they are recorded here in the interest of future experimental designs and that these general surveys of post-translational modifications in cardiac mitochondria may be subjects of future investigations.

My initial hypothesis was that the protein charge variants may represent differential protein phosphorylation and acetylation on different individual molecules of the protein pool. Protein phosphorylation targets serine, threonine, and tyrosine residues and acetylation targets lysine; both are highly common protein modifications in the mitochondrion. Both modifications are reversible, are protein- and site- specific, respond to stimuli, and function as important regulators of cellular signaling. Both modifications are small, and charge-altering (phosphorylation introduces a negative phosphate whereas acetylation neutralizes the positive charge on lysine). This matches the 2D electrophoresis profile we observed (horizontal but not vertical shifts), although not the directionality. Both protein modifications have been implicated in protein degradation signals in other cellular compartments. Recent studies implicate histone acetylation to be a direct recognition signal in lieu of ubiquitination for 20S proteasomes bound to PA200 regulatory complex (Qian et al., 2013). In systems where propagation of signaling is dependent on the inhibition of selective degradation such as the Wnt signaling pathway (Clevers, 2006), phosphorylation acts as the permissive signal to regulate the rate of degradation.
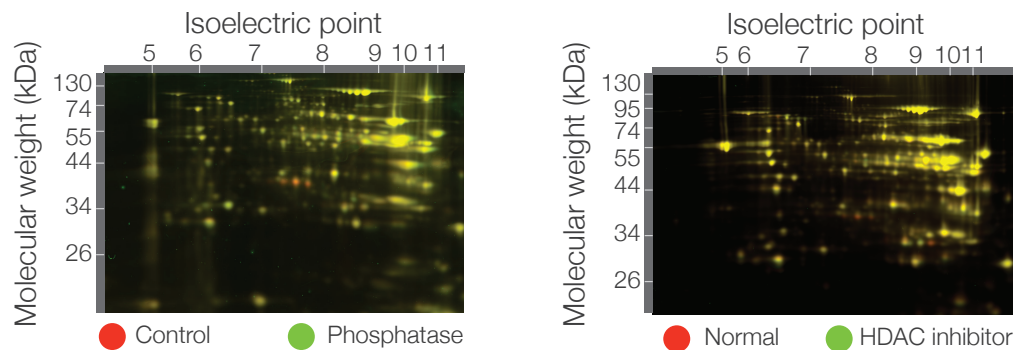
FIGURE 3.12   2DE patterns of protein phosphorylation and acetylation

FIGURE 3.12 displays two representative gel images from 2D-DIGE experiments designed to determine whether the degradation-susceptible gel spots were enriched in protein phosphorylation or acetylation. (Left) Untreated mitochondrial proteins (Cy 5; red) were compared with those treated with lambda phosphatase (New England Biolabs) (Cy3; green). (Right) Mitochondrial proteins isolated from untreated mouse hearts (Cy5; red) were compared with those isolated from mice treated with histone deacetylase (HDAC) inhibitors (suberoylanilide hydroxamic acid and sodium valproate) for 6 hours in vivo prior to euthanasia (Cy3; green). The proteins were resolved with IEF-SDS PAGE as above. It can be seen that relatively few changes in the implicated isoforms were present and the patterns of changes did not conform to the patterns of substrate susceptibility of the protein degradation map. We used an alternative strategy to detect endogenous protein phosphorylation patterns using a phosphate-binding fluorescent gel stain (Pro-Q Diamond) and likewise did not detect matching phosphorylation patterns that may discriminate the charge variants (data not shown). Hence we did not observe any evidence that the protease substrate preference was due to protein phosphorylation or acetylation.

It is possible that protein phosphorylation or acetylation nevertheless acts as endogenous degradation signals but that their roles were obscured in the experiments above. For example, the HDAC inhibitors we used are thought to inhibit mostly class I and class II HDACs, whereas class III HDAC sirtuins (SIRT3, SIRT4 and SIRT5) exist in the mitochondria that may be the biologically relevant deacetylating agents. Future investigations may employ sirtuin inhibitors (e.g., sirtinol) to examine their effects on mitochondrial proteolysis. Secondly, it is possible that the protein charge isoforms on the 2D-DIGE gels represent differential multiples of a combination of modification moieties (e.g., having 8, 7, 6 and 5 phosphates and 5 acetyl-lysine moieties, etc.), which would complicate their distinction under perturbation.

My next hypothesis was that the charge variants might represent an oxidative modification, of which many types exist including cysteine thiol oxidation, nitrosylation, and protein carbonylation. The reported preference of LONP1 to degrade mildly oxidized aconitase (Bota and Davies, 2002) suggested oxidative protein modifications to be another potential cause of the observed degradation preferences. Our first strategy was to detect the staining patterns for protein carbonylation (using Millipore OxyBlot) and lysine 4-hydroxy-2-nonenal (4-HNE) modification with immunoblotting.
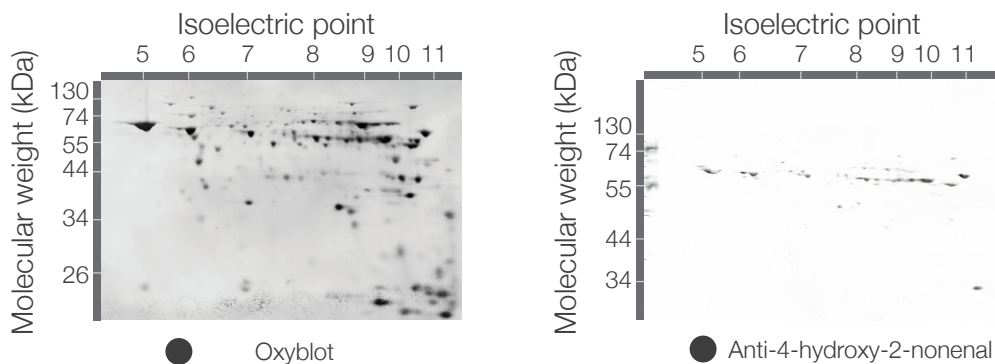
FIGURE 3.13   2DE patterns of oxidative post-translational modifications

FIGURE 3.13 displays two representative blot images from 2DE experiments designed to determine whether the degradation-susceptible gel spots were enriched in protein carbonylation (Left) or 4-HNE modifications (Right). Neither patterns conclusively confirmed that the isoform charge variant trains corresponded to differential amounts of oxidative modifications, although for some proteins Oxyblot appeared to react preferentially with the spots on more acidic side, which would be consistent with charge-reducing carbonylation of positively-charged residues.

These experiments do not rule out the involvement of other oxidative modifications, including cysteine oxidative modification to sulfonic acid, which has been shown to confer similar charge train patterns in other proteins by increasing the isoelectric point of the protein spots (Fujiwara et al., 2007). We next explored whether in vitro perturbations of ROS levels may shift the migration patterns of the mitochondrial proteins.
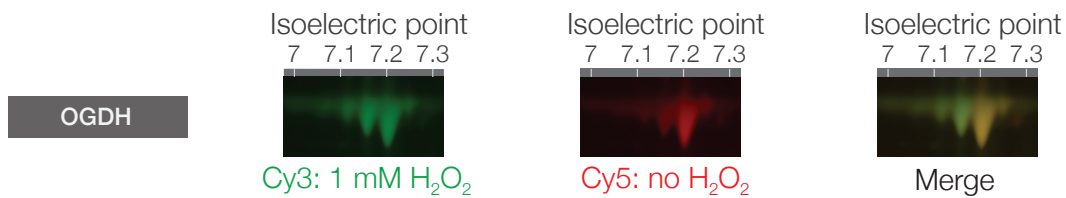
FIGURE 3.14   Charge isoform patterns following in vitro oxidation

FIGURE 3.14 shows the shift in isoform charge variants following exposure to 1 mM of H_2O_2 for 30 minutes in vitro, as compared using 2D-DIGE. Exposing mitochondrial lysate to H_2O_2 shifted the isoelectric pattern toward the anode, as may be expected from the carbonylation modifications of positively charged residues. It is, however, not clear whether this may be connected to the substrate preference of mitochondrial proteases, as such hypothesis would suggest that mitochondrial proteases preferentially degrade un-damaged proteins! Nevertheless, it is worth noting that as described previously in this chapter, ROS decreased the general capacity of isolated mitochondria to degrade fluorescein-labeled casein. An intriguing possibility is that mitochondrial proteases become ineffectual in the presence of excessive ROS on both the protease and substrate levels.

We conducted additional experiments to assay the 2DE patterns other post-translational modifications may present, including glycosylation using Pro-Q Emerald stains or glycosidase treatment (data not shown). Altogether, these data suggest that although mitochondrial proteases may influence protein turnover by targeting substrates that possess a potential degradation signal, at present the identity of the degradation signal remains elusive.

Can proteasomes degrade mitochondrial proteins?

As noted previously in this chapter, a number of mitochondrial proteins do not appear susceptible to the endogenous proteolytic activity of the mitochondrion. These proteins may normally

turn over via extra-mitochondrial factors including autophagy and the ubiquitin-proteasome system. Proteasome degrades the majority of cellular proteins including in the cytosol, the ER, and the nucleus (Lee and Goldberg, 1998). Although proteasomes are not known to reside within the mitochondrion, multiple lines of evidence are converging to implicate the involvement of cytosolic proteasomes in mitochondrial protein homeostasis (Azzu and Brand, 2010; Radke et al., 2008).

Ubiquitination is a post-translational modification commonly associated with proteasomal degradation of the modified protein. Surprisingly, large-scale profiling experiments have revealed that ubiquitinated proteins exist not only on the mitochondrial surface facing the cytosol (e.g., mitofusin) (Livnat-Levanon and Glickman, 2011) but also on the inner membrane isolated from the cytosolic contents, including in all five of the respiratory complexes (Kim et al., 2011). Two inner-membrane proteins, the uncoupling protein 2 and uncoupling protein 3 (UCP2 and UCP3), have been investigated in further details and were found to require both proteasomes and an intact outer membrane in order to turn over effectively in cultured cells (Azzu and Brand, 2010; Azzu et al., 2010). These studies lend credence to the notion that particular mitochondrial proteins may in fact be degraded through proteasomal pathways in physiologic conditions, perhaps after being exported through an unknown retrograde transportation mechanism to the cytosol that has been proposed (Heo et al., 2010; Livnat-Levanon and Glickman, 2011; Xu et al., 2011). Retrograde transport may occur with the aid of the transitional endoplasmic reticulum ATPase (VCP) protein or nuclear protein localization protein 4 homolog (NPL4), both of which function in endoplasmic reticulum-assisted degradation (ERAD)- associated retrotranslocation (Heo et al., 2010), and both of which have unexpectedly been found to associate with the mitochondrion (Livnat-Levanon and Glickman, 2011). Alternatively, this process may also be facilitated by heat-shock protein 90 (HSP90), a pleiotropic chaperone protein involved in mitochondrial protein import and homeostasis that has also been shown to be involved in the retrotranslocation of the F_1F_0 ATP synthase complex subunit OSCP to the

outer membrane and its subsequent proteasomal degradation (Margineantu et al., 2007). Corroborating this, previous studies in the Ping laboratory have observed mitochondrial proteins accumulate in the cytosol of diseased hearts (Zhang et al., 2008b), which would permit encounters with proteasomes. Lastly, proteasome inhibitors including bortezomib, epoxomicin, and MG115 can disrupt mitochondrial functions, morphology, and turnover in vitro and in vivo (Nowis et al., 2010; Sullivan et al., 2004) , although this may be due to direct inhibition of protein degradation or an indirect effect on mitochondrial dynamics.

Given these supporting evidences, I hypothesized that proteasomes possess a previously under-appreciated capacity to degrade multiple mitochondrial proteins. It would therefore be an objective of interest to determine in an unbiased manner the extent to which the homeostasis of mitochondrial proteins may be affected by proteasomes in vitro, and whether disrupted proteasome capacity mechanistically alters mitochondrial dynamics in vivo. I first designed experiments to address whether any of the cardiac mitochondrial proteins are possible substrates of 20S proteasomes using the 2D-DIGE strategy as previously described in the chapter.
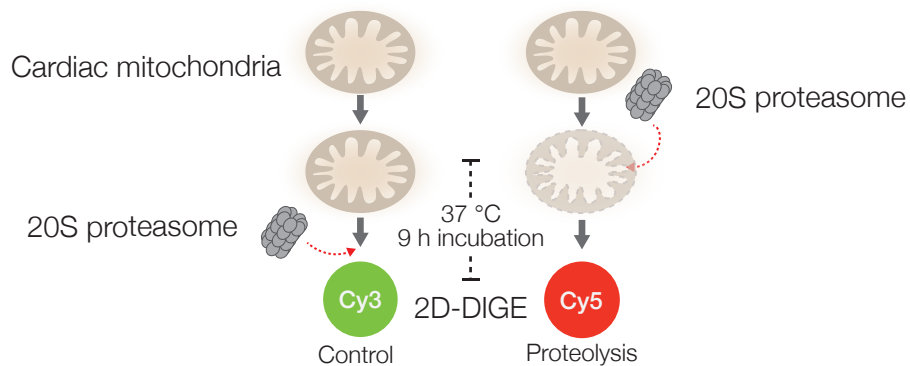
FIGURE 3.15   **Experimental design to identify 20S degradation targets**

FIGURE 3.15 illustrates the experimental design for measuring the proteolytic substrates of 20S proteasomes using the 2D-DIGE approach. In the proteolysis sample, cardiac mitochon-

dria were incubated with 1:50 molar ratios of mouse cardiac 20S proteasomes at 37 °C for 9 hours. Control samples were not incubated. The two samples were labeled with Cy3 and Cy5 dye, mixed, and resolved with 2DE. The degrees of proteolysis were measured via the percentage of residual proteins in the proteolysis sample as previously described in the chapter.
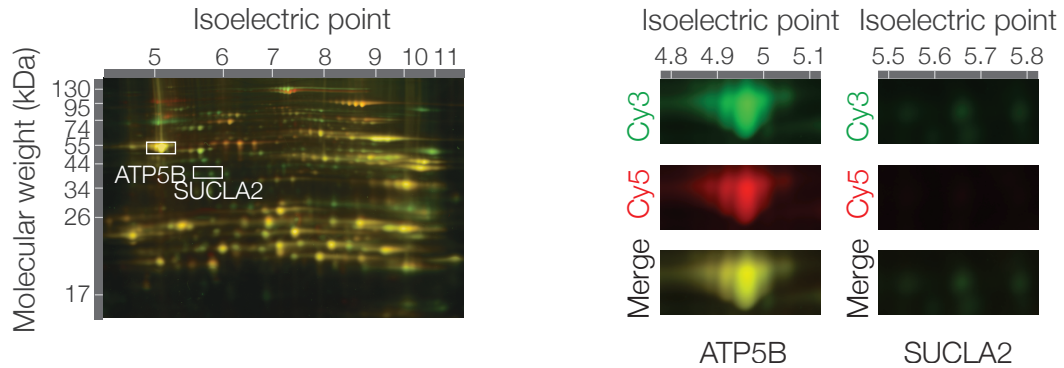
FIGURE 3.16   In vitro 20S-mediated degradation of mitochondrial proteins

FIGURE 3.16 shows a representative 2D-DIGE experiment aimed at identifying the in vitro substrate of 20S proteasome in the cardiac mitochondrion. (Left) Substrate preference may be discerned from the differential degradation patterns of individual protein spots, as described earlier in the chapter. (Right) Zoomed-in images from the 2D gel shows that ATP synthase beta subunit (ATP5B) was not susceptible to 20S proteasome-mediated degradation, as an equal amount of the protein remained in both the proteolytic and control samples; whereas succinyl-CoA ligase [ADP-forming] subunit beta (SUCLA2) was effectively degraded, as virtually no protein remained in the proteolysis sample and the combined 2D-DIGE spot was green.
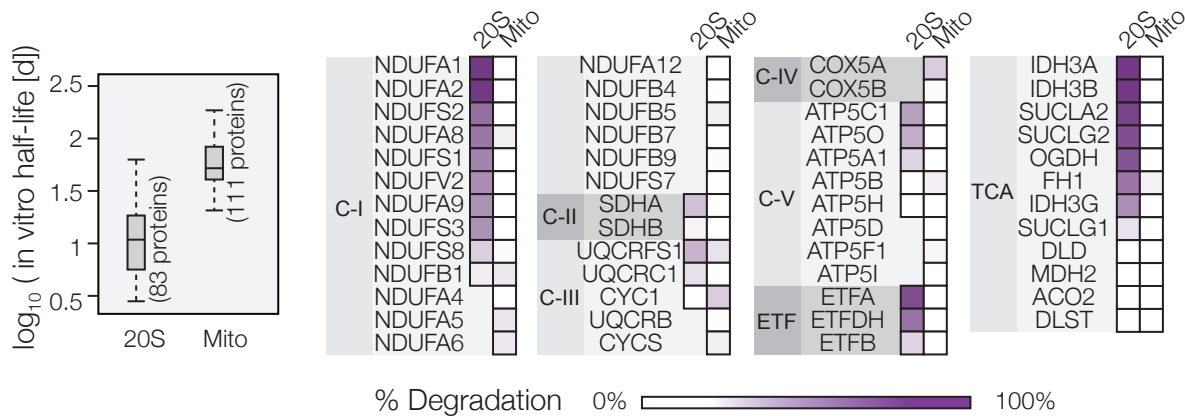
FIGURE 3.17   Substrate preferences of 20S proteasomes and proteases

FIGURE 3.17 summarizes and compares the observed substrate preferences of the mitochondrial proteases with that of the 20S proteasome. Differences in in vitro proteolytic rates (Left) and in substrate preferences (Right) between the two proteolytic mechanisms are apparent. The protein degradation profiles were correlated with functional categories or multi-protein complex association. The tricarboxylic acid cycle and the NADH:ubiquinone oxidoreductase complex contained more proteins susceptible to the 20S proteasome. The identified NADH:ubiquinone oxidoreductase components exhibited a median in vitro half-life of 7.1 hours under 20S proteasome ($5^{th} - 95^{th}$ percentile: 3.4 – 17.1 hours). In comparison, proteins belonging to other respiratory chain complexes had over twice the median half-life, at 15.7 hours, in the same experiments ($5^{th} - 95^{th}$ percentile: 9.2 – 44.4 hours). This discrepancy in degradation rates could not be satisfactorily correlated to any examined biophysical parameters including hydrophobicity, abundance, isoelectric point, and molecular weight (data not reproduced here from our publication (Lau et al., 2012)). The data therefore favor the hypothesis that biological properties confer substrate selectivity in proteolysis.

To determine whether proteasome-mediated degradation of mitochondrial proteins may in fact occur in vivo, we conducted a pilot experiment to compare the protein turnover rates of normal mice and mice treated in vivo with epoxomicin, an irreversible proteasome inhibitor with no activity against the Lon protease. Twenty-eight wild-type C57BL/6J mice were randomized into

145

two groups, receiving daily injection of 0.5 mg·kg^{-1}·d^{-1} epoxomicin or vehicle, respectively, whilst labeled with ^2H_2O simultaneously. Protein turnover rates from the two groups were measured as described.
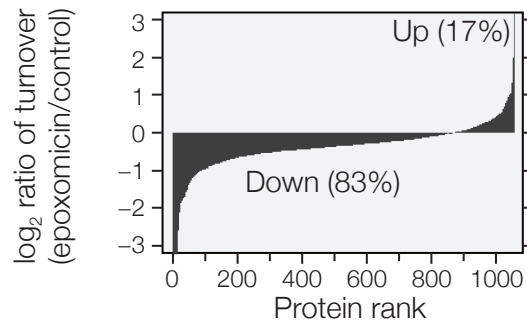
FIGURE 3.18   Effect of in vivo epoxomicin stimulus on protein turnover

FIGURE 3.18 shows the results of the above experiment and the comparison of protein turnover rates. Amongst 1,056 compared proteins, 83% exhibited an expected decrease in overall turnover rates following epoxomicin stimulus, consistent with the inhibition of proteasomes leading to a decrease in replacement of the majority of cellular proteins that are ordinarily degraded through the ubiquitin-proteasome system; whereas 17% of proteins exhibited an increase in overall turnover rates. The bottom 10% of proteins (with most drastically decreased turnover rates) were significantly enriched in proteins involvedin focal adhesion including collagens and caveolins (3.6-fold enrichment, Fisher's Exact P: 6.9×10^{-5}; Benjamini-Hochberg P: 0.02), whereas the top 10% of proteins (with increased turnover rates following epoxomicin) were suggestively enriched in proteases (3.2-fold enrichment, Fisher's Exact P: 2.6×10^{-4}; Benjamini-Hochberg P: 0.19), and include several 19S and 20S proteasome subunits (PSMA4, PSMA5, and PSMC5).
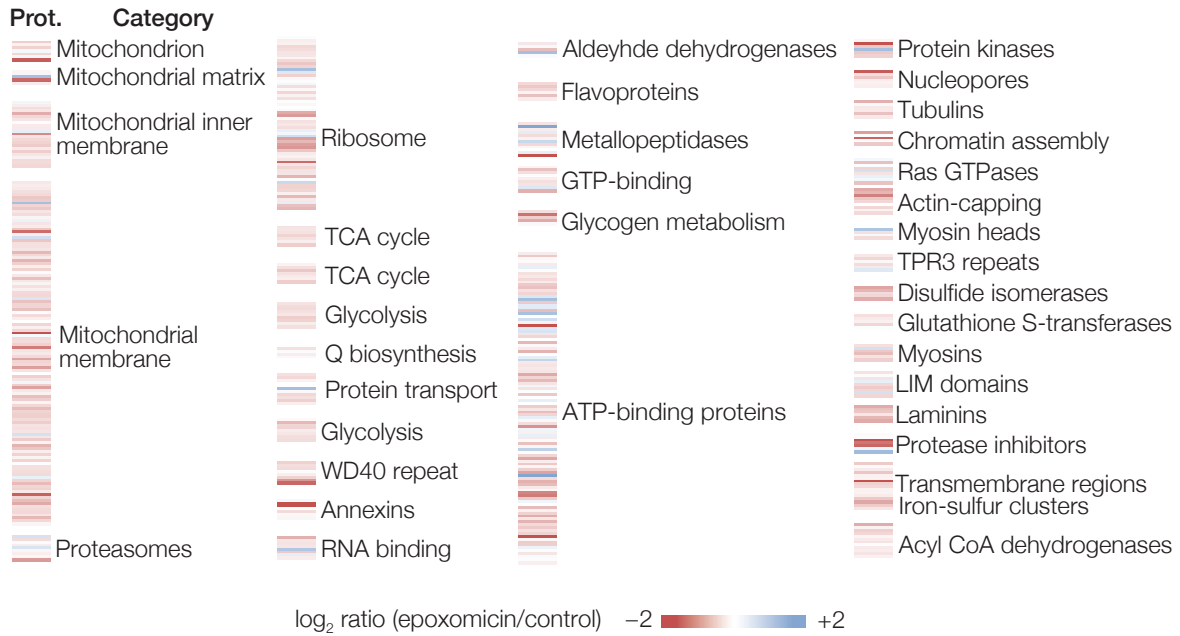
FIGURE 3.19   Epoxomicin-sensitive turnover rates in functional clusters

FIGURE 3.19 shows the functional categories of quantified cardiac proteins along with the ratio of their turnover rates in epoxomicin vs. vehicle treatment. A number of mitochondrial proteins are amongst the majority of proteins, which exhibited a decrease in protein turnover. The data are therefore consistent with cytosolic proteasomes being able to influence the dynamics of mitochondrial proteins, and suggest that a number of mitochondrial proteins are potential proteasome substrate in vivo. However, a major limitation of the experimental results is that they do not distinguish secondary effects (such as the decreased degradation of mitofusion 2 affecting mitochondrial dynamics) from direct proteolysis of mitochondrial proteins by proteasomes.

To summarize this chapter, our results corroborate accumulating evidence on alternative mechanisms of mitochondrial protein turnover in vitro and in vivo. We showed that the stability and degradation of the cardiac mitochondrial proteins provide a mechanism for altered mitochondrial protein turnover in the diseased heart, where the inhibition of oxidative metabolism

and the accumulation of metabolic byproducts in the mitochondria are known to directly contribute to the etiology of myocardial dysfunction. The failure to contain mitochondrial protein damage and restore protein homeostasis would result in the disruption of key metabolic and energetic subsystems and serve a molecular trigger of further pathogenesis. The interrelationship among cardiac mitochondria, ROS, and protein quality control suggests an axis where disrupted protein dynamics of the mitochondria plays a decisive role in the course of cardiac remodeling. As misfolded proteins are typically degraded through multiple pathways, several effectors may act in concert to modulate mitochondrial proteome turnover. The UPS presents a recent candidate contributor of extra-mitochondrial degradation mechanisms, and the 20S proteasome is here shown to independently degrade mitochondrial proteins in the absence of ubiquitination. We hypothesize a working model where the 20S proteasomes may act as an oxidative stress response to modulate mitochondrial protein dynamics under different physiological and pathological conditions. These findings should stimulate further investigations on the roles of alternative protein degradation mechanisms on the homeostasis of cardiac mitochondria in normal and stressed conditions.

Materials and methods

Method summary: Hsd:ICR (CD-1) mouse cardiac mitochondria and 20S proteasomes were isolated as previously described (Zhang et al., 2008b; Zong et al., 2006). The mitochondrial proteome was set up to undergo proteolysis either by its endogenous proteases, or by exogenous, active 20S cardiac proteasomes. Relative protein abundances following proteolysis were determined by two-dimensional differential gel electrophoresis (2D-DIGE), then identified by LC-MS.

Reagents. All chemicals were purchased from Sigma-Aldrich unless specified. Milli-Q (Millipore) filtered water (18.2 MΩ) was used throughout the study.

Study approval: Mouse experiments were conducted in accordance with the Guide for the Care and Use of Laboratory Animals by the National Research Council and approved by University of California, Los Angeles. Animals were euthanized with an overdose of pentobarbital (150 mg·kg^{-1} i.p.) or cervical dislocation in accordance with guidelines established by the American Veterinary Medical Association Panel on Euthanasia.

Isolation of cardiac mitochondria: Male Hsd:ICR (CD-1) outbred mice (Harlan laboratories) at 8 – 12 weeks of age were used for the study. To isolate mitochondria from the heart, we euthanized ≈20 mice and performed thoracotomy to excise the hearts. The heart was immediately minced and homogenized using a Dounce glass homogenizer (≈25 strokes) in a sucrose buffer (250 mmol·L^{-1} sucrose, 10 mmol·L^{-1} HEPES, and 10 mmol·L^{-1} Tris-HCl, pH 7.5). The sucrose buffer for mitochondrial preparations used for studying endogenous proteolytic activities contained no protease inhibitors, whereas the preparations for other experiments contained in addition 1 mmol·L^{-1} EGTA, protease inhibitors (Roche Complete, 1×), phosphatase inhibitors (Sigma Phosphatase Inhibitor Cocktail II and III, 1×), and 10 mmol·L^{-1} of dithiothreitol (Sigma). The heart homogenate was centrifuged (800 rcf, 4 °C, 7 minutes) to remove debris. The supernatant was centrifuged (4,000 rcf, 4 °C, 20 minutes) to pellet crude mitochondria. The mitochondrial pellets were washed once, then resuspended in 19% Percoll (Sigma) (v/v) in sucrose buffer, overlaid on 30% and 60% Percoll and ultracentrifuged (12,000 rcf, 4 °C, 20 minutes) to remove microsomal contamination. Purified mitochondria were collected from the 30%/60% Percoll interface and washed twice in the sucrose buffer, followed by centrifugation (4,000 rcf, 4 °C, 20 minutes) to remove the residual Percoll. We quantified the yield of isolated mitochondria by rupturing an aliquot of intact mitochondria through sonication in a hypotonic

buffer (10 mmol·L^{-1} Tris-HCl, pH 7.4), followed by bicinchoninic acid assays using pure bovine serum albumins as standards (Pierce).

Isolation of cardiac 20S proteasome: To purify 20S proteasomes for in vitro reactions, we euthanized ≈100 Hsd:ICR mice and performed thoracotomy to excise the hearts. The hearts were immediately minced and homogenized using a Dounce glass homogenizer (≈25 strokes) in a buffer (20 mmol·L^{-1} Tris-HCl, 5 mmol·L^{-1} MgCl$_2$, protease inhibitors (Roche Complete, 1×), phosphatase inhibitors (Sigma Phosphatase Inhibitor Cocktail II and III, 1×), and 0.5 mmol·L^{-1} dithiothreitol, pH 7.8). We centrifuged the homogenate (25,000 rcf, 4 °C, 2 hours) to collect the cytosolic fraction in the supernantant, where the majority of proteasomes reside. We precipitated this cytosolic supernatant sequentially using 20%, 40%, and 60% ammonium sulfate to yield the 20S proteasome-containing fraction, which precipitates at 40% ammonium sulfate. This fraction was dialyzed against 20 mmol·L^{-1} Tris-HCl, 5 mmol·L^{-1} MgCl$_2$, 0.5 mmol·L^{-1} dithiothreitol, pH 7.4 at 4 °C overnight, then further purified using ion-exchange chromatography on a Q Fast Flow XK26/40 column (Amersham). The crude 20S proteasomes was resolved by isocratic steps of 270 mmol·L^{-1}, 450 mmol·L^{-1} and 600 mmol·L^{-1} KCl, dissolved in 20 mmol·L^{-1} Tris-HCl, 5 mmol·L^{-1} MgCl$_2$, 0.5 mmol·L^{-1} dithiothreitol, 10% glycerol, pH 7.4, at a flow-rate of 5 mL·min^{-1}, at 4 °C. The eluent from 450 mmol·L^{-1} KCl was collected and ultracentrifuged (205,000 rcf, 4 °C, 19 hours) to sediment the proteasomal complexes. The resulting pellets were resuspended in 20 mmol·L^{-1} Tris-HCl, 5 mmol·L^{-1} MgCl$_2$, 0.5 mmol·L^{-1} dithiothreitol, 10% glycerol, pH 7.4 and further resolved by ion-exchange chromatography on a Mono Q HR5/50 column using identical solvents as above. The purified 20S-proteasome eluted at ≈360 mmol·L^{-1} KCl under the following gradient: 0 – 270 mmol·L^{-1} KCl for 7.875 column-volumes, 270 – 450 mmol·L^{-1} KCl for 21 column-volumes and 450 – 600 mmol·L^{-1} KCl for 4.375 column-volumes, at the flow rate of 0.5 mL·min^{-1}, at 4 °C. My colleagues in the Ping laboratory have previously used this method to successfully acquire highly purified 20S proteasome complexes (Drews et al., 2010; Wang et al., 2011a; Zong et al., 2006). We quantified the 20S proteasome yield with

bicinchoninic acid assays using pure bovine serum albumin as standards (Thermo Pierce), and further assessed the purity of the preparation using SDS-PAGE and Coomassie Blue staining. The activities of 20S proteasomes were validated using established fluorescent substrates of 20S proteasomes (Z-LLC-AMC for caspase-like activity, Boc-LSTR-AMC for trypsin-like activity, and Suc-LLVY-AMC for chymotrypsin-like activity) as previously described (Zong et al., 2006).

In vitro proteolysis of cardiac mitochondrial proteins: To assess the effect of endogenous proteolytic activities on degrading the cardiac mitochondrial proteome in vitro, we incubated isolated mitochondria (150 μg polypeptide equivalent) in 100 μL of sucrose buffer and 100 mmol·L^{-1} ATP at 37 °C for ~15 hours. The effect of 20S proteasome-mediated degradation was examined by adding murine cardiac 20S proteasome to ruptured mitochondria (150 μg polypeptide equivalent) and incubating the mixture in 100 μL of 50 mmol·L^{-1} HEPES, 100 mmol·L^{-1} KCl, 10 mmol·L^{-1} MgCl$_2$, and 100 mmol·L^{-1} CaCl$_2$, pH 7.6 at 37 °C for 9 hours. Mitochondria and 20S proteasomes were incubated separately in the proteasome-negative control. In the reaction mix, the molar ratio of 20S proteasome to mitochondrial proteins was ≈ 1:50, assuming an average molecular weight of mitochondrial proteins of 55,000 Da and that of the 20S proteasome complex to be 750,000 Da. Following incubation, the proteins were frozen at −20 °C to deactivate enzymatic activities and acetone-precipitated using the GE Healthcare Amersham Ettan 2D Clean-up Kit according to the manufacturer's instructions.

Measurement of proteolytic activities of mitochondrial proteases: We estimated the endogenous proteolytic activity of mitochondria by incubating 100 μg of isolated murine cardiac mitochondria with 100 mmol·L^{-1} ATP and 10 μL of fluorescein-labeled casein (Sigma Protease Fluorescent Detection Kit) at 37 °C in the dark for 2 hours. Any undigested proteins were precipitated by incubation with 150 μL of 0.6 N trifluroacetic acid at 37 °C for 30 minutes, followed by centrifugation (10,000 rcf, ambient temperature, 10 minutes). To detect the amount of di-

gested peptides, we mixed 10 μL of the supernatant with 200 μL of 500 mmol·L^{-1} Tris, pH 8.5, and measured the fluorescence at 485 nm/527 nm using a Thermo Fluoroska Nascent microplate spectrofluorometer.

Fluorescence labeling and separation of mitochondrial proteins: To resolve and quantify the mitochondrial proteins following in vitro proteolysis, we resuspended the acetone-precipitated digests in 30 μL of deionized 8 mol·L^{-1} urea, 2 mol·L^{-1} thiourea, and 4% (w/v) 3-[(3-cholamidopropyl)dimethylammonio]-1-propanesulfonate (CHAPS). Protein labeling was carried out with 150 pmol Cy3 or Cy5 fluorescent cyanine dyes using the CyDye^{TM} DIGE Fluor (minimal dye) Labeling Kit (GE Healthcare) on ice for 3 hours according to manufacturer's instruction. Furthermore, aliquots from replicate experiments were combined and labeled with Cy2 fluorescent dyes as internal loading standards of each gel. The labeling reaction was quenched with 20 nmol L-lysine. The Cy2, Cy3 and Cy5 samples of each experiment were combined and diluted to 340 μL with deionized 8 mol·L^{-1} urea, 2 mol·L^{-1} thiourea, and 4% (w/v) 3-[(3-cholamidopropyl)dimethylammonio]-1-propanesulfonate (CHAPS), 2% (v/v) tributylphosphine (Sigma), 1% (v/v) carrier ampholite (GE IPG buffer 3 – 11 non-linear), 1% (v/v) GE deStreak reagent, and 1.5% (w/v) dithiothreitol. IEF was conducted on 18-cm Immobiline DryStrip pH 3-11 non-linear IPG strips (GE Healthcare) on an Ettan IPGphor 3 instrument (GE Healthcare) with the following profile: 30 V, 8 hours; 150 V, 2 hours; 300 V, 2 hours; 600 V, 2 hours; 1000 V, 2 hours; 1000 – 8000 V ramping, 1 hour; 8000 V until 60000 V·hr. The IPG strips were equilibrated in 50 mmol·L^{-1} Tris-HCl, 8% (w/v) SDS, 6 mmol·L^{-1} urea, 30% (v/v) glycerol, 1% (w/v) dithiothreitol, pH 8.8, at ambient temperature in the dark, for 30 minutes, followed by 50 mmol·L^{-1} Tris-HCl, 8% (w/v) SDS, 6 mmol·L^{-1} urea, 30% (v/v) glycerol, 4% (w/v) iodoacetamide, pH 8.8, for 30 minutes. We then separated the charge-resolved proteins by size using SDS-PAGE on a 12% Tris-glycine acrylamide gel at 80 V at ambient temperature in the dark for 19 hours. 2D-DIGE gels were scanned on a Typhoon 9410 workstation (Amersham) near 489 nm/506 nm, 550 nm/570 nm, and 650 nm/670 nm for each of the Cy dyes using the manufacturer's scanner

control software. The protein spots from fluorescent signal scans were recognized and quantified using the Progenesis SameSpots software (v.4) (Nonlinear Dynamics).

Identification of protein species using LC-MS: Following quantification, the gels were silver-stained and protein spots were manually excised and digested with 1:50 (w/w) modified sequencing-grade trypsin (Promega) using a standard in-gel digestion protocol my colleagues in the Ping laboratory has previously utilized(Wang et al., 2011a). The extracted peptides were separated on a 300-Å-pore, 5-μm-particle, 75 μm × 150 mm C_{18} reverse-phase nanoLC column (New Objective) and analyzed on a Thermo LTQ-XL linear ion-trap mass spectrometer, controlled using the XCalibur v.1.5 software with typical parameters for routine protein identification. The acquired spectra were searched using the SEQUEST algorithm in Thermo Bioworks v.3.3.1, against the UniProt mouse database (2011-07-27; 55,744 entries). The identified peptides were further grouped into non-redundant protein sets with Scaffold v.2.0 (Proteome Software). Gel spots that did not result in the unambiguous assignment to a single protein claiming a preponderance of unique peptides were excluded from quantitative analyses.

In a parallel set of experiments, we also assessed the relative abundances of proteins from isolated mitochondria using shotgun proteomics and spectral counts as previously described (Paoletti et al., 2006). Briefly, we defined the spectral abundance factor of a protein as the sum of peptide spectral counts divided by its length. The spectral abundance factors of all proteins identified in an experiment are normalized within the population to give the normalized spectral abundance factor (NSAF) as a quantitative measurement of relative protein expression levels in the mouse heart.

Measurement of protein turnover rates: Protein processing, MS analysis and bioinformatics workflows were as reported in Chapter II unless otherwise specified. Hierarchical clustering analysis was performed with the software program Cluster (v.3.0 for Mac OS X) by Michael

153

Eisen (Eisen et al., 1998) using Spearman's correlation as similarity matrix and complete link-age clustering, then visualized as a scalable heat map with JTreeView (v.3.0) (Saldanha, 2004).

IV. Translational potential and future perspectives

This chapter begins with a discussion on some ongoing applications of the presented methods to measure protein turnover in vivo in animal models, including the use of six inbred mouse strains with different outcomes after isoproterenol challenge as a model to distinguish proteomic features associated with susceptibility to cardiac hypertrophy. I then explore the challenges and outlook on how protein turnover studies can be translated to studying human diseases of the heart and of other systems. My colleagues and I devised a non-linear kinetic model that accounts for the rate constant of isotope enrichment in human experiments, and demonstrate that it can be used to measure the turnover rates of over 500 human plasma proteins. The material composing this chapter was published and can be found in our publications (Lam et al., 2014; Wang et al., 2014).

Approaches for further applications and data validation

We utilized a genetic model as a differential to further categorize candidate proteins and identify potential disease drivers. To do so, we performed the turnover experiment in multiple strains of inbred mice from the hybrid mouse diversity panel (HMDP). Susceptibility to and progression of HF are governed in no small part by genetic variability (Bleumink et al., 2004), thus environmental stressors must be viewed within the diverse context of biochemical individuality – the genetic canvas that distinguishes one person from another and contributes to the molecular phenotypes that determine disease susceptibility. The Lusis lab has pioneered the use of a panel of >100 laboratory mouse strains with variable traits and fully defined genotypes to ex-

amine the genetic basis of common traits (Ghazalpour et al., 2012; van Nas et al., 2013; Parks et al., 2013).
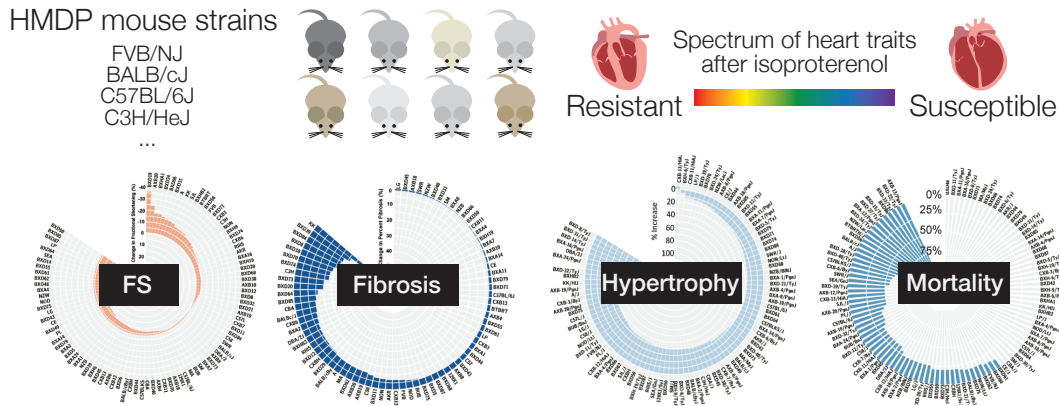
FIGURE 4.1   Spectrum of cardiac phenotypes in mice

FIGURE 4.1 shows the spectrum of cardiac phenotype in different mouse strains. (Top) Like individuals in a human population, the HMDP mouse strains exhibit individual differences in heart failure traits, and their polymorphic genetic makeup profoundly influences outcome in the isoproterenol-induced heart failure model. Data are shown on various traits including fractional shortening (FS), hypertrophy, fibrosis, and survival following 21 days of isoproterenol challenge (data from (Rau, 2013)). These variations also manifest during disease development as variable intermediate phenotypes (e.g., RNA and protein levels) that can be exploited for systems level interrogations (Civelek and Lusis, 2014). The HMDP mice therefore constitute a renewable systems biology resource for studying the molecular complexity that underlies why some individuals are predisposed to common diseases, while others are not.

In order to carry out such analyses, however, the question of whether protein dynamics is influenced by genetic must first be addressed. Recent studies have shown that absolute protein abundance is a heritable trait that influences phenotype (Wu et al., 2013) and holds prom-

ise for clinical diagnosis (Gerszten et al., 2011). We therefore asked whether protein half-life is an intrinsic trait that varies greatly by genetic backgrounds in the HMDP strains by comparing the measured turnover data from several distinct strains in the following preliminary studies, which will determine whether we may leverage the genetic differences of distinct mouse strains to identify causal disease associations in conjunction with the power protein dynamics to reveal non-steady-state perturbations.

Mouse strain	Mortality	Fibrosis	Hypertrophy	Fractional shortening
FVB/NJ	Resistant (0-25%)	Resistant	Moderate (20-40%)	Decrease
CE/J	Resistant (0%)	Resistant	Resistant (0-20%)	Increase
C57BL/6J	Moderate (25-50%)	Resistant	Moderate (20-40%)	No change
BALB/cJ	Susceptible (50-75%)	Susceptible	Moderate (20-40%)	No change
A/J	Susceptible (50-75%)	Moderate	Susceptible (40-60%)	Decrease
DBA/2J	Moderate (25-50%)	Susceptible	Susceptible (40-60%)	No change

TABLE 4.1   **Expected phenotypes of examined mouse strains**

TABLE 4.1 lists the expected phenotypes of the mouse strains used, based on data following isoproterenol challenge in (Rau, 2013). For reason of throughput, we limited the number of mouse strains to six (FVB/NJ, BALB/cJ, C57BL/6J, DBA/2J, A/J, CE/J). FVB/NJ, CE/J, and C57BL/6J are considered to be resistant to isoproterenol-mediated cardiac remodeling, based on mortality, fibrosis, hypertrophy, and fractional shortening data from (Rau, 2013); BALB/cJ, A/J, and DBA/2J are considered to be susceptible to isoproterenol, although it may be seen that susceptibility of a strain depends on the trait being measured (in addition to the heart failure model being employed). For our purpose in locating the extreme strains, we considered hypertrophy and mortality with priority. Note that these studies were not designed to map causal polymorphisms for heart failure, but rather would use the above strains which was demonstrated to show extreme phenotypes (very resistant or very susceptible to isoproterenol-induced heart failure) as differentials to generate hypotheses and prioritize candidates for

validation studies; e.g., a bona fide disease driver is likely to have particularly perturbed half-life in susceptible strains, whereas a protective proteome change may present in resistant strains.
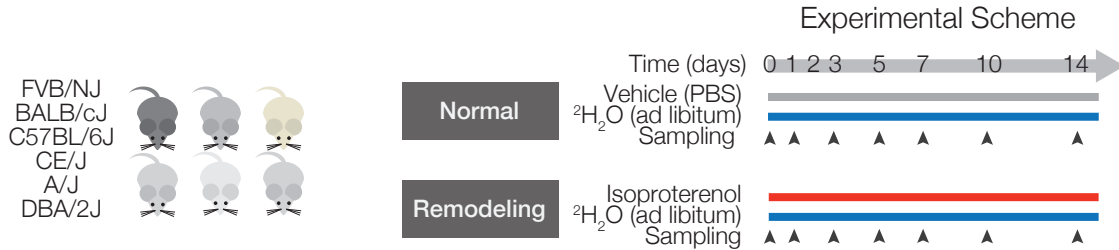
FIGURE 4.2   Experimental design of mouse strain study

FIGURE 4.2 illustrates the experimental scheme. For each of the six mouse strains, 28 male animals (9 – 12 weeks of age) were randomized to receive either vehicle (normal hearts) or 20 mg·kg^{-1}·d^{-1} isoproterenol (remodeling hearts) for up to 14 days. Labeling with ^2H_2O was initiated simultaneously as described in previous chapters. Samples were collected at day 0, 1, 3, 5, 7, 10, 14 following the initiation of labeling, and analyzed for protein turnover with MS and Pro-Turn as described.
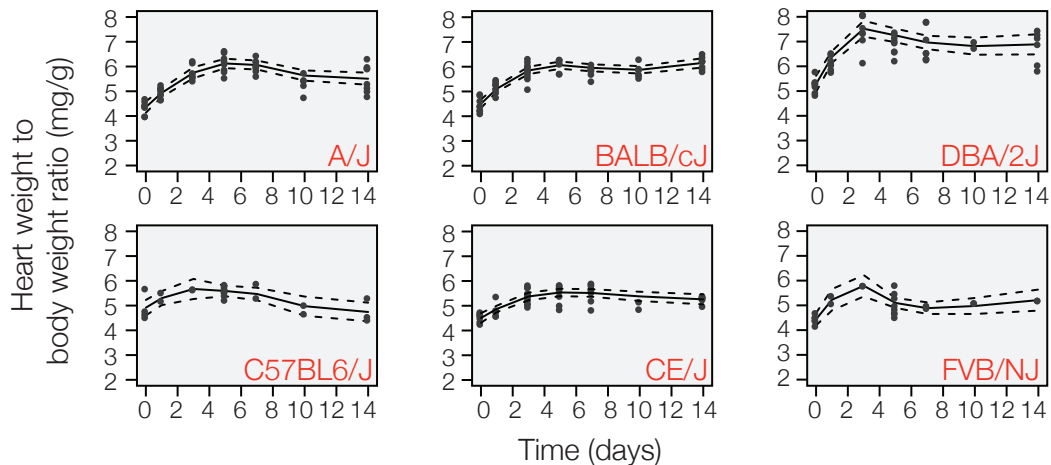
FIGURE 4.3   Hypertrophic responses of resistant and susceptible strains

FIGURE 4.3 plots the experimental heart-weight-to-body-weight ratios of the six mouse strains following isoproterenol treatment in our laboratory. As expected, the susceptible mouse strains (top) exhibited substantially higher degrees of hypertrophy following isoproterenol than the resistant strains (bottom). Each data point represents an individual animal; solid and dashed line represents local regression and 95% confidence interval.

Strain	Turnover rate (control)	Turnover rate (isoproterenol)	Quantified proteins* (control, isoproternol)	Median deviation (control, isoproterenol)
FVB/NJ	0.15 [0.04 - 0.64]	0.11 [0.03 - 0.48]	1421, 1078	17.7%, 18.2%
CE/J	0.11 [0.03 - 0.45]	0.13 [0.03 - 0.52]	1599, 1420	17.8%, 18.4%
C57BL/6J	0.09 [0.03 - 0.45]	0.13 [0.03 - 0.45]	1168, 1824	19.3%, 19.2%
BALB/cJ	0.12 [0.04 - 0.58]	0.12 [0.03 - 0.50]	1038, 1130	17.7%, 18.0%
A/J	0.11 [0.03 - 0.52]	0.13 [0.04 - 0.46]	1625, 1745	22.0%, 18.7%
DBA/2J	0.13 [0.03 - 0.54]	0.14 [0.04 - 0.45]	1742, 1630	19.3%, 17.8%
Hsd:ICR	0.10 [0.03 - 0.51]	0.13 [0.03 - 0.43]	2271, 2439	22.1%, 20.0%

TABLE 4.2   Summary and statistics of examined mouse strains

TABLE 4.2 summarizes the results of the MS experiments on the six mouse strains. Turnover rates (d^{-1}) are given as median [5th to 95th percentile]. The median deviation is given as the median of all median absolute deviations of turnover rates amongst peptides belonging to the each protein. Data from Hsd:ICR mice are reproduced from Chapter II for reference.
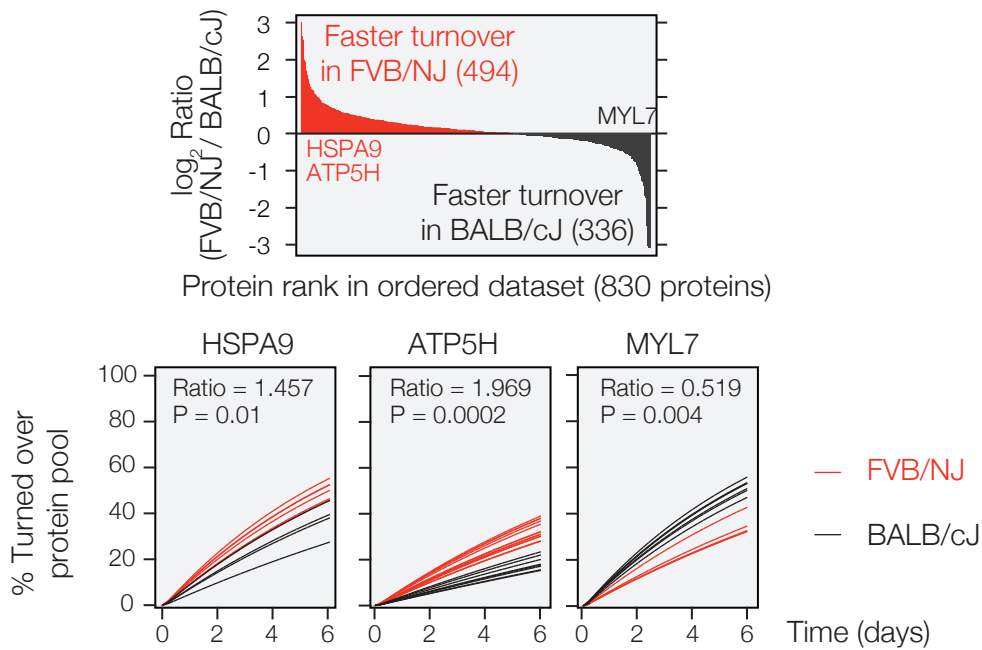
FIGURE 4.4   Strain differences in protein turnover rates

FIGURE 4.4 demonstrates how basal protein half-life varies significantly between two inbred mouse strains with differential susceptibility to heart failure, indicating half-life data can be co-mapped with genetic differences in the HMDP strains to cardiac traits of interest. (Top) Preliminary data from 830 compared proteins show that basal protein turnover differ between two mouse strains. (Bottom) Each graph shows the percentage of protein pool that has been turned over at different time points. Each line represents an independent measurement, e.g., ~60% of the mitochondrial heat shock protein HSPA9 molecules turned over after 6 days in FVB/NJ mice, as opposed to ~40% in BALB/cJ mice, suggesting HSPA9 has higher turnover rates in the FVB/NJ strain. Similarly, the mitochondrial ATP synthase subunit ATP5H turns over faster in FVB/NJ mice, whereas the myosin light chain protein MYL7 turns over faster in BALB/cJ mice. The variability observed between mouse strains was greater than the variability from independent replicate observations within the same strain, suggesting the difference was due to genetic backgrounds. Future multivariate analysis will determine whether particular proteins exhibit turnover behaviors that segregate with phenotypic classifications.

We next considered the potential validation workflows for large-scale protein turnover datasets, e.g., the data from this and the previous chapters which identified a number mitochondrial proteins whose disrupted degradation with impaired proteolysis. From these data one may hypothesize that selected mitochondrial proteins normally maintained in homeostasis by intra-mitochondrial proteases, exhibit impaired proteolysis during remodeling that may contribute to further disease development. Although it lies beyond the current scope of investigation, it would be of interest to theorize how such findings may be validated to identify causal disease drivers.

In the simplest iteration, candidate disease drivers can be genetically manipulated to simulate enhanced or diminished protein abundance as may occur during isoproterenol remodeling. Although we are identifying protein targets that may not show overt steady-state abundance changes, silencing or overexpression will nevertheless change their turnover dynamics and allow us to test whether the protein may modulate disease phenotypes. High-priority targets may be tested with siRNA or adenoviral vectors followed by functional assays in H9c2 rat cardiomyoblast cells or neonatal rat ventricular myocytes (NRVM) to determine whether perturbing such the discovered protein targets may affect phenotypes. These experiments may be carried out under a hypertrophic remodeling stimulus (48 hours of stimulation of 10 µmol·L^{-1} phenylephrine or 1 nmol·L^{-1} endothelin-1). Cellular remodeling may be assessed using cell size, cell morphology, growth rate, respiratory rates, and apoptosis, whereas qRT-PCR can be performed to quantify expression of the fetal gene program (e.g., ANF, beta-MHC), with the goal of testing whether manipulating protein targets can ameliorate expected transformations to hypertrophic phenotypes.

More sophisticated in vitro genetic manipuation studies will validate whether the candidates can causally modulate hypertrophy phenotypes via the discovered turnover changes. Methods to modulate protein turnover genetically (e.g., N-end rule and ubiquitin fusion modifications (Dantuma et al., 2000)) have been described that may be considered. If a validated degradation signal exists (e.g., phosphorylation or acetylation), tagged constructs can be made for the candidate proteins in which discovered modification sites can be mutated (S/T -> A for non-phosphorylatable; S/T -> D/E for phosphomimetic; K -> R for non-acetylatable, K -> Q for acetyl-mimetic) to measure their effects on protein degradation and cardiac phenotypes. Cardiac-specific and/or muscle specific (tinC-Gal4 or Dmef2-Gal4) UAS-RNAi drosophila lines (from VDRC) may be used to directly test their effects in cardiac parameters and in tissue metabolic functions. Once we home in on several candidate disease proteins, we may also formally test the hypothesis that the differential turnover of these proteins contributes to heart disease development by expanding to 50 or more HMDP mouse strains to measure their half-life using highly targeted, high-throughput assays such as multiple-reaction monitoring (MRM) mass spectrometry, from which turnover quantitative trait loci may be mapped.

We envision that these and other future experiments will help establish the causality of protein dynamics regulations in effecting cardiac remodeling, which will be indispensible to the search for actionable targets and interventional strategies that modulate turnover. In the long-term, however, the utility of protein turnover studies will hinge upon the ability to validate the data in other model systems and in human, with the eventual objective of measuring protein turnover in the hearts of heart failure patients and LVAD patients in order to understand the anatomy, behavior, and time-evolution of human heart disease as well as to identify new markers for disease sub-classifications. To achieve this goal, an indispensible first step is to validate and optimize the analytical approach and to determine whether it may be applicable to other model systems and human.

Protein turnover in non-linear enrichment systems

A primary rationale for ^2H_2O labeling in our studies is that ^2H_2O is unique among protein tracers in its compatibility with human clinical investigations. Several advantages of ^2H_2O over other isotope tracers as described in Chapter I are particularly applicable to future clinical studies. Firstly, contrary to labeled amino acids or ^{15}N tracers, ^2H_2O oral uptake is straightforward to administer without dietary modifications, which would obviously present additional difficulty in subject recruitment and administration, as the subject would have to ingest an enriched meal in place of usual foodstuff. Secondly, the ability to monitor body water enrichment from any body fluid is especially beneficial for clinical studies as it minimizes the number of procedures and potential inconvenience or invasiveness. Thirdly, ^2H_2O is sufficiently inexpensive to remain financially feasible within the scale of human consumption. A labeling regiment would consume approximately 0.75 to 1.5 L of 70% ^2H_2O, depending on body mass, to achieve up to 2% labeling for up to 14 days, which would cost approximately \$500 per subject at the time of writing. By contrast, equivalent isotope enrichment with ^{13}C-labeled leucine would cost approximately \$5,000 per subject based on 3 g of total leucine intake per day. Thirdly, ^2H_2O has a well-established safety record in human going back decades (Busch et al., 2007; Price et al., 2012a). No physiological effects have been reported at the proposed dosage (~2%).

Nevertheless, several technical constraints hinder the application of ^2H_2O labeling to validate disease drivers in the clinical setting, which we aimed to address in a pilot study. Firstly, human has slower metabolism and protein turnover than in smaller animal models, which decreases the amount of labels incorporated into the subject during the labeling period, which favors experiments with longer labeling duration to be able to effectively measure protein turnover rates. However, procedurally it would be desirable to minimize the labeling duration in

a human study so as to minimize the impact of the labeling regimen to the human subject. In addition, a viable strategy to acquire cardiac protein turnover rates must be able to deduce protein turnover from only a single time point, given the severely limited surgical availability of cardiac samples and the impossibility to acquire repeated biopsy samples in most cases. In patients, samples procurements are only available at specific points, such as during LVAD installation, cardiac transplant, or the routine biopsies of post-transplant surveillance.

Secondly, a lower dose of ^2H_2O enrichment is targeted for human subjects (2%) as compared to animal studies (5%), which limits the amount of isotopes that are incorporated into proteins. Since fixed variations in the measured isotopomer fractional abundance by the mass spectrometer will translate into larger errors in measured protein turnover rates, we expect that the median absolute deviations of turnover rates from peptides in the same protein will be larger as a result. To maintain data integrity, the data analysis workflow must needs incorporate more stringent filtering criteria, which will exclude some proteins with lower abundance from taken into consideration.

Thirdly, human subjects take in ^2H_2O through small boluses. In rodent models, one can administer an initial i.p. injection of almost isotopically pure ^2H_2O into the animal to quickly reach the desired level of enrichment, which amounts to approximately 1 mL of ^2H_2O in a 40-g outbred Hsd:ICR (CD-1) mouse, assuming 60% body mass of water. An equivalent booster in human would unfeasibly require an injection of 1 L of ^2H_2O into the subject at once. Hence, label enrichment in body water rises gradually before reaching the target level, which complicates data analysis workflows, as described below.
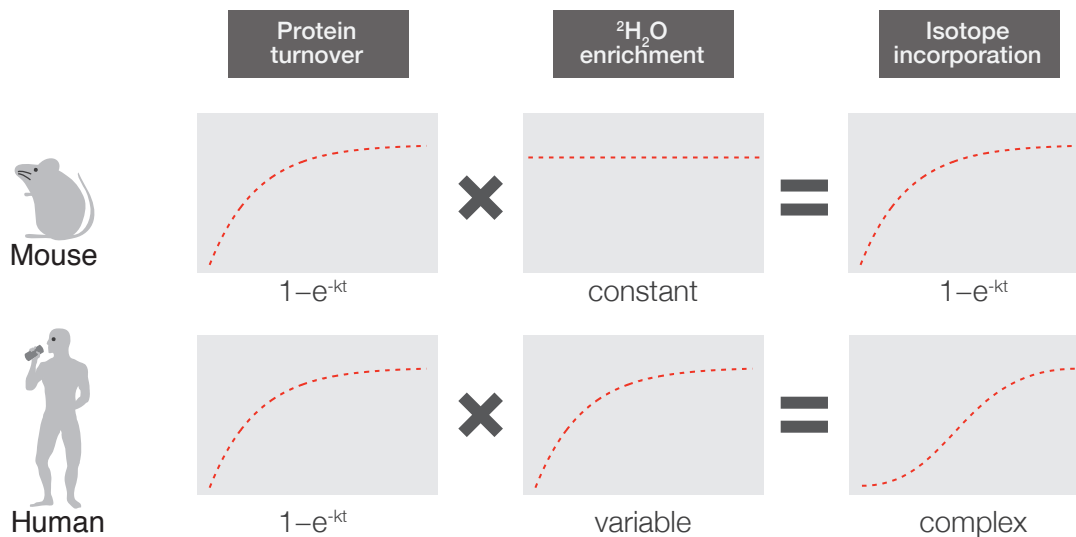
FIGURE 4.5   Complications for ^2H_2O labeling in human

FIGURE 4.5 illustrates the analytical complications that may arise from the slow enrichment of labels in human patients. The top half of the figure shows the principles of isotope incorporation in mice, as has been previously discussed. Protein turnover is assumed to follow first-order kinetics. For instance, if we consider the proportion of protein molecules in a protein pool that are newly synthesized after a certain point in time, this value should be a function of time that follows an exponential rise curve: the more newly synthesized proteins are present, the more newly synthesized proteins will be degraded, thus tapering the rise of the proportion of new proteins as it approaches the plateau. Couple this to a constant background of ^2H_2O label enrichment, such that every new protein molecule is labeled with a constant amount of isotopes, and we get the same first-order exponential rise curve in the appearance of higher-mass protein isotope in the mass spectrometer. By contrast, the scenario is slightly different in human as shown in the bottom half of the figure. Protein turnover still follows the same natural laws and display first-order kinetics, yet the enrichment of ^2H_2O is by necessity variable. As a result, a protein molecule that is made shortly after labeling begins will contain less labels than one that is made later when label enrichment is higher, thus jeopardizing the pattern of higher-mass isotopes in the MS data, and forbidding straightforward interpretation of the data. As

stated above, the reason for such discrepancy of label enrichment is largely due to the in hu-

man patients, labels have to be introduced slowly and gradually.

Several strategies account for this discrepancy. Firstly, one can compare within samples with-

out parametrizing the turnover rate constant k. Direct comparisons of enrichment level for

equivalent peptides can give a qualitative measures of whether a particular protein may be

turning over faster, or slower, in a system, which has been demonstrated by several groups. In

a pioneering study, Emson et al. administered psoriasis patients with ^2H_2O and collected skin

samples with tape (Emson et al., 2013). The authors found ^2H_2O-label appearance on keratin

samples from psoriasis-affected skin to be significantly quicker than in healthy skin, suggesting

increased keratin synthesis is a quantitative biomarker of psoriasis that may be useful as a

non-invasive clinical indicator of treatment response. Since the study analyzed total label in-

corporation from the acid hydrolysate of isolated proteins, the weighted average of all protein

turnover rates was measured. As our approach allows the turnover rate of individual protein

species in human to be quantified separately, we anticipate that it can avail similar translational

strategies and greatly expand the scope of investigations.

Secondly, a method has been described by Marc Hellerstein and colleagues to correct for

fractional synthesis calculation under non-steady-state enrichment, which involves manual

calculation using MIDA to deduce the enrichment rate from the isotope distribution data at

each time point (Price et al., 2012a). This method was demonstrated in four healthy subjects

and deduced the protein turnover rates of approximately 100 plasma proteins.

Our solution is to model the precursor enrichment using a first-order kinetics model using a

unified a combined equation. This method has several advantages, e.g., it forgoes the labori-

ous manual data processing required to generating the resulting data table to calculate the

precursor enrichment at each time point individually, and will be described below.

Following our initial analytical workflow described in Chapter I, we identified several areas in which improvements may be made to our data analysis methods, with the goal being to increase the scope of half-life characterization to cover more of the proteome, in more diverse biological systems, and in a manner such that it is rigorous and sensitive enough to compare changes in protein half-life between health and disease.

Firstly, we devised a new mathematical model that does not involve free three-parameter fitting. The three-parameter method has many tangible advantages, such as the option to forgo GC measurement and its independence from the MIDA parameters which makes it feasible to characterize protein turnover in systems where the amino acid incorporation may be unknown, such as in vitro system with variable amino acid compositions in the culturing medium. However, several drawbacks also limit the utility of the method to disease models, for instance, the method still requires the kinetic curve to have elapsed sufficiently long for the plateau to be accurately predicted. In certain experimental systems with slow turnover (mouse mitochondria, human neurons, etc.) where proteins require a long period of time to plateau to their maximum isotope incorporation, the method is likely to perform poorly without extended labeling. This shortcoming is compounded by the fact that some disease models preclude a long period of labeling, e.g., the isoproterenol challenge model which we will utilize to simulate cardiac remodeling functions as intended to mimic cardiac remodeling within a time frame of 7 to 14 days, after which the mouse develops into full failure and insights into early cardiac remodeling can no longer be gained. Hence my colleagues and I devised an alternative approach, which defines the initial and plateau values of peptide isotope enrichment with MIDA parameters but additionally incorporate the rate constant of precursor enrichment to calculate protein turnover under non-steady-state $^{2}H_{2}O$ enrichment level.

Constant labeling

change in labeling $\dfrac{dA_0}{dt} = k \cdot (A_{0,max} - A_0)$ difference in labeling between current protein pool and newly-synthesized proteins

$A_{0,max} = a \cdot (1-p)^N$ combinatorial probability of a peptide having only light isotopes

Non-steady state labeling

^2H_2O in body $\quad p = p_{ss} \cdot (1 - e^{-k_p t})$ modeled with 1 − exponential decay

change in labeling $\dfrac{dA_0}{dt} = k \cdot \{ a\,[1 - p_{ss} \cdot (1 - e^{-k_p t})]^N - A_0 \}$
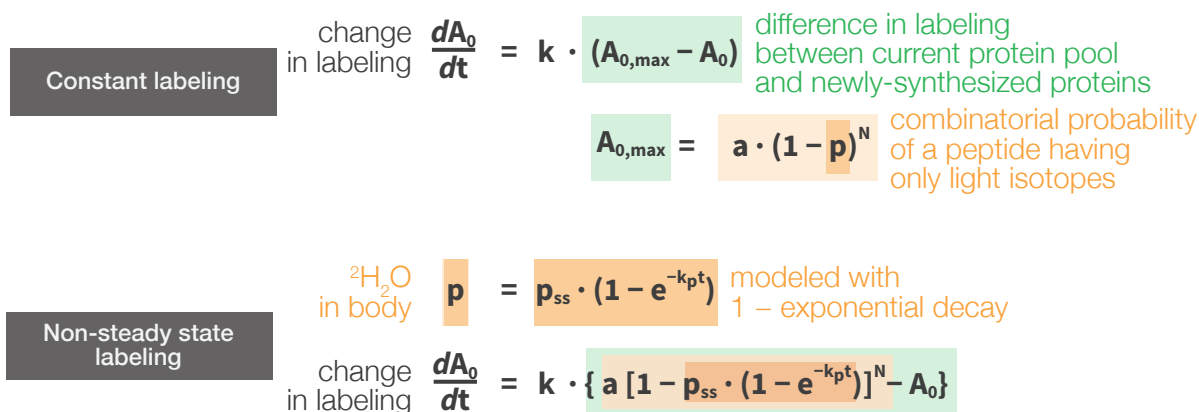
FIGURE 4.6   Principles of kinetic model for non-linear label intake

FIGURE 4.6 illustrates the principle of the non-steady-state enrichment model. A protein molecule that is synthesized shortly after labeling begins therefore would contain fewer isotope labels than one synthesized later, which complicates the ascertainment of the fraction of newly synthesized proteins from the MS data. In both constant labeling and non-steady-state labeling, protein turnover can be assumed to follow first-order kinetics. Under constant labeling, each new molecule of protein being synthesized will introduce a fixed amount of label into the label pool; hence the resulting peptide isotope distribution follows first-order kinetic curves. Under gradual enrichment scheme, label incorporation into proteins deviates from the first-order exponential decay function. To correct for the variable label enrichment, we further derived a nonlinear mathematical function that incorporates the rate constant of ^2H_2O enrichment (k_p) and the rate constant of protein turnover (k).

To correctly resolve isotopomer shifts by accounting for, both the rate constants of ^2H_2O enrichment and protein turnover need to be accounted for. The gradual incorporation of isotope labels in a proteolytic peptide can be represented by the decrease in the fractional abundance of the 0th isotopomer, A_0, i.e., the fraction of peptides devoid of any heavy isotopes. We followed the assumption that the decrease in fractional abundance of the unlabeled (0th) peptide

isotopomer (dA_0/dt) upon ^{2}H incorporation follows the kinetics of protein pool replacement. Thus the rate of decrease is strictly the result of protein turnover and follows first-order kinetics, where k is the protein turnover rate constant and $A_{0,max}$ is the fractional abundance of the 0th isotopomer in the newly-synthesized, labeled peptide, i.e., the amount of label that is entering the peptide pool. The component ($A_{0,max} - A_0$) therefore represents the difference between the steady-state label and the protein label at a particular time.

The amount of label entering the protein is governed by the number of labeling sites on the peptide, N, the precursor enrichment level, p, and the natural fractional abundance of the 0th isotopomer prior to labeling, a. In a simplified scenario where fast and constant precursor label enrichment can be achieved (e.g., in cell cultures following change of medium), $A_{0,max}$ is constant and represents the fractional abundance of the 0th isotopomer when the peptide is fully labeled as dictated by the precursor level, i.e., the fractional abundance when the peptide has reached the plateau and undergoes no additional changes. The resulting exponential decay equation reflects first-order kinetics as expected. However, in most realistic labeling situations, p and therefore $A_{0,max}$ are time-dependent given slow label intake, and a simple exponential decay equation no longer adequately describes the changes of A_0. This is due to the fact that when an organism intakes ^{2}H$_2$O, the pre-existing unlabeled H$_2$O predominates in molar ratio, and relative isotope abundance of ^{2}H rises slowly. We further reasoned that the time-dependent change of relative isotope abundance itself follows first-order kinetics with the steady-state level p_{ss} and the rate constant of k_p.

In a human labeling experiment, this sigmoidal function resolves isotopomer shifts by accounting for both the initial lag of available isotopes and the rise-to-plateau kinetics of protein turnover. Under fast enrichment, such as in mice, where $k_p \gg k$, the function approximates a first-order exponential decay function. Thus this nonlinear model could handle a wide range of labeling scenarios in mice, in human, and in other organisms with gradual label enrichment

including drosophila. This model is analogous in some aspects to more complex multi-compartment models with multiple rate constants that have been proposed for ^{15}N labeling (Guan et al., 2012), with a notable difference that the unified single kinetic equation facilitates curve-fitting and error estimation.

The solution to the differential equation can be found in the Supplemental Information of our publication (Lam et al., 2014) and is not reproduced here. The following contains a brief analysis of the properties of the equation, which is a function of five parameters: (i) k, the turnover rate of the protein to which the peptide belongs. This is the parameter of interest. (ii) p_{ss}, the plateau level of enrichment of ^2H_2O in the biological system. This parameter was readily measured from body fluid samples with gas chromatography-mass spectrometry. (iii) k_p, the rate constant of the rise-to-plateau kinetics of body water ^2H_2O enrichment. This parameter could be acquired from fitting gas chromatography measurements of body fluid samples at regular time points following the initiation of labeling to a first-order kinetics equation. (iv) a, which represents the unlabeled fractional abundance of the 0th isotopomer of the particular peptide. The value of a could be readily calculated from the peptide sequence and the natural biological abundance of heavy isotopes of carbon, nitrogen, oxygen, and sulfur, using the formula:

$$a = (1 - 0.011)^{N_C} \times (1 - 0.00366)^{N_N} \times (1 - 0.0238)^{N_O} \times (1 - 0.0498)^{N_S}$$

where N_C, N_N, N_O, N_S denote the number of carbon, nitrogen, oxygen, and sulfur atoms in the peptide, respectively. Lastly, (v), N, which represents the number of deuterium-accessible labeling sites on the peptide sequence. N could then be calculated as the sum of the known average accessible deuterium/tritium labeling sites on individual amino acids (N_{aa}) in mice, as has been reported in the literature (Commerford et al., 1983). It may be seen from experimental data that the values of a and N accurately predict the plateau values of A_0 of identified peptides, which is given by $a \cdot (1 - p_{ss})^N$. The values of a and N may be further adjusted in cases of

methionine oxidation, serine/threonine/tyrosine phosphorylation, lysine acetylation, and the lysine ubiquitination remnant diglycine, based on their respective atomic compositions.

The values for p_{ss} and k_p, for an experiment, together with the values of a and N for each individual peptide, were then substituted into the kinetic model, which could now be fitted using the Nelder-Mead method (Nelder and Mead, 1965) for the optimal value of k that minimizes the residual values between the model and the experimental data points. In systems where the target enrichment levels are quickly achieved ($k_p \gg k$) such as in mouse models, $A_{0,max}$ is effectively constant and the nonlinear model approaches a simple first-order exponential decay function. The nonlinear model is therefore applicable to both gradual and fast labeling experiments and can be used in both the mouse and human labeling studies.

A second development that occurred after our initial experiment in Chapter I and in parallel with the experiments in Chapter II was the acquisition of a more capable mass spectrometer in the form of a Thermo Orbitrap Elite instrument coupled to an Easy-nLC ultra-high performance liquid chromatography system. The new instrument gave higher intrinsic performance by virtue of its new ion guide design and smaller Orbitrap construction that allows shorter ion transient time. The new instrument allows experiments to be run at R = 60,000 resolution (at m/z 400) (as opposed to R = 7,500 on the Orbitrap XL) without sacrificing precision in measuring mass isotopomer relative abundance, which greatly increased performances in protein identification and peak integration. Details and performance comparison data are omitted here for brevity.

A third development took place as my colleagues and I built on top of the algorithm a complete software package with graphical user interface, which we named ProTurn.

| Read protein ID list and locate peptides from mass spectra | ▶ | Integrate isotopomers and calculate fractional abundance | ▶ | Perform nonlinear fitting of data time series to kinetic model | ▶ | Output optimized results in text and graphical formats |

FIGURE 4.7   Simplified flowchart of ProTurn

FIGURE 4.7 is a simplified workflow schematic of ProTurn. ProTurn is written in-house by programmers in the Ping lab and contains approximately 30 classes in approximately 30,000 lines of code in Java. My colleague Maggie Lam and I directed four student Java programmers (Brian Bleakley, Louie Liu, Tevfik Dincer, and Hannah Chou) to work on the user interface. A primary distinction of the user interface and the up to five-fold improved speed performance from previous work is that it allows all fitting parameters to be quickly optimized and iterated.

FIGURE 4.8   The graphical user interface of ProTurn
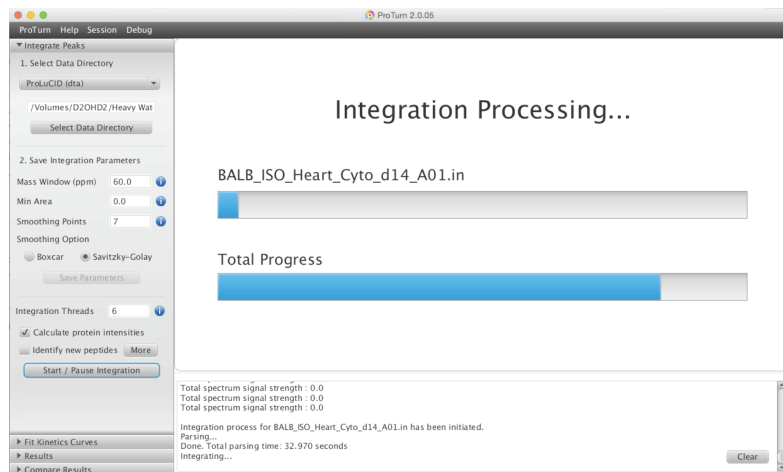
FIGURE 4.8 shows the user interface of a current build of ProTurn (2.0.5). Several elements are visible. The accordion menu to the left allows the user to choose between options and execution of the peak integration, kinetic curve-fitting, result display, and dataset comparison functions. Options from the peak integration page are shown, which house user-interactive

172

elements for selecting file source and format, inputting the preferred integration mass window, adjusting smoothing options, and the option to automatically calculate peak areas. The progress bar and console are also visible at the center of the interface.

Following these developments, I embarked on a series of incremental improvements to the overall analytical workflow. Operational and filtering parameters in the workflow were heuristically optimized based on the criterion that an improved parameter should either **(i)** maximize the number of protein species being quantified or **(ii)** minimize the variance of turnover rates among peptides of the same protein, without negatively impacting the other. Given the scarce amount of in vivo protein half-life data in the literature and the absence of true protein turnover standards, the assumption that all proteolytic peptides originating from the same protein molecule ought to have the same turnover rate provides a good standard with which to optimize the methods. This was estimated by the median of the median absolute deviation of the turnover rates of all peptides belonging to each protein in the sample. The additive effects of multiple changes were recorded to the best of abilities but for the reason of time and resources not every combination of parameters were tested.

Some progresses of the ongoing parameter optimization are briefly summarized here. (i) We included in ProTurn the option to perform Savitzky-Golay filtering for noise removal prior to peak are integration. Previously only box-car smoothing was performed. Savitzky-Golay filtering was found to be more effective in handling the inaccuracy of protein isotope fractional abundance measurement for some peptides with low signals. Seven-point smoothing was found to maximize performance. (ii) We used a more stringent 60-ppm integration window as opposed to the previous 100-ppm, which helps avoid overlapping peptides with similar mass-to-charge ratios and retention time but different isotopic patterns. (iii) Included a dual fitting error filter utilizing both goodness-of-fit (r) and standard error of estimate to include slow turnover proteins, whose flat kinetic curves naturally resulted in low r values.

These optimization efforts were time consuming but important to the overall research goal. Parameter optimization meant that the number of analyzed proteins in the normal mouse cytosol increased by more than 60%. Coupled to the increased performance of the Orbitrap Elite instrument and improved sample pre-fractionation methods, throughout this period the scope of our mitochondrial turnover measurements leaped from covering approximately 400 proteins in the mitochondrial samples as presented in Chapter I to over 800 in Chapter II, which laid the foundation for a high-coverage global analysis of protein dynamics in disease samples.

The non-linear equation has utilities in multiple animals in which a priming dose is not possible and enrichment is gradual. Potential applications range from human subjects, where individuals consume ^2H_2O gradually via small, regular boluses; to drosophila, where ^2H_2O is introduced while the cornmeal/ molasses/ yeast fly media is formed. To demonstrate the utility of this method, we characterized the plasma protein samples from ten human subjects, reasoning that plasma proteins are less invasive to acquire and have immediate translational potential as diagnostic markers.

Phase I Subjects	Age (yr)	Gender	Weight (kg)	Height (cm)	BMI	Ethnicity
Subject 1	51	F	68	175	22.7	Asian
Subject 2	39	M	82	178	25.8	Asian
Subject 4	35	M	108	188	30.5	Asian
Subject 6	21	F	64	168	22.7	Caucasian
Phase II Subjects						
Subject 5	21	M	87	180	26.7	Caucasian
Subject 7	23	M	84	180	25.8	Caucasian
Subject 8	21	F	59	168	20.9	Caucasian
Subject 9	21	F	51	160	19.9	Caucasian
Subject 10	27	M	82	175	26.6	Caucasian
Subject 11	25	M	88	175	28.6	Asian-Indian

TABLE 4.3   Demographics of human subjects

TABLE 4.3 lists the demographic information of the 10 human subjects we recruited for a longitudinal study. Initially, four healthy volunteers were recruited for Phase I in a longitudinal study. Six more subjects were subsequently recruited via open advertisement at UCLA for Phase II, which brought the total number of subjects to 10. The average age of the subjects was 26 ± 3 (range: 21 – 51) years; body weights averaged 76 ± 5 (range: 51 – 108) kg; heights ranged 160 – 188 cm; body mass index values were 19.9 – 30.5, altogether indicating a representative distribution of body types.
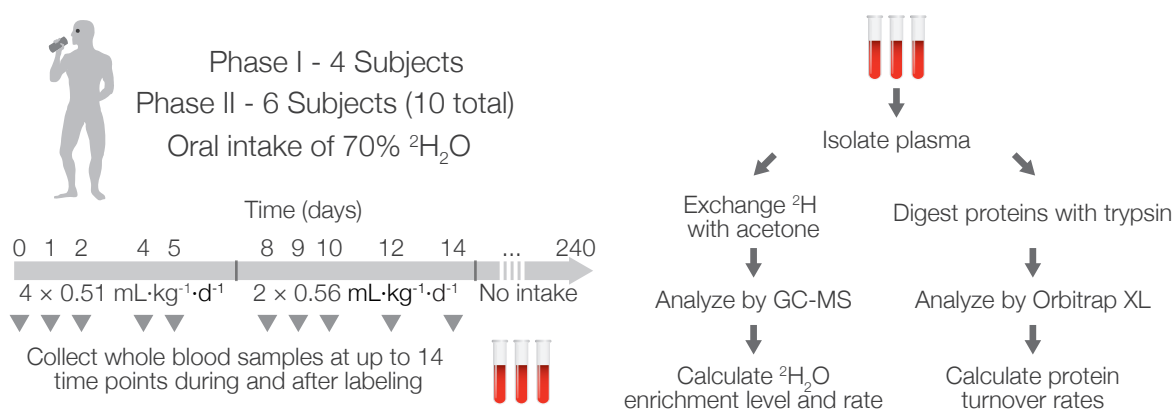
FIGURE 4.9   Labeling protocol and sample processing workflow

FIGURE 4.9 illustrates the labeling protocol and sample processing workflow of the study. The procedure comprised regular boluses of 70% ^2H_2O for 14 days and procurement of 3 mL peripheral blood at 10–15 time points (daily in Phase I; day 0, 1, 2, 4, 5, 8, 9, 10, 12, 14 of administration in Phase II) to extract plasma and erythrocyte proteins for analysis. In addition, saliva (0.5 mL) was collected at each time point for body water enrichment analysis (not shown). The intake dosage was weight adjusted where each subject consumed 0.51 mL·kg^{-1} of ^2H_2O over four daily doses per os during the first 7 days, followed by 0.56 mL·kg^{-1} over two doses per os during the second period of 7 days; with the exception of the first of the two replicate procedures for Subject #1, where the subject consumed 0.66 and 0.74 mL·kg^{-1} in the first and second week, respectively. Monitoring and regular body fluid sampling occurred after consumption concludes for up to 240 days following the start of labeling. The entire procedure including recruitment, label administration, and the acquisition of approximately 1,400 mass spectrometry experiments took approximately one year to complete.
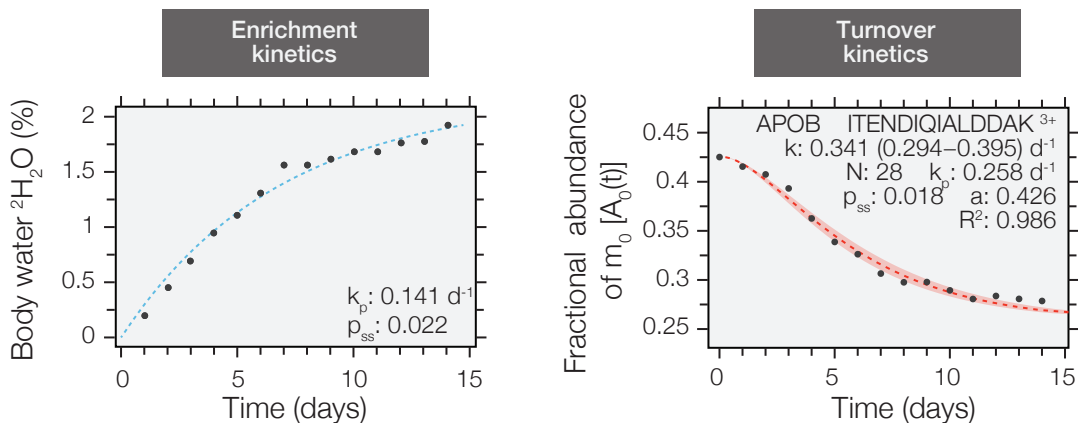
FIGURE 4.10   Enrichment and turnover kinetics in human

FIGURE 4.10 The gradual enrichment of ^2H_2O in the body water of the subjects can be modeled by a first-order exponential decay function to deduce the enrichment rate (k_p) and level

(p_{ss}) that are used in turn to model the turnover kinetics of peptide isotopomers. (Left) Experimentally measured values of body water enrichment in a subject from 0 to 15 days of labeling is modeled with an exponential rise curve. Upon labeling, the body water ^2H_2O level of the subjects followed first-order kinetics as expected, gradually approaching ≈1.6–2.2% at the enrichment rates of 0.15–0.25 d^{-1}. After termination of labeling, the enrichment level of body ^2H_2O gradually subsided in the subjects at a rate of ≈0.1 d^{-1}. The volunteers were further monitored for up to 6 months after labeling and reported no adverse effects. (Right) Experimental data and kinetic curve fitting of a human plasma peptide (EQLGEFYEALDCLCIPR[3+]). The fractional abundance of the unlabeled isotopomer (m_0/m_i) decreases in a sigmoidal curve that reflects the two rate constants of ^2H_2O ramping (k_p) and protein turnover (k). Red shade: upper and lower limits of fitting.
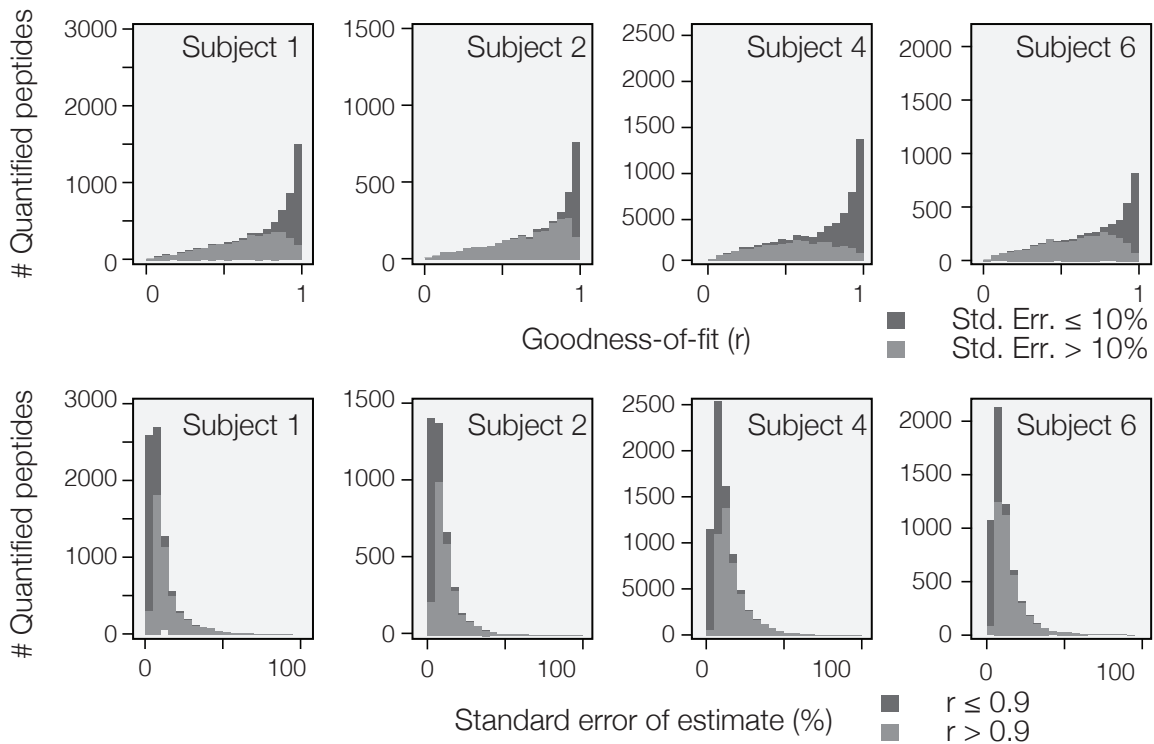
FIGURE 4.11   Kinetic curve fitting in labeled human plasma samples

FIGURE **4.11** contains histograms of goodness-of-fit of the nonlinear fitting model in healthy human subjects (Subjects #1, #2, #4, and #6). Only peptides explicitly identified in ≥ 4 time points and containing quantifiable mass isotopomer information are included. The top row graphs tally the distributions of goodness-of-fit (r) values in all quantified peptides in each subject, with the dark gray shading corresponding to whether those peptides also returned a low standard errors of estimates of ≤ 10%. The bottom row graphs tally the distributions of the standard errors of estimates in all quantified peptides in each subject, with the dark gray shading corresponding to whether those peptides also returned a good r value. The two filtering mechanisms worked complementarily to include well-fitted peptide time-series in turnover rate calculation. In these subjects, the nonlinear fitting method implemented in ProTurn modeled at least 32 – 47% of the consistently observed peptides closely ($r \geq 0.9$ or standard error of estimate of 4 to 9%) in each plasma sample, whereas more than 50% of consistently identified proteins yielded turnover rates, indicating our approach does not negatively impact the scope and coverage of proteomics inquiries.
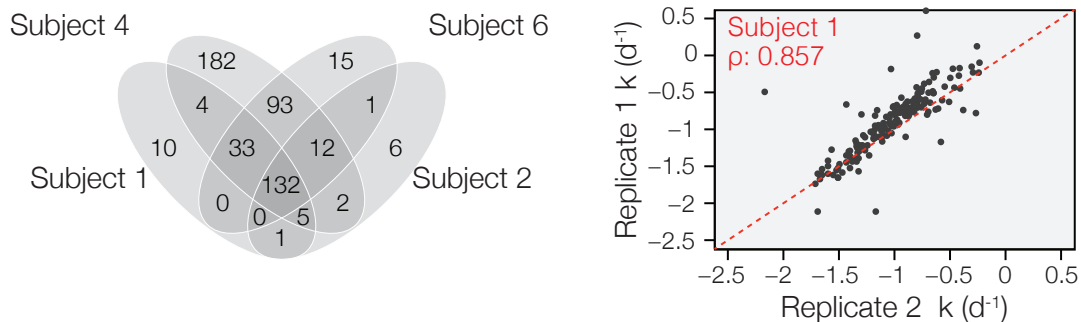
FIGURE 4.12   Number of quantified proteins and technical reproducibility

FIGURE **4.12** enumerates the number of quantified proteins from each of the four subjects in the phase I study, and the reproducibility of the labeling procedure. (Left) Venn diagram of the commonly and uniquely quantified proteins in four healthy human subjects (Subjects #1, #2, #4

and #6). The turnover rates of 496 human plasma proteins were confidently quantified, with 182 proteins quantified in at least three subjects. (Right) Scatter plot and Spearman's correlation coefficient of turnover rates, showing the reproducibility of protein turnover rates in two labeling procedures and mass spectrometry experiments conducted on the same subject (Subject #1), who was recalled six months following the first labeling experiment to initiate a second round of labeling. Each data point represents a commonly quantified individual protein. Despite the different ^2H_2O enrichment level (1.8% vs. 1.4%) and enrichment rate in the replicate experiments, due to the introduction of weight-adjusted ^2H_2O dose in the second enrichment in line with the labeling protocol of all other subjects, we acquired reproducibly quantified kinetics with relatively little variation (Spearman's correlation coefficient ρ: 0.857).
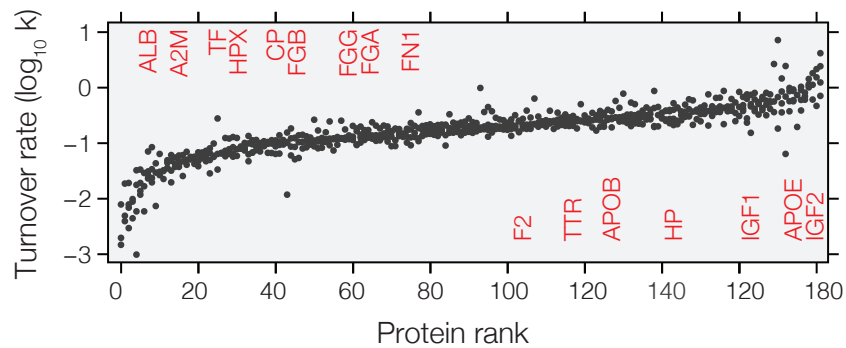
FIGURE 4.13   Range of protein turnover rates in the human subjects

FIGURE 4.13 shows the range of protein turnover rates in the human subjects. A total of 182 plasma proteins that were quantified in three or more subjects are shown, ranked by ascending average turnover rates in all subjects where the protein is quantified. From human serum albumin (ALB), which has an average half-life of 18.3 days in the subjects, to insulin-like growth factor 2 (IGF2), with an average half-life of 8 hours, the measured turnover rates spanned over two orders of magnitude. The relative turnover rates of fourteen other commonly studied human serum proteins are listed on the graph. By contrast, the 59 proteins we also quantified

from transcriptionally quiescent erythrocytes had negligible turnover, with half-life of more than 50 days (data not shown here). The full dataset can be found in the Supplemental Data of our publication (Wang et al., 2014) and is not reproduced here. The results confirm that the designed labeling procedure, to a very low level of ≤ 2% enrichment, was safe and sufficient to monitor large-scale protein turnover in human.
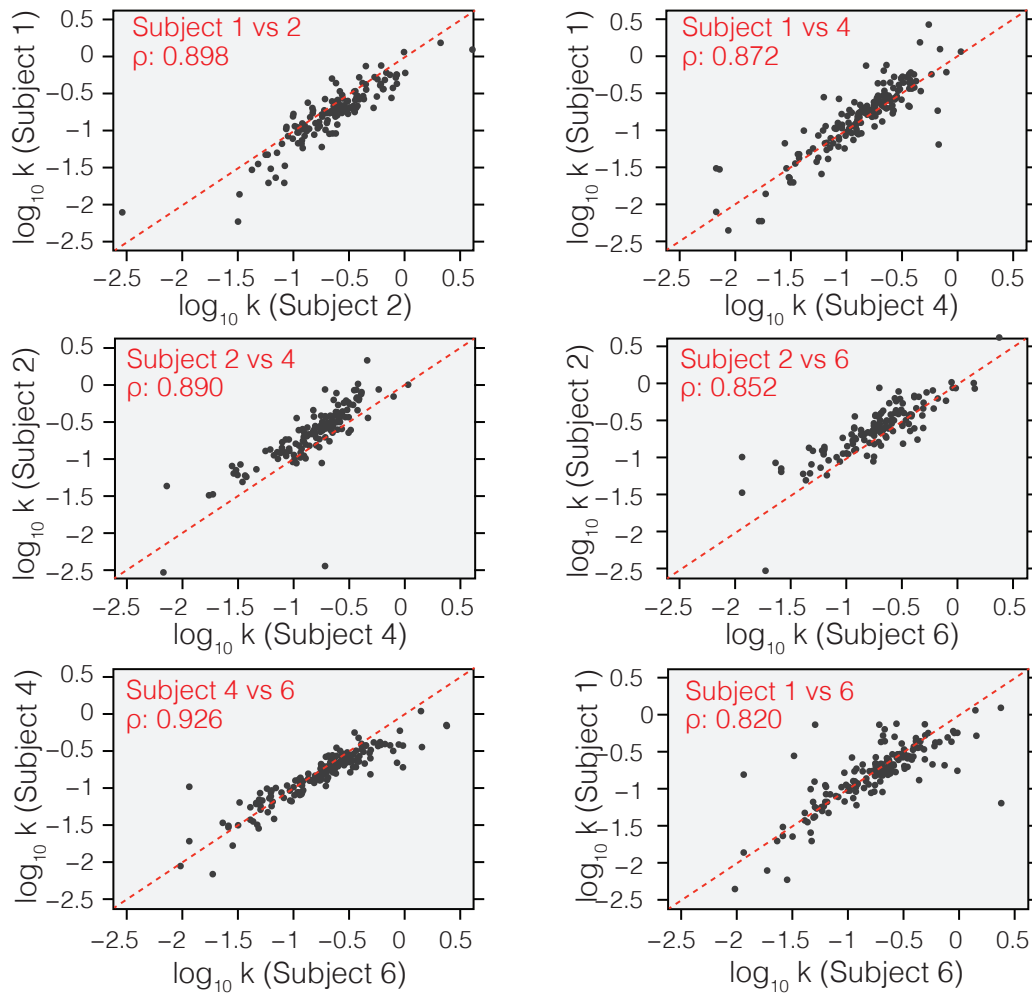
FIGURE 4.14   Biological variability of turnover in human

FIGURE 4.14 shows the biological variability of the measurements, represented as scatter plots and Spearman's correlation coefficient of turnover rates of proteins commonly quantified in any pairwise combination of the four human subjects. Overall, good correlation (Spearman's correlation coefficient ρ: 0.85 – 0.83) between subjects was observed. Altogether, these data demonstrate the robustness of large-scale protein kinetics quantitation in human, and constitute to our knowledge the largest human protein kinetics dataset to-date. Future studies are required that will better define the possible sources of variability in human protein turnover, e.g., the impact of age and gender, and whether the low isotope enrichments contribute disproportionately to the standard errors of half-life of slow-turnover proteins. The human study presented here serves to validate our approach and software. The dataset will benefit future investigations by providing critical reference for experimental designs and power analysis to determine sample size.

Following these results, we initiated Phase II of labeling experiment, during which we expanded the number of subjects from four to ten. In addition, we continued to monitor the label enrichment level and general wellbeing of the subjects for up to eight months after the end of their label intake in order to determine the safety of the enrichment procedure and the clearance of the label from the body.
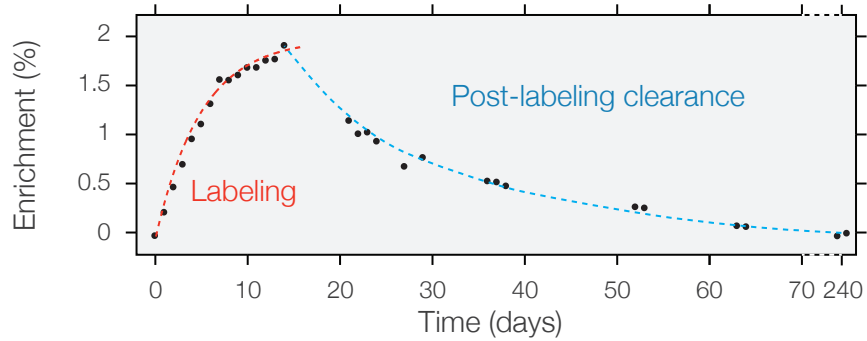
FIGURE 4.15   Label clearance after labeling course finishes

FIGURE 4.15 traces the label enrichment of a subject (Subject #2) as measured from peripheral blood samples using GC-MS at various time points throughout and after the labeling procedure. Each data point represents the average reading of the percentage of ^2H_2O in plasma; red line denotes the best-fit exponential rise curve of the data points during labeling, as defined by k_p and p_{ss}; blue line denotes the exponential decay curve of enrichment post-labeling. A gradual increase during the first week of the protocol was observed, following by gradual plateauing in the next 7 days. The enrichment kinetic curve is expected to plateau at 2.15% of body water, but this actual enrichment level was never reached because labeling was terminated on schedule before the kinetic curve plateaued. ^2H_2O enrichment was also measured from the saliva sample and gave virtually identical results (R^2: 0.985) as presented in our publication (Wang et al., 2014).

The cessation of ^2H_2O intake is followed by a typical physiological clearance of ^2H_2O, with a characteristic half-life of approximately seven days. By day 240, approximately eight months after the completion of intake, we recalled three subjects (Subject #1, #2, and #4) to follow up on their body water ^2H_2O enrichment, and detected virtually no trace of deuterium remaining in their body fluids (plasma or saliva).
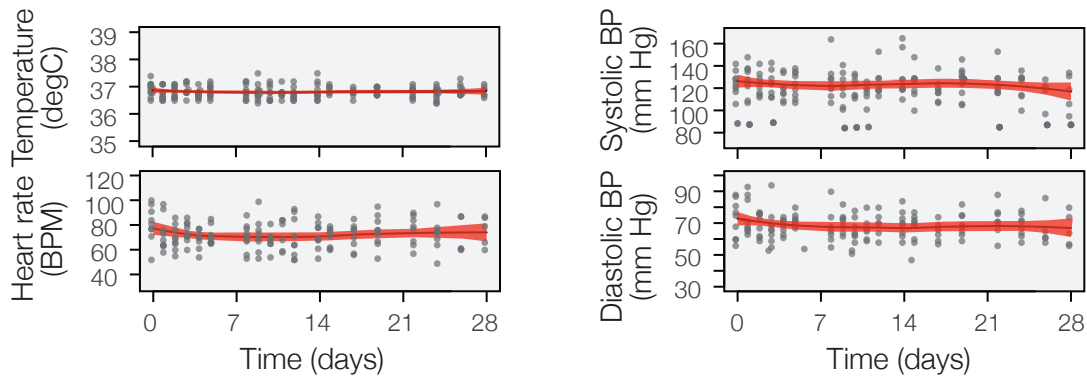
FIGURE 4.16   Vital signs of human subjects during and after labeling

FIGURE 4.16 shows the vital signs and hemodynamics of the 10 subjects during the course of labeling. Aggregated data of body temperature, heart rate, systolic and diastolic blood pressure (BP) are shown. Each data point represents an individual reading from a subject; red area indicates the 95% confidence range of local regression analysis. Both aggregate analysis and individual line charts (not shown here) indicate that the vital signs from the 10 human subjects were within normal ranges, and did not alter significantly over time for each individual as well as the group average, suggesting the specified dosage and duration had no discernible effect on vital signs and hemodynamics of healthy subjects.

Phase I Subjects	k_p (d^{-1})	p_{ss}	# Proteins	Median k (d^{-1})
Subject 1	0.258	1.78%	185	0.181
Subject 2	0.147	2.15%	159	0.234
Subject 4	0.151	2.12%	424	0.14
Subject 6	0.159	1.62%	283	0.195
Phase II Subjects				
Subject 5	0.238	1.02%	229	0.189
Subject 7	0.176	1.72%	282	0.184
Subject 8	0.281	1.36%	246	0.163
Subject 9	0.303	1.05%	187	0.199
Subject 10	0.275	1.21%	233	0.1835
Subject 11	0.181	2.05%	330	0.173

TABLE 4.4   Summary of enrichment and turnover data

TABLE 4.4 summarizes the enrichment kinetics and protein turnover quantification results from 10 human subjects. The columns show the precursor enrichment rate (kp), precursor plateau level (pss), number of proteins with quantified turnover rates in each subject (# Proteins), and the median of the turnover rate values acquired (Median k). In the experiment, the subjects showed a range of plateau enrichment level due to individual differences in metabolism and total water intake, which ranges from 1.02% to 2.12% (predicted plateau). The rate of enrichment likewise varied between 0.147 d^{-1} to 0.303 d^{-1}.

We observed no correlation between the median protein turnover rate constant (k) and the precursor enrichment rate constant (k_p) (Pearson's correlation coefficient r: 0.07, *P* value of trend: 0.85); nor between k and the steady-state precursor enrichment level (p_{ss}) (r: -0.07, *P*: 0.85), suggesting the enrichment curve fitting does not have a measurable impact on the measured protein turnover rate. We also did not observe a significant correlation between the measured protein turnover rates with the age of the subjects (r: 0.06, *P*: 0.87) or their body mass index (r: -0.32, *P*: 0.35).

However, a potential trend may exist between the enrichment level (pss) with the number of proteins with quantified turnover rates. Although the correlation is not significant (r: 0.40, P: 0.25), such correlation may be expected since higher enrichment will lead to more label incor-

poration, which leads to more proteins' shift being appreciably measured. This correlation becomes more apparent when the quality of data fitting is concerned as described below.
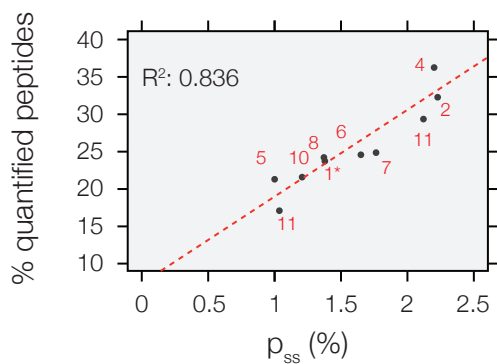
FIGURE 4.17   Correlation between enrichment and data quality

FIGURE 4.17 shows a linear regression analysis between the plateau enrichment value within a particular subject and the proportion of quantifiable peptides in the MS experiment. Each data point represents an individual subject as labeled in red. Data from subject 1 came from a replicate experiment from the data shown previously in this chapter. The quantifiability of peptide was determined by a variable filter that minimizes variations amongst peptides. Dashed line: linear regression; coefficient of determination R2: 0.836. The data suggest a positive correlation between enrichment level and the proportion of total quantified peptides that yielded confident protein turnover rates. Thus although a minimal labeling of 1% was sufficient to acquire protein turnover information, a substantial benefit is observed in data quality at 2% enrichment. This likely reflects the fact that at low enrichment levels the small amount of isotopes incorporated into the protein pool is technically difficult to discern by MS, especially for long-half-life proteins that are slow to accumulate deuterium. We conclude that our original intended target enrichment of 1.5% – 2% approximates a cost-effective trade-off between minimal intake and experimental performance for current technological platforms.

In total, these experiments obtained from the 10 human subjects the temporal dynamics of 542 plasma proteins, 325 of which were quantified in ≥ 3 subjects. To our knowledge, this dataset is among the largest collections of human protein dynamics to-date, both in terms of proteome coverage and in the number of biological replicates. The quantified proteins belong to diverse functional categories as evident from GO terms and include proteins of intracellular origins, consistent with the notion that proteins from cell leakage can be accessed and measured in the plasma. Consecutive technical triplicate MS experiments showed that the technical CV of > 90% of quantified peptides were ≤ 5%. The proteome dynamics data were generally reproducible among the tested subjects despite their differences in age and lifestyle, with ~25% median CV. As expected, the measured protein half-life was virtually independent from protein expression over 3+ orders of magnitude of abundance (ρ: 0.109). Consumption of ^2H_2O had no discernible effect on protein abundance, as measured by spectral counts before and after the ^2H_2O intake protocol in the 10 subjects (Benjamini-Hochberg adjusted *P*: 0.49 – 1.00). The full dataset is in our publication (Wang et al., 2014) and is not reproduced here.

A germane consideration is whether the quantified proteins are of interest to biomarker discovery or cardiovascular disease study. The total plasma proteome presents a formidable 10^{12} dynamic range of concentration. Recent HUPO Plasma Proteome Project efforts reported the concentration of 1,243 plasma based on spectral count information, spanning over 6 orders of magnitude (Farrah et al., 2011). Given that a single typical MS experiment can only sample a $10^4 – 10^6$ –fold dynamic range of protein concentrations, but that the plasma proteome is thought to have a dynamic range of concentration of 10^{10} to 10^{12} (Anderson and Anderson, 2002), some underrepresentation of the plasma proteome is inevitable in the current investigation. Nevertheless, proteins of interest can be found across the sampled concentration range. Previous HUPO annotations have identified 338 out of ~3,000 plasma proteins with known relevance to cardiovascular diseases (Berhane et al., 2005). The present dataset revealed the

turnover of 119 of these proteins, with disease relevance ranging from cardioprotection to myocardial infarction markers. The quantification of their turnover rates serves as a blueprint for future comparisons with cardiac disease patients.

Finally, we validated the accuracy of our method by comparing the data from the present large-scale study to the range of known human plasma protein turnover rates from past single-protein studies in the literature, wherever such data may exist:

Protein	Gene name	k (d^{-1})	Replicates	Avg ± s.d.	Literature Range
Albumin	ALB	0.02 - 0.07	6	0.04 ± 0.01	0.03 - 0.06
Ceruloplasmin	CP	0.05 - 0.14	10	0.09 ± 0.01	0.14 - 0.20
Fibrinogen α chain	FGA	0.10 - 0.21	10	0.15 ± 0.01	0.14 - 0.19
Fibrinogen β chain	FGB	0.06 - 0.12	5	0.09 ± 0.01	0.14 - 0.19
Fibrinogen γ chain	FGG	0.07 - 0.19	6	0.12 ± 0.02	0.14 - 0.19
Fibronectin	FN1	0.12 - 0.23	10	0.15 ± 0.02	0.30 - 0.40
Haptoglobin	HP	0.23 - 0.44	10	0.31 ± 0.02	0.17 - 025
Prothrombin	F2	0.18 - 0.28	10	0.20 ± 0.01	0.21 - 0.30
Transferrin	TF	0.04 - 0.14	8	0.09 ± 0.01	0.07 - 0.20
Transthyretin	TTR	0.16 - 0.31	9	0.21 ± 0.02	0.22 - 0.31

TABLE 4.5   Comparison of human turnover data with literature values

TABLE 4.5 compares the turnover rate data from the 10 human subjects against the range of reported literature values, for 10 plasma proteins with previous turnover rate data from single-protein studies in the literature. The known turnover rates in the literature were extracted from References (Carraro et al., 1991; Katz, 1961; Kekki et al., 1966; Krauss, 1969; de Sain-van der Velden et al., 1998; Shapiro and Martinez, 1969; Socolow et al., 1965).

Proteomes across time and space

The role of mitochondrial dynamics in cardiac research is being increasingly recognized. Mito-chondria in the heart undergo continual fission, fusion, biogenesis, and engulfment through mitophagy in order to maintain cardiac health and functions. Both the spatial and temporal

distributions and dynamism of mitochondria are vital to cellular functions, and disruptions of either process often ends with catastrophic consequences (Gottlieb and Gustafsson, 2011; Hammerling and Gustafsson, 2014). At the same time, proteins in the cell are highly dynamic both across space and time even in the absence of overt organelle changes. Protein molecules traffic to various locales at various cell states, and protein pools renew at characteristic rates.

We envision that the protein turnover studies here will be part of ongoing method developments that will increase our capability to understand the complexity of the proteome and its dynamisms across time and space. The proteome is a collection of orthogonal properties over the lifetime of its constituent proteins. As a cardiac protein is expressed, it is modified co-translationally or post-translationally, localizes to one or more specific cellular compartments, interacts with other proteins or metabolites, and performs its signaling, structural, or catalytic functions, before being commissioned for degradation under tightly controlled schedule and mechanism. As discussed in the beginning of this dissertation, although current large-scale proteomics experiments have focused disproportionally on a few particular parameters such as abundance or phosphorylation, many such aspects in the life of a protein may be perturbed in disease, and thus each may constitute a potential untapped source of new knowledge regarding disease mechanisms and therapies. We conclude this chapter and the dissertation by discussing some future challenges in translating the presented methods to measure mitochondrial protein turnover in the human heart to identify disease-associated proteins.

In the experiments shown earlier in this chapter we examined protein turnover in the human plasma. The plasma was chosen as a sample because of its immediate translational potential as diagnostic indicators as well as its accessibility. Although the general features of our method are expected to be applicable to other human tissues in preclinical studies, currently no FDA-approved protocol exists for the use of ^2H_2O in clinical research and diagnostic applications. This can in part be attributed to a lack of standardized protocols for ^2H_2O administration,

or detailed documentation of physical parameters relevant to clinical interests and safety precautions. For instance, if ^2H_2O is to be approved for measuring cardiac protein turnover rate in human heart failure patients, it would be imperative to have a detailed understanding of the hemodynamic responses in human subjects, especially those with compromised health conditions. Thus the prospects of clinical research and diagnostics are contingent upon preclinical efforts that meticulously document the potential outcomes of labeling protocols in human subjects.

It is hoped that these preliminary studies will buttress future investigations in the cardiovascular research community to characterize protein turnover kinetics of many important cardiac functional groups, including metabolic regulation, calcium signaling, contractile function, and protein trafficking. In order to achieve these goals, several present challenges must be overcome, including the observation that gross protein turnover appears to be inversely proportional to the metabolic rate of the animal, which suggests many human organ tissue samples will turn over at much slower rate than is accommodated in the present experimental design. Human plasma proteins turn over much slower than their mouse counter parts, and cardiac proteins have slower turnover than plasma proteins. Thus human cardiac proteins will have exceedingly long half-life that may be beyond the detection limit allowed by the sampling time points, e.g., if the normal turnover rate of a particular protein in the heart is 200 days, then labeling a subject for 10 days is unlikely to give useful information on protein kinetics change irrespective of the mass spectrometry techniques, since the protein pool will have only turned over 5% during the labeling period and would have only incorporated very little isotopes. Initial studies may therefore be limited to only regulatory proteins that may have higher turnover rates.

Moreover, proteome turnover measurements in the heart will be hindered by clinical accessibility of tissue samples. Previous ^2H_2O labeling methods invariably required repeated sample

biopsies, which presents unnecessary distress and is impractical in many clinical settings. This limitation is alleviated by the described nonlinear fitting model, in which the initial and final isotopomer abundances of a peptide in the MS (i.e., the unlabeled and fully turned over protein, respectively) can be precisely defined by the peptide sequence and ^2H_2O enrichment in the body water. A single data point acquired in between could therefore effectively demarcate the trajectory of the kinetic curve.
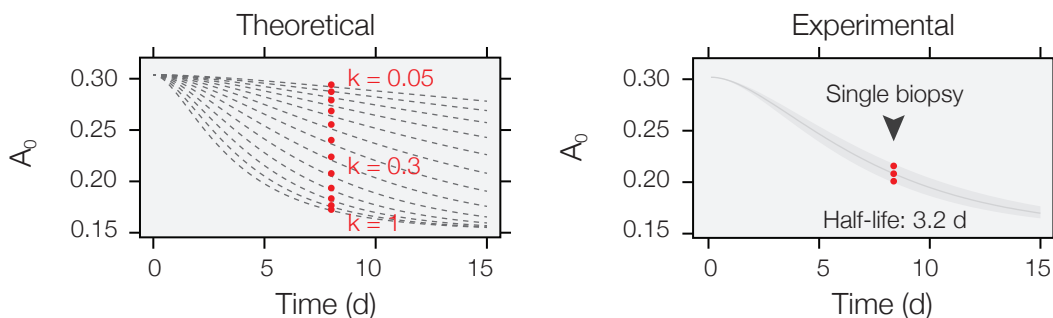
FIGURE 4.18   Measuring protein turnover from a single time point

FIGURE 4.18 illustrates how protein turnover rates may be measured by sampling the tissue of interest at only one time point using the described fitting method. (Left) Theoretical kinetic curves for a particular peptide, (EQLGEFYEALDCLCIPR[3+]) from the human plasma protein AGP2, at different hypothetical turnover rates from 0.05 d^{-1} to 1 d^{-1}. The fractional abundance of the unlabeled isotopomer (m_0/m_i) decreases in a sigmoidal curve that reflects the two rate constants of ^2H_2O ramping (k_p) and protein turnover (k). Since k determines the kinetic curve, a single measurement of mass isotopomer fractional abundance (A_0) is sufficient to capture turnover rate if at the sampling time point the protein has accumulated sufficient isotopes but the kinetic curve has not yet reached its plateau. The puncta denote the corresponding A_0 that would have been measured from a single-time-point experiment with a sample on day 8 of labeling. (Right) Actual experimental data and fitting of the same peptide sequence from a single-point experiment from the day 8 plasma sample of Subject #1. The triplicate data points

acquired from the single sample define the kinetic curve to the same effect as the multiple data points from different time points, demonstrating the feasibility to acquire protein kinetics information without a time-course experiment.

To demonstrate the feasibility of deducing protein kinetics deduction from a single, non-time-course measurement, we performed triplicate MS experiments on human plasma samples from each of three individual time points (day 4, day 8, and day 12 of labeling) in two subjects
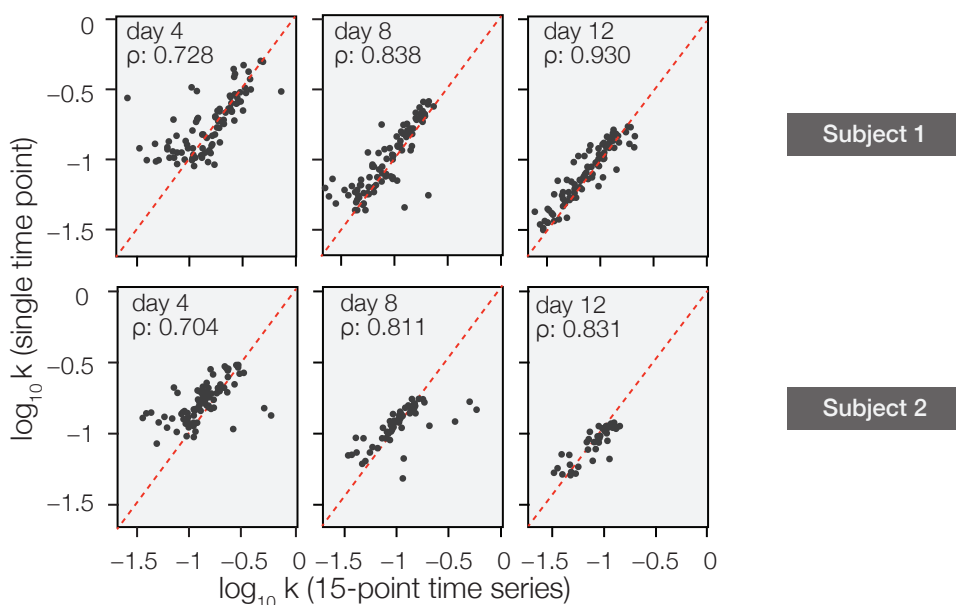
FIGURE 4.19   Accuracy of turnover rate measurements from one time point

FIGURE 4.19 plots the turnover rates of proteins when measured from a technical triplicate from a single-time-point sample against those from curve-fitting of a 15-point time course. Correlations in turnover rates between peptides commonly analyzed from single-point sampling and 15-point time course experiments, from Subject #1 (Top row) and Subject #2 (Bottom row), sampled at either day 4 (Left), day 8 (Middle), or day 12 (Right) after the initiation of labeling. A filter is used such that only proteins with fitted turnover rates that would cause the sampling time point to fall between 0.5 and 3 half-lives to be accepted. A protein with a particular

turnover rate needs therefore to be measured at an appropriate time point designed to capture its kinetics. We found that although the day 4 samples presented more variations – possibly due to limited label incorporation by that time, both the day-8 and the day-12 single-point measurements were highly consistent with 15-point time-course data. Overall, good correlation was observed between the single-point and time-course data (Spearman's correlation coefficient ρ: 0.74 – 0.93). The average peptide relative standard error was approximately 20% compared to the time-course experiment.

Because cardiac proteins have limited surgical accessibility and are typically only available during cardiac transplant or ventricular assist device implantation, the described method opens opportunities for kinetic investigations of the human heart, among other invasive tissue samples.
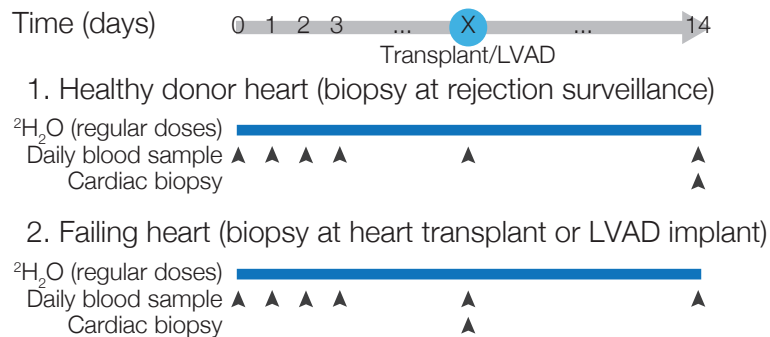
FIGURE 4.20   Hypothetical workflow for human heart sample measurements

FIGURE 4.20 illustrates a hypothetical protocol to measure mitochondrial protein turnover in the human heart. For clinical investigations of protein dynamics in human diseases, case-control studies can compare the plasma protein turnover of age-matched healthy subjects and early- or late-stage heart failure patients (NYHA Class I – IV) to identify novel biomarkers and to sub-classify patients. In this protocol, following enrolment into the study and decision to com-

mence labeling, the human subjects may drink 4 doses of 0.51 mL·kg^{-1} sterile 70% ^{2}H$_2$O at 11 am, 2 pm, 6 pm, and 9 pm daily for 7 days (approximately 150 mL·d^{-1} for a 75-kg subject), followed by two doses of 0.56 mL·kg^{-1} sterile 70% ^{2}H$_2$O at 11 am and 9 pm daily for 7 days. In parallel to the 2-week ^{2}H$_2$O-drinking period, blood/saliva specimens will be collected daily for 14 days. Healthy subjects will have all received a donor heart with normal cardiac functions, and will act as healthy heart controls. Following heart transplantation, endomyocardial biopsies from the donor heart are routinely scheduled for rejection surveillance (monthly for the first year after transplant). Two weeks prior to a scheduled biopsy, the enrolled patient may start a two-week ^{2}H$_2$O intake protocol to label the myocardium. We will procure and analyze the procured biopsy (~8 mm^3), which in our hands yield ~500 μg total proteins. For heart failure subjects, we may enroll high-priority patients anticipated to receive one of the 300 heart transplants project-ed to take place at UCLA in the next 5 years, until we obtain 15 labeled cardiac samples. After enrollment, subjects will be labeled as above, where a 10-day window exists after labeling begins for labeled cardiac samples to be procured. An average high-priority patient will under-go operation with a median waiting time of 30 days. If heart transplantation occurs within the labeling period, a myocardial biopsy labeled with ^{2}H$_2$O will be procured from the explanted heart for analysis. If no operation takes place, labeling will terminate.

The discovered protein turnover biomarkers may be used to detect, analyze, or predict patient response to medical or surgical intervention (e.g., after angiotensin-converting-enzyme inhibitor or left-ventricular-assist-device-mediated mechanical unloading). Because the presented method is capable of quantifying protein turnover from as few as one time point, future studies can be envisioned that directly compare the proteome dynamics of healthy and diseased human hearts, such as can be acquired from routine clinical biopsies during surgical interven-tion or post-transplant allograft rejection surveillance. Similar studies can be envisioned in the future such that therapeutic designs in other diseases may also benefit from further insights into protein removal mechanisms. The stability of protein targets will directly influence the

efficacy and pharmacokinetics of drugs such as cardioprotective agents. The half-life of crucial therapeutic mediators could conceivably be prolonged if their primary removal mechanisms are simultaneously inhibited while the drug is active; alternatively, parallel mechanisms could be exploited to intervene in cell death pathways and minimize injury.

Materials and methods

Method summary. Human participants were administered regular boluses of ^2H_2O over a 2-week period. Saliva and blood samples were collected at 10 time points and analyzed by GC-MS and LC-MS to deduce ^2H_2O enrichment rate and protein half-life using a modified kinetics equation to account for gradual labeling.

Study approval. Human procedures were performed in compliance with UCLA Institutional Review Boards (IRB#12-000899). All participants gave written informed consent.

Reagents. ^2H_2O (70% and 99.9% molar ratio) was purchased from Cambridge Isotope Laboratories and filtered through 0.1-μm polyethersulfone membranes (VWR). Other chemical reagents were from Sigma-Aldrich unless specified. High-performance liquid chromatography-grade water (J.T.Baker) was used for all analytical solvent preparations. Milli-Q (Millipore) filtered water (18.2 MΩ) was used for all other preparations.

Enrollment and labeling of human participants. Ten healthy participants (Subjects #1, #2, #4 – #11) gave written informed consent and enrolled in the study. To label body water with ^2H_2O, we instructed the participants to intake 4 boluses of 0.51-mL·kg^{-1} (body mass) sterile 70% molar ratio ^2H_2O daily at 11:00 am, 2:00 pm, 6:00 pm, and 9:00 pm for the first 7 days; and 2

boluses of 0.56-mL·kg^{-1} sterile 70% molar ratio ^2H_2O daily at 11:00 am and 9:00 pm for the next 7 days; with the exception of the first replicate of Subject #1, where body-mass adjustment was not performed and the first- and second- week boluses were 0.66 mL·kg^{-1} and 0.74 mL·kg^{-1}, respectively.

During labeling, participants were given daily general physical examinations and inquired with a concise medical health questionnaire for any signs of discomforts by the clinical coordinator David Liem. Vital signs were monitored by measuring blood pressure, heart rate, and temperature on a daily basis. From day 0 to day 14 at 10 to 15 time points, 3 mL of whole blood samples were collected by qualified phlebotomists in the clinical laboratory of the UCLA Ronald Reagan Medical Center at 12:00 noon. The participants were monitored for 14 days to 6 months post-administration, and indicated no discomfort or side effects throughout the labeling and monitoring periods. Compliance with the intake protocol was ensured by the surveillance of body water enrichment level, by the return of ^2H_2O vials for counting, and by oral inquiry. All subjects maintained normal food and fluid intake during the study and routine daily activities.

Isolation and digestion of labeled human blood proteins. The human whole blood sample was collected in lithium heparin tubes and separated into plasma and blood cells by centrifugation (800 rcf, 4 °C, 5 minutes). Erythrocytes were isolated by centrifugation on 1:1 Histopaque-1077 (400 rcf, 4 °C, 30 minutes) followed by washing twice with phosphate-buffered saline. Plasma samples (7 µL; approximately 500 µg proteins at 70 g·L^{-1}) were immunodepleted of the 14 most abundant proteins in the human plasma using Agilent Hu14 Multiple Affinity Removal System columns (Agilent Technologies). The immunodepleted plasma proteins were digested on 10,000 Da polyethersulfone filters (Nanosep; Pall Life Sciences) as described (Wisniewski et al., 2009). Sample buffer was exchanged on-filter with 100 mmol·L^{-1} ammonium bicarbonate. The samples were then heated at 70 °C with 3 mmol·L^{-1} dithiothreitol for 5

minutes, followed by alkylation with 9 mmol·L^{-1} iodoacetamide in the dark at ambient temperature. Proteins were digested with 50:1 (w/w) sequencing grade trypsin (Promega) on-filter for 16 hours at 37 °C. Human erythrocyte protein samples were separately digested in-solution; 200 µg of proteins were heated at 80 °C with 0.2% (w/v) Rapigest (Waters) for 5 minutes, then heated at 70 °C with 3 mmol·L^{-1} dithiothreitol for 5 minutes, followed by alkylation with 9 mmol·L^{-1} iodoacetamide in the dark at ambient temperature. Proteins were digested with 50:1 sequencing grade trypsin (Promega) for 16 hours at 37 °C, then acidified with 1% (v/v) tri-fluoroacetic acid (Thermo Pierce).

Separation of peptides by two-dimensional liquid chromatography. To resolve the human plasma samples and improve sample coverage, we separated the depleted peptides with two-dimensional reversed-phase/reversed-phase LC prior to MS analysis (Lam et al., 2011; Lau et al., 2011). First-dimension (high-pH) separation for human plasma samples was conducted on a Phenomenex C$_{12}$ reversed-phase column (Jupiter Proteo C$_{12}$, 4 µm particle, 90 Å pore, 100 mm length × 1 mm inner diameter) at high pH using a Finnigan Surveyor LC system. The solvent gradient was as follows: 0th – 2nd minute, 0 – 5% B; 3rd – 32nd minute, 5 – 35% B; 32nd – 37th minute, 80% B; 50 µL·min^{-1}; A: 20 mM ammonium formate, pH 10; B: 20 mM ammonium formate, 90% (v/v) acetonitrile, pH 10. We then injected 50 µg of proteolytic peptides with a syringe into a manual 6-port/2-position switch valve. Twelve fractions from 16 – 40 minute were collected, lyophilized and re-dissolved in 20 µL of 0.5% (v/v) formic acid with 2% (v/v) acetonitrile prior to low-pH reversed-phase separation.

We then performed second-dimension (low-pH) reversed-phase chromatography using an Easy-nLC 1000 nano-UPLC system (Thermo Scientific) on an EasySpray C$_{18}$ reversed-phase column (PepMap, 3-µm particle, 100-Å pore; 150 mm length × 75 µm dimension; Thermo Scientific) held at 50 °C. The solvent gradient was 0th – 110th minute: 0–40% B; 110th – 117th minute: 40–80% B; 117th – 120th minute: 80% B; 300 nL·min^{-1}; A: 0.1% (v/v) formic acid, 2%

(v/v) acetonitrile; B: 0.1% (v/v) formic acid, 80% (v/v) acetonitrile. The autosampler on the Easy-nLC 1000 nano-UPLC system then injected 10 µL of each high-pH fraction into the solvent flow path.

Protein identification and quantification using mass spectrometry. Mass spectrometry was performed on an LTQ Orbitrap Elite mass spectrometer (Thermo Fisher Scientific) controlled by XCalibur (v.2.1.0) coupled to the Easy-nLC 1000 nano-UPLC system through a Thermo EasySpray interface. Each survey scan was analyzed inside the Orbitrap at 60,000 resolving power in profile mode, followed by data-dependent collision-induced dissociation MS2 scans on the top 15 ions inside the ion trap. MS1 and MS2 target ion accumulations were 1×10^4 and 1×10^6, respectively. We set dynamic exclusion to 90 seconds to avoid acquisition of redundant spectra. We further used an MS1 scan lock mass of m/z 425.120025 for internal mass calibration.

Protein identification was performed with ProLuCID (Xu et al., 2006) against a reverse-decoyed database (Uniprot human Reference Proteome Reviewed, February 9th, 2013, 20,241 entries). The search allowed for static cysteine carbamidomethylation (+57.02146 Da) modification and up to 3 variable modifications, including methionine oxidation (+15.9949 Da), lysine acetylation (+42.0106 Da), serine/threonine/tyrosine phosphorylation (+79.9663 Da), or lysine ubiquitylation (+114.0403 Da). Tryptic, semi-tryptic, and non-tryptic peptides within a 20-ppm mass window surrounding the candidate precursor mass were searched under separate confidence calculation. Protein identifications were filtered by DTASelect (Tabb et al., 2002) .requiring ≤ 1% global peptide false discovery rate and two unique peptides per protein. ProLuCID performs multiple iterations of database search for every spectrum, first to identify only unmodified peptides and then to assume variable mass shifts of unmodified peptides (Wong et al., 2007). DTASelect, with the –modstat parameter set to on, then applies separate statistical filters to the modified and unmodified peptides to identify variable modifications using separate protein

identification confidence calculations, which would explain why searching with variable modifications in our typical workflow did not negatively impact protein identification performance. Note that modified peptides (other than methionine oxidation) were not considered for comparative analyses as we await rigorous validations of the number of label-accessible atoms on the modification moieties. However, scenarios exist where performing database search with modifications would nevertheless improve coverage – because a protein may be confidently identified by an unmodified and a modified peptide at two different sites to satisfy the two-peptide rule, and the unmodified peptide could go on to yield kinetic information. On a related note, so far in our unpublished data we have not observed any systematic difference in turnover rates between modified and unmodified peptides of the same proteins.

For protein abundance calculation based on spectral counts, normalized spectral abundance factors were calculated in DTASelect. Additional protein identification was performed using MaxQuant/Andromeda (Cox and Mann, 2008; Cox et al., 2011) for comparison. A two-stage, probabilistic strategy to handle variable modifications is also employed in MaxQuant/Andromeda.

Computational workflow for protein kinetics analysis: Proteins were identified from the acquired mass spectra using ProLuCID (Xu et al., 2006) Protein functional information and Gene Ontology entries were queried through NCBI DAVID (Huang da et al., 2009) and COPaKB (Zong et al., 2013). Protein turnover kinetics was quantified with ProTurn. The nonlinear fitting parameters utilized to deduce protein turnover rates were as follows. Orbitrap spectra were input to ProTurn after conversion into the open [.mzML] format using MSConvert (Chambers et al., 2012). ProTurn was then instructed to select only confidently identified peptides that were uniquely assigned to a protein from the ProLuCID search result [.dta] file.

For each identified peptide, all isotopomer areas-under-curves over a 60-ppm window of the peptide mass were integrated from the raw mass spectra, at the retention time in the MS1 extracted ion chromatograph as indicated by the scan number in the protein identification list. Savizky-Golay filters over 7 data points were applied to the MS1 chromatograph prior to it-negration (Savitzky and Golay, 1964). False positive identifications were further controlled by the requirement of a peptide to be explicitly identified in at least 4 time points before it is considered for kinetics calculation. Turnover rates were extracted by multivariate optimization to a nonlinear function. Peptide isotopomer time-series were accepted if they fit to the model with r ≥ 0.9, or alternatively with a sliding standard error of estimate of ≤ 5 – 9%, which was heuristically determined in each subject such that the median of the median absolute deviations of the measured turnover rates of peptides belonging to each protein was approximately 30% to 35%.

For single-point analyses, the peptide isotopomer data were filtered without a priori knowledge of the true turnover rates from the full time-course datasets. For a fitting to be considered valid, the coefficient of variance of the measured peptide isotopomer fractional abundance in the triplicate mass spectrometry experiments must be ≤ 10%, whereas the residual sum of squares of fitting must be ≤ 1.5%, and the fitted turnover must lie within 0.5 to 3 half-lives at the sampling time.

For iBAQ-based label-free quantification in ProTurn, the integrated isotopomer peak areas were summed up as the peptide cluster area. Protein areas were defined as the sum of all peptide areas from identified peptides, normalized to the total spectral intensity, then normalized to the potential number of peptides (six or more amino acids in length) that may be produced from the protein sequence in an in silico tryptic digest.

APPENDIX A. ORIGINAL PROPOSED AIMS

Aim 1: Temporal dynamics of the mitochondrial proteome in cardiac remodeling. Using a stable isotope labeling method we recently developed, we will measure the in vivo turnover rates of mitochondrial proteins in mice undergoing isoproterenol-stimulated cardiac remodeling, post-stimulus reverse-remodeling, or oxidative stress. These experiments are designed to identify protein turnover changes in key pathways that may parallel aberrations in cardiac functions.

Aim 2: Regulatory mechanisms of mitochondrial protein degradation in health and disease. We will assay the effect of mitochondrial proteases and cytosolic proteasomes on mitochondrial protein turnover in vitro. These experiments will test the hypothesis that individual protein degradation mechanisms are differentially regulated in the stressed heart to instigate protein remodeling in cardiac mitochondria.

Aim 3: Translational models for proteome turnover analysis in human subjects. Following a UCLA IRB-approved human ^2H_2O labeling protocol, we will enroll healthy human subjects to study basal human plasma proteome turnover rates. These pilot studies will help us develop the labeling and computational methods for future clinical investigations on protein kinetics.

REFERENCES

Abel, E.D., and Doenst, T. (2011). Mitochondrial adaptations to physiological vs. pathological cardiac hypertrophy. Cardiovasc Res *90*, 234–242.

Albin, R., Dowell, R.T., Zak, R., and Rabinowitz, M. (1973). Synthesis and degradation of mitochondrial components in hypertrophied rat heart. Biochem J *136*, 629–637.

Allard, M.F., Schonekess, B.O., Henning, S.L., English, D.R., and Lopaschuk, G.D. (1994). Contribution of oxidative metabolism and glycolysis to ATP production in hypertrophied hearts. Am J Physiol *267*, H742–H750.

Altieri, D.C., Stein, G.S., Lian, J.B., and Languino, L.R. (2012). TRAP-1, the mitochondrial Hsp90. Biochim. Biophys. Acta - Mol. Cell Res. *1823*, 767–773.

Andersen, J.S., Lam, Y.W., Leung, A.K., Ong, S.E., Lyon, C.E., Lamond, A.I., and Mann, M. (2005). Nucleolar proteome dynamics. Nature *433*, 77–83.

Anderson, N.L., and Anderson, N.G. (2002). The human plasma proteome: history, character, and diagnostic prospects. Mol Cell Proteomics *1*, 845–867.

Anderson, M.E., Brown, J.H., and Bers, D.M. (2011). CaMKII in myocardial hypertrophy and heart failure. J. Mol. Cell. Cardiol. *51*, 468–473.

Artimo, P., Jonnalagedda, M., Arnold, K., Baratin, D., Csardi, G., de Castro, E., Duvaud, S., Flegel, V., Fortier, A., Gasteiger, E., et al. (2012). ExPASy: SIB bioinformatics resource portal. Nucleic Acids Res *40*, W597–W603.

Augustin, S., Nolden, M., Müller, S., Hardt, O., Arnold, I., and Langer, T. (2005). Characterization of Peptides Released from Mitochondria. J Biol Chem *280*, 2691–2699.

Azzu, V., and Brand, M.D. (2010). Degradation of an intramitochondrial protein by the cytosolic proteasome. J Cell Sci *123*, 578–585.

Azzu, V., Mookerjee, S.A., and Brand, M.D. (2010). Rapid turnover of mitochondrial uncoupling protein 3. Biochem. J. *426*, 13–17.

Balaban, R.S. (1990). Regulation of oxidative phosphorylation in the mammalian cell. Am J Physiol *258*, C377–C389.

Balaban, R.S., Nemoto, S., and Finkel, T. (2005). Mitochondria, oxidants, and aging. Cell *120*, 483–495.

Balakumar, P., Singh, A.P., and Singh, M. (2007). Rodent models of heart failure. J Pharmacol Toxicol Methods *56*, 1–10.

Balch, W.E., Morimoto, R.I., Dillin, A., and Kelly, J.W. (2008). Adapting proteostasis for disease intervention. Science (80-.). *319*, 916–919.

Barnes, J.A., and Gomes, A. V. (2002). Proteolytic signals in the primary structure of annexins. Mol. Cell. Biochem. *231*, 1–7.

Bayot, A., Gareil, M., Rogowska-Wrzesinska, A., Roepstorff, P., Friguet, B., and Bulteau, A.-L. (2010). Identification of Novel Oxidized Protein Substrates and Physiological Partners of the Mitochondrial ATP-dependent Lon-like Protease Pim1. J. Biol. Chem. *285* , 11445–11457.

Beardslee, M.A., Laing, J.G., Beyer, E.C., and Saffitz, J.E. (1998). Rapid turnover of connexin43 in the adult rat heart. Circ Res *83*, 629–635.

Bender, T., Leidhold, C., Ruppert, T., Franken, S., and Voos, W. (2010). The role of protein quality control in mitochondrial protein homeostasis under oxidative stress. Proteomics *10*, 1426–1443.

Bender, T., Lewrenz, I., Franken, S., Baitzel, C., and Voos, W. (2011). Mitochondrial enzymes are protected from stress-induced aggregation by mitochondrial chaperones and the Pim1/LON protease. Mol. Biol. Cell *22*, 541–554.

Benevolensky, D., Belikova, Y., Mohammadzadeh, R., Trouve, P., Marotte, F., Russo-Marie, F., Samuel, J.L., and Charlemagne, D. (2000). Expression and localization of the annexins II, V, and VI in myocardium from patients with end-stage heart failure. Lab Invest *80*, 123–133.

Berhane, B.T., Zong, C., Liem, D.A., Huang, A., Le, S., Edmondson, R.D., Jones, R.C., Qiao, X., Whitelegge, J.P., Ping, P., et al. (2005). Cardiovascular-related proteins identified in human plasma by the HUPO Plasma Proteome Project pilot phase. Proteomics *5*, 3520–3530.

Beynon, R.J., and Pratt, J.M. (2005). Metabolic labeling of proteins for proteomics. Mol Cell Proteomics *4*, 857–872.

Bezawork-Geleta, A., Saiyed, T., Dougan, D.A., and Truscott, K.N. (2014). Mitochondrial matrix proteostasis is linked to hereditary paraganglioma: LON-mediated turnover of the human flavinylation factor SDH5 is regulated by its interaction with SDHA. FASEB J.

Van Bilsen, M., Smeets, P.J., Gilde, A.J., and van der Vusse, G.J. (2004). Metabolic remodelling of the failing heart: the cardiac burn-out syndrome? Cardiovasc Res *61*, 218–226.

Bleumink, G.S., Schut, A.F.C., Sturkenboom, M.C.J.M., Deckers, J.W., van Duijn, C.M., and Stricker, B.H.C. (2004). Genetic polymorphisms and heart failure. Genet. Med. *6*, 465–474.

Boisvert, F.-M., Ahmad, Y., Gierlinski, M., Charriere, F., Lamont, D., Scott, M., Barton, G., and Lamond, A.I. (2012). A Quantitative Spatial Proteomics Analysis of Proteome Turnover in Human Cells. Mol. Cell. Proteomics *11*, M111.011429–M111.011429.

Borek, E., Ponticorvo, L., and Rittenberg, D. (1958). Protein Turnover in Micro-Organisms. Proc Natl Acad Sci U S A *44*, 369–374.

Bota, D.A., and Davies, K.J.A. (2002). Lon protease preferentially degrades oxidized mitochondrial aconitase by an ATP-stimulated mechanism. Nat Cel Biol *4*, 674–680.

Bota, D.A., Van Remmen, H., and Davies, K.J. (2002). Modulation of Lon protease activity and aconitase turnover during aging and oxidative stress. FEBS Lett. *532*, 103–106.

Brunner, G., and Neupert, W. (1968). Turnover of outer and inner membrane proteins of rat liver mitochondria. FEBS Lett. *1*, 153–155.

Bugger, H., Schwarzer, M., Chen, D., Schrepper, A., Amorim, P.A., Schoepe, M., Nguyen, T.D., Mohr, F.W., Khalimonchuk, O., Weimer, B.C., et al. (2010). Proteomic remodelling of mitochondrial oxidative pathways in pressure overload-induced heart failure. Cardiovasc Res *85*, 376–384.

Busch, R., Kim, Y.K., Neese, R.A., Schade-Serin, V., Collins, M., Awada, M., Gardner, J.L., Beysen, C., Marino, M.E., Misell, L.M., et al. (2006). Measurement of protein turnover rates by heavy water labeling of nonessential amino acids. Biochim Biophys Acta *1760*, 730–744.

Busch, R., Neese, R.A., Awada, M., Hayes, G.M., and Hellerstein, M.K. (2007). Measurement of cell proliferation by heavy water labeling. Nat Protoc *2*, 3045–3057.

Cambridge, S.B., Gnad, F., Nguyen, C., Bermejo, J.L., Krüger, M., and Mann, M. (2011). Systems-wide proteomic analysis in mammalian cells reveals conserved, functional protein turnover. J. Proteome Res. *10*, 5275–5284.

Carraro, F., Rosenblatt, J., and Wolfe, R.R. (1991). Isotopic determination of fibronectin synthesis in humans. Metabolism *40*, 553–561.

Chambers, M.C., Maclean, B., Burke, R., Amodei, D., Ruderman, D.L., Neumann, S., Gatto, L., Fischer, B., Pratt, B., Egertson, J., et al. (2012). A cross-platform toolkit for mass spectrometry and proteomics. Nat Biotechnol *30*, 918–920.

Chan, X.C., Black, C.M., Lin, A.J., Ping, P., and Lau, E. (2014). Mitochondrial protein turnover: methods to measure turnover rates on a large scale. J. Mol. Cell. Cardiol. *In Print*.

Chen, Q., Liu, J.B., Horak, K.M., Zheng, H., Kumarapeli, A.R.K., Li, J., Li, F., Gerdes, A.M., Wawrousek, E.F., and Wang, X. (2005). Intrasarcoplasmic amyloidosis impairs proteolytic function of proteasomes in cardiomyocytes by compromising substrate uptake. Circ. Res. *97*, 1018–1026.

Civelek, M., and Lusis, A.J. (2014). Systems genetics approaches to understand complex traits. Nat Rev Genet *15*, 34–48.

Claydon, A.J., and Beynon, R. (2012). Proteome dynamics: revisiting turnover with a global perspective. Mol Cell Proteomics *11*, 1551–1565.

Claydon, A., Thom, M., Hurst, J., and Beynon, R.J. (2012). Protein turnover: measurement of proteome dynamics by whole animal metabolic labelling with stable isotope labelled amino acids. Proteomics *In press*.

Clevers, H. (2006). Wnt/beta-catenin signaling in development and disease. Cell *127*, 469–480.

Commerford, S.L., Carsten, A.L., and Cronkite, E.P. (1983). The distribution of tritium among the amino acids of proteins obtained from mice exposed to tritiated water. Radiat Res *94*, 151–155.

Cox, J., and Mann, M. (2008). MaxQuant enables high peptide identification rates, individualized p.p.b.-range mass accuracies and proteome-wide protein quantification. Nat Biotechnol *26*, 1367–1372.

Cox, J., Neuhauser, N., Michalski, A., Scheltema, R.A., Olsen, J. V, and Mann, M. (2011). Andromeda: a peptide search engine integrated into the MaxQuant environment. J Proteome Res *10*, 1794–1805.

Dai, D.F., Hsieh, E.J., Liu, Y., Chen, T., Beyer, R.P., Chin, M.T., MacCoss, M.J., and Rabinovitch, P.S. (2012). Mitochondrial proteome remodelling in pressure overload-induced heart failure: the role of mitochondrial oxidative stress. Cardiovasc Res *93*, 79–88.

Dai, D.F., Hsieh, E.J., Chen, T., Menendez, L.G., Basisty, N.B., Tsai, L., Beyer, R.P., Crispin, D.A., Shulman, N.J., Szeto, H.H., et al. (2013). Global proteomics and pathway analysis of pressure-overload-induced heart failure and its attenuation by mitochondrial-targeted peptides. Circ. Heart Fail. *6*, 1067–1076.

Dantuma, N.P., Lindsten, K., Glas, R., Jellne, M., and Masucci, M.G. (2000). Short-lived green fluorescent proteins for quantifying ubiquitin/proteasome-dependent proteolysis in living cells. Nat. Biotechnol. *18*, 538–543.

Day, S.M. (2013). The ubiquitin proteasome system in human cardiomyopathies and heart failure. Am. J. Physiol. Heart Circ. Physiol. *304*, H1283–H1293.

Dehlinger, P.J., and Schimke, R.T. (1970). Effect of size on the relative rate of degradation of rat liver soluble proteins. Biochem Biophys Res Commun *40*, 1473–1480.

Dice, J.F., and Goldberg, A.L. (1975a). A statistical analysis of the relationship between degradative rates and molecular weights of proteins. Arch Biochem Biophys *170*, 213–219.

Dice, J.F., and Goldberg, A.L. (1975b). Relationship between in vivo degradative rates and isoelectric points of proteins. Proc Natl Acad Sci U S A *72*, 3893–3897.

Divald, A., Kivity, S., Wang, P., Hochhauser, E., Roberts, B., Teichberg, S., Gomes, A. V, and Powell, S.R. (2010). Myocardial ischemic preconditioning preserves postischemic function of the 26S proteasome through diminished oxidative damage to 19S regulatory particle subunits. Circ Res *106*, 1829–1838.

Doherty, M.K., and Beynon, R.J. (2006). Protein turnover on the scale of the proteome. Expert Rev Proteomics *3*, 97–110.

Doherty, M.K., Whitehead, C., McCormack, H., Gaskell, S.J., and Beynon, R.J. (2005). Proteome dynamics in complex organisms: Using stable isotopes to monitor individual protein turnover rates. Proteomics *5*, 522–533.

Doherty, M.K., Hammond, D.E., Clague, M.J., Gaskell, S.J., and Beynon, R.J. (2009). Turnover of the human proteome: determination of protein intracellular stability by dynamic SILAC. J Proteome Res *8*, 104–112.

Doherty, M.K., Brownridge, P., Owen, M.A.G., Davies, S.J., Young, I.S., and Whitfield, P.D. (2012). A proteomics strategy for determining the synthesis and degradation rates of individual proteins in fish. J. Proteomics *75*, 4471–4477.

Dorn 2nd, G.W. (2013). Mitochondrial dynamics in heart disease. Biochim Biophys Acta *1833*, 233–241.

Doroudgar, S., and Glembotski, C.C. (2013). New concepts of endoplasmic reticulum function in the heart: programmed to conserve. J Mol Cell Cardiol *55*, 85–91.

Drews, O., Tsukamoto, O., Liem, D., Streicher, J., Wang, Y., and Ping, P. (2010). Differential regulation of proteasome function in isoproterenol-induced cardiac hypertrophy. Circ Res *107*, 1094–1101.

Eisen, M.B., Spellman, P.T., Brown, P.O., and Botstein, D. (1998). Cluster analysis and display of genome-wide expression patterns. Proc. Natl. Acad. Sci. U. S. A. *95*, 14863–14868.

Emson, C.L., Fitzmaurice, S., Lindwall, G., Li, K.W., Hellerstein, M.K., Maibach, H.I., Liao, W., and Turner, S.M. (2013). A pilot study demonstrating a non-invasive method for the measurement of protein turnover in skin disorders: application to psoriasis. Clin Transl Med *2*, 12.

Fanara, P., Wong, P.Y., Husted, K.H., Liu, S., Liu, V.M., Kohlstaedt, L.A., Riiff, T., Protasio, J.C., Boban, D., Killion, S., et al. (2012). Cerebrospinal fluid-based kinetic biomarkers of axonal transport in monitoring neurodegeneration. J Clin Invest *122*, 3159–3169.

Farrah, T., Deutsch, E.W., Omenn, G.S., Campbell, D.S., Sun, Z., Bletz, J.A., Mallick, P., Katz, J.E., Malmstrom, J., Ossola, R., et al. (2011). A high-confidence human plasma proteome reference set with estimated concentrations in PeptideAtlas. Mol Cell Proteomics *10*, M110 006353.

Fujiwara, N., Nakano, M., Kato, S., Yoshihara, D., Ookawara, T., Eguchi, H., Taniguchi, N., and Suzuki, K. (2007). Oxidative modification to cysteine sulfonic acid of Cys111 in human copper-zinc superoxide dismutase. J. Biol. Chem. *282*, 35933–35944.

Gaussin, V., Tomlinson, J.E., Depre, C., Engelhardt, S., Antos, C.L., Takagi, G., Hein, L., Topper, J.N., Liggett, S.B., Olson, E.N., et al. (2003). Common genomic response in different mouse models of beta-adrenergic-induced cardiomyopathy. Circulation *108*, 2926–2933.

Gerszten, R.E., Asnani, A., and Carr, S.A. (2011). Status and prospects for discovery and verification of new biomarkers of cardiovascular disease by proteomics. Circ Res *109*, 463–474.

Getz, G.S. (2013). Murray Rabinowitz. Biogr Mem Natl Acad Sci.

Ghazalpour, A., Rau, C.D., Farber, C.R., Bennett, B.J., Orozco, L.D., van Nas, A., Pan, C., Allayee, H., Beaven, S.W., Civelek, M., et al. (2012). Hybrid mouse diversity panel: a panel of inbred mouse strains suitable for analysis of complex genetic traits. Mamm Genome *23*, 680–692.

Gianni, D., Li, A., Tesco, G., McKay, K.M., Moore, J., Raygor, K., Rota, M., Gwathmey, J.K., Dec, G.W., Aretz, T., et al. (2010). Protein aggregates and novel presenilin gene variants in idiopathic dilated cardiomyopathy. Circulation *121*, 1216–1226.

Giordano, F.J. (2005). Oxygen, oxidative stress, hypoxia, and heart failure. J Clin Invest *115*, 500–508.

Glass, R.D., and Doyle, D. (1972). On the measurement of protein turnover in animal cells. J Biol Chem *247*, 5234–5242.

Glembotski, C.C. (2012). Clarifying the cardiac proteasome paradox: protein quality control. Circ Res *111*, 509–512.

Go, A.S., Mozaffarian, D., Roger, V.L., Benjamin, E.J., Berry, J.D., Borden, W.B., Bravata, D.M., Dai, S., Ford, E.S., Fox, C.S., et al. (2013). Heart disease and stroke statistics-2013 update: A Report from the American Heart Association. Circulation *127*.

Gomes, A. V, Zong, C., and Ping, P. (2006). Protein degradation by the 26S proteasome system in the normal and stressed myocardium. Antioxid Redox Signal *8*, 1677–1691.

Goonasekera, S.A., Hammer, K., Auger-Messier, M., Bodi, I., Chen, X., Zhang, H., Reiken, S., Elrod, J.W., Correll, R.N., York, A.J., et al. (2012). Decreased cardiac L-type Ca(2)(+) channel activity induces hypertrophy and heart failure in mice. J Clin Invest *122*, 280–290.

Gottlieb, R.A., and Gustafsson, A.B. (2011). Mitochondrial turnover in the heart. Biochim Biophys Acta *1813*, 1295–1301.

Guan, S., Price, J.C., Prusiner, S.B., Ghaemmaghami, S., and Burlingame, A.L. (2011). A Data Processing Pipeline for Mammalian Proteome Dynamics Studies Using Stable Isotope Metabolic Labeling. Mol. Cell. Proteomics *10*, M111.010728–M111.010728.

Guan, S., Price, J.C., Ghaemmaghami, S., Prusiner, S.B., and Burlingame, A.L. (2012). Compartment modeling for mammalian protein turnover studies by stable isotope metabolic labeling. Anal. Chem. *84*, 4014–4021.

Guitart, M., Osorio-Conles, Ó., Pentinat, T., Cebrià, J., García-Villoria, J., Sala, D., Sebastián, D., Zorzano, A., Ribes, A., Jiménez-Chillarón, J.C., et al. (2014). Fatty Acid Transport Protein 1 (FATP1) Localizes in Mitochondria in Mouse Skeletal Muscle and Regulates Lipid and Ketone Body Disposal. PLoS One *9*, e98109.

Hamada, H., Suzuki, M., Yuasa, S., Mimura, N., Shinozuka, N., Takada, Y., Nishino, T., Nakaya, H., Koseki, H., and Aoe, T. (2004). Dilated cardiomyopathy caused by aberrant endoplasmic reticulum quality control in mutant KDEL receptor transgenic mice. Mol Cell Biol *24*, 8007–8017.

Hammerling, B.C., and Gustafsson, Å.B. (2014). Mitochondrial Quality Control in the Myocardium: Cooperation between Protein Degradation and Mitophagy. J. Mol. Cell. Cardiol. *75*, 122–130.

Hawkins, A.J.S. (1991). Protein Turnover: A Functional Appraisal. Funct. Ecol. *5*, 222–233 CR – Copyright © 1991 British Ecolog.

Hedhli, N., and Depre, C. (2010). Proteasome inhibitors and cardiac cell growth. Cardiovasc Res *85*, 321–329.

Hellerstein, M.K., and Neese, R.A. (1999). Mass isotopomer distribution analysis at eight years: theoretical, analytic, and experimental considerations. Am. J. Physiol. *276*, E1146–E1170.

Heo, J.M., Livnat-Levanon, N., Taylor, E.B., Jones, K.T., Dephoure, N., Ring, J., Xie, J., Brodsky, J.L., Madeo, F., Gygi, S.P., et al. (2010). A stress-responsive system for mitochondrial protein degradation. Mol. Cell *40*, 465–480.

Hinkson, I. V, and Elias, J.E. (2011). The dynamic state of protein turnover: It's about time. Trends Cell Biol *21*, 293–303.

Hipkiss, A.R. (2011). Energy metabolism and ageing regulation: metabolically driven deamidation of triosephosphate isomerase may contribute to proteostatic dysfunction. Ageing Res Rev *10*, 498–502.

Hoshino, A., Okawa, Y., Ariyoshi, M., Kaimoto, S., Uchihashi, M., Fukai, K., Iwai-Kanai, E., and Matoba, S. (2014). Oxidative post-translational modifications develop LONP1 dysfunction in pressure overload heart failure. Circ. Hear. Fail. *7*, 500–509.

Houser, S.R., Margulies, K.B., Murphy, A.M., Spinale, F.G., Francis, G.S., Prabhu, S.D., Rockman, H.A., Kass, D.A., Molkentin, J.D., Sussman, M.A., et al. (2012). Animal models of heart failure: a scientific statement from the American Heart Association. Circ Res *111*, 131–150.

Houtkooper, R.H., Mouchiroud, L., Ryu, D., Moullan, N., Katsyuba, E., Knott, G., Williams, R.W., and Auwerx, J. (2013). Mitonuclear protein imbalance as a conserved longevity mechanism. Nature *497*, 451–457.

Hsieh, E.J., Shulman, N.J., Dai, D.F., Vincow, E.S., Karunadharma, P.P., Pallanck, L., Rabinovitch, P.S., and MacCoss, M.J. (2012). Topograph, a software platform for precursor enrichment corrected global protein turnover measurements. Mol Cell Proteomics *11*, 1468–1474.

Huang da, W., Sherman, B.T., and Lempicki, R.A. (2009). Systematic and integrative analysis of large gene lists using DAVID bioinformatics resources. Nat Protoc *4*, 44–57.

Huttlin, E.L., Jedrychowski, M.P., Elias, J.E., Goswami, T., Rad, R., Beausoleil, S.A., Villen, J., Haas, W., Sowa, M.E., and Gygi, S.P. (2010). A tissue-specific atlas of mouse protein phosphorylation and expression. Cell *143*, 1174–1189.

Ideker, T., Thorsson, V., Ranish, J.A., Christmas, R., Buhler, J., Eng, J.K., Bumgarner, R., Goodlett, D.R., Aebersold, R., and Hood, L. (2001). Integrated genomic and proteomic analyses of a systematically perturbed metabolic network. Science *292*, 929–934.

Janssen, R.J.R.J., Nijtmans, L.G., van den Heuvel, L.P., and Smeitink, J. a M. (2006). Mitochondrial complex I: structure, function and pathology. J. Inherit. Metab. Dis. *29*, 499–515.

Jayapal, K.P., Sui, S., Philp, R.J., Kok, Y.J., Yap, M.G.S., Griffin, T.J., and Hu, W.S. (2010). Multitagging proteomic strategy to estimate protein turnover rates in dynamic systems. J. Proteome Res. *9*, 2087–2097.

Jin, S.M., Lazarou, M., Wang, C., Kane, L.A., Narendra, D.P., and Youle, R.J. (2010). Mitochondrial membrane potential regulates PINK1 import and proteolytic destabilization by PARL. J. Cell Biol. *191*, 933–942.

John, S., Weiss, J.N., and Ribalet, B. (2011). Subcellular localization of hexokinases I and II directs the metabolic fate of glucose. PLoS One *6*.

Kalderon, B., Gopher, A., and Lapidot, A. (1986). Metabolic pathways leading to liver glycogen repletion in vivo, studied by GC-MS and NMR. FEBS Lett. *204*, 29–32.

Kaser, M., and Langer, T. (2000). Protein degradation in mitochondria. Semin. Cell Dev. Biol. *11*, 181–190.

Kasumov, T., Ilchenko, S., Li, L., Rachdaoui, N., Sadygov, R.G., Willard, B., McCullough, A.J., and Previs, S. (2011). Measuring protein synthesis using metabolic (2)H labeling, high-resolution mass spectrometry, and an algorithm. Anal Biochem *412*, 47–55.

Kasumov, T., Dabkowski, E.R., Shekar, K.C., Li, L., Ribeiro Jr., R.F., Walsh, K., Previs, S.F., Sadygov, R.G., Willard, B., and Stanley, W.C. (2013). Assessment of Cardiac Proteome Dynamics with Heavy Water: Slower Protein Synthesis Rates in Interfibrillar than Subsarcolemmal Mitochondria. Am J Physiol Hear. Circ Physiol.

Kato, T., Niizuma, S., Inuzuka, Y., Kawashima, T., Okuda, J., Tamaki, Y., Iwanaga, Y., Narazaki, M., Matsuda, T., Soga, T., et al. (2010). Analysis of metabolic remodeling in compensated left ventricular hypertrophy and heart failure. Circ. Heart Fail. *3*, 420–430.

Katz, A.M. (2010). Physiology of the Heart (Lippincott Williams & Wilkins).

Katz, J.H. (1961). Iron and protein kinetics studied by means of doubly labeled human crystalline transferrin. J Clin Invest *40*, 2143–2152.

Kekki, M., Koskelo, P., and Nikkila, E.A. (1966). Turnover of iodine-131-labelled ceruloplasmin in human beings. Nature *209*, 1252–1253.

Kennedy, E.P. (2001). Hitler's gift and the era of biosynthesis. J Biol Chem *276*, 42619–42631.

Khmelinskii, A., Keller, P.J., Bartosik, A., Meurer, M., Barry, J.D., Mardin, B.R., Kaufmann, A., Trautmann, S., Wachsmuth, M., Pereira, G., et al. (2012). Tandem fluorescent protein timers for in vivo analysis of protein dynamics. Nat Biotechnol *30*, 708–714.

Kim, T.Y., Wang, D., Kim, A.K., Lau, E., Lin, A.J., Liem, D.A., Zhang, J., Zong, N.C., Lam, M.P., and Ping, P. (2012). Metabolic labeling reveals proteome dynamics of mouse mitochondria. Mol Cell Proteomics *11*, 1586–1594.

Kim, W., Bennett, E.J., Huttlin, E.L., Guo, A., Li, J., Possemato, A., Sowa, M.E., Rad, R., Rush, J., Comb, M.J., et al. (2011). Systematic and quantitative assessment of the ubiquitin-modified proteome. Mol. Cell *44*, 325–340.

Kohler Jr., R.E. (1977). Rudolf Schoenheimer, Isotopic Tracers, and Biochemistry in the 1930's. Hist. Stud. Phys. Sci. *8*, 257–298.

Kolwicz Jr., S.C., and Tian, R. (2011). Glucose metabolism and cardiac hypertrophy. Cardiovasc Res *90*, 194–201.

Krauss, S. (1969). Haptoglobin metabolism in polycythemia vera. Blood *33*, 865–876.

Kresge, N., Simoni, R.D., and Hill, R.L. (2005). David Rittenberg: Exploring Porphyrin Synthesis with Duck Blood and Isotope Tracers. J Biol Chem *280*, e12.

Kristensen, A.R., Gsponer, J., and Foster, L.J. (2013). Protein synthesis rate is the predominant regulator of protein expression during differentiation. Mol. Syst. Biol. *9*, 689.

Kubli, D.A., and Gustafsson, A.B. (2012). Mitochondria and mitophagy: the yin and yang of cell death control. Circ Res *111*, 1208–1221.

Kyte, J., and Doolittle, R.F. (1982). A simple method foKyte, J., & Doolittle, R. F. (1982). A simple method for displaying the hydropathic character of a protein. Journal of Molecular Biology, 157, 105–132. doi:10.1016/0022-2836(82)90515-0r displaying the hydropathic character of a protein. J. Mol. Biol. *157*, 105–132.

Lam, M.P., Lau, E., Siu, S.O., Ng, D.C., Kong, R.P., Chiu, P.C., Yeung, W.S., Lo, C., and Chu, I.K. (2011). Online combination of reversed-phase/reversed-phase and porous graphitic carbon liquid chromatography for multicomponent separation of proteomics and glycoproteomics samples. Electrophoresis *32*, 2930–2940.

Lam, M.P., Scruggs, S.B., Kim, T.Y., Zong, C., Lau, E., Wang, D., Ryan, C.M., Faull, K.F., and Ping, P. (2012). An MRM-based workflow for quantifying cardiac mitochondrial protein phosphorylation in murine and human tissue. J Proteomics *75*, 4602–4609.

Lam, M.P., Lau, E., Scruggs, S.B., Wang, D., Kim, T.Y., Liem, D.A., Zhang, J., Ryan, C.M., Faull, K.F., and Ping, P. (2013). Site-specific quantitative analysis of cardiac mitochondrial protein phosphorylation. J Proteomics *81*, 15–23.

Lam, M.P., Wang, D., Lau, E., Liem, D., Kim, A.K., Ng, D.C., Liang, X., Bleakley, B.J., Liu, C., Tabaraki, J.D., et al. (2014). Protein kinetic signatures of the remodeling heart following isoproterenol stimulation. J Clin Invest *124*, 1734–1744.

Lamant, M., Smih, F., Harmancey, R., Philip-Couderc, P., Pathak, A., Roncalli, J., Galinier, M., Collet, X., Massabuau, P., Senard, J.-M., et al. (2006). ApoO, a novel apolipoprotein, is an original glycoprotein up-regulated by diabetes in human heart. J. Biol. Chem. *281*, 36289–36302.

Lane, D.J.R., Huang, M.L.-H., Ting, S., Sivagurunathan, S., and Richardson, D.R. (2013). Biochemistry of cardiomyopathy in the mitochondrial disease Friedreich's ataxia. Biochem. J. *453*, 321–336.

Lau, E., Lam, M.P., Siu, S.O., Kong, R.P., Chan, W.L., Zhou, Z., Huang, J., Lo, C., and Chu, I.K. (2011). Combinatorial use of offline SCX and online RP-RP liquid chromatography for iTRAQ-based quantitative proteomics applications. Mol Biosyst *7*, 1399–1408.

Lau, E., Wang, D., Zhang, J., Yu, H., Lam, M.P., Liang, X., Zong, N., Kim, T.Y., and Ping, P. (2012). Substrate- and isoform-specific proteome stability in normal and stressed cardiac mitochondria. Circ Res *110*, 1174–1178.

Lee, D.H., and Goldberg, A.L. (1998). Proteasome inhibitors: Valuable new tools for cell biologists. Trends Cell Biol. *8*, 397–403.

Leonhard, K., Guiard, B., Pellecchia, G., Tzagoloff, A., Neupert, W., and Langer, T. (2000). Membrane protein degradation by AAA proteases in mitochondria: extraction of substrates from either membrane surface. Mol. Cell *5*, 629–638.

Li, J., Powell, S.R., and Wang, X. (2011). Enhancement of proteasome function by PA28α overexpression protects against oxidative stress. FASEB J *25*, 883–893.

Li, L., Willard, B., Rachdaoui, N., Kirwan, J.P., Sadygov, R.G., Stanley, W.C., Previs, S., McCullough, A.J., and Kasumov, T. (2012). Plasma proteome dynamics: analysis of lipoproteins and acute phase response proteins with 2H2O metabolic labeling. Mol Cell Proteomics *11*, M111 014209.

Lin, C.S., Sun, Y.L., and Liu, C.Y. (2003). Structural and biochemical evidence of mitochondrial depletion in pigs with hypertrophic cardiomyopathy. Res. Vet. Sci. *74*, 219–226.

Lindner, H., and Helliger, W. (2001). Age-dependent deamidation of asparagine residues in proteins. Exp Gerontol *36*, 1551–1563.

Lindsey, M.L., Goshorn, D.K., Comte-Walters, S., Hendrick, J.W., Hapke, E., Zile, M.R., and Schey, K. (2006). A multidimensional proteomic approach to identify hypertrophy-associated proteins. Proteomics *6*, 2225–2235.

Lipsky, N.G., and Pedersen, P.L. (1981). Mitochondrial turnover in animal cells. Half-lives of mitochondria and mitochondrial subfractions of rat liver based on [14C]bicarbonate incorporation. J Biol Chem *256*, 8652–8657.

Livnat-Levanon, N., and Glickman, M.H. (2011). Ubiquitin-Proteasome System and mitochondria - Reciprocity. Biochim Biophys Acta Gene Regul. Mech. *1809*, 80–87.

Lombardi, R., Betocchi, S., Losi, M.A., Tocchetti, C.G., Aversa, M., Miranda, M., D'Alessandro, G., Cacace, A., Ciampi, Q., and Chiariello, M. (2003). Myocardial collagen turnover in hypertrophic cardiomyopathy. Circulation *108*, 1455–1460.

Lotz, C., Lin, A.J., Black, C.M., Zhang, J., Lau, E., Deng, N., Wang, Y., Zong, N., Choi, J., Tao, X., et al. (2013). The Characterization, Design, and Function of the Mitochondrial Proteome: From Organs to Organisms. J Proteome Res *Epub DOI: .*

Lukashchuk, N., and Vousden, K.H. (2007). Ubiquitination and degradation of mutant p53. Mol. Cell. Biol. *27*, 8284–8295.

Lyon, D., Castillejo, M.A., Staudinger, C., Weckwerth, W., Wienkoop, S., and Egelhofer, V. (2014). Automated protein turnover calculations from 15n partial metabolic labeling lc/ms shotgun proteomics data. PLoS One *9*.

Maier, T., Güell, M., and Serrano, L. (2009). Correlation of mRNA and protein in complex biological samples. FEBS Lett. *583*, 3966–3973.

Maier, T., Schmidt, A., Güell, M., Kühner, S., Gavin, A.-C., Aebersold, R., and Serrano, L. (2011). Quantification of mRNA and protein and integration with protein turnover in a bacterium. Mol. Syst. Biol. *7*, 511.

Major, T., von Janowsky, B., Ruppert, T., Mogk, A., and Voos, W. (2006). Proteomic Analysis of Mitochondrial Protein Turnover: Identification of Novel Substrate Proteins of the Matrix Protease Pim1. Mol Cell Biol *26*, 762–776.

Marcillat, O., Zhang, Y., Lin, S.W., and Davies, K.J. (1988). Mitochondria contain a proteolytic system which can recognize and degrade oxidatively-denatured proteins. Biochem. J. *254*, 677–683.

Margineantu, D.H., Emerson, C.B., Diaz, D., and Hockenbery, D.M. (2007). Hsp90 inhibition decreases mitochondrial protein turnover. PLoS One *2*, e1066.

Marin-Garcia, J., Goldenthal, M.J., and Moe, G.W. (2001). Mitochondrial pathology in cardiac failure. Cardiovasc Res *49*, 17–26.

Martin, A.F. (1981). Turnover of cardiac troponin subunits. Kinetic evidence for a precursor pool of troponin-I. J Biol Chem *256*, 964–968.

Matsushima, Y., Goto, Y., and Kaguni, L.S. (2010). Mitochondrial Lon protease regulates mitochondrial DNA copy number and transcription by selective degradation of mitochondrial transcription factor A (TFAM). Proc. Natl. Acad. Sci. U. S. A. *107*, 18410–18415.

McLelland, G.L., Soubannier, V., Chen, C.X., McBride, H.M., and Fon, E.A. (2014). Parkin and PINK1 function in a vesicular trafficking pathway regulating mitochondrial quality control. EMBO J. *33*, 282–295.

Meng, C., Jin, X., Xia, L., Shen, S.M., Wang, X.L., Cai, J., Chen, G.Q., Wang, L.S., and Fang, N.Y. (2009). Alterations of mitochondrial enzymes contribute to cardiac hypertrophy before hypertension development in spontaneously hypertensive rats. J Proteome Res *8*, 2463–2475.

Miller, B.F., Robinson, M.M., Bruss, M.D., Hellerstein, M., and Hamilton, K.L. (2012). A comprehensive assessment of mitochondrial protein synthesis and cellular proliferation with age and caloric restriction. Aging Cell *11*, 150–161.

Millward, D.J., Garlick, P.J., Stewart, R.J., Nnanyelugo, D.O., and Waterlow, J.C. (1975). Skeletal-muscle growth and protein turnover. Biochem. J. *150*, 235–243.

Miro-Casas, E., Ruiz-Meana, M., Agullo, E., Stahlhofen, S., Rodríguez-Sinovas, A., Cabestrero, A., Jorge, I., Torre, I., Vazquez, J., Boengler, K., et al. (2009). Connexin43 in cardiomyocyte mitochondria contributes to mitochondrial potassium uptake. Cardiovasc. Res. *83*, 747–756.

Miwa, S., Lawless, C., and von Zglinicki, T. (2008). Mitochondrial turnover in liver is fast in vivo and is accelerated by dietary restriction: application of a simple dynamic model. Aging Cell *7*, 920–923.

Molkentin, J.D. (2004). Calcineurin-NFAT signaling regulates the cardiac hypertrophic response in coordination with the MAPKs. Cardiovasc. Res. *63*, 467–475.

Nagaraj, N., Wisniewski, J.R., Geiger, T., Cox, J., Kircher, M., Kelso, J., Paabo, S., and Mann, M. (2011). Deep proteome and transcriptome mapping of a human cancer cell line. Mol Syst Biol *7*, 548.

Van Nas, A., Pan, C., Ingram-Drake, L.A., Ghazalpour, A., Drake, T.A., Sobel, E.M., Papp, J.C., and Lusis, A.J. (2013). The systems genetics resource: a web application to mine global data for complex disease traits. Front Genet *4*, 84.

Neely, J.R., and Morgan, H.E. (1974). Relationship Between Carbohydrate and Lipid Metabolism and the Energy Balance of Heart Muscle. Annu. Rev. Physiol. *36*, 413–459.

Nelder, J.A., and Mead, R. (1965). A simplex-method for function minimization. Comput. J. *7*, 308–313.

Neubauer, S. (2007). The failing heart--an engine out of fuel. N Engl J Med *356*, 1140–1151.

Ngo, J.K., and Davies, K.J. (2009). Mitochondrial Lon protease is a human stress protein. Free Radic. Biol. Med. *46*, 1042–1048.

Ngo, J.K., Pomatto, L.C.D., Bota, D.A., Koop, A.L., and Davies, K.J.A. (2011). Impairment of Lon-Induced Protection Against the Accumulation of Oxidized Proteins in Senescent Wi-38 Fibroblasts. J Gerontol A Biol Sci Med Sci.

Nojiri, H., Shimizu, T., Funakoshi, M., Yamaguchi, O., Zhou, H., Kawakami, S., Ohta, Y., Sami, M., Tachibana, T., Ishikawa, H., et al. (2006). Oxidative stress causes heart failure with impaired mitochondrial respiration. J Biol Chem *281*, 33789–33801.

Noor, N., Patel, C.B., and Rockman, H.A. (2011). Beta-arrestin: a signaling molecule and potential therapeutic target for heart failure. J Mol Cell Cardiol *51*, 534–541.

Nowis, D., Maczewski, M., Mackiewicz, U., Kujawa, M., Ratajska, A., Wieckowski, M.R., Wilczyński, G.M., Malinowska, M., Bil, J., Salwa, P., et al. (2010). Cardiotoxicity of the anticancer therapeutic agent bortezomib. Am. J. Pathol. *176*, 2658–2668.

Paoletti, A.C., Parmely, T.J., Tomomori-Sato, C., Sato, S., Zhu, D.X., Conaway, R.C., Conaway, J.W., Florens, L., and Washburn, M.P. (2006). Quantitative proteomic analysis of distinct mammalian Mediator complexes using normalized spectral abundance factors. Proc Natl Acad Sci U S A *103*, 18928–18933.

Papa, L., Gomes, E., and Rockwell, P. (2007). Reactive oxygen species induced by proteasome inhibition in neuronal cells mediate mitochondrial dysfunction and a caspase-independent cell death. Apoptosis *12*, 1389–1405.

Papageorgopoulos, C., Caldwell, K., Shackleton, C., Schweingrubber, H., and Hellerstein, M.K. (1999). Measuring protein synthesis by mass isotopomer distribution analysis (MIDA). Anal. Biochem. *267*, 1–16.

Parks, B.W., Nam, E., Org, E., Kostem, E., Norheim, F., Hui, S.T., Pan, C., Civelek, M., Rau, C.D., Bennett, B.J., et al. (2013). Genetic control of obesity and gut microbiota composition in response to high-fat, high-sucrose diet in mice. Cell Metab *17*, 141–152.

Petrak, J., Pospisilova, J., Sedinova, M., Jedelsky, P., Lorkova, L., Vit, O., Kolar, M., Strnad, H., Benes, J., Sedmera, D., et al. (2011). Proteomic and transcriptomic analysis of heart failure due to volume overload in a rat aorto-caval fistula model provides support for new potential therapeutic targets - monoamine oxidase A and transglutaminase 2. Proteome Sci *9*, 69.

Prakash, S., Tian, L., Ratliff, K.S., Lehotzky, R.E., and Matouschek, A. (2004). An unstructured initiation site is required for efficient proteasome-mediated degradation. Nat. Struct. Mol. Biol. *11*, 830–837.

Pratt, J.M., Petty, J., Riba-Garcia, I., Robertson, D.H.L., Gaskell, S.J., Oliver, S.G., and Beynon, R.J. (2002). Dynamics of protein turnover, a missing dimension in proteomics. Mol. Cell. Proteomics *1*, 579–591.

Predmore, J.M., Wang, P., Davis, F., Bartolone, S., Westfall, M. V., Dyke, D.B., Pagani, F., Powell, S.R., and Day, S.M. (2010). Ubiquitin proteasome dysfunction in human hypertrophic and dilated cardiomyopathies. Circulation *121*, 997–1004.

Price, J.C., Guan, S., Burlingame, A., Prusiner, S.B., and Ghaemmaghami, S. (2010). Analysis of proteome dynamics in the mouse brain. Proc Natl Acad Sci U S A *107*, 14508–14513.

Price, J.C., Holmes, W.E., Li, K.W., Floreani, N.A., Neese, R.A., Turner, S.M., and Hellerstein, M.K. (2012a). Measurement of human plasma proteome dynamics with (2)H(2)O and liquid chromatography tandem mass spectrometry. Anal Biochem *420*, 73–83.

Price, J.C., Khambatta, C.F., Li, K.W., Bruss, M.D., Shankaran, M., Dalidd, M., Floreani, N.A., Roberts, L.S., Turner, S.M., Holmes, W.E., et al. (2012b). The effect of long term calorie restriction on in vivo hepatic proteostatis: a novel combination of dynamic and quantitative proteomics. Mol Cell Proteomics *11*, 1801–1814.

Prilusky, J., Felder, C.E., Zeev-Ben-Mordehai, T., Rydberg, E.H., Man, O., Beckmann, J.S., Silman, I., and Sussman, J.L. (2005). FoldIndex: a simple tool to predict whether a given protein sequence is intrinsically unfolded. Bioinformatics *21*, 3435–3438.

Qian, M.X., Pang, Y., Liu, C.H., Haratake, K., Du, B.Y., Ji, D.Y., Wang, G.F., Zhu, Q.Q., Song, W., Yu, Y., et al. (2013). Acetylation-mediated proteasomal degradation of core histones during DNA repair and spermatogenesis. Cell *153*, 1012–1024.

Rabinowitz, M. (1973). Protein synthesis and turnover in normal and hypertrophied heart. Am J Cardiol *31*, 202–210.

Rabinowitz, M., and Zak, R. (1975). Mitochondria and cardiac hypertrophy. Circ Res *36*, 367–376.

Rachdaoui, N., Austin, L., Kramer, E., Previs, M.J., Anderson, V.E., Kasumov, T., and Previs, S.F. (2009). Measuring proteome dynamics in vivo: as easy as adding water? Mol Cell Proteomics *8*, 2653–2663.

Radke, S., Chander, H., Schäfer, P., Meiss, G., Krüger, R., Schulz, J.B., and Germain, D. (2008). Mitochondrial Protein Quality Control by the Proteasome Involves Ubiquitination and the Protease Omi. J Biol Chem *283*, 12681–12685.

Rau, C.D. (2013). A systems genetics approach to the identification of causal genes in heart failure using a large mouse panel. University of California, Los Angeles.

Razeghi, P., Young, M.E., Alcorn, J.L., Moravec, C.S., Frazier, O.H., and Taegtmeyer, H. (2001). Metabolic gene expression in fetal and failing human heart. Circulation *104*, 2923–2931.

Rep, M., and Grivell, L.A. (1996). The role of protein degradation in mitochondrial function and biogenesis. Curr. Genet. *30*, 367–380.

Rittenberg, D., and San Pietro, A. (1953). A STUDY OF THE RATE OF PROTEIN SYNTHESIS IN HUMANS: II. MEASUREMENT OF THE METABOLIC POOL AND THE RATE OF PROTEIN SYNTHESIS. J Biol Chem *201*, 457–473.

De Riva, A., Deery, M.J., McDonald, S., Lund, T., and Busch, R. (2010). Measurement of protein synthesis using heavy water labeling and peptide mass spectrometry: Discrimination between major histocompatibility complex allotypes. Anal Biochem *403*, 1–12.

Rockman, H.A., Chien, K.R., Choi, D.J., Iaccarino, G., Hunter, J.J., Ross Jr., J., Lefkowitz, R.J., and Koch, W.J. (1998). Expression of a beta-adrenergic receptor kinase 1 inhibitor prevents the development of myocardial failure in gene-targeted mice. Proc Natl Acad Sci U S A *95*, 7000–7005.

Rogers, S., Wells, R., and Rechsteiner, M. (1986). Amino acid sequences common to rapidly degraded proteins: the PEST hypothesis. Science (80-.). *234*, 364–368.

Rosca, M.G., and Hoppel, C.L. (2010). Mitochondria in heart failure. Cardiovasc Res *88*, 40–50.

Rosca, M.G., Vazquez, E.J., Kerner, J., Parland, W., Chandler, M.P., Stanley, W., Sabbah, H.N., and Hoppel, C.L. (2008). Cardiac mitochondria in heart failure: decrease in respirasomes and oxidative phosphorylation. Cardiovasc Res *80*, 30–39.

De Sain-van der Velden, M.G., Kaysen, G.A., de Meer, K., Stellaard, F., Voorbij, H.A., Reijngoud, D.J., Rabelink, T.J., and Koomans, H.A. (1998). Proportionate increase of fibrinogen and albumin synthesis in nephrotic patients: measurements with stable isotopes. Kidney Int *53*, 181–188.

Saita, S., Shirane, M., and Nakayama, K.I. (2013). Selective escape of proteins from the mitochondria during mitophagy. Nat. Commun. *4*, 1410.

Sakamaki, J., Daitoku, H., Ueno, K., Hagiwara, A., Yamagata, K., and Fukamizu, A. (2011). Arginine methylation of BCL-2 antagonist of cell death (BAD) counteracts its phosphorylation and inactivation by Akt. Proc. Natl. Acad. Sci. U. S. A. *108*, 6085–6090.

Salazar, N.C., Chen, J., and Rockman, H.A. (2007). Cardiac GPCRs: GPCR signaling in healthy and failing hearts. Biochim. Biophys. Acta - Biomembr. *1768*, 1006–1018.

Saldanha, A.J. (2004). Java Treeview - Extensible visualization of microarray data. Bioinformatics *20*, 3246–3248.

Savas, J.N., Toyama, B.H., Xu, T., Yates, J.R., and Hetzer, M.W. (2012). Extremely Long-Lived Nuclear Pore Proteins in the Rat Brain. Science (80-.). *335*, 942–942.

Savitzky, A., and Golay, M.J.E. (1964). Smoothing and differentiation of data by simplified least squares procedures. Anal Chem *36*, 1627–1639.

Schaper, J., Meiser, E., and Stämmler, G. (1985). Ultrastructural morphometric analysis of myocardium from dogs, rats, hamsters, mice, and from human hearts. Circ. Res. *56* , 377–391.

Schoenheimer, R., Ratner, S., and Rittenberg, D. (1939). STUDIES IN PROTEIN METABOLISM: X. THE METABOLIC ACTIVITY OF BODY PROTEINS INVESTIGATED WITH l (-)-LEUCINE CONTAINING TWO ISOTOPES. J Biol Chem *130*, 703–732.

Schubert, U., Antón, L.C., Gibbs, J., Norbury, C.C., Yewdell, J.W., and Bennink, J.R. (2000). Rapid degradation of a large fraction of newly synthesized proteins by proteasomes. Nature *404*, 770–774.

Schuster, M.K., and Grabner, M. (1986). http://emboss.bioinformatics.nl/cgi-bin/emboss/epestfind.

Schwanhausser, B., Busse, D., Li, N., Dittmar, G., Schuchhardt, J., Wolf, J., Chen, W., and Selbach, M. (2011). Global quantification of mammalian gene expression control. Nature *473*, 337–342.

Shapiro, S.S., and Martinez, J. (1969). Human prothrombin metabolism in normal man and in hypocoagulable subjects. J Clin Invest *48*, 1292–1298.

Sheikh, F., Raskin, A., Chu, P.H., Lange, S., Domenighetti, A.A., Zheng, M., Liang, X., Zhang, T., Yajima, T., Gu, Y., et al. (2008). An FHL1-containing complex within the cardiomyocyte sarcomere mediates hypertrophic biomechanical stress responses in mice. J Clin Invest *118*, 3870–3880.

Shekar, K.C., Li, L., Dabkowski, E.R., Xu, W., Ribeiro, R.F., Hecker, P.A., Recchia, F. a, Sadygov, R.G., Willard, B., Kasumov, T., et al. (2014). Cardiac mitochondrial proteome dynamics with heavy water reveals stable rate of mitochondrial protein synthesis in heart failure despite decline in mitochondrial oxidative capacity. J. Mol. Cell. Cardiol. *75*, 88–97.

Shemin, D., and Bentley, R. (2001). David Rittenberg. Biogr Mem Natl Acad Sci *80*, 257–274.

Simoni, R.D., Hill, C.P., and Vaughan, M. (2002). The Use of Isotope Tracers to Study Intermediary Metabolism: Rudolf Schoenheimer. J Biol Chem *277*, e31.

Simpson, D.G., Sharp, W.W., Borg, T.K., Price, R.L., Terracio, L., and Samarel, A.M. (1996). Mechanical regulation of cardiac myocyte protein turnover and myofibrillar structure. Am J Physiol *270*, C1075–C1087.

Smith, C.K., Baker, T.A., and Sauer, R.T. (1999). Lon and Clp family proteases and chaperones share homologous substrate-recognition domains. Proc. Natl. Acad. Sci. U. S. A. *96*, 6678–6682.

Smith, P.K., Krohn, R.I., Hermanson, G.T., Mallia, A.K., Gartner, F.H., Provenzano, M.D., Fujimoto, E.K., Goeke, N.M., Olson, B.J., and Klenk, D.C. (1985). Measurement of protein using bicinchoninic acid. Anal Biochem *150*, 76–85.

Socolow, E.L., Woeber, K.A., Purdy, R.H., Holloway, M.T., and Ingbar, S.H. (1965). Preparation of I-131-labeled human serum prealbumin and its metabolism in normal and sick patients. J Clin Invest *44*, 1600–1609.

Song, G., Campos, B., Wagoner, L.E., Dedman, J.R., and Walsh, R.A. (1998). Altered cardiac annexin mRNA and protein levels in the left ventricle of patients with end-stage heart failure. J Mol Cell Cardiol *30*, 443–451.

Soubannier, V., McLelland, G.L., Zunino, R., Braschi, E., Rippstein, P., Fon, E.A., and McBride, H.M. (2012). A vesicular transport pathway shuttles cargo from mitochondria to lysosomes. Curr. Biol. *22*, 135–141.

Stansfield, W.E., Tang, R.H., Moss, N.C., Baldwin, A.S., Willis, M.S., and Selzman, C.H. (2008). Proteasome inhibition promotes regression of left ventricular hypertrophy. Am J Physiol Hear. Circ Physiol *294*, H645–H650.

Sullivan, P.G., Dragicevic, N.B., Deng, J.H., Bai, Y., Dimayuga, E., Ding, Q., Chen, Q., Bruce-Keller, A.J., and Keller, J.N. (2004). Proteasome inhibition alters neural mitochondrial homeostasis and mitochondria turnover. J Biol Chem *279*, 20699–20707.

Suzuki, C.K., Suda, K., Wang, N., and Schatz, G. (1994). Requirement for the yeast gene LON in intramitochondrial proteolysis and maintenance of respiration. Science *264*, 273–276.

Tabb, D.L., McDonald, W.H., and Yates 3rd, J.R. (2002). DTASelect and Contrast: tools for assembling and comparing protein identifications from shotgun proteomics. J Proteome Res *1*, 21–26.

Tanaka, K., Ii, K., Ichihara, A., Waxman, L., and Goldberg, A.L. (1986). A high molecular weight protease in the cytosol of rat liver. I. Purification, enzymological properties, and tissue distribution. J Biol Chem *261*, 15197–15203.

Tang, M., Li, J., Huang, W., Su, H., Liang, Q., Tian, Z., Horak, K.M., Molkentin, J.D., and Wang, X. (2010). Proteasome functional insufficiency activates the calcineurin-NFAT pathway in cardiomyocytes and promotes maladaptive remodelling of stressed mouse hearts. Cardiovasc Res *88*, 424–433.

Taniguchi, Y., Choi, P.J., Li, G.-W., Chen, H., Babu, M., Hearn, J., Emili, A., and Xie, X.S. (2010). Quantifying E. coli proteome and transcriptome with single-molecule sensitivity in single cells. Science *329*, 533–538.

Tokoro, T., Ito, H., Maenishi, O., and Suzuki, T. (1995). Mitochondrial abnormalities in hypertrophied myocardium of stroke-prone spontaneously hypertensive rats. Clin. Exp. Pharmacol. Physiol. Suppl. *22*, S268–S269.

Trnka, J., Blaikie, F.H., Logan, A., Smith, R.A.J., and Murphy, M.P. (2009). Antioxidant properties of MitoTEMPOL and its hydroxylamine. Free Radic. Res. *43*, 4–12.

Tsukamoto, O., Minamino, T., Okada, K.I., Shintani, Y., Takashima, S., Kato, H., Liao, Y., Okazaki, H., Asai, M., Hirata, A., et al. (2006). Depression of proteasome activities during the progression of cardiac dysfunction in pressure-overloaded heart of mice. Biochem. Biophys. Res. Commun. *340*, 1125–1133.

Tsutsui, H., Kinugawa, S., and Matsushima, S. (2009). Mitochondrial oxidative stress and dysfunction in myocardial remodelling. Cardiovasc Res *81*, 449–456.

Varshavsky, A. (1996). The N-end rule: functions, mysteries, uses. Proc. Natl. Acad. Sci. U. S. A. *93*, 12142–12149.

Varshavsky, A. (2011). The N-end rule pathway and regulation by proteolysis. Protein Sci.

Vogel, C., and Marcotte, E.M. (2012). Insights into the regulation of protein abundance from proteomic and transcriptomic analyses. Nat. Rev. Genet.

Vogt, J.A., Hunzinger, C., Schroer, K., Hölzer, K., Bauer, A., Schrattenholz, A., Cahill, M.A., Schillo, S., Schwall, G., Stegmann, W., et al. (2005). Determination of Fractional Synthesis Rates of Mouse Hepatic Proteins via Metabolic 13C-Labeling, MALDI-TOF MS and Analysis of Relative Isotopologue Abundances Using Average Masses. Anal. Chem. *77*, 2034–2042.

Vögtle, F.-N., Wortelkamp, S., Zahedi, R.P., Becker, D., Leidhold, C., Gevaert, K., Kellermann, J., Voos, W., Sickmann, A., Pfanner, N., et al. (2009). Global analysis of the mitochondrial N-proteome identifies a processing peptidase critical for protein stability. Cell *139*, 428–439.

Wang, X., and Robbins, J. (2006). Heart failure and protein quality control. Circ Res *99*, 1315–1328.

Wang, D., Zong, C., Koag, M., Wang, Y., Drews, O., Fang, C., Scruggs, S.B., and Ping, P. (2011a). Proteome Dynamics and Proteome Function of Cardiac 19S Proteasomes. Mol Cell Proteomics *10*.

Wang, D., Liem, D.A., Lau, E., Ng, D.C., Bleakley, B.J., Cadeiras, M., Deng, M.C., Lam, M.P., and Ping, P. (2014). Characterization of human plasma proteome dynamics using deuterium oxide. Proteomics Clin Appl.

Wang, X., Li, J., Zheng, H., Su, H., and Powell, S.R. (2011b). Proteasome functional insufficiency in cardiac pathogenesis. Am J Physiol Hear. Circ Physiol *301*, H2207–H2219.

Weber, K., and Osborn, M. (1969). The reliability of molecular weight determinations by dodecyl sulfate-polyacrylamide gel electrophoresis. J Biol Chem *244*, 4406–4412.

Weintraub, S.J., and Deverman, B.E. (2007). Chronoregulation by asparagine deamidation. Sci STKE *2007*, re7.

Westman-Brinkmalm, A., Abramsson, A., Pannee, J., Gang, C., Gustavsson, M.K., von Otter, M., Blennow, K., Brinkmalm, G., Heumann, H., and Zetterberg, H. (2011). SILAC zebrafish for quantitative analysis of protein turnover and tissue regeneration. J. Proteomics *75*, 425–434.

Wisniewski, J.R., Zougman, A., Nagaraj, N., and Mann, M. (2009). Universal sample preparation method for proteome analysis. Nat Methods *6*, 359–362.

Wolstencroft, K., Haines, R., Fellows, D., Williams, A., Withers, D., Owen, S., Soiland-Reyes, S., Dunlop, I., Nenadic, A., Fisher, P., et al. (2013). The Taverna workflow suite: designing and executing workflows of Web Services on the desktop, web or in the cloud. Nucleic Acids Res *41*, W557–W561.

Wong, C.C., Xu, T., Rai, R., Bailey, A.O., Yates 3rd, J.R., Wolf, Y.I., Zebroski, H., and Kashina, A. (2007). Global analysis of posttranslational protein arginylation. PLoS Biol *5*, e258.

Wu, L., Candille, S.I., Choi, Y., Xie, D., Jiang, L., Li-Pook-Than, J., Tang, H., and Snyder, M. (2013). Variation and genetic control of protein abundance in humans. Nature *499*, 79–82.

Xu, S., Peng, G., Wang, Y., Fang, S., and Karbowski, M. (2011). The AAA-ATPase p97 is essential for outer mitochondrial membrane protein turnover. Mol Biol Cell *22*, 291–300.

Xu, T., Venable, J.D., Park, S.K., Cociorva, D., Lu, B., Liao, L., Wohlschlegel, J., Hewel, J., and Yates 3rd, J.R. (2006). ProLuCID, a fast and sensitive tandem mass spectra-based protein identification program. Mol Cell Proteomics *5*, S174.

Yang, H., and Zubarev, R.A. (2010). Mass spectrometric analysis of asparagine deamidation and aspartate isomerization in polypeptides. Electrophoresis *31*, 1764–1772.

Yen, H.-C.S., Xu, Q., Chou, D.M., Zhao, Z., and Elledge, S.J. (2008). Global protein stability profiling in mammalian cells. Science *322*, 918–923.

Young, V.R., Steffee, W.P., Pencharz, P.B., Winterer, J.C., and Scrimshaw, N.S. (1975). Total human body protein synthesis in relation to protein requirements at various ages. Nature *253*, 192–194.

Zak, R., Martin, A.F., Prior, G., and Rabinowitz, M. (1977). Comparison of turnover of several myofibrillar proteins and critical evaluation of double isotope method. J Biol Chem *252*, 3430–3435.

Zhang, G.X., Kimura, S., Nishiyama, A., Shokoji, T., Rahman, M., Yao, L., Nagai, Y., Fujisawa, Y., Miyatake, A., and Abe, Y. (2005). Cardiac oxidative stress in acute and chronic isoproterenol-infused rats. Cardiovasc. Res. *65*, 230–238.

Zhang, J., Li, X., Mueller, M., Wang, Y., Zong, C., Deng, N., Vondriska, T.M., Liem, D.A., Yang, J.-I., Korge, P., et al. (2008a). Systematic characterization of the murine mitochondrial proteome using functionally validated cardiac mitochondria. Proteomics *8*, 1564–1575.

Zhang, J., Liem, D.A., Mueller, M., Wang, Y., Zong, C., Deng, N., Vondriska, T.M., Korge, P., Drews, O., MacLellan, W.R., et al. (2008b). Altered Proteome Biology of Cardiac Mitochondria Under Stress Conditions. J Proteome Res *7*, 2204–2214.

Zhang, J., Lin, A., Powers, J., Lam, M.P., Lotz, C., Liem, D., Lau, E., Wang, D., Deng, N., Korge, P., et al. (2012). Perspectives on: SGP symposium on mitochondrial physiology and medicine: mitochondrial proteome design: from molecular identity to pathophysiological regulation. J Gen Physiol *139*, 395–406.

Zhang, Y., Reckow, S., Webhofer, C., Boehme, M., Gormanns, P., Egge-Jacobsen, W.M., and Turck, C.W. (2011). Proteome scale turnover analysis in live animals using stable isotope metabolic labeling. Anal. Chem. *83*, 1665–1672.

Zong, C., Gomes, A. V, Drews, O., Li, X., Young, G.W., Berhane, B., Qiao, X., French, S.W., Bardag-Gorce, F., and Ping, P. (2006). Regulation of murine cardiac 20S proteasomes: role of associating partners. Circ Res *99*, 372–380.

Zong, N., Li, H., Lam, M.P., Jimenez, R.C., Kim, C.S., Deng, N., Kim, A.K., Choi, J.H., Zelaya, I., Liem, D.A., et al. (2013). Integration of Cardiac Proteome Biology and Medicine by a Specialized Knowledgebase. Circ Res *113*, 1043–1053.